

## **Materials Science**



## XANES and EXAFS Studies of Plutonium(III, VI) Sorbed on Thorium Oxide

The study of plutonium sorption mechanisms on mineral surfaces seems very interesting considering radwaste management and, in particular, for underground disposal after advanced reprocessing. Indeed, radionuclides retention processes on engineered or geological barriers could enhance retardation. Thus, it appears important to understand such phenomena at both the macroscopic and molecular levels.<sup>1,2</sup> In this context, as plutonium is a very radiotoxic element, it is necessary to model its behavior in the geosphere and its interaction with natural minerals. Such an investigation is complicated by the existence of several oxidation states for plutonium. Then, sorption mechanisms could be different considering Pu(III), (IV), or (VI). This work deals with the influence of the oxidation state of plutonium on the structure of the sorbed complex. X-ray absorption spectroscopy has been chosen to perform this study. We have considered thorium oxide as a retention matrix because, on one hand, it is a sparingly soluble material; thus, dissolution processes of the solid can be neglected during sorption experiments. On the other hand, only one type of sorption site is expected, which allows us to simplify the study.

Thorium oxide has been obtained by heating thorium oxalate at 900°C. Its specific surface area measured by the N<sub>2</sub>-BET method is around 5 m<sup>2</sup>.g<sup>-1</sup>. The synthesized compound has been characterized by X-ray powder diffraction. Moreover, a thorium oxide doped plutonium(IV) (Pu/Th around 0.01) has been synthesized and characterized as well. This later compound has been used as a reference solid for extended X-ray absorption fine structure (EXAFS) analysis.

In order to avoid Pu(OH)<sub>4</sub> colloid formation or precipitation, it is necessary to adjust the pH of the aqueous phase to very low values. But for such conditions, no retention phenomenon can occur. Therefore, we have only performed experiments with Pu(III) and Pu(VI).

Plutonium solutions were prepared from a Pu(IV) stock solution. The Pu(III) solution was prepared by reducing Pu(IV) with zinc powder while the Pu(VI) solution was prepared by oxidizing Pu(IV) with ammonium persulfate. Then, these two solutions were respectively adjusted to pH = 5 and 3 for Pu(III) and Pu(VI) with a 0.1 M NaOH solution, and the concentrations were determined by spectrophotometry. The initial concentrations were around 5.10<sup>-3</sup> M.

Sorption experiments were performed by shaking, for 3 hours, a weighed amount of ThO<sub>2</sub> (previously equilibrated with the aqueous phase) with the plutonium solutions. Then the supernatant was removed, and the solid was dried at room temperature. Both samples were pressed into pellets and sealed with Kapton tape, which served as an X-ray transparent window.

The spectroscopic investigation was performed at the Stanford Synchrotron Radiation Laboratory. X-ray absorption near-edge structure (XANES) and EXAFS spectra were collected at the Pu L<sub>III</sub> absorption edge. EXAFS data were extracted from the raw absorption spectra by standard methods using in-house codes,<sup>3</sup> and single scattering approximation was used for the quantitative fitting procedure. The backscattering phases and amplitudes have been extracted from the initially

**R. Drot,**  
**E. Ordonez-Regil,**  
**E. Simoni**  
*Institut de Physique  
Nucléaire, Université  
Paris Sud, Groupe de  
Radiochimie,  
91406 Orsay Cedex,  
France*

**Ch. Den Auwer,**  
**Ph. Moisy**  
*CEA Marcoule, DCC/  
DRRV/SEMP, Valrhô,  
30207 Bagnols-sur-  
Cèze, France*

calculated EXAFS spectrum of the model solid, ThO<sub>2</sub> doped Pu (1%), using FEFF7 code.<sup>4</sup> The obtained results indicate that the plutonium is sorbed as an inner-sphere complex. By studying the XANES part of the X-ray absorption spectra, it is possible to identify the oxidation state of sorbed plutonium. Previous published works<sup>5</sup> have shown that the position of the Pu L<sub>III</sub> white line depends on the oxidation state of the plutonium species. The obtained results show that the plutonium is not sorbed at the same oxidation state as when it was initially introduced in solution. This seems to indicate that, in our experimental conditions, no oxidation or reduction phenomena occur in the electrical double layer.

### References

1. Manceau A. et al., *Applied Clay Science*, 7, 201 (1992).
2. Drot R. et al., *Langmuir*, 15, 14, 4820 (1999).
3. Michalowicz A., Thesis, Université du Val de Marne, France, 624 pp. (1990).
4. Ankoudinov A., Thesis, Washington University, 119 pp. (1996).
5. Conradson S. D. et al., *Polyhedron*, 17, 4, 599 (1998).

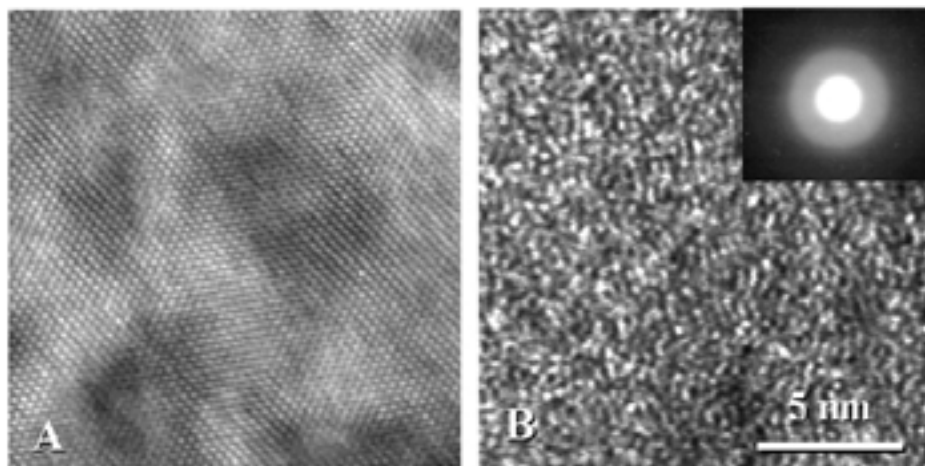
## Effects of Fission Product Accumulation in Cubic Zirconia\*

The disposition and disposal of plutonium from the dismantlement of nuclear weapons and from the reprocessing of the commercial nuclear fuel have led to increased interest in the possibility of “burning” actinides in non-fertile or so-called inert-matrix fuels (e.g., fuels without  $^{238}\text{U}$ ).<sup>1,2</sup> This strategy prevents the further production of plutonium by neutron capture reactions and subsequent beta decay. The recently adopted strategy in selecting materials for inert matrix fuel has been to consider not only the properties of the material as a fuel, but also the waste form properties of the inert-matrix fuel. Such an approach would allow direct disposal without reprocessing after once-through burnup.

Yttria stabilized cubic-zirconia (YSZ) is a promising candidate material for both inert matrix fuel and waste form based on its high solubility for actinides, high chemical durability and its reported exceptional stability under radiation.<sup>3,4</sup> Because the incorporation of fission and other transmutation products during burnup may significantly affect the radiation response and the chemical durability of cubic zirconia, the solubility and mobility of the fission product nuclides in the inert matrix fuel at high temperatures (reactor fuel conditions) and low temperatures (repository conditions) are important.

In this study, we have investigated the effects of fission product incorporation on the microstructure of YSZ (with 9.5 mol. % of yttria) by ion implantation (using 70-400 keV  $\text{Cs}^+$ ,  $\text{Xe}^+$ ,  $\text{Sr}^+$  and  $\text{I}^+$  ions) and transmission electron microscopy (TEM). The ion implantation was conducted in a temperature range between 300 to 873 K to doses up to  $1 \times 10^{21}$  ions/ $\text{m}^2$ . *In situ* TEM was conducted on pre-thinned TEM samples to follow the microstructure evolution during ion implantation using the IVEM-Tandem Facility at Argonne National Laboratory. Cross-sectional TEM was performed after implantation of the bulk samples to reveal the depth-dependent microstructure induced by ion implantation.

*In situ* TEM during the 70 keV  $\text{Cs}^+$  implantation at the room temperature revealed a high density of defect clusters on the nanometer scale after  $\sim 2 \times 10^{20}$   $\text{Cs}/\text{m}^2$ . The defect clusters with characteristics of interstitial type dislocation loops are interpreted to be the result of planar precipitates of Zr and/or O interstitials displaced from their original lattice site by the collisional events. Amorphous domains in thin regions of the specimen were observed after  $1 \times 10^{21}$   $\text{Cs}/\text{m}^2$  with high resolution TEM (HRTEM) and nanobeam electron diffraction (Fig. 1).

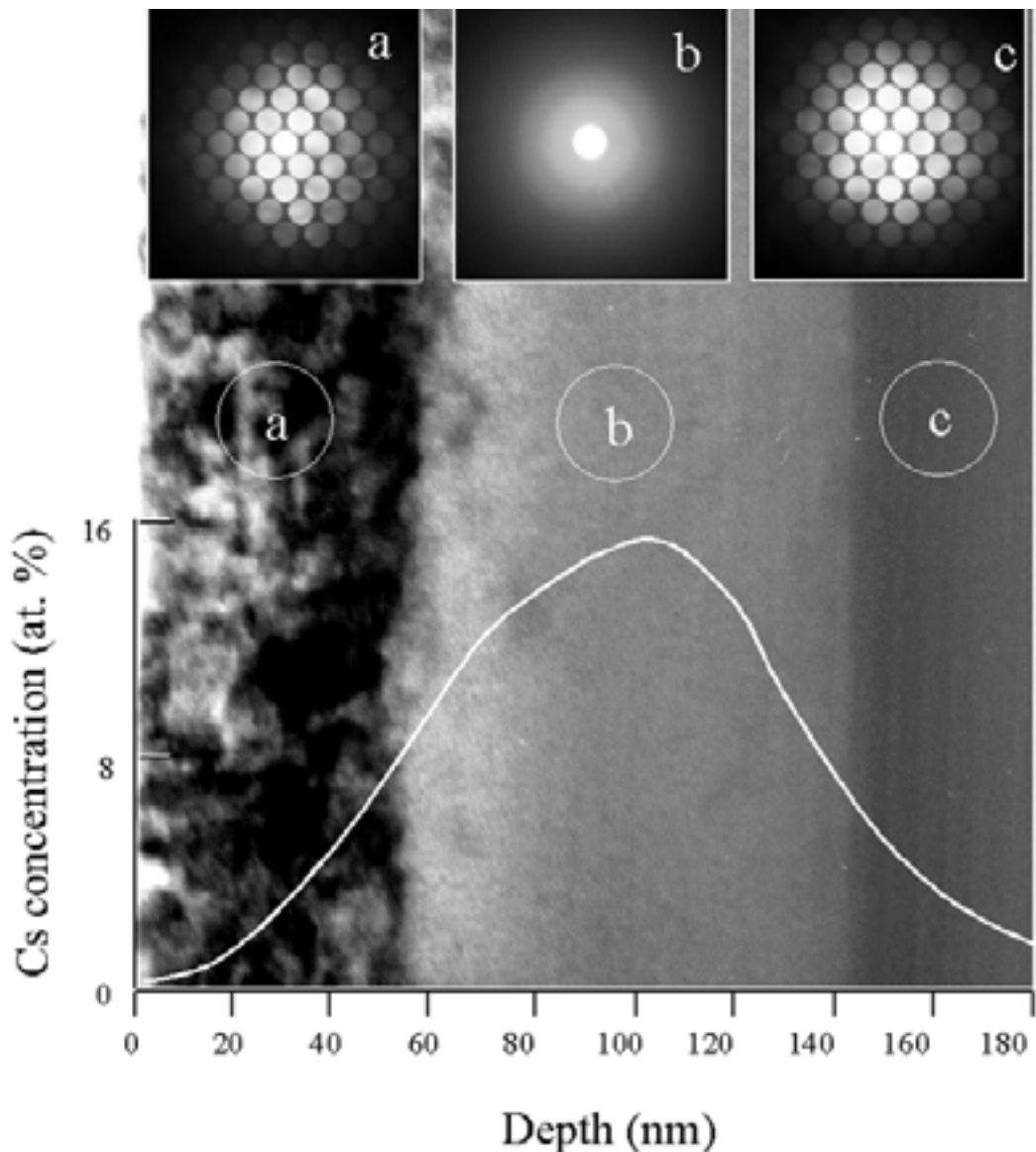


L.M. Wang,  
S.X. Wang, S. Zhu  
R.C. Ewing,  
University of Michigan,  
Ann Arbor, MI 48109,  
USA

Figure 1. Plan-view high resolution TEM micrographs from various regions of a cubic zirconia sample (stabilized by 9.5 mol. % of yttria) after 70 keV  $\text{Cs}^+$  implantation to  $1 \times 10^{21}$   $\text{Cs}/\text{m}^2$  at room temperature. (A) from a region with ~7 at.% Cs; (B) from a region with ~11 at.% Cs.

Cross-sectional TEM of a specimen after 400 keV Cs<sup>+</sup> implantation to 1x10<sup>21</sup> Cs/m<sup>2</sup> at the room temperature has revealed an amorphous band in a depth range where Cs concentration is greater than 8 at.% (Fig. 2). Although the front edge of the amorphous layer overlaps with the displacement damage peak that reached 330 displacement per atom (dpa), we suggest that the amorphization is mainly due to the incorporation of Cs rather than from the displacement damage as the center of the amorphous layer overlaps with the peak Cs concentration. This interpretation is consistent with previous results of radiation damage studies in YSZ that reached damage levels as high as 680 dpa but without amorphization.<sup>3</sup> Amorphization of YSZ is caused by the large size incompatibility and low mobility of cesium ions in the YSZ structure at room temperature, reflecting a relatively low solubility of Cs in YSZ. Nevertheless, the Cs concentration at which amorphization of YSZ occurred (~8 at. %) is well above the value that will likely be reached in an inert fuel matrix (~5 at. % assuming a 30 at.% Pu loading).

**Figure 2. Cross-sectional bright-field TEM micrograph with associated electron diffraction pattern showing the formation of an amorphous band in a cubic zirconia sample (stabilized by 9.5 mol. % of yttria) after 70 keV Cs<sup>+</sup> implantation to 1x10<sup>21</sup> Cs/m<sup>2</sup> at room temperature. The overlay of the Cs concentration profile is based on the results of analytical TEM that has been normalized by the results of a Monte Carlo computer simulation using the SRIM code.**



Various types of nanometer-scaled defect clusters (e.g., dislocation loops or small gas bubbles) were apparent in samples implanted by the other three ions after  $1 \times 10^{20}$  ions/m<sup>2</sup>. However, other than Xe bubbles, no secondary phase precipitates were apparent in YSZ implanted with Xe, Sr or I ions even after  $1 \times 10^{21}$  ions/m<sup>2</sup>. No amorphization was observed after 400 keV I<sup>+</sup> implantation to  $1 \times 10^{21}$  ions/m<sup>2</sup> at 973 K, even though iodine has a larger ionic radius than cesium, due to the relatively high mobility of iodine in YSZ at the high temperature.

### References

1. Boczar, P.G. et al., Advanced CANDU systems for plutonium destruction, Can. Nucl. Soc. Bull. **18**, 2 (1997).
2. Oversby, V. M., McPheeters, C. C., Degueldre C. and Paratte, J. M. Control of civilian plutonium inventories using burning in a non-fertile fuel, J. Nucl. Mater. **245**, 17 (1997).
3. Sickafus, K.E. et al. Burn and bury option for plutonium, Ceram. Bull. **78**(1), 69 (1999).
4. Degueldre, C. and Paratte, J.-M. Basic properties of a zirconia-based fuel material for light water reactors, Nucl. Tech. **123**, 21 (1998).

\*Work supported by US DOE under Grant DE-FG07-99ID13767.

# Identification of a Physical Metallurgy Surrogate for the Plutonium— 1 wt. % Gallium Alloy

Frank E. Gibbs,  
David L. Olson,  
William Hutchinson  
*Los Alamos National  
Laboratory, Los  
Alamos, NM 87545,  
USA and Colorado  
School of Mines*

## Introduction

Future plutonium research is expected to be limited due to the downsizing of the nuclear weapons complex and an industry focus on environmental remediation and decommissioning of former manufacturing and research facilities. However, the need to further the understanding of the behavior of plutonium has not diminished. Disposition of high level residues, long-term storage of wastes, and certification of the nuclear stockpile through the Stockpile Stewardship Program are examples of the complex issues that must be addressed. Limited experimental facilities and the increasing cost of conducting plutonium research provide a strong argument for the development of surrogate materials. The purpose of this work was to identify a plutonium surrogate based on fundamental principles such as electronic structure, and then to experimentally demonstrate its viability.

A fundamental link between cerium and plutonium has been reported in several references.<sup>1,2,3,4,5,6</sup> Both materials exhibit low melting temperatures, non-symmetrical crystal structures, and multiple allotropic forms which undergo large volume changes during transformation. This behavior has been attributed to the degree of localization of f electrons in each material (plutonium – 5f, cerium – 4f). Each element is located on the periodic table where f-electrons are in transition to a localized state and, as a result, exhibit similar bulk properties and phase transformation characteristics. The fundamental similarities between plutonium and cerium set the stage for the identification of a material surrogate.

## Description of the Work

The well characterized plutonium – 1 wt. % gallium alloy was used to establish a link to potential surrogate alloys. This alloy exhibits solid-state solute microsegregation upon cooling through the  $\epsilon$ -Pu (BCC) +  $\delta$ -Pu (FCC) two-phase region that can affect its behavior during mechanical processing or affect the final material properties. The resulting microstructure is shown in Figure 1. Homogenization is required to redistribute gallium and stabilize the room-temperature  $\delta$ -Pu (FCC) phase.<sup>7,8</sup> Two cerium-based alloys (Ce-5 wt. % Nd and Ce-5 wt. % La) were identified and experimentally shown to exhibit similar solid-state microsegregation in a transformation between  $\delta$ -Ce (BCC) +  $\gamma$ -Ce (FCC). An initial photomicrograph and the electron microprobe results for the Ce- 5 wt. % La alloy are shown in Figure 2. The rate of homogenization of lanthanum in the cored surrogate was then used to measure the activation energy for diffusion and to establish an analytical correlation between the two alloys. An example of these data are shown in Figure 3.

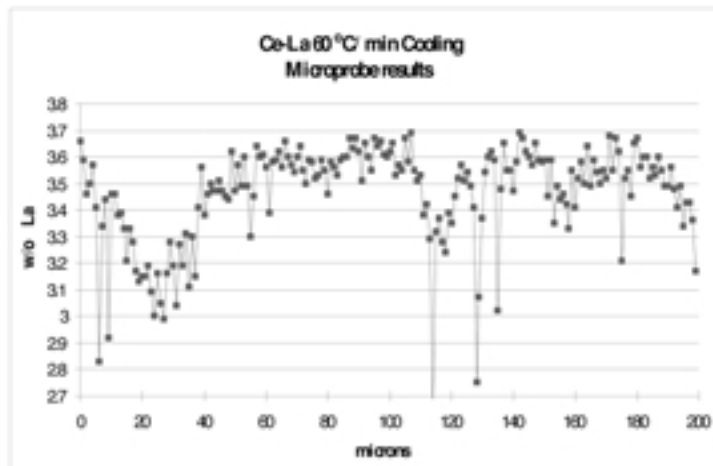
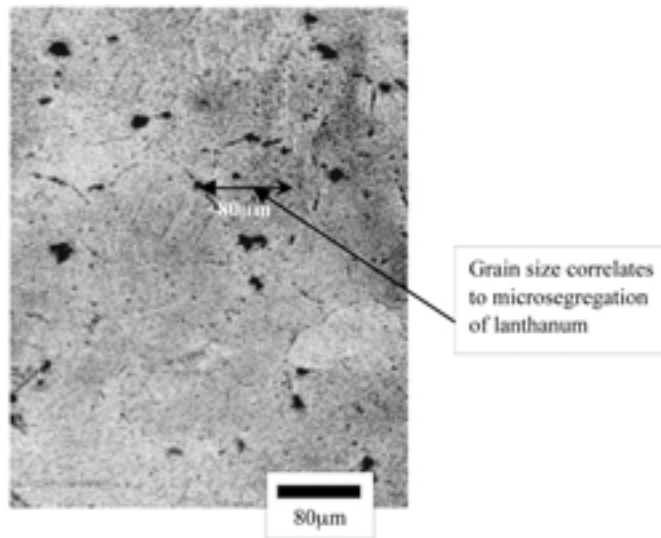
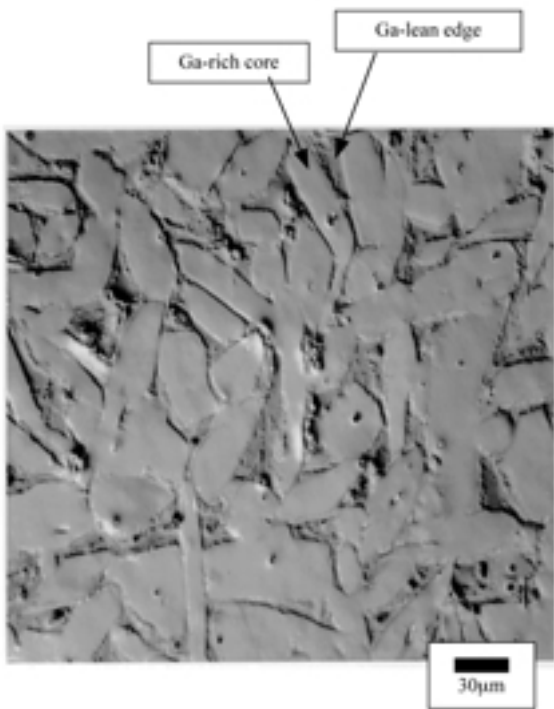
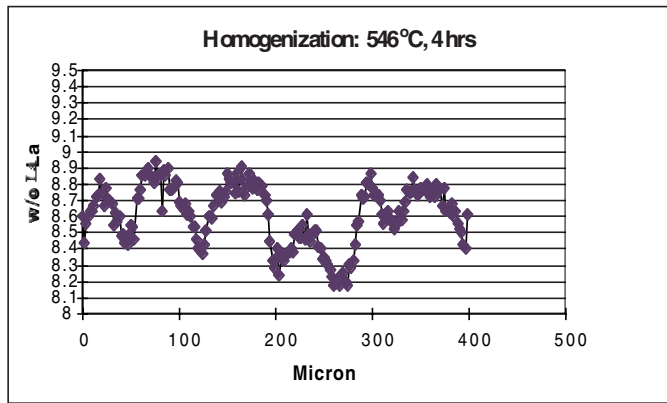


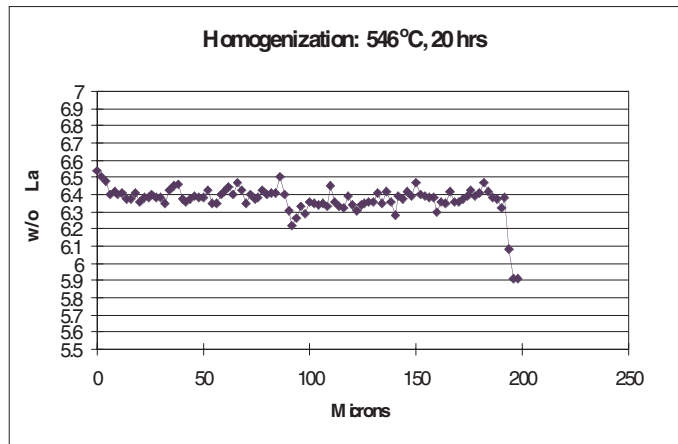
Figure 1. Typical cored microstructure of the Pu – 1 wt. % Ga alloy. Gallium microsegregation occurs upon cooling from the melt. Electron microprobe measurements show Ga-rich grain centers (~1.6 wt. % Ga) and Ga-lean boundaries that have been correlated to the equilibrium Pu-Ga phase diagram. The darker, Ga-lean regions result in metastable  $\delta$ -phase or lower temperature phases as defined by the phase diagram.

Figure 2. Electron microprobe results for a Ce- 5 wt. % La alloy subjected to a cooling rate of 60°C/min cooling rate through the  $\gamma+\delta$  region. A 200  $\mu\text{m}$  trace was run which indicates microsegregation of lanthanum at a frequency that approximately corresponds to the grain size. Further study is required to fully characterize the cerium phase equilibria and phase transformations, but the distribution is similar to the Pu – 1 wt. % Ga alloy. Lanthanum detection limit was  $\pm 0.05$  wt. %.

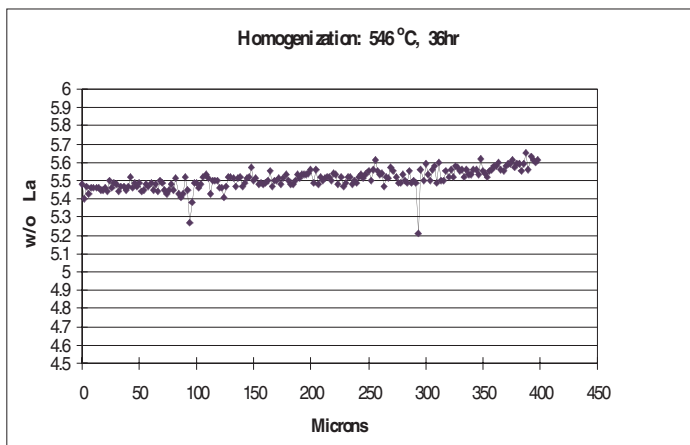
Figure 3. Example of homogenization data for Ce – 5 wt. % La alloy. The rate of homogenization for three different temperatures (546°C, 585°C, and 633°C) was used to determine the activation energy for diffusion (30,200 cal/mole). This value was used to establish an analytical link to the Pu – 1 wt. % Ga alloy. The variation in the nominal lanthanum concentration was due to macrosegregation during casting. This variation can be reduced via induction melting.



Ce – 5 wt. % La alloy initially cored by rapid cooling through the  $\gamma+\delta$  region and then homogenized at 546°C for 4 hours.



Ce – 5 wt. % La alloy initially cored by rapid cooling through the  $\gamma+\delta$  region and then homogenized at 546°C for 20 hours.



Ce – 5 wt. % La alloy initially cored by rapid cooling through the  $\gamma+\delta$  region and then homogenized at 546°C for 36 hours.

## Results

Cerium is an excellent plutonium surrogate candidate because of the correlation to electronic structure that is manifested in similar bulk properties and phase transformation characteristics. The specific correlation of the Ce-5 wt. % La alloy to the Pu-1 wt. % Ga alloy establishes an important link. Cerium surrogate studies can potentially provide important insights into important issues such as the effect of fabrication processes (wrought versus cast), the role of impurities such as iron, or the impact of high strain-rates. Such Pu surrogates can advance the understanding of plutonium behavior while reducing the amount of plutonium work required and ultimately reducing operational risks and costs.

## References

1. Raraz, Alcides G., Optimization of Plutonium Electrorefining Through modeling and Model Materials, PhD Thesis T4306, Colorado School of Mines, Golden Colorado, June 24, 1994.
2. N. M. Edelstein, "Comparison of the Electronic Structure of the Lanthanides and Actinides," J. Alloys and Compounds 223 (1995) 197-203.
3. Johansson, B., "Crystal and Electronic Structure Connections Between the 4f and the 5f Transition Metals," J. Alloys and Compounds, 223 (1995) 211-215.
4. M. S. S. Brooks, O. Eriksson, B. Johansson, "From the Transition Metals to the Rare Earths - Via the Actinides," J. Alloys and Compounds 223 (1995) 204-210.
5. Dariel, M. P., "Diffusion of  $^{140}\text{La}$  in b.c.c. -Lanthanum and -Cerium," Philosophical Magazine, 1973, Vol. 28, page 915-922.
6. Haire, R. G., "Comparison of the Chemical and Physical Properties of f-element Metals and Oxides: Their Dependence on Electronic Properties," J. Alloys and Compounds 223 (1995) 185-196.
7. Ferrera, D. W., Doyle, J. H., Harvey M. R., "Gallium Coring Profiles for Plutonium-1 Weight Percent Gallium Alloys," RFP-1800, Rocky Flats Plant, Golden, Colorado, May 11, 1972.
8. Johnson, K. A., "Homogenization of Gallium-Stabilized Delta-Phase Plutonium," LA-2989, UC-25, Metals, Ceramics, and Materials, TID-4500 (26th edition), Los Alamos National Laboratory of the University of California, February 28, 1964.

## Innovative Concepts for the Plutonium Facilities at La Hague

**B. Gillet,**  
**A. Gresle**  
*Cogema, Velizy*  
*Villacoublay 78141,*  
*France*

**F. Drain**  
*SGN, Saint Quentin*  
*en Yvelines 78182,*  
*France*

The commercial strategy of COGEMA is now based on a combined reprocessing-conditioning-recycling proposal: the reprocessing plants at La Hague ensure plutonium recovery, purification, and conditioning, and the mixed-oxide (MOX) fuel fabrication plant MELOX at Marcoule ensures its recycling into MOX nuclear fuel. This strategy is enabled thanks to technological and process innovations resulting from an extensive R&D program over the past twenty years. First, the UP3 plant (the T4 plutonium facility in particular) have benefited from these innovations. Second, experience gained from the UP3 plant and new developments have been integrated into the UP2-800 plutonium facilities (R4, URP, UCD) to continue cost reduction and performance optimizing.

### Plutonium Facilities at La Hague

The reprocessing-conditioning-recycling strategy is based on the MELOX plant and on the plutonium facilities at the La Hague plant.

- T4 facility, which started in active operation in 1990, and future R4 facilities [1], which will start in active operation in 2001, include three main units:
  - Purification of plutonium nitrate, conducted in pulsed columns or in multi-stage centrifugal extractors in one or two cycles.
  - Oxalate conversion into PuO<sub>2</sub>. Plutonium oxalate is formed continuously by precipitation. The precipitate is separated from the mother liquors by continuous filtration. The pulp is then dried and calcinated into a screw calciner.
  - Plutonium oxide conditioning in stainless steel cans. Five cans are placed in a canister which itself is placed in a container for interim storage.
- The Plutonium Redissolution Unit (URP started in active operation in 1994), which enables the dissolution of PuO<sub>2</sub> after an interim storage step using a silver dissolution process. Plutonium nitrate is then decontaminated in the PUREX process to separate plutonium and americium.
- An industrial-scale alpha waste decontamination facility known as the Centralized Alpha Waste Treatment facility (UCD started in active operation in 1997), which ensures plutonium removal from technological plutonium-bearing waste (metallic or plastic) by a silver leach process. Depending on the waste type, a mechanical treatment could be necessary before leaching to enable a high decontamination rate. The objective is, on one hand, to downgrade the waste to make it suitable for near-surface disposal and, on the other hand, to recycle the largest possible amount of plutonium in the main reprocessing line [2]. More than 95% of the silver used as an oxidizing agent is recovered in a complementary unit of UCD using an electrochemical process and recycled.

### Technological and Process Innovations

An extensive R&D program has enabled innovations necessary to design and operate the plutonium purification facilities, UCD, and URP, including the following in particular:

- Development of equipment: multi-stage centrifugal extractor to perform plutonium purification by liquid-liquid extraction, crushing function to reduce

waste size and thus guarantee plutonium-bearing waste mixing during silver decontamination, electrolyser of high power with the associated electric distribution and insulation, leach tank and its internals to perform the plutonium-bearing waste treatment with a high plutonium recovery rate and good operating conditions, tube bundle tanks, on-line analysers installed directly on the process piping.

- Development of new process: purification of plutonium in pulsed columns using specific packing technology which guarantees a good wettability and short residence time in centrifugal extractors, decontamination of plutonium-bearing waste and plutonium oxide dissolution using electrogenerated silver as an oxidizing agent, silver recovery from nitric acid solution with high efficiency.
- Optimizing of engineering rules [3] and, in particular, containment rules (static or dynamic).
- Large scale use of on-line analyses and remote control to enable supervision from a remote control room and minimization of operating cost.
- Optimizing of process automation to avoid human intervention during both normal operations and maintenance, thus greatly reducing the dose rate to personnel.
- Optimizing of equipment size and arrangement to reduce building size and cost.

### Conclusion

The experience gained by COGEMA from the new reprocessing plants at La Hague in the past ten years demonstrates that the plutonium facility enables a high level of performance:

- The planned capacity and throughput are achieved while complying with safety requirements.
- A constant plutonium quality is obtained.
- A reduction of dose rate to personnel is observed in spite of more stringent isotopic plutonium composition thanks to containment quality and remote operation.
- Process optimizing and development both ensure the reduction of solid plutonium-bearing waste production and of radioactive releases to the environment.

Consequently, COGEMA's plutonium technologies (purification using pulsed columns, the electrochemical process in particular) have already been selected for pilot or industrial applications in Japan and the United States, for instance.

### References

1. G. Bertolotti, B. Gillet, I.-V. de Laguerie, R. Richter, "R4 Innovative Concept for Plutonium Finishing Facility." RECOD, 5<sup>th</sup> International Nuclear Conference on Recycling, Conditioning and Disposal, p.11. Vol. 1, Nice, France, October 25-28, 1998.
2. J.-J. Izquierdo, A. Lavenu, B. Kniebihli, "The Centralized Alpha Waste Treatment Facility (UCD) at La Hague." RECOD, 5<sup>th</sup> International Nuclear Conference on Recycling, Conditioning and Disposal, p.11. vol. 1, Nice, France, October 25-28, 1998.
3. G. Bertolotti, F. Drain, G. Dubois, P. Mathieu, J. Monnatte, "French Engineering and Operating Rules for Plutonium Facilities." RECOD, 5<sup>th</sup> International Nuclear Conference on Recycling, Conditioning and Disposal, p.11. vol. 1, Nice, France, October 25-28, 1998.

# Anisotropic Expansion of Pu through the $\alpha$ - $\beta$ - $\gamma$ Phase Transitions While Under Radial Compressive Stress

Dane R. Spearing,  
D. Kirk Veirs,  
F. Coyne Prenger  
*Los Alamos National  
Laboratory, Los  
Alamos, NM 87545*

## Introduction

In support of the new US Department of Energy (DOE) standard for the stabilization, packaging, and storage of plutonium bearing materials, the effects of the volume expansion associated with the  $\alpha/\beta$  and  $\beta/\gamma$  transformations of Pu metal on the integrity of a stainless steel storage container were examined. Within current proposed storage facilities, credible scenarios exist in which local temperatures could exceed the Pu  $\alpha/\beta$  and  $\beta/\gamma$  transition temperatures. Thus, tightly wedged pieces of  $\alpha$ -phase Pu metal within a 3013-type stainless steel storage container could pose a threat to the integrity of the canister. Therefore, understanding the mechanical effects of the volume expansions associated with the Pu  $\alpha/\beta$  and  $\beta/\gamma$  phase transitions on the integrity of said storage containers is a crucial step in the certification of the storage standards and facilities. In addition, an attempt is made to correlate the observed mechanical properties with the behavior of Pu through the phase transitions at a crystallographic scale.

## Experiment Description

Two separate experiments were performed: one to examine the effect of the expansion associated with the Pu  $\alpha/\beta$  phase transition on storage can integrity, and one to examine the cumulative effects of both the  $\alpha/\beta$  and  $\beta/\gamma$  phase transitions. In each of the experiments, a ~3.5 kg chill-cast monolithic cylindrical ingot of  $\alpha$ -phase Pu was placed in the axial center of an annealed stainless steel cylinder with an inner diameter less than 0.006" larger than the outer diameter of the ingot. This geometry maximizes the strength of the plutonium ingot with respect to the confining stainless steel cylinder and represents one "worst case" geometry for assessing the possibility of containment failure. Strain gages placed on the outside of the cylinder measured the hoop and axial strain response. The ingot was thermally cycled through the  $\alpha/\beta$  (first experiment) and  $\alpha$ - $\beta$ - $\gamma$  (second experiment) phase transitions until equilibrium in the strain response was reached. In addition, the thickness and diameter of the Pu ingot was measured following each cycle. Prior to and after each experiment, samples were collected from each ingot, and the grain sizes and orientation were examined via reflected light metallography.

## Results

The total hoop strain per cycle and cumulative plastic strain observed in the stainless steel storage cylinders are summarized in Figure 1.

In both experiments, the maximum strain was accumulated during the first cycle. For the  $\alpha$ - $\beta$  experiment, additional plastic strain was accumulated in the storage cylinder through four cycles, whereas no additional plastic strain was accumulated after the first cycle in the  $\alpha$ - $\beta$ - $\gamma$  experiment. The accumulated plastic strain levels have been determined to be within ASME code levels and have been modeled by Savannah River Site (SRS) using finite element analysis, which concluded that the observed expansion poses no threat to the integrity of the storage containers.

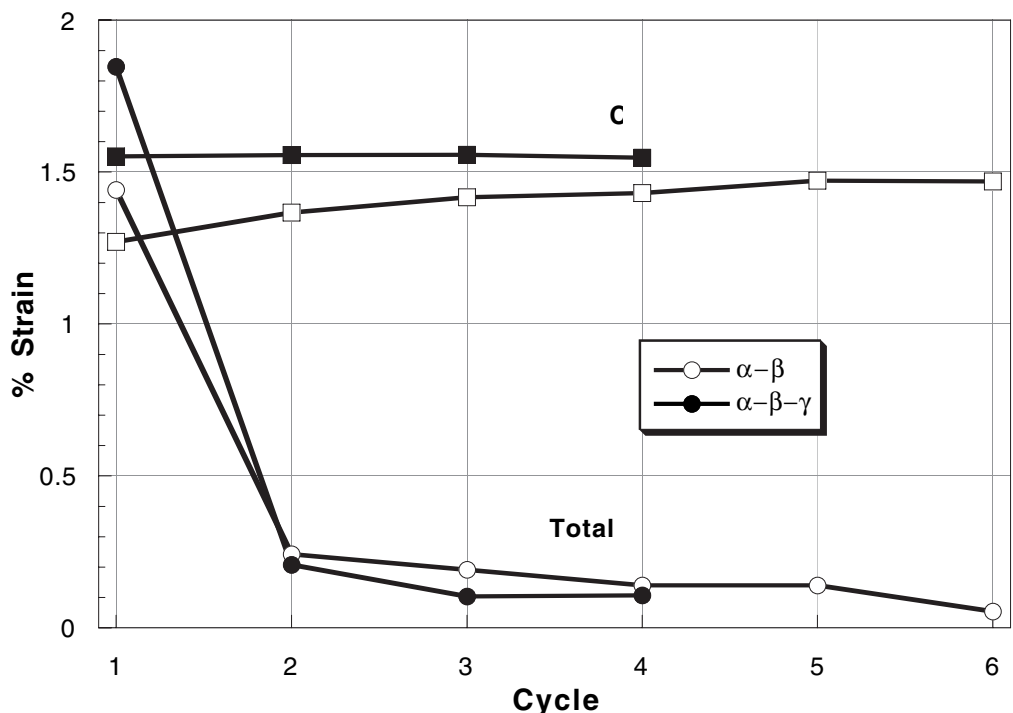


Figure 1. % strain vs. cycle. Circles: Total Strain/Cycle, Squares: Cumulative Plastic Strain

During the course of these experiments, it was observed that the Pu ingots did not expand isotropically, nor did they return to their original dimensions. Rather, the ingots expanded more along the axial direction and less radially. In Figure 2 the room temperature diameter and thickness of the ingot used in the  $\alpha$ - $\beta$ - $\gamma$  experiment are shown as measured at the end of each cycle.

The radial compressive stress on the Pu ingot was calculated to be approximately 1,200 psi, which is substantially less than the compressive yield strengths of  $\alpha$ -Pu (~60,000 psi)  $\beta$ -Pu (~20,000 psi), and  $\gamma$ -Pu (~5,000 psi). Therefore, the axial deformation observed in the Pu ingot must be due to some mechanism other than simple compressive yield. Reflected light metallographic images of the cycled

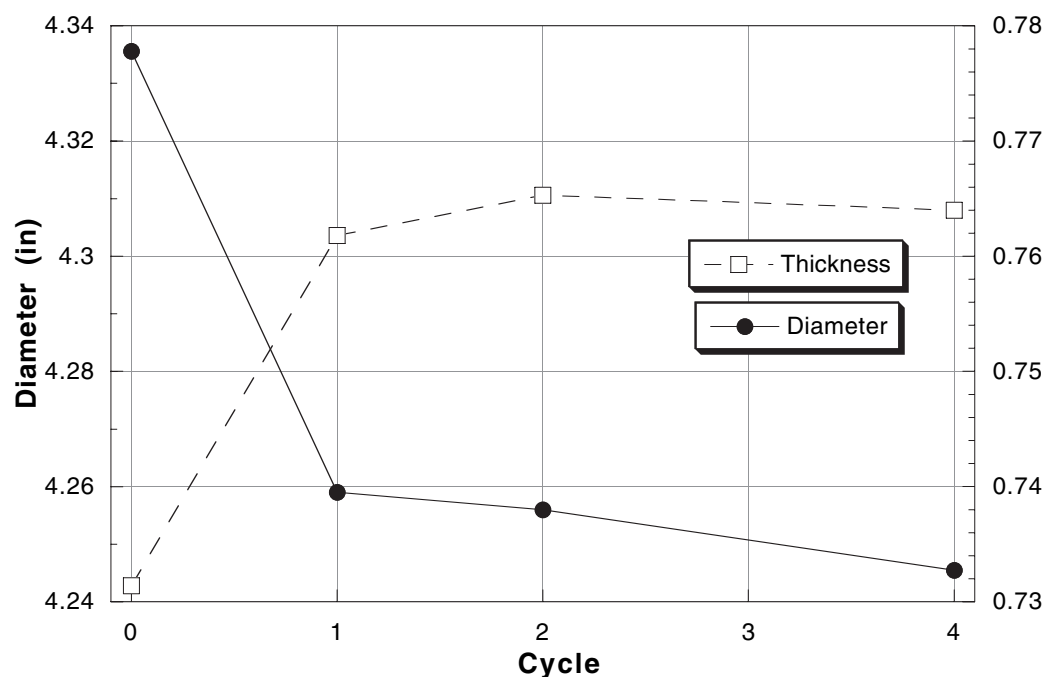
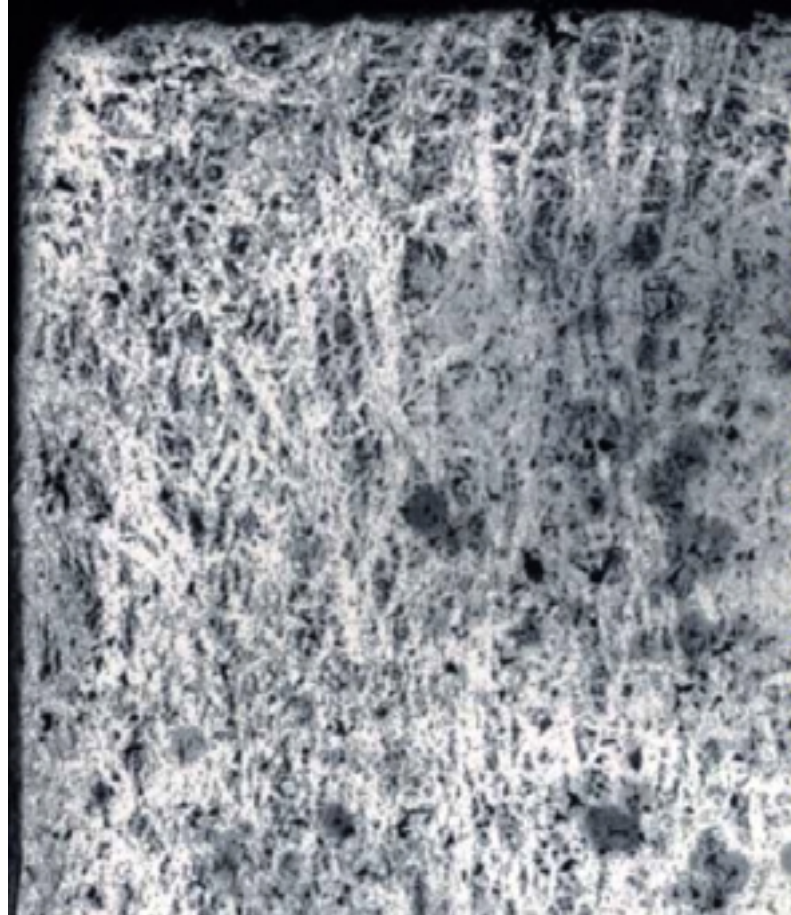


Figure 2. Ingot diameter and thickness vs. cycle for  $\alpha$ - $\beta$ - $\gamma$  experiment.

ingots show a “veining” phenomenon characteristic of Pu that has been cycled through the  $\alpha$ - $\beta$  phase transition. These veins tend to run perpendicular to the axial stress direction imposed upon the ingot by the canister wall, suggesting that the anisotropic expansion is due to alignment of the grains in response to the stresses during the phase transition.

**Figure 3.**  
Metallographic image  
of  $\alpha$ -Pu cycled  
through the  $\alpha$ - $\beta$   
phase transition.  
Width is approx.  
1/4 in.



## Contribution of Water Vapor Pressure to Pressurization of Plutonium Dioxide Storage Containers

Pressurization of long-term storage containers filled with materials meeting the US DOE storage standard is of concern.<sup>[1,2]</sup> For example, temperatures within storage containers packaged according to the standard and contained in 9975 shipping packages that are stored in full view of the sun can reach internal temperatures of 250°C.<sup>[3]</sup> Twenty five grams of water (0.5 wt. %) at 250°C in the storage container with no other material present would result in a pressure of 412 psia, which is limited by the amount of water. The pressure due to the water can be substantially reduced due to interactions with the stored material. Studies of the adsorption of water by PuO<sub>2</sub> and surface interactions of water with PuO<sub>2</sub> show that adsorption of 0.5 wt. % of water is feasible under many conditions and probable under high humidity conditions.<sup>[4,5,6]</sup> However, no data are available on the vapor pressure of water over plutonium dioxide containing materials that have been exposed to water.

A complete monolayer of water on plutonium dioxide should result in water adsorption of 0.22 mg m<sup>-2</sup>. Models of the interaction of water with the surface of plutonium dioxide have been proposed where the first layer is a hydroxide layer arising from the chemisorption of the equivalent of 1/2 monolayer of water with a heat of adsorption of 41 kcal mol<sup>-1</sup>.<sup>[7,4]</sup> The second layer of water is a complete monolayer that physisorbs with a heat of adsorption of 20 kcal mol<sup>-1</sup>. Subsequent layers are postulated to physisorb with a heat of adsorption equivalent to that of liquid water, 10 kcal mol<sup>-1</sup>, although there is no experimental data for these layers. The range of specific surface areas of plutonium dioxide commonly found at Los Alamos National Laboratory is between 50–0.5 m<sup>2</sup> g<sup>-1</sup>. Within this range, 0.5 wt. % water could be adsorbed within the strongly bound chemisorbed layer or almost completely as physisorbed liquid water.

Using the physical model and thermodynamic parameters described above, we have developed a method to calculate the vapor pressure of water over plutonium dioxide. Results at 240°C support a strong dependence upon the specific surface area (SSA) of the plutonium dioxide, ranging from essentially no contribution from water for material with a SSA of 50 m<sup>2</sup> g<sup>-1</sup> to over 400 psia pressure due to water for material with a SSA of 0.1 m<sup>2</sup> g<sup>-1</sup>. We will report on experiments to measure the vapor pressure of water as a function of temperature over plutonium dioxide at various water content, SSA of the material, and salt content. These experiments will be a guide to refine our model and provide data to estimate the heat of adsorption of adsorbed water layers beyond the second monolayer.

### References

1. U. S. Department of Energy, "Stabilization and storage of plutonium-containing materials," U. S. DOE DOE-STD-5XXX-99 (1999).
2. P. G. Eller, R. E. Mason, D. E. Horrell, S. D. McKee, N. A. Rink, and C. S. Leasure, "Gas pressurization from calcined plutonium oxides," LA-UR-99-3804, Los Alamos National Laboratory (1999).

D. Kirk Veirs,  
John S. Morris,  
Dane R. Spearing  
Los Alamos National  
Laboratory, Los  
Alamos, NM 87545,  
USA

3. S. J. Hensel, "Thermal analyses of the 9975 as a plutonium storage container," Westinghouse Savannah River Company, Aiken, SC 29802, WSRC-TR-98-00203 (1999).
4. J. L. Stakebake, "A thermal desorption study of the surface interactions between water and plutonium dioxide," *J. Phys. Chem.* **77**, 581 (1973).
5. J. M. Haschke and T. E. Ricketts, "Adsorption of water on plutonium dioxide," *J. Alloys Comp.* **252**, 148 (1997).
6. D. M. Smith, M. P. Neu, E. Garcia, and L. A. Morales, "Hydration of plutonium oxide and process salts, NaCl, KCl, CaCl<sub>2</sub>, MgCl<sub>2</sub>: effect of calcination on residual water and rehydration," LA-UR-99-261, Los Alamos National Laboratory, Los Alamos, NM 87545 (1999).
7. M. Paffett, private communication based on a reinterpretation of the data in Ref. 4.

# Surveillance of Sealed Containers with Plutonium Oxide Materials (ms163)

## Introduction

DOE is embarking upon a program to store large quantities of plutonium-bearing materials for up to fifty years. Materials destined for long-term storage include metals and oxides that are stabilized and packaged according to the DOE storage standard, where the packaging consists of two nested, welded, stainless steel containers.<sup>1</sup> Experience with pure PuO<sub>2</sub> and with impure materials has shown that gases generated by catalytic and/or radiolytic processes may accumulate.<sup>2-10</sup> Of concern are the generation of H<sub>2</sub> gas from adsorbed water and the generation of HCl or Cl<sub>2</sub> gases from the radiolysis of chloride-containing salts. The DOE 94-1 Program has initiated a surveillance plan where an integral part includes the monitoring of gas generation and compositional changes over oxide materials in sealed storage containers. The goal is to establish parameters for safe storage of plutonium bearing materials in the 3013 containers.

## Description of the Actual Work

The Los Alamos National Laboratory based surveillance project has two parallel studies. Many small (10-g) samples are monitored for relatively short time periods, and a limited number of large samples equivalent in size to the storage can capacity will be monitored for long periods of time. The small samples will allow a database of many material types prepared for storage in various ways and in contact with various gases to be compiled. Large samples will give the precise behavior of a limited number of samples. The instrumented sealed containers will be loaded with representative oxide materials and monitored for gas compositional changes over time. Baseline plutonium oxides, oxides exposed to high-humidity atmospheres, and oxides containing chloride salt impurities are planned. Comparison between the two sample types will determine the degree of confidence in small sample experiments and fundamental measurements in predicting the long-term behavior of real materials.

## Results

We have designed instrumented storage containers that mimic the inner storage can specified in the 3013 standard at both full- and small-scale capacities (2.4 liter and 0.005 liter, respectively), Figures 1 and 2. The containers are designed to maintain the volume to material mass ratio while allowing the gas composition and pressure to be monitored over time. The full-scale cans are instrumented with a Raman fiber optic probe, a mass spectrometer sampling port, an acoustic resonance chamber, two corrosion monitors, and pressure and temperature transducers. Preliminary Raman spectroscopy results indicate that detection levels of at least 0.2 torr of H<sub>2</sub> are easily achievable with a fiber optic system for light collection and delivery. Data collection for the containers is automated in order to reduce worker exposure. The small-scale containers are designed with microliter gas sampling capability and pressure and temperature sensors. These containers will be stored in a heated array in order to reproduce the increased temperatures arising from radioactive self-heating.

Laura Worl,  
John Berg,  
Doris Ford,  
Max Martinez,  
Jim McFarlan,  
John Morris,  
Dennis Padilla,  
Karen Rau,  
Coleman Smith,  
Kirk Veirs,  
Dallas Hill,  
Coyne Prenger  
*Los Alamos National  
Laboratory, Los  
Alamos, NM 87545,  
USA*

Figure 1. Full-scale (5000g) instrumented can assembly for gas surveillance.

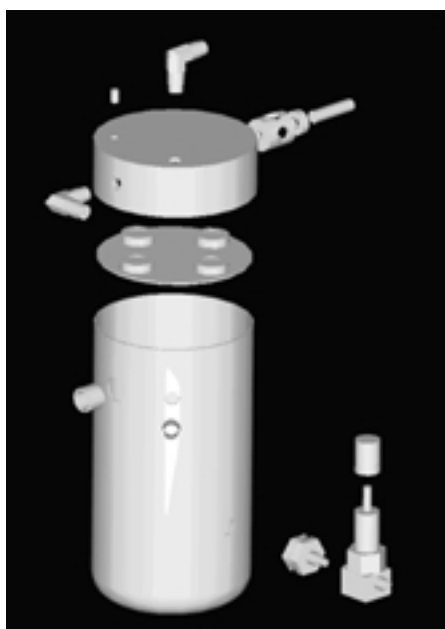


Figure 2. Small-scale (10g) instrumented container assembly for gas surveillance.



Oxide materials representing inventories destined for long-term storage throughout the DOE complex will be monitored. The oxide materials for the small-scale study will be selected to address known existing uncertainties in gas generation associated with specific material types being considered for storage. They will also reproduce the materials going into the large-scale study and offer data validity with ongoing efforts.<sup>9</sup> The large-scale containers will examine characterized oxide material in varying forms (pure  $\text{PuO}_2$ ,  $x\% \text{H}_2\text{O}/\text{PuO}_2$ ,  $\text{PuO}_2$  with salt,  $\text{PuO}_2$  with other material (plastics), etc.). The details of the materials and expected results will be discussed.

### References

1. "Stabilization, Packaging, and Storage of Plutonium-Bearing Materials," DOE-STD-3013-99, U. S. Department of Energy, Washington, DC.
2. Haschke, J. M. and T. E. Ricketts, "Plutonium Dioxide Storage: Conditions for Preparation and Handling," Los Alamos National Laboratory report, LA-12999-MS, 1995.
3. Haschke, J. M. and J. C. Martz, *Plutonium Storage*, 1998, John Wiley and Sons, Inc.: New York.
4. Allen, T. H. and J. M. Haschke, "Interactions of Plutonium Dioxide with Water and Oxygen-Hydrogen Mixtures," Los Alamos National Laboratory report, LA-13537-MS, 1999.
5. Stakebake, J. L., D. T. Larson, and J. M. Haschke, "Characterization of the Plutonium-water Reaction II: Formation of a Binary Oxide Containing Pu(IV)," *Journal of Alloys and Compounds*, 1993. **202**: p. 251.
6. Morales, L.A., "Preliminary Report on the Recombination Rates of Hydrogen and Oxygen over Pure and Impure Pu Oxides," Los Alamos National Laboratory report, LA-UR-98-5200, 1998.

7. Eller, P. G.; Mason, R. E.; Horrell, D. R.; McKee, S. D.; Rink, N. A.; Leasure, C. S., "Gas Pressurization from Calcined Plutonium Oxides," Los Alamos National Laboratory report LA-UR-00-3804, and reference therein.
8. Hagan, R.; Fry, D. A., "Report, Radiographic Surveillance of 3013 Containers," Los Alamos National Laboratory internal memorandum NMT-04-99-70, April 29, 1999.
9. Mason, R.; Allen, T.; Morales, L.; Rink, N.; Hagan, R.; Fry, D.; Foster, L.; Wilson, E.; Martinez, C.; Valdez, M.; Hampel, F.; Peterson, O., "Materials Identification and Surveillance: June 1999 Characterization Status Report," Los Alamos National Laboratory unclassified release, LA-UR-99-1231 (June 1999).
10. Livingston, R., "Gas Generation Test Support for Transportation and Storage of Plutonium Residue Materials," Westinghouse Savannah River Company Report #WSRC-TR-99-00223 (1999).

## **PuO<sub>2</sub> Surface Catalyzed Reactions: Recombination of H<sub>2</sub> and O<sub>2</sub> and the Effects of Adsorbed Water on Surface Reactivity**

**Luis Morales**  
*Los Alamos National  
Laboratory, Los  
Alamos, NM 87544,  
USA*

The Department of Energy/Environmental Management (DOE/EM) is responsible for the management and long-term disposition of a variety of materials located at Rocky Flats Environmental Test Site (RFETS), Hanford, Savannah River, and other DOE sites. The new plutonium storage standard, set to replace DOE 3013, requires thermal stabilization of the materials prior to packaging for storage. The Pu content of those materials can vary from ~86 weight percent, (essentially pure PuO<sub>2</sub>), down to ~30 weight percent. With such a range of compositions, the presumed plutonium dioxide can be in contact with a variety of other materials. Typically, these "impurities" include alkali metal chlorides, MgO, MgCl<sub>2</sub>, CaCl<sub>2</sub>, Fe<sub>2</sub>O<sub>3</sub> and other materials which are not well characterized. In addition, these solid mixtures are in contact with the gas phase under which the materials were packaged; the moisture content may not be known or well controlled. The new plutonium stabilization standard does not set accepted glovebox moisture levels nor does it prescribe the time duration between calcination and packaging.

The current storage standard contains an equation that predicts the total pressure build-up in the can over the anticipated storage time of fifty years. This equation was meant to model a worst-case scenario to insure pressures would not exceed the strength of the container at the end of 50 years. As a result, concerns about pressure generation in the storage cans, both absolute values and rates, have been raised with regard to rupture and dispersal of nuclear materials (1). Similar issues have been raised about the transportation of these materials around the complex.

The technical basis for the pressure equation given in the standard has not been fully established. The pressure equation contains two major assumptions, (a) that hydrogen and oxygen generated from radiolysis do not react to form water and (b) that the oxygen generated by radiolysis reacts with the oxide material and does not contribute to the pressure in the container. With regard to the first assumption, if the formation of water from hydrogen and oxygen is important, then the calculated pressures would be dramatically reduced. The formation of water is thermodynamically favored.

The reaction rates for oxidation, corrosion, and gas generation are affected by the nature of oxide surfaces and interfaces. In addition, water vapor present on metal oxide surfaces can influence the reaction rates and the chemistry which may occur. Because of the important role water vapor plays in solid-gas reactions, it is important to understand the interaction between plutonium dioxide and water vapor and its effects on the surface reactivity.

The purpose of this work is to measure the recombination rates of hydrogen/oxygen mixtures in contact with pure and impure plutonium oxides and to test the effects of adsorbed water on the surface reactivity. This was accomplished by using a calibrated pressure-volume-temperature (PVT) apparatus to measure the recombination rates, in a fixed volume, as the gas mixture was brought into contact with oxide powders whose temperatures ranged from 50°C to 300°C.

These conditions were selected in order to bracket the temperature conditions expected in a typical storage can. In addition, a 2% H<sub>2</sub>/air mixture was included in the study since this composition encompasses storage scenarios in which the cans are sealed in air and over time various amounts of hydrogen are formed.

The recombination of hydrogen and oxygen has been studied over a 250°C temperature range. Pressure-time curves and mass spectrometric results were obtained during gas mixture exposure to pure and impure plutonium oxides. The pure oxide was obtained from oxidation of alpha metal. The impure oxide was obtained through the Defense Nuclear Facilities Safety Board (DNFSB) 94-1 R & D program's Materials Identification and Surveillance (MIS) project and selected due to its low plutonium content, 29 weight percent and its high chloride content. Analysis by x-ray powder diffraction shows that the impure oxide is a mixture of plutonium dioxide, sodium chloride and potassium chloride.

The experiments suggest that the oxide surface is an active catalyst for the recombination reaction. The concentration of active surface sites governs the kinetics of recombination early on, and as the reaction proceeds, certain moieties (OH or H<sub>2</sub>O for example) occupy these surface sites thereby reducing the rate of recombination. Similar results, reduced recombination rates, are obtained when water is absorbed on the oxide surface. Above 100°C enough thermal energy is provided to maintain a larger fraction of the active sites available for recombination. A sharp break in the 100°C pressure-time curve shows how dramatically the recombination rate is reduced when the active sites become blocked. This type of behavior would not be expected for a recombination reaction dominated by radiolytic formation of radicals in the gas phase.

The results of these kinetic experiments also show that steady-state gas compositions are reached indicating the rates of recombination and water radiolysis become equal under these experimental conditions, although the recombination rate is dramatically faster than the radiolysis of adsorbed water initially. For a mixture 2% H<sub>2</sub>/air mixture, the steady-state gas composition is calculated to be below the flammable limit. The rates of water formation were calculated from the pressure-time curves and reported.

The implications of this work on the extended storage of materials are discussed. The rate of recombination serves to limit the potential pressure in the container from water radiolysis. With regard to hydrogen-oxygen recombination, radiolysis of water, or the reaction of plutonium oxide with water, an equilibrium state is indicated. Therefore, the pressure reaches a steady-state value, which may be calculated from the properties of the materials involved and the pertinent chemical reactions. In order to carry out such calculations, both aspects, kinetics and thermodynamics, are required to properly address the long-term storage issues.

### Reference

1. "Assessment of Plutonium Storage Safety Issues at Department of Energy Facilities," US DOE Report DOE/DP/0123T, US Department of Energy, Washington, D.C., 1994.

## Kinetics of the Reaction between Plutonium Dioxide and Water from 25°C to 350°C: Formation and Properties of the Phase PuO<sub>2+x</sub>

**L. Morales,**

**T. Allen**

*Los Alamos National  
Laboratory, Los  
Alamos, NM 87545  
USA*

**J. Haschke**

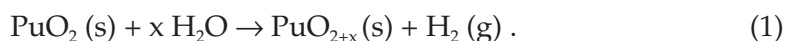
*Actinide Consulting  
Waco, TX 76712, USA*

In the areas of plutonium waste disposition and storage, and medium to long-term retrievable Pu materials storage, the issue of water and other small molecule interactions with pure or impure Pu oxide materials and metal has become a major concern. Small molecule reactions in these types of systems has led to changes in materials stoichiometry, containment breaches and dispersal of material resulting from pressurization, corrosion of the containment, and the collapse of sealed containers due to the formation of partial vacuum. The exact nature of these reactions and the resulting implications for medium to long-term storage are not well understood, although there have been studies which attempted to explain them from a large body of observations and experiments [1-3].

The interaction of PuO<sub>2</sub> with water was investigated from 100°C to 350°C using a suite of experimental techniques which include microbalance and pressure-volume-temperature (PVT) methods, thermal gravimetric analysis (TGA), mass spectrometry (MS), x-ray and neutron diffraction. Reaction rates and oxide compositions were determined from measured increases in sample mass or pressure over time (t). Gaseous and solid products were analyzed using MS and diffraction methods, respectively. Oxide products have also been characterized by x-ray photoelectron spectroscopy (XPS). The plutonium oxide specimens used in this study were formed by oxidation of electrorefined alpha-phase metal containing approximately 100 ppm Am as the major metallic impurity. The specific surface area of the oxide was 4.8 m<sup>2</sup>/g. The initial oxide stoichiometry was determined to be PuO<sub>1.97</sub> based on the measured lattice parameter and data from the correlation of the cubic lattice parameter (a<sub>o</sub>) at fixed O:Pu ratios with temperature reported by Gardner et al. [4].

PVT and microbalance measurements were made at 200°C to 350°C using techniques similar to those described for kinetic measurements at 25°C [5]. Accurately weighed samples (0.05-0.1 g) of oxide contained in Pt or Au crucibles were placed in volume-calibrated (36 cm<sup>3</sup>) gold coated, stainless steel reactors sealed with nickel-gasket closures. After evacuation, a reactor was filled with H<sub>2</sub>O vapor (24 Torr) supplied by a water reservoir held at constant temperature throughout the test. The sample temperature was measured by a thermocouple located near the specimen and was maintained at the desired constant value using a programmable controller. The system pressure was measured as a function of time using a capacitance manometer and was recorded using digital methods. After completion of the P-t measurements, samples of the gas and solid phase were obtained for MS and for XRD (or XPS analyses), respectively.

Results of PVT and microbalance measurements during exposure of plutonium dioxide to water vapor at 200°C to 350°C and 24 Torr show linear increases in pressure and mass as a function of time. Mass spectrometric analysis of gas samples taken after termination of the tests show that only H<sub>2</sub>O and H<sub>2</sub> were present in the gas phase. These results are identical to those observed at 25°C [5] and suggest the following reaction:



This equation implies that a fraction of the plutonium is oxidized to an oxidation state greater than Pu(IV); although difficult to unambiguously prove in an ex-situ setting, this result is consistent with earlier XPS data [2]. The kinetic results from the microbalance and PVT measurements are described by a single relationship:

$$\ln R = -6.441 - (4706/T) . \quad (2)$$

The activation energy for reaction is  $9.4 \pm 0.6$  kcal/mol. The uncertainty in  $E_a$  results primarily from the uncertainty in the average  $R$  at  $25^\circ\text{C}$  [5]. Rates from microbalance measurements are in good agreement with those from PVT data, but are consistently higher because of water adsorption on the microbalance and the sample.

X-ray diffraction data show that the oxide product formed during reaction (1) has a fluorite-related fcc structure derived from that of the dioxide. The results of eight measurements with calculated O:Pu ratios from 2.016 to 2.169 show that the lattice parameter of  $\text{PuO}_{2+x}$  is a linear function of composition:

$$a_o \text{ (Å)} = 5.3643 + 0.01764 \text{ O:Pu} . \quad (3)$$

When the  $\text{PuO}_{2+x}$  oxide product was heated above  $400^\circ\text{C}$  in subsequent TGA experiments, a mass loss was observed at approximately  $360^\circ\text{C}$  and the lattice constant of the resulting oxide returns to that of  $\text{PuO}_2$ , indicating that  $\text{PuO}_{2+x}$  is stable only up to  $360^\circ\text{C}$ . The O:Pu ratio calculated from the measured mass loss in the TGA experiments and the hydrogen generation from the PVT experiments are in excellent agreement.

Kinetic results for oxidation of plutonium dioxide by water shows that the reaction has a normal temperature dependence over the  $25^\circ\text{C}$  to  $350^\circ\text{C}$  range. The temperature dependence observed for the rate demonstrates that the reaction of  $\text{PuO}_2$  with  $\text{H}_2\text{O}$  is primarily chemical instead of radiolytic. The rate of a purely radiolytic process is expected to be temperature independent at a fixed water pressure. At isobaric conditions, the measured activation energy of a radiolytic process might actually be slightly positive because the rate is expected to decrease as the equilibrium surface concentration of  $\text{H}_2\text{O}$  adsorbed on the oxide decreases with increasing temperature. If formation of  $\text{PuO}_{2+x}$  is promoted by radiolysis of  $\text{H}_2\text{O}$ , the largest fractional contribution to the oxidation rate is anticipated at low temperature in a system with a high surface concentration of water.

The Vegard's law behavior shown by Equation 3 assists in defining important solid-state properties of  $\text{PuO}_{2+x}$ . The continuous variation of  $a_o$  with composition indicates that  $\text{PuO}_{2+x}$  is a solid-solution. Neutron diffraction studies indicate that additional oxygen is accommodated on interstitial sites in the fluorite lattice of  $\text{PuO}_2$ . Whereas oxidation of Pu(IV) on cationic sites of dioxide would tend to shrink the lattice, accommodation of oxide ions on vacant sites causes lattice expansion. The opposing changes are apparently of comparable magnitude, and the net effect is a low dependence of  $a_o$  on the composition of  $\text{PuO}_{2+x}$ .

## References

1. "Reactions of Plutonium and Uranium with Water: Kinetics and Potential Hazards," J. Haschke, LA-13069-MS, December 1995.
2. "Characterization of the plutonium-water reaction II: Formation of a binary oxide containing Pu(VI)" J. L. Stakebake, D. T. Larson, and J. Haschke, *J. Alloys and Compounds*, 202, 1993, 251.
3. "Plutonium Dioxide Storage: Conditions for Preparation and Handling", J. M. Haschke, and T. E. Ricketts, LA-12999-MS, 1995.
4. E. R. Gardner, T. L. Markin, and R. S. Street, *J. Inorg. Nucl. Chem.*, **27**, (1965), 541.
5. "Interactions of Plutonium Dioxide and Water and Oxygen-Hydrogen Mixtures," J. M. Haschke and T. H. Allen, LA-13537-MS, January 1999.

## A Conceptual and Calculational Model for Gas Formation from Impure Calcined Plutonium Oxides

Safe transport and storage of pure and impure plutonium oxides requires an understanding of processes that may generate or consume gases in a confined storage vessel. We have formulated conceptual and calculational models for gas formation from calcined materials. The conceptual model for impure calcined plutonium oxides is based on the data collected to date,<sup>1</sup> the anticipated post-calcination behavior of plutonium oxide and of the dominant impurities. By its very nature, a conceptual model does not solve all technical aspects of an issue. Instead, a conceptual model provides an intellectual framework for evaluating a broad range of data and for posing relevant hypotheses that can be tested through additional work. The conceptual model is thereby improved as additional data is acquired. The conceptual model assumes that plutonium in calcined impure oxides exists predominantly as plutonium dioxide. Dominant impurity phases are assumed to be chloride salts, binary and complex oxides of transition metals, and alkaline earth oxides.

The dominant issue from gas evolution is the increase of pressure that could burst or damage the container. The pressure increase could result from the following three sources:

1. Thermal Heating. Internal heating of container fill gas from radioactive decay of the plutonium oxide material and the external ambient environment will increase pressure in storage containers. Thermal modeling has been performed for packages containing oxide generating nineteen watts under various conditions.<sup>3,4</sup> For a bounding shipping scenario with direct solar exposure of the shipping packages, Hensel reports an average gas temperature of about 211°C, which increases the gas pressure increases to 23 psia. This would occur within days or weeks.
2. Helium from Radioactive Decay. Helium is produced by alpha radioactive decay. Appendix B of the proposed standard<sup>5</sup> contains a calculation of the amount of helium produced from 12.4 watts (typical of five kilograms of pure weapons-grade plutonium oxide) during storage. In a typical package configuration with an average gas temperature of 204°C, the theoretical helium pressure was calculated to be about 13 psia after fifty years. The actual helium gas pressure will be less than that due to trapping in the solid matrices.
3. Radiolytic and Chemical Degradation. Both the current and proposed standards specify calcination at 950°C to minimize or eliminate potential gas-generating constituents such as organic compounds, adsorbed moisture and hydroxides, halides, and oxyanions such as nitrate, sulfate and carbonate. Both standards also specify storage in leak-tested gas-tight steel containers to eliminate the possibility of adsorption of gas-generating constituents during storage. Moisture re-adsorption between calcination and storage is required to be less than 0.5 wt. %. Calcining also reduces the material surface area to about 5 m<sup>2</sup>/g of material, which influences surface reactions. A recent peer-reviewed report<sup>2</sup> summarizing plutonium storage package failures supports the adequacy of the standards' calcination conditions. It states that no gas

John L. Lyman,  
P. Gary Eller  
Los Alamos National  
Laboratory, Los  
Alamos, NM 87545,  
USA

pressurization failures have been documented for reasonably stabilized and packaged oxide materials.

The calculational model follows from the calculational model and is based on gas evolution by both radiolytic and chemical processes. It reflects the physical characteristics of the 3013 transport container and its contents. It solves a set of ordinary differential equations to give the temporal dependence of the concentration of different gaseous species, surface species, condensed species, and molecular layers of water and plutonium oxide for a given set of initial conditions. It uses measured (and estimated) rates of the radiolytic and chemical processes and is written in visual basic for a PC.

Some of the chemical and radiolytic processes are radiolytic generation of helium, surface adsorption of water, desorption of water, formation of the plutonium hydroxide, radiolysis of adsorbed water to H<sub>2</sub> and other species, radiolytic recombination of H<sub>2</sub> and O<sub>2</sub> to water, catalytic recombination of H<sub>2</sub> and O<sub>2</sub> to water, oxidation of PuO<sub>2</sub> to PuO<sub>2+x</sub>, and reduction of PuO<sub>2+x</sub> to PuO<sub>2</sub>. The rate of a reverse reaction is taken from the rate of the forward reaction and the equilibrium constant. The adsorption and desorption of water is an example. The plutonium hydroxide formation rate and equilibrium constant is based on the work of Stakebake,<sup>6</sup> as modified by Paffett.<sup>7</sup> The rate of adsorbed water radiolysis was taken from the G factor suggested by Hyder.<sup>8</sup> The catalytic and radiolytic recombination rates published sources. The controversial PuO<sub>2+x</sub> production is from the recent *Science* article,<sup>9</sup> and its equilibrium properties were estimated by comparison with lower plutonium oxides and the oxides of uranium and neptunium. Reactions of the three types of impurity phases are treated similarly to the reactions of water on plutonium oxide. The alkaline chlorides may adsorb some water. Radiolysis to gaseous chlorides may also occur. The transition metal oxides also have the potential to undergo oxidation/reduction reactions. Some of the alkaline earth oxides adsorb considerably more water than plutonium oxide. The information necessary to model reactions involving these impurities is taken from available published thermodynamic and kinetic data.

The paper reports the model concepts and conclusions from its use.

## References

1. P. Gary Eller, Richard E. Mason, David R. Horrell, Steven D. McKee, Nora A. Rink and Craig S. Leasure, "Gas pressurization from calcined plutonium oxides," Los Alamos National Laboratory report LA-UR-99-3804, 1999.
2. P. G. Eller, R. W. Szempruch, and J. W. McClard, "Summary of Plutonium Oxide and Metal Storage Package Failures," Los Alamos National Laboratory report LA-UR-99-2896, July 1999.
3. S. J. Hensel, "Thermal Analyses of the 9975 Package with the 3013 Configuration during Normal Conditions of Transport," Westinghouse Savannah River Company report WSRC-TR-98-00420, February 1999.
4. S. J. Hensel, "Thermal Analyses of the 9975 as a Plutonium Storage Container," Westinghouse Savannah River Company report WSRC-TR-98-00203, February 1999.
5. U. S. Department of Energy, "Stabilization and Storage of Plutonium-Containing Materials," U. S. DOE proposed standard DOE-STD-3013-99, September, 1999.

6. J. L. Stakebake, *J. Phys. Chem.* (1973) **77**, 581.
7. Mark Paffett, private communication, Aug. 17, 1999.
8. M. L. Hyder, "Calculations in Support of Plutonium Oxide Storage," unpublished memo, 11/8/98, to R. A. Penneman.
9. J. M. Haschke, T. H. Allen, and L. A. Morales, *Science* **287**, 285 (1000).

## Status of the Pit Disassembly and Conversion Facility

**Warren T. Wood,**  
**Lowell T. Christensen**  
*Los Alamos National  
Laboratory, Los  
Alamos, NM 87545,  
USA*

A planned new facility, the Pit Disassembly and Conversion Facility (PDCF), will be used to disassemble the nation's inventory of surplus nuclear weapons pits and convert the plutonium from those pits into a form suitable for storage, international inspection, and final disposition. Sized to handle 35 metric tons of plutonium from pits and other sources over its 10-year operating life, the PDCF will apply the Advanced Recovery and Integrated Extraction System (ARIES) technology. ARIES process technology has been developed at Los Alamos National Laboratory (LANL) and Lawrence Livermore National Laboratory (LLNL), and an integrated system is being demonstrated at LANL. The Los Alamos National Laboratory is the lead for technical design oversight of the PDCF. Technical data gained from the ARIES demonstrations is integral for the proper design of the PDCF.

A hardened structure, the PDCF will be capable of receiving pits and plutonium metal and producing an oxide product suitable for disposition. The PDCF includes support functions needed to handle all the parts and waste generated from pit disassembly. A design-only conceptual design report, which estimated the size, cost, and staffing for the facility, was prepared by LANL to support the funding request by the Department of Energy (DOE) Office of Fissile Materials Disposition (OFMD). Four sites were originally considered for locating the PDCF: Pantex Plant, Savannah River Site (SRS), Idaho National Engineering and Environmental (INEEL), and the Hanford Site. The Savannah River Site was selected late last year by the DOE. Raytheon Engineers and Constructors was selected as the Architect Engineering (A/E) firm last year and will finish 30% Title I design in early 2000. The schedule for construction of the PDCF is aggressive with normal operations commencing by 2006.

## Plutonium Packaging and Long-Term Storage

It has been demonstrated that the Advanced Recovery and Integrated Extraction System (ARIES) packaging line at Los Alamos National Laboratory can successfully package plutonium to meet DOE requirements for safe long-term storage. The ARIES system has just completed the disassembly and conversion of its first cores (“pits”) for nuclear weapons.

In this demonstration, the plutonium is separated from other pit components and reduced to an unclassified and stable form suitable for long-term storage. Because the operation occurs within the confines of a contaminated glovebox environment the container’s surface becomes radiologically contaminated. The DOE-STD-3013-96 “Criteria for Preparing and Packaging Plutonium Metals and Oxides for Long-Term Storage,” requires the surfaces of the inner container meet the contamination limits specified in 10-CFR-835 Appendix D. This regulation pertains to the respiratory exposure protection of workers to airborne contamination, the limits are set at 20 dpm/100 cm<sup>2</sup> for removable contamination and 500 dpm/100cm<sup>2</sup> of fixed contamination. This operation has been well tested in a full production operation.

The Decontamination of the inner container employed an electrolytic technique. This cleaning process uses an aqueous solution that generates remarkably little solid or liquid waste. Once the inner container is processed through the decontamination system, it is removed from the glovebox line and packaged to a secondary “boundary” container. This final package is then assayed to verify content and placed under surveillance to monitor changes in head-space pressure or weight.



**Jane A. Lloyd,  
Douglas E. Wedman**  
*Los Alamos National  
Laboratory, Los  
Alamos, NM 87545,  
USA*

**The first DOE-STD-3013-99 inner container of plutonium oxide processed through the ARIES packaging line at Los Alamos National Laboratory.**

## Phase Composition of Murataite Ceramics for Excess Weapons Plutonium Immobilization

**I. A. Sobolev,**  
**S. V. Stefanovsky**  
*SIA Radon, Moscow*  
 119121 Russia

**B. F. Myasoedov,**  
**Y. M. Kuliako**  
*Institute of*  
*Geochemistry*

**S. V. Yudinsev**  
*Institute of Geology of*  
*Ore Deposits*

Among the host phases for actinides immobilization, murataite (cubic, space group  $Fm\bar{3}m$ ) with the general formula  $A_4B_2C_7O_{22-x}$  ( $A=Ca, Mn, Na, Ln, An$ ;  $B=Mn, Ti, Zr, An^{IV}$ ;  $C=Ti, Al, Fe$ ;  $0 < x < 1.5$ ) is a promising matrix due to high isomorphous capacity and low leaching of actinides. One feature of murataite actinide zoning is an order-of-magnitude difference in concentration between the core and the rim.[1,2] Investigation of murataite ceramics in detail has shown occurrence of several murataite varieties with three-, five-, and eight-fold fluorite unit cells.[1-3] The goal of the present step of work is to study an effect of waste elements on phase composition of murataite ceramic and isomorphous capacity of waste elements.

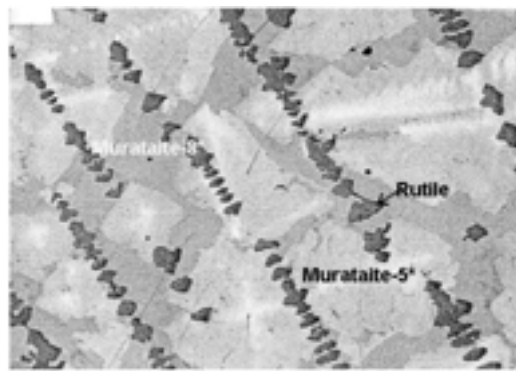
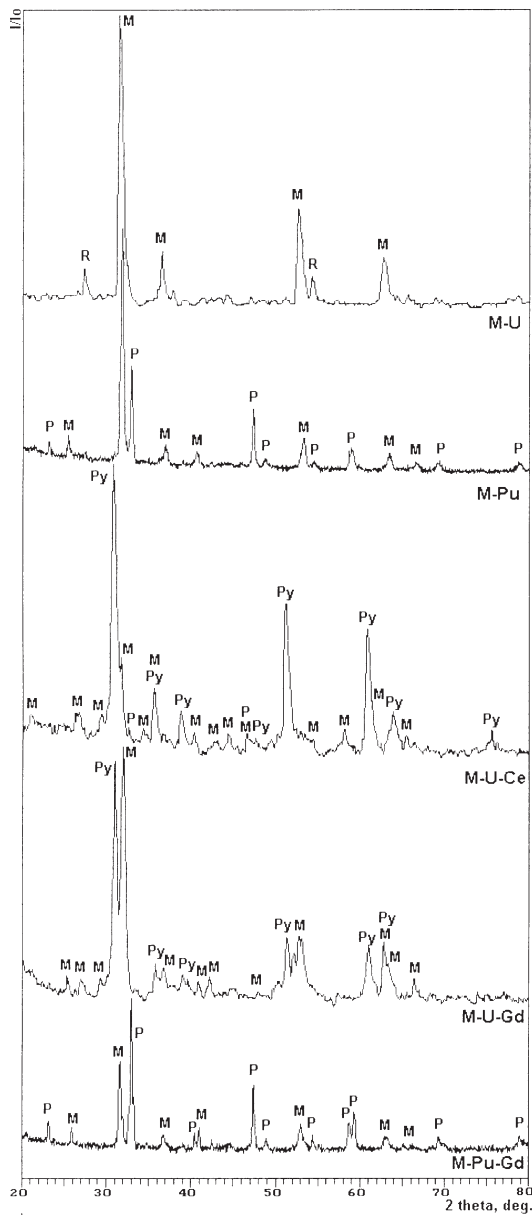
Pu-free samples (Table I) were prepared by melting of oxide mixtures in platinum crucibles at 1450°C–1500°C followed by controlled cooling to crystallize melts. Pu-doped ceramics were fabricated at the same temperatures in graphite dies. The samples were examined with X-ray diffraction (XRD), scanning and transmission electron microscopy with energy dispersive system (SEM/EDS and TEM).

**Table I. Nominal Chemical Compositions of the Samples (in wt. %).**

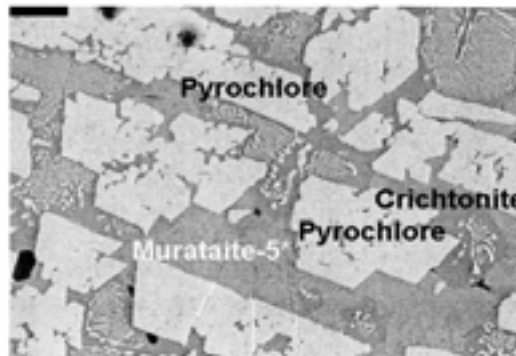
Samples	Al <sub>2</sub> O <sub>3</sub>	CaO	TiO <sub>2</sub>	MnO	Fe <sub>2</sub> O <sub>3</sub>	ZrO <sub>2</sub>	UO <sub>2</sub>	PuO <sub>2</sub>	CeO <sub>2</sub>	Gd <sub>2</sub> O <sub>3</sub>
M-U	5	10	55	10	5	5	10	-	-	-
M-Pu	5	10	55	10	5	5	-	10	-	-
M-U-Ce	4	8	44	8	4	4	8	-	20	-
M-U-Gd	4	8	44	8	4	4	8	-	-	20
M-Pu-Gd	4	8	44	8	4	24	-	8	-	20

The sample with baseline composition (M-U) is composed of major murataite (>90 vol.% of total) and minor rutile (Figure 1,2). As follows from TEM data, two murataite varieties with five- (murataite-5<sup>x</sup>) and eight-fold (murataite-8<sup>x</sup>) fluorite cells are present. Murataite-5<sup>x</sup> has zoned structure (Figure 2) with formulae  $Ca_{2.25}U_{0.39}Zr_{0.58}Mn_{1.36}Ti_{6.82}Fe_{0.64}Al_{0.96}O_{21.59}$  (bulk) and  $Ca_{2.70}U_{0.51}Zr_{0.90}Mn_{1.16}Ti_{6.69}Fe_{0.51}Al_{0.51}O_{21.59}$  (core). Core (light-coloured on SEM-image) is enriched with Ca, U, Zr and depleted with Mn, Ti, Fe, and Al as compared to bulk and rim. Maximum uranium content in the core of murataite with five-fold fluorite cell reaches 0.51 formula units (f.u.) or 14 wt. % UO<sub>2</sub>. Composition of murataite-8<sup>x</sup> ( $Ca_{2.02}U_{0.26}Zr_{0.26}Mn_{1.62}Ti_{6.70}Fe_{0.84}Al_{1.30}O_{21.29}$ ) is more uniform over the bulk of the grains. Representative rutile composition is  $Ti_{0.93}Zr_{0.03}U_{0.01}Mn_{0.01}Al_{0.01}Fe_{0.01}O_{2.00}$ . Relative content of the phases (in vol.%) may be estimated as 60%–70 % murataite-5<sup>x</sup>, 20%–30% murataite-8<sup>x</sup>, and ~10% rutile. Pu substitution for U yields product with murataite as the major phase (Figure 1) but also significant perovskite content (~25%–0% of total). No rutile has been found from the XRD data. SEM study of the Pu-doped samples is under performance now.

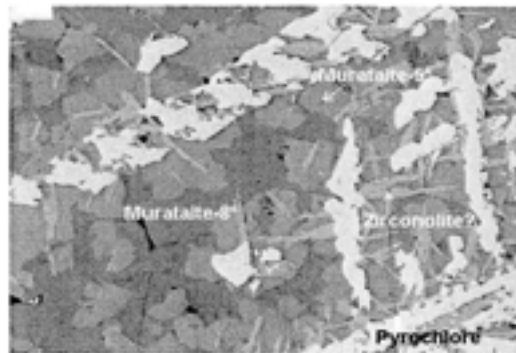
Incorporation of Ce in the amount of 20 wt. % (sample M-U-Ce) resulted in formation of pyrochlore (60–70 vol. %) - murataite (20–30 vol. %) - minor crichtonite (~10%) assemblage. Representative compositions of pyrochlore, murataite, and crichtonite are  $Ca_{0.64}Mn_{0.28}Ce^{III}_{0.04}Ce^{IV}_{0.64}Zr_{0.16}U_{0.16}Ti_{1.96}Fe_{0.04}Al_{0.08}O_{7.00}$ ,  $Ca_{1.56}Ce^{IV}_{0.78}Zr_{0.13}U_{0.13}Mn_{1.56}Ti_{6.37}Fe_{0.91}Al_{1.56}O_{21.65}$ , and  $Ca_{0.79}Ce^{IV}_{0.81}Zr_{0.36}Mn_{2.00}Ti_{12.16}Fe_{1.95}Al_{3.92}O_{38.00}$ , respectively.



M-U



M-U-Ce



M-U-Gd

Figure 1. XRD patterns of the samples.

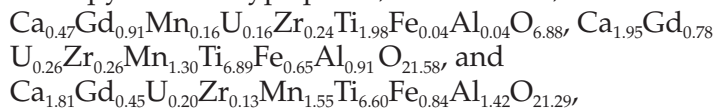
M – murataite,  
P – perovskite,  
Py – pyrochlore,  
R – rutile

Figure 2. SEM images of the ceramics.

Scale markers – 50 μm.

In samples the M-U murataite compound is abundant in the uranium-bearing phase. Unlike M-U the M-U-Ce pyrochlore-structured phase concentrates uranium along with murataite, whereas crichtonite contains only traces of uranium (~1.1 wt. % UO<sub>2</sub>).

Replacement of Ce by Gd (Sample M-U-Gd) affects phase composition of the ceramic. The bulk of the sample is composed of pyrochlore-murataite assemblage but with different ratios of the phases (approximately 1:1). Representative formulae of pyrochlore-type phase, murataite-5<sup>x</sup>, and murataite-8<sup>x</sup> are



respectively. Moreover, one more minor phase, whose composition may be recalculated to zirconolite formula:  $\text{Ca}_{0.40}\text{Mn}_{0.16}\text{Gd}_{0.52}\text{Zr}_{0.32}\text{U}_{0.04}\text{Ti}_{2.13}\text{Fe}_{0.16}\text{Al}_{0.24}\text{O}_{7.00}$ , has been found (Figure 2). Major diffraction peaks of this phase are overlapped with pyrochlore reflections, and it can be seen on SEM images only as light-gray elongated grains being lighter than murataite-5<sup>x</sup> but darker than pyrochlore (Figure 2). Approximate amount of the phases may be estimated as ~50% pyrochlore + 10% zirconolite and 20%–30% each of murataite-5<sup>x</sup> and murataite-8<sup>x</sup>. Presence of all of these phases has been also confirmed by TEM data.

Incorporation of Pu instead of U (Sample M-Pu-Gd) affects significantly the phase composition of the ceramic. Pyrochlore- and zirconolite-type phases disappear, and the perovskite-type phase becomes predominant (Figure 1). This sample consists of about 60%–65% perovskite-type phase and 35%–40% murataite varieties.

So, a specific feature of Pu-containing murataite ceramics is the appearance of a perovskite-type phase. Formation of this phase is connected with occurrence of Pu(III). Positions of major diffraction peaks of perovskite phase (2.714–2.718, 1.918–1.922, 3.842–3.850) somewhat differ from those for nominal  $\text{CaTiO}_3$  (2.701, 1.911, 3.824 – JCPDS 22-153). It is seen from comparison of XRD patterns of samples M-Pu and M-Pu-Gd that a fraction of the perovskite phase grows in the presence of  $\text{Gd}_2\text{O}_3$  (Figure 1), and positions of major diffraction peaks are shifted to lower angles. This demonstrates an important role of Gd in the perovskite phase formation. In the Gd-free sample, M-Pu the generalized perovskite formula is approximately  $(\text{Ca},\text{Pu}^{3+})(\text{Ti}^{4+},\text{Ti}^{3+})\text{O}_3$ , whereas in the Gd-containing sample, the chemical composition of the perovskite phase is more complex (solid solution  $\text{CaTiO}_3$ - $\text{PuTiO}_3$ - $\text{GdTiO}_3$ - $\text{GdAlO}_3$ ) and may be represented as  $(\text{Ca},\text{Gd},\text{Pu}^{3+})(\text{Ti}^{4+},\text{Ti}^{3+},\text{Al})\text{O}_3$ .

### Acknowledgments

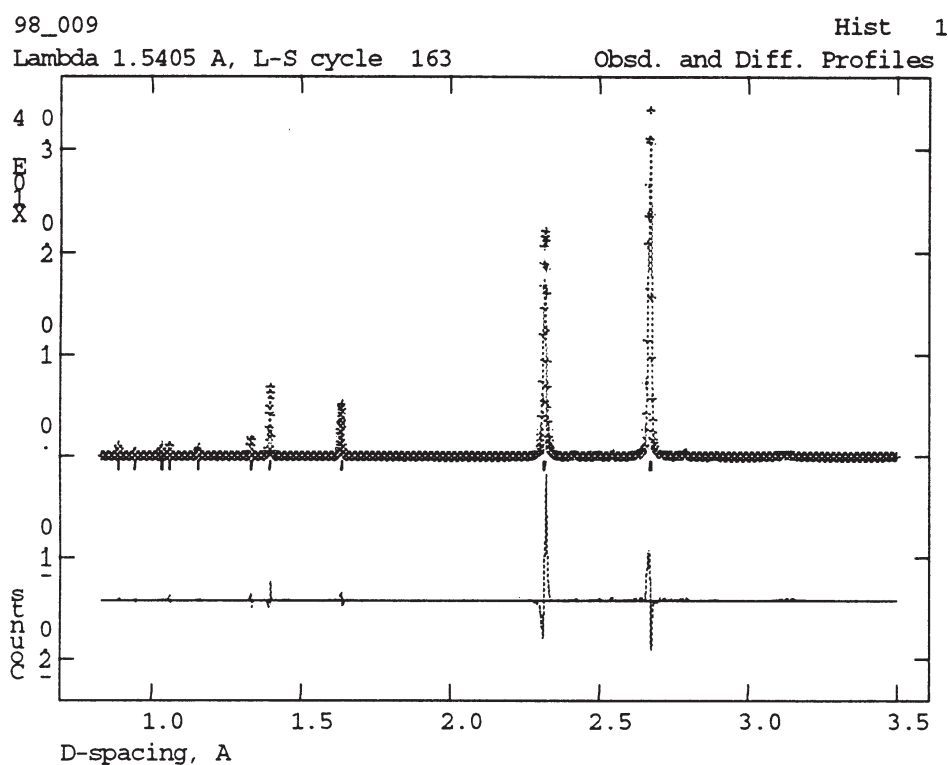
The authors gratefully acknowledge the help of A. G. Ptashkin (SIA Radon), M. I. Lapina, A. V. Sivtsov and B. S. Nikonov (IGEM RAS) in synthesis and SEM/TEM study of the Pu-free samples.

### References

1. A. Sobolev, S. V. Stefanovsky, S. V. Ioudintsev, B. S. Nikonov, B.I. Omelianenko, A. V. Mokhov, *Mat. Res. Soc. Symp. Proc.* **465** (1997) 363.
2. N. P. Laverov, S. V. Yudintsev, B. I. Omelianenko, B. S. Nikonov, S. V. Stefanovsky, *Geol. Ore Deposits* **41** (1999) 99.
3. S. V. Stefanovsky, S. V. Yudintsev, B. S. Nikonov, B. I. Omelianenko, A. G. Ptashkin, *Mat. Res. Soc. Symp. Proc.* **556** (1999) 121.

## Analysis of Strain Anisotropy in Delta Stabilized Pu-Ga Alloys

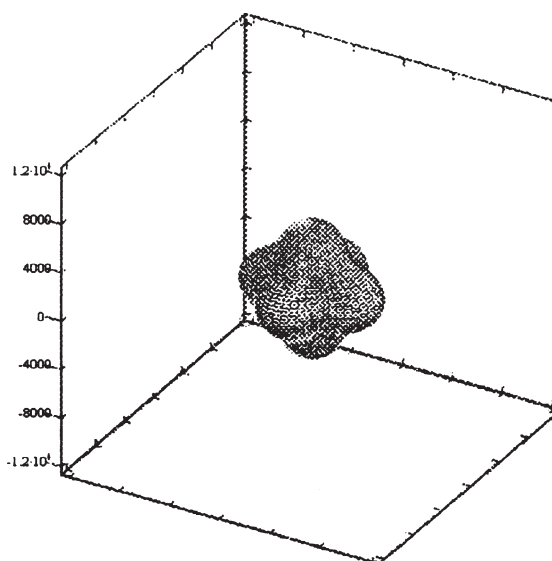
Optimal extraction of information from powder diffraction patterns requires an accurate description of the diffraction line shape. Most refinement techniques, such as Rietveld, treat the diffraction line width as a smooth function of d-spacing or diffraction angle. Anisotropic line-shape broadening, in which the peak width is not a smooth function of d spacing, is sometimes observed in powder patterns and has been difficult to model with whole pattern fitting or Rietveld techniques. Recently this technical problem has been overcome by incorporating the anisotropic broadening model of Stephens into the GSAS Rietveld refinement package.<sup>1,2</sup> If the influence of stacking faults can be neglected, the broadening of the diffraction line shape can be attributed mainly to the strain fields surrounding dislocations and the domain size or ordering length. In particular, this dislocation model of the mean square strain, which is related to the peak width, employs a knowledge of the individual contrast factors,  $C$ , of dislocations related to particular Burgers vectors as well as to the elastic constants of the material of interest.<sup>3,4</sup> Such an approach has been applied to the understanding of the anisotropic line broadening now identified in various delta stabilized Pu-Ga alloys. As an example, Figure 1 shows the diffraction pattern of a typical Pu-Ga alloy in which the peak widths (microstrain) and their dependence on the d spacings were obtained from a Rietveld analysis. Figure 2 provides the variance of the microstrain as a function of the crystallographic directions. The microstrain broadening is assumed to be a measure of dislocations induced by processing and aging. We will discuss our measurements of domain size and approximate dislocation density for various Pu-Ga samples.



Luis Morales,  
Andrew Lawson,  
John Kennison  
Los Alamos National  
Laboratory, Los  
Alamos, NM 87545  
USA

Figure 1. Diffraction pattern of a Pu-Ga alloy. The +s are the observations, the line through the +s is a Rietveld fit, and the lower curve is the difference between the observations and the fit.

Figure 2. The variance of the microstrain plotted as a function of the xyz crystallographic directions. This is obtained by measuring the d- and hkl-dependence of the peak width and correcting for the domain size broadening.



### References

1. Stephens, P. W., 1999, *J. Appl. Cryst.* **32** 281.
2. Larson, A. C., and Von Dreele, R. B., 1986, Los Alamos National Laboratory Report LA-U- 86-748, Los Alamos, NM.
3. Ungár, T., Leoni, M. and Scardi, P., 1999, *J. Appl. Cryst.* **32** 290.
4. Ungár, T., and Tichy, G., 1999, *Phys. Stat. Sol. (a)* **171** 425.

## Preparation of Actinide Boride Materials via Solid-State Metathesis Reactions and Actinide Dicarbollide Precursors

Information gaps exist in the knowledge base needed for choosing among the alternate processes to be used in the safe conversion of fissile materials to optimal forms for safe interim storage, long-term storage, and ultimate disposition. The current baseline storage technology for various wastes uses borosilicate glasses.<sup>1</sup> While this waste form has many desirable characteristics such as chemical inertness and stability to radiolytic decay, borosilicate glasses can crystallize and crack, can accommodate only low actinide loadings (<25% by weight),<sup>2</sup> and require temperatures in excess of 1200°C for the vitrification process. This work focuses on metal borides as alternative actinide storage forms since these would have many of the desirable characteristics of borosilicate glasses but are capable of encapsulating greater quantities of plutonium. The area of actinide borides has been underdeveloped, no doubt in part due to the high temperatures (>1500°C) required to produce these materials. The focus of this paper is the synthesis of actinide-containing ceramic materials at low and moderate temperatures (200°C–1000°C) using molecular and polymeric actinide borane and carborane complexes.

The sum total of known binary plutonium-boride phases includes PuB, PuB<sub>2</sub>, PuB<sub>4</sub>, PuB<sub>6</sub>, PuB<sub>12</sub>, and PuB<sub>100</sub> (Table 1). These materials are known to be refractory, but other properties such as chemical behavior or inertness have not been evaluated. Similarly, in the thorium and uranium systems only ThB<sub>4</sub>, ThB<sub>6</sub>, ThB<sub>66</sub> and UB<sub>12</sub>, UB<sub>2</sub>, UB<sub>4</sub>, UB<sub>12</sub> have been identified with no information reported on their chemical properties.<sup>3</sup> In contrast, many transition metal and lanthanide borides, such as ZrB<sub>2</sub> and LaB<sub>6</sub>, have been extensively studied.<sup>4</sup> These borides have been used as refractory materials and corrosion resistant coatings. It is therefore expected that some actinide-boride phases will also be corrosion resistant. To date actinide borides have been made exclusively by high temperature methods.

	Th	U	Pu
<b>MB</b>			X
<b>MB<sub>2</sub></b>		X	X
<b>MB<sub>4</sub></b>	X	X	X
<b>MB<sub>6</sub></b>	X		X
<b>MB<sub>12</sub></b>		X	X
<b>MB<sub>66</sub></b>	X		X
<b>MB<sub>100</sub></b>			X

During the past two decades significant advances have been made in the low-temperature synthesis of highly refractory materials.<sup>5,6</sup> New methods, such as low-temperature molten salts, chemical vapor deposition, sol-gel and hydrothermal synthesis, self-propagating high-temperature synthesis (SHS), solid-state metathesis reactions (SSM), molecular precursors, and preceramic polymers virtually eliminate the problems associated with solid-state diffusion by mixing the constituents of the ceramic at a molecular level. In some cases, structural elements of the precursor such as chemical bonds and coordination environment

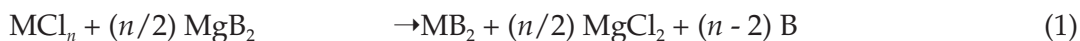
Anthony J. Lupinetti,  
Julie Fife,  
Eduardo Garcia,  
Kent D. Abney  
Los Alamos National  
Laboratory Los  
Alamos, NM 87545,  
USA

Table 1. Known Actinide Boride Phases of Thorium, Uranium, and Plutonium.

are preserved in the final ceramic. The key is identification of suitable precursors leading to ceramic materials having the physical properties to produce the desired form.

Polyhedral boranes and carboranes are ideally suited for the formation of actinide-containing ceramics due to the high degree of crosslinking reaction between the polyhedra at moderate temperatures.<sup>7</sup> Sneddon has shown that pentaborane ( $B_5H_9$ ) can be polymerized with acetylene to form a boron-containing polymeric ceramic precursor.<sup>8</sup> This material is cross-linked via the pentaborane pendent by heating to 140°C to form B-B linkages. Thermal data show that a pyrolytic exotherm of this material occurs rapidly between 200°C and 350°C to form black, lustrous, amorphous boron carbide. Once formed, it may be converted to crystalline boron carbide by heating to 1450°C. Cerium and gadolinium borides have likewise been made by pyrolysis of  $M_2(B_{10}H_{10})_3$  complexes. The onset of boron-boron bond formation occurs at approximately 200°C and is complete by 400°C.<sup>9</sup> Although transition-metal carborane complexes have been extensively explored, few analogous actinide complexes have been isolated. We recently reported an efficient synthetic route to uranium- and thorium-containing dicarbollide complexes with the first reports on their stability and reactivity. Incorporation of these complexes into polymers and subsequent pyrolysis should lead to dense, critical safe, actinide-bearing ceramics with high boron content at low temperatures.

Initial work has focused on the solid-state metathesis reactions of actinide halides with alkali-earth borides ( $MgB_2$  and  $CaB_6$ ) and *closo*-boranes ( $K_2B_{10}H_{10}$  and  $K_2B_{12}H_{12}$ ). The proposed reaction of the actinide halides and  $MgB_2$  is shown in Scheme 1.<sup>10</sup> Typical reactions were carried out in evacuated, sealed quartz tubes at 850°C for 24 hours.



(M = Th,  $n = 4$ ; U,  $n = 3, 4$ ; Pu,  $n = 3$ )

Preliminary results of the pyrolysis of newly synthesized actinide dicarbollide complexes will also be discussed.

## References

1. Jacquet-Francillon, N.; Bonniaud, R.; Sombret, C.; *Akademisch Verlagsgesellschaft, Wiesbaden* **1978**, 231.
2. "The RENUW Dry Halide Process for Nuclear Fuel Reprocessing, Phase I Final Report," AC-WC31-31; August 14, **1991**.
3. Katz, J. J.; Seaborg, G. T.; Morss, L. R. *The Chemistry of the Actinide Elements*; Chapman and Hall: New York, NY, 1986, pp. 56, 280, 317 for Th, U, and Pu respectively.
4. Su, K.; Sneddon, L. G. *Chem. Mater.* **1993**, *5*, 1659.
5. Wynne, K. J.; Rice, R. W. *Ann. Rev. Mater. Sci.* **1984**, *14*, 297-334.
6. Rice, R. W. *Am. Ceram. Soc. Bull.* **1983**, *62*, 889-892.
7. Onak, T.; Dunks, G. B.; Searcy, I. W.; Spielman, J. *Inorg. Chem.* **1967**, *6*, 1465-1471.

8. Mirabelli, M. G. L.; Sneddon, L. G. *J. Am. Chem. Soc.* **1988**, *110*, 3305-3307.
9. Itoh, H.; Tsuzuki, Y.; Yogo, T.; Naka, S. *Mat. Res. Bull.* **1987**, *22*, 1259-1266.
10. Rao, L.; Gillian, E. G.; Kaner, R. B. *J. Mater. Res.* **1995**, *10*, 353-361.

## The Self-Irradiation Driven Enhancement of Diffusion Processes in Nuclear-Safe Ceramics

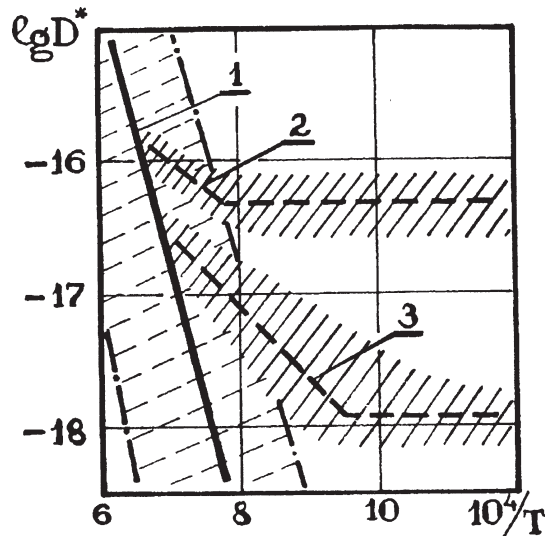
**E. A. Smirnov**  
Moscow State  
Engineering Physics  
Institute (Technical  
University), Moscow  
115409, Russia

**L. F. Timofeeva**  
All-Russia Scientific  
Research A. A.  
Bochvar Institute of  
Inorganic Materials,  
Moscow 123060,  
Russia

The problem of long-term storage of nuclear-safe ceramics (NSC) supposedly containing plutonium, transition and rare-earth metals oxides is connected first with the necessity of the plutonium isotope enhanced diffusional release prognostication at storage temperatures. Assuming the prevailing impact of irradiation on the enhancement of diffusion processes at low temperatures, only self-irradiation effects in stock piled NSC must be taken into account. For lack of experimental features on diffusion processes in NSC, our estimations are based on the literature data for thermal-activated and radiation-enhanced diffusion (TAD and RED, respectively) of U and Pu in  $\text{UO}_2$  and  $(\text{U, Pu})\text{O}_2$  oxides. Experimental data on diffusion of  $^{233}\text{U}$  and  $^{238}\text{Pu}$  in  $\text{UO}_2$  and  $(\text{U, Pu})\text{O}_2$  [1] measured during fission in nuclear reactor (fission rate  $5 \times 10^{12} \text{ f/cm}^3 \cdot \text{s}$ ) may be presented for temperatures  $1293 \text{ K} \leq T \leq 1673 \text{ K}$  as follows (Fig. 1):

$$D_{RED}^{*U, Pu} = (5.67_{-1.50}^{+2.04}) \times 10^{-14} \exp\left(-\frac{0.78 \pm 0.01 \text{ eV}}{kT}\right), \text{ cm}^2/\text{s}. \quad (1)$$

**Figure 1.** The temperature dependencies of TAD (1), RED (2) and EDSI (3) in  $\text{UO}_2$  and  $(\text{U, Pu})\text{O}_2$ ; - - - - - the limiting data on TAD.



One can assume by analogy with RED in metals that Eq. 1 corresponds to appropriate solution of the rate equations for steady-state defect concentrations when a mutual recombination is the dominant mechanism of defect annealing. In such case,  $D_{RED}^*$  varies with the square root of the point defect production rate (PDPR) and  $Q_{RED}^* \approx E_m^v / 2$ . The approximate estimation of the vacancy migration energy,  $E_m^v$  (eV)  $\approx (0.37 \pm 0.03) Q_{TAD}^* \approx 1.56 \pm 0.02$ , agrees with results [2]. Here, the activation energy of TAD  $Q_{TAD}^*$  was evaluated from the averaged temperature dependence of  $D_{TAD}^*$  (Fig. 1) obtained by treatment of the most reliable data on cation diffusion in  $\text{UO}_2$  and  $(\text{U, Pu})\text{O}_2$ :

$$D_{TAD}^{*U, Pu} = (1.47_{-1.40}^{+34.72}) \times 10^{-2} \exp\left(-\frac{4.24 \pm 0.39 \text{ eV}}{kT}\right), \text{ cm}^2/\text{s}. \quad (2)$$

Thus, the radiation enhancement of metallic diffusion in NSC with the tentative melting point  $T_m \approx 3000 \text{ K}$  may be presented as

$$R = D_{RED}^* / D_{TAD}^* \approx (3.86_{-3.65}^{+55.71}) \times 10^{-12} \exp[(13.38 \pm 1.47)T_m / T], \quad (3)$$

conforming with data [3] when PDPR is about of  $10^{-8} \div 10^{-7} \text{ dpa/s}$ .

Consequently, the model for RED in metals can be taken as the first approximation for RED in ceramics.

The calculation method [4] for the determination of the number of atoms decaying at self-irradiation of Pu was applied to NSC taking into account their density and atomic weight. It allowed us to estimate the fission rate,  $10^{10} \div 10^{11} \text{ at/cm}^3 \cdot \text{s}$ . Using the fission rate parabolic dependence of RED in nuclear ceramics fuel [1], maximum enhancement of diffusion processes at self-irradiation (EDSI) is

$$D_{EDSI}^* \approx (1.66_{-1.56}^{+25.63}) \times 10^{-13} \exp\left(-\frac{1.07 \pm 0.4 \text{ eV}}{kT}\right), \text{ cm}^2/\text{s}; \quad (4)$$

here, the fission rate is about of  $10^{11 \pm 0.2} \text{ at/cm}^3 \cdot \text{s}$ ,  $1073 \text{ K} \leq T \leq 1473 \text{ K}$ . With the linear fission rate dependence of athermal  $D_{RED}^*$  [1] the athermal  $D_{EDSI}^*$  can be estimated as  $(1.20 \pm 0.35) \times 10^{-18} \text{ cm}^2/\text{s}$  for temperatures below  $\sim 1050 \text{ K}$ .

It follows from Eq. 4 that the parameter  $R$  for EDSI can be presented as

$$R \approx (1.1 \pm .3) \times 10^{-11} \exp[(12.25 \pm 152)T_m / T], \quad (5)$$

conforming with data [3] for PDPR of  $10^{-9} \div 10^{-8} \text{ dpa/s}$ .

For example, at the storage temperature  $\sim 723 \text{ K}$  the value of  $R$  is  $\sim (2.8_{-2.6}^{+42.2}) \times 10^{13}$ , that is, the effect of self-irradiation on the enhancement of diffusion processes in NSC may be as much as  $12 \div 14$  of orders; it significantly exceeded the influence of other factors.

The mechanisms of EDSI and the effect of alloying on EDSI in NSC are also discussed.

## References

1. H. Matzke, Radiation Effects 75 (1983) 317.
2. E. A. Smirnov, A. A. Shmakov, Defect and Diffusion Forum 165&166 (1999) 63.
3. E. A. Smirnov, A. A. Shmakov, Defect and Diffusion Forum 175&176 (1999) 13.
4. R. O. Elliott, C. E. Olsen, Self-Irradiation of Plutonium and Its Alloys. In: Studies in Radiation Effects (Gordon & Breach Sci. Publ., Inc., N.Y., Vol. 1, 1966), pp. 1–71.

## The Regularities of Diffusion Processes in the Low-Temperature Phases of Neptunium and Plutonium

**E. A. Smirnov,  
A. A. Shmakov**  
Moscow State  
Engineering Physics  
Institute (Technical  
University), Moscow  
115409, Russia

At present there are no experimental data about the key features and characteristics of diffusion processes in the low-temperature phases of Np and Pu. This paper has the aim to predict the temperature dependencies of the self-diffusion coefficients in  $\alpha$ -Np and  $\alpha$ -Pu.

The activation energy of self-diffusion  $Q^*$  in  $\alpha$ -Np and  $\alpha$ -Pu was drawn using the general relation,

$$Q^*(\text{eV}) = (1535 \pm 0.028) \times 10^{-3} T_m^f, \quad (1)$$

derived from data on the closed-packed phases of light actinides ( $\alpha$ -Th,  $\alpha$ -U and  $\beta$ -,  $\gamma$ -,  $\delta$ -Pu). Here,  $T_m^f$  is the melting temperature for the corresponding phase  $f$  estimated by means of the empirical Ardell's method.

The pre-exponential factor  $D_0$  for self-diffusion in  $\alpha$ -Pu has been estimated by expressions for the compensation effect obtained using the data on self-diffusion in  $\beta$ -,  $\gamma$ - and  $\delta$ -Pu:

$$D_0(\text{cm}^2/\text{s}) = (4.3_{-3.1}^{+11.5}) \times 10^{-11} \exp(Q^*/B), \quad (2)$$

$$B(\text{eV}) \approx (5.57 \pm 0.36) \times 10^{-2}.$$

In the case of  $\alpha$ -Np, the following approximation for the  $\alpha$ -Th,  $\alpha$ -U and  $\alpha$ - $\delta$ -Pu self-diffusion data was used:

$$\lg D_0 \approx - (11.30 \pm 0.33) + (0.44 \pm 0.03) Q^*/B. \quad (3)$$

Here, parameter  $B$  defining the compensation effect can be evaluated within the framework of the elastic model [1]:

$$B \approx - (3.91 \pm 0.34) \times 10^{-3} \Omega. \quad (4)$$

where  $\Omega = G_0 / \left. \frac{dG}{dT} \right|_0$  and  $G_0$  is the shear modulus at 0 K;  $\Omega$  is equal to 1990 K and 1440 K for  $\alpha$ -Np and  $\alpha$ -Pu, respectively.

Thus, the temperature dependencies of the self-diffusion coefficients in  $\alpha$ -Np and  $\alpha$ -Pu may be presented as follows (Fig. 1):

$$D_{\alpha\text{-Pu}}^* = (2.72_{-0.28}^{+0.48}) \times 10^{-4} \exp\left(-\frac{0.87 \pm 0.02 \text{ eV}}{kT}\right), \text{ cm}^2/\text{s}, \quad (5)$$

$$D_{\alpha\text{-Np}}^* = (1.26_{-0.92}^{+5.76}) \times 10^{-5} \exp\left(-\frac{1.12 \pm 0.02 \text{ eV}}{kT}\right), \text{ cm}^2/\text{s}. \quad (6)$$

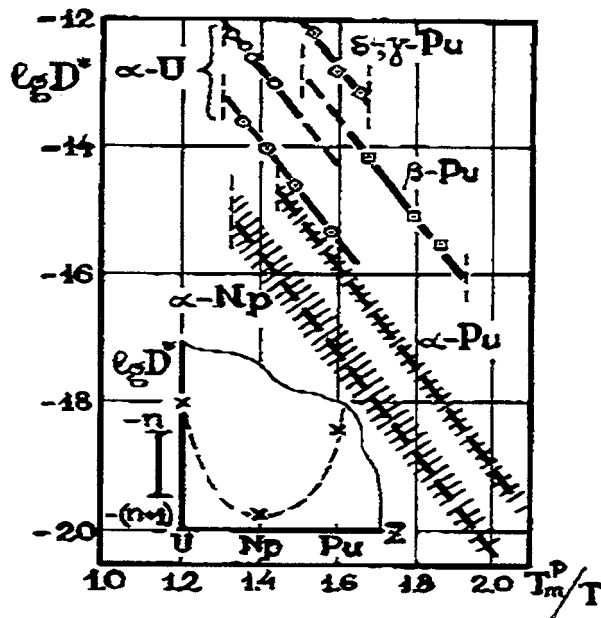


Figure 1. Self-diffusion in the low-temperature phases of actinides. The points and shaded lines are experimental data and our estimations, respectively.

Comparative analysis of diffusion data on the close-packed phases of actinides shows: 1) the proximity of diffusion mechanisms; 2) among all self-diffusion coefficients the  $D_{\sigma np}^*$  values are minimal at any  $T_m^f / T$ . It seems, the second fact is caused by the peculiarities of electronic building of  $\alpha$ -Np [2].

Presuming that the orthorhombic ( $\alpha$ -Np) and monoclinic ( $\alpha$ -Pu) structures have the quasi-hexagonal nature, using our model for  $\alpha$ -U [3], one can predict the temperature dependencies of self-diffusion anisotropy  $D_A = D_c/D_a$ :

$\alpha$ Np( $\Delta_{c/a} = -0.1335$ ,  $T_m^\alpha = 730 \pm 6K$ ):

$$D_A = (1.42 \pm 0.05) \exp\left(-\frac{0.047 \pm 0.002 eV}{kT}\right); \quad (7)$$

$\alpha$ Pu( $\Delta_{c/a} = -0.0863$ ,  $T_m^\alpha = 568 \pm 5K$ ):

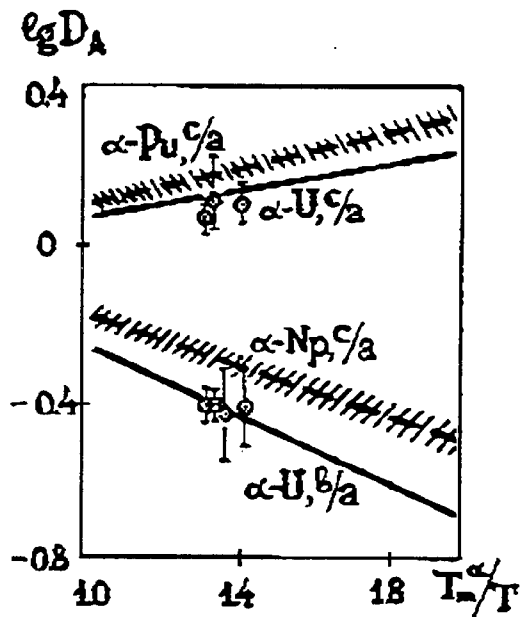
$$D_A = (0.80 \pm 0.02) \exp\left(-\frac{0.024 \pm 0.001 eV}{kT}\right), \quad (8)$$

where  $\Delta_{c/a} = (c/1.633a) - 1$ .

As well as it was found for  $\alpha$ -U [3], only slight anisotropy of self-diffusion appears in both  $\alpha$ -Np and  $\alpha$ -Pu (Fig. 2).

Using our previously reported model [4] and relations (4), (5) the radiation-enhanced self-diffusion coefficients and the vacancy migration energies may be estimated for  $\alpha$ -Np and  $\alpha$ -Pu when the mutual recombination of radiation defects dominates. In this case, the estimated  $E_m^v$  values,  $(0.5 \pm 0.05) Q^*$ , agree with our preliminary findings [4].

Figure 2. Self-diffusion anisotropy for the low-temperature phases of actinides. The points are experimental data for  $\alpha$ -U.



#### References

1. E. A. Smirnov, K. E. Smirnov, The Diffusion Processes in BCC Phases of Actinides, Preprint of Moscow Engineering Physics Institute, 013-92 (1992, in Russian).
2. O. A. Alexeev, V. S. Kurilo, E. A. Smirnov, A. A. Shmakov, Thermodynamics and Kinetics of Actinides with Zirconium Interaction (Moscow, VNIINM, 1999, in Russian).
3. E. A. Smirnov, A. A. Shmakov, Metallofiz. Noveishie Tekhnol. 21 (1999) 12.
4. E. A. Smirnov, A. A. Shmakov, Defect and Diffusion Forum 165&166 (1999) 63.

## Interdiffusion in U–Pu–Zr and U–Zr–Ti Solid Solutions

There is extremely scanty diffusion information on both light actinides (Th, U, Np, Pu) and their alloys with transition metals at present. We recently reported some of our data for actinide-zirconium systems [1–3]. In this study, interdiffusion is examined for the b.c.c. phases of the ternary U–Pu–Zr and U–Zr–Ti alloys.

Thermodynamic analysis of the limiting binary sub-systems and the Kohler interpolation equations gives mathematical expressions for the excess Gibbs energy of ternary alloys and allows us to calculate the solidus temperatures  $T_s$  for the U–Pu–Zr [1] and U–Zr–Ti (Fig. 1) systems (See Fig. 1).

Based on the most reliable experimental data on self-diffusion and impurity diffusion in pure  $\gamma$ -U,  $\epsilon$ -Pu,  $\beta$ -Ti and  $\beta$ -Zr as well as in their alloys, the following semi-empirical expressions were obtained for the estimation of component self-diffusion in ternary solid solution:

$$D_k^*(C, t) = [D_k^{*1}(T_1)]^{C_1} [D_k^{*2}(T_2)]^{C_2} [D_k^{*3}(T_3)]^{C_3} \exp[G^M(C, T) / RT] \quad (k = 1, 2, 3) ,$$

where  $C_i$  are the component concentrations (atom fractions);  $D_k^*$  is the coefficient of either self-diffusion in metal  $k$  (if  $k \neq j$ ) or impurity diffusion of element  $k$  in matrix  $j$  (if  $k \neq j$ );  $G^M$  is the free Gibbs energy of mixing;  $T_i = T_i^m / T_s$ ,  $T_i^m$  is the melting point for metal  $i$ .

Using the obtained expressions for  $G^M$  and  $D_k^*$ , within the framework of the irreversible process theory [4], full matrix of the interdiffusion coefficients (IC) was determined for each system. It was found that the main IC calculated for the U–Pu–Zr alloys in the concentration and temperature ranges:

$$0.7 \leq C_U < 0.9, \quad 0.05 \leq C_{PuZr} \leq 0.25, \quad 1073\text{K} \leq T < T_s ,$$

may be presented by the following expressions:

$$\lg \tilde{D}_{ZrZr}^U = (-2.49 \pm 0.07) - (5.295 \pm 0.063)T_s / T , \quad (1)$$

$$\lg \tilde{D}_{PuPu}^U = (1.04 \pm 0.25) - (11.31 \pm 0.44)T_s / T + (3.17 \pm 0.19)T_s / T)^2 . \quad (2)$$

Here and further diffusion coefficients are given in  $\text{cm}^2/\text{s}$ . The above results (Eqs. 1, 2) are compared in Fig. 2 with our and literary experimental data.

The main IC calculated for the U–Zr–Ti alloys in the temperature range  $1173\text{K} \leq T < T_s$  are described by the next equations:

$$\lg \tilde{D}_{ZrZr}^U = (-3.51 \pm 0.05) - (6700 \pm 70) / T . \quad 0.01 \leq C_{U, Ti, Zr} \leq 0.8 ;$$

$$\lg \tilde{D}_{TiTi}^U = (-3.82 \pm 0.06) - (6440 \pm 90) / T . \quad 0.1 \leq C_{U, Zr} \leq 0.6, \quad 0.2 \leq C_n \leq 0.6 .$$

Diffusion data calculated for this system are compared with our experiments in Table I.

**O. A. Alexeev**  
All-Russia Scientific  
Research A. A.  
Bochvar Institute of  
Inorganic Materials,  
Moscow 123060,  
Russia

**A. A. Shmakov,**  
**E. A. Smirnov**  
Moscow State  
Engineering Physics  
Institute (Technical  
University), Moscow  
115409, Russia

Figure 1. Absolute solidus temperatures calculated for the U–Zr–Ti system.

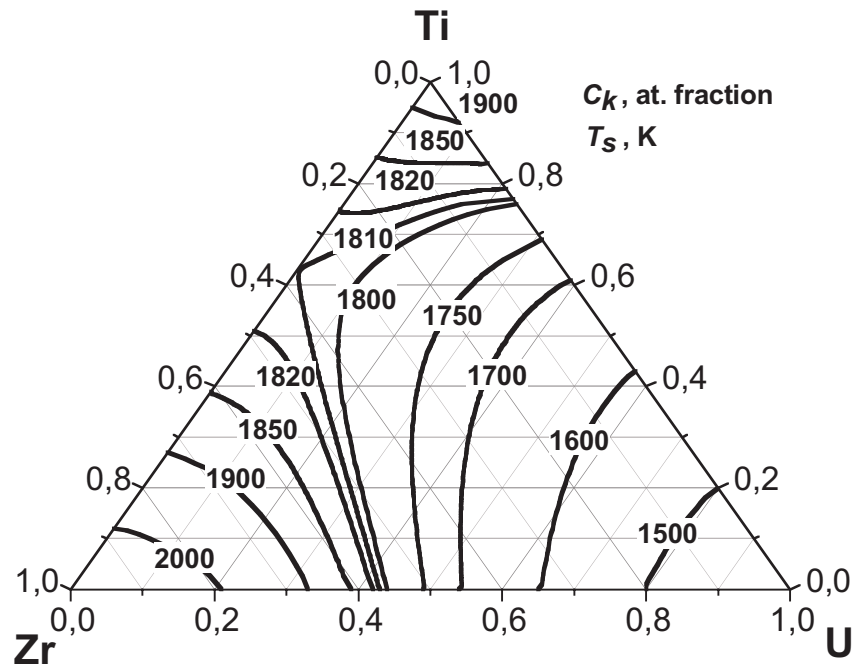
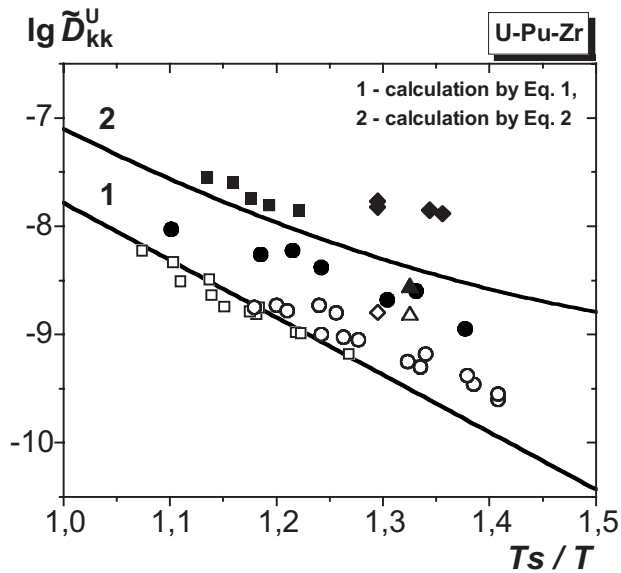


Figure 2. The main interdiffusion coefficients in the U–Pu–Zr system, light and dark symbols denote the  $\tilde{D}_{ZrZr}^U$  and  $\tilde{D}_{PuPu}^U$  data, respectively. Calculation: Lines 1 and 2 were calculated by Eq. 1 and 2, respectively;  $\triangle$ ,  $\blacktriangle$  are taken from Ref. 5. Experiment:  $\circ$ ,  $\bullet$  represent our data (partly published [1, 2]);  $\blacklozenge$  – is taken from Ref. 6. Interdiffusion in binary systems:  $\square$  – U–Zr is taken from Ref. 7;  $\blacksquare$  – U–Pu is taken from Ref. 8.



Alloy composition, at. fractions		Experiment, $10^{-9}$ cm <sup>2</sup> /s		Calculation, $10^{-9}$ cm <sup>2</sup> /s		Solidus temperature
U	Zr					$T_s$ , K
0.18	0.53	1.2	0.94	1.2	1.7	1832
0.30	0.30	1.2	0.875	1.4	1.6	1740
0.325	0.25	1.1	1.1	1.4	1.5	1723
0.12	0.52	1.4	1.2	1.3	2.0	1833
0.285	0.29	0.73	0.975	1.4	1.6	1743
0.22	0.23	1.3	0.9	1.4	1.9	1762
0.13	0.475	1.6	1.7	1.4	2.1	1818

Fig. 2 and Table I demonstrate that for both systems under consideration the calculated IC are in satisfactory agreement with experiment. It allows us to consider the proposed calculation method as a realistic alternative to the long and expensive experiments.

### References

1. O. A. Alexeev, V. S. Kurilo, E. A. Smirnov, A. A. Shmakov, Thermodynamics and Kinetics of Actinides with Zirconium Interaction (Moscow, VNIINM, 1999, in Russian).
2. O. A. Alexeev, V. S. Kurilo, A. A. Shmakov, E. A. Smirnov, Metallofiz. Noveishie Tekhnol., 1999, v. 21, 1, p. 61.
3. O. A. Alexeev, A. A. Shmakov, E. A. Smirnov, Defect & Diffusion Forum, 1999, vs. 175 & 176, p. 23.
4. The Processes of Interdiffusion in Alloys, K. P. Gurov, Ed., (Moscow, Nauka, 1973, in Russian).
5. M. Ishida, T. Ogata, M. Kinoshita, Nucl. Technol., 1993, v. 104, p. 37.
6. M. C. Petri, M. A. Dayananda, J. Nucl. Mater., 1997, v. 240, p. 131.
7. Y. Adda, J. Philibert, Comp. Rend. Acad. Sci., 1956, v. 242, ? 26, p. 3081.
8. M. C. Petri, A. G. Hins, J. E. Sanecki, M. A. Dayananda, J. Nucl. Mater., 1994, v. 211, p. 1.

# Research in the Patterns of Time-Related Change in the Structure and Properties of Plutonium Dioxide Produced with Different Process Streams

E. M. Glagovskiy,  
V. A. Zhmak,  
V. Ye. Klepatskiy,  
L. N. Konovalov,  
A. V. Laushkin,  
V. K. Orlov,  
Ya. N. Chebotarev  
*State Science Center  
of the Russian  
Federation  
Academician A. A.  
Bochvar All-Russia  
Research Institute of  
Inorganic Materials,  
123060, g. Moskva,  
Russia*

## Introduction

The scientific and technical literature has a quite a few experimental results indicating that  $\text{Pu}^{+4}$  represents the highest degree of oxidation of plutonium in its compounds in solid state and that the most stable form of that valent state is the dioxide. Apparently, that underlies the idea of the design for the storage of plutonium in the form of a dioxide and the use of the latter as a component of nuclear fuel for various reactors.

The work reported in this paper represents the first step in a study of the changes that plutonium dioxide experiences when it is stored in air. Using x-ray analysis methods, we studied the changes in the phase composition, the crystal structure, the size of crystallites, and the level of micro-distortions of the lattice that are the result of the action of the  $\alpha$ -particles given off by the plutonium in natural radioactive decay (self-irradiation). In addition, an attempt is made here to elucidate the effect that the method for producing the dioxide has on the course of the above-enumerated processes when the dioxide is stored.

## Experimental Results and Discussion

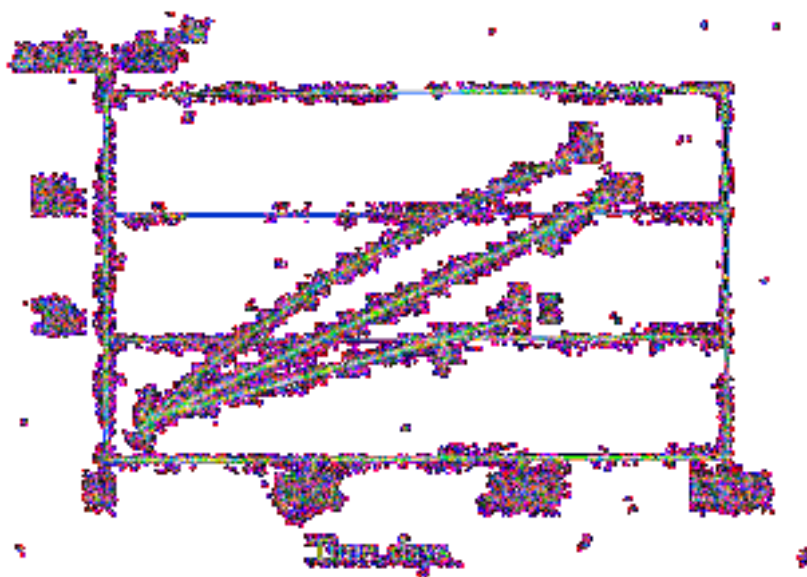
The study of the effect of self-irradiation on the structure of plutonium dioxide during lengthy storage was done with x-ray diffraction in the following manner. A phase analysis was first performed. The crystal lattice spacing was determined from continuous-recording diffractograms, whereas the dimensions of the coherent scattering fields and the number of micro-deformations were ascertained from the materials of a point-by-point survey done on a DRON-3M diffractometer. Chosen for the study were dioxide samples produced with oxalate precipitation (series 1) after storage in air at room temperature for 100, 820, and 1,000 days and samples produced with ammonia precipitation (series 2) after 100, 1,020, and 1,200 days of storage under the same conditions. In work done earlier,<sup>1</sup>  $\Delta A/a_0$  was used to describe the increase in the crystal lattice spacing of plutonium dioxide during storage, and the following experimental formula was derived for describing the dependence of the increase in crystal lattice spacing on storage time:

$$A/a_0 = 3.9 \cdot 10^{-3} \cdot [1 - \exp(-0.87 \cdot 10^3 \cdot t)] \quad (1)$$

where  $t$  is the storage time in days. We also used  $\Delta A/a_0$  in our work to describe the enlargement of the crystal lattice spacing. For  $a_0$ , we used a baseline value of 0.53961 nm, which corresponds to the crystal lattice spacing of the freshly prepared  $\text{PuO}_2$  produced with both technologies.

The results of the x-ray analysis studies are given in Table 1 and Figure 1. In Figure 1, curve 3 was plotted from Raud<sup>1</sup> with formula (1); curve 2 is for ammonium dioxide; and curve 1, for oxalate precipitation.

Sample code (storage time)	Crystal lattice spacing $a$ , nm	$\Delta A = a - a_0 \cdot 10^{-4}$	$\Delta A/a_0 \cdot 10^{-4}$
Oxalate precipitation:			
1.1 (100 days)	0.53985±0.0005	2.4±0.5	4.4±1.0
1.2 (820 days)	0.54010±0.0002	4.9±0.2	9.1±0.4
1.3 (1,000 days)	0.54032±0.0005	7.1±0.5	13.2±1.0
Ammonia precipitation:			
2.1 (100 days)	0.53978±0.0005	1.7±0.5	1.7±1.0
2.2 (1,020 days)	0.54058±0.0005	9.7±0.5	18.0±1.0
2.3 (1,200 days)	0.54076±0.0005	11.5±0.5	21.3±1.0



1—oxalate precipitation samples; 2—ammonia precipitation samples; 3—design curve.

From the results in Table 1 and Figure 1, one can conclude that the growth in the crystal lattice spacing of  $\text{PuO}_2$  for the samples of the different batches is around 0.1%-0.2% for 1,000-1,200 days of storage. The shapes of the curves for the growth of crystal lattice spacing (see Fig. 1) show that the process associated with the structural changes over the storage times indicated does not reach saturation, and the rate of crystal lattice spacing growth for the samples produced with ammonia precipitation is higher than for the oxalate samples. For the  $\text{PuO}_2$  samples after lengthy storage, the values of the physical widening for a number of reflexes were determined, and the sizes of the coherent scattering fields and micro-deformations (see Table 2) were calculated.

Sample code (storage time)	Size of coherent scattering fields, $\mu\text{m}$	Micro-deformations, %
Oxalate precipitation:		
1.2 (820 days)	0.012	0.2
1.3 (1,000 days)	0.013	0.2
Ammonia precipitation:		
2.2 (1,020 days)	0.025	0.1
2.3 (1,200 days)	0.031	0.1

Table 1. Study of the change in the crystal lattice spacing of  $\text{PuO}_2$  in samples after different times for storage in air.

Fig. 1. Dependence of values for crystal lattice spacing of  $\text{PuO}_2$  on storage time.

Table 2. Sizes of coherent scattering fields and levels of micro-deformation of lattice of  $\text{PuO}_2$  in samples with different storage times.

The data of Table 2 show that as a result of self-irradiation (with an increase in storage time) the dimensions of the crystallites (coherent scattering fields) increase in the PuO<sub>2</sub> samples, while the degree of deformation of the lattice remains unchanged. The fact that the degree of micro-deformation of the lattice remains constant while the self-irradiation time increases makes it possible to exclude radiogenic helium as a cause of the increase in crystal lattice spacing because experience in studying plutonium and its alloys shows that during aging even a smaller increase in crystal lattice spacing as a result of helium accumulation leads to a marked increase in the level of micro-deformations of the lattice.

Apparently, as a result of the irradiation-induced defects, the crystal lattice of PuO<sub>2</sub> experiences a structural reorganization that is accompanied by an enlargement in the crystal lattice spacing. An example of such reorganization is the formation of plutonium oxide with a fluorite structure (PuO<sub>2</sub> type), but with a considerable shortage of oxygen. Such a compound is known as a high-temperature phase of  $\alpha'$ -Pu<sub>2</sub>O<sub>3</sub>.

As noted earlier, the process attending structural changes that result in an enlargement in the crystal lattice spacing of samples of plutonium oxide does not reach saturation over 1,000-1,200 days of storage. From that it follows that a detailed determination of the structural changes of PuO<sub>2</sub> and of the change in its properties over time requires continuing the structural studies of samples of plutonium dioxide with longer storage times.

### Conclusion

As a result of the x-ray diffraction study of samples of plutonium dioxide produced with different process streams, the following was established after different lengths of storage in air at room temperature:

- during storage of the samples, the crystal lattice spacing is observed to increase (1,000-1,200 days—0.1%-0.2%), and that increase maintains a trend for further growth over the indicated storage time;
- the rate of growth of the crystal lattice spacing of the PuO<sub>2</sub> in samples produced with ammonia technology is markedly greater than in the oxalate samples;
- the increase in the crystal lattice spacing of the PuO<sub>2</sub> is accompanied by an increase in the size of the crystallites (coherent scattering fields), but the level of micro-deformation of the lattice does not change.

A possible reason for the structural changes in the plutonium dioxide during storage is the change in the crystal structure of the dioxide. A detailed study of the changes in the crystal lattice of plutonium dioxide is proposed for samples with storage times exceeding 1,200 days.

### Reference

1. M. H. Raud. *Nature*, 195, 567 (1962).

### Additional Bibliography

1. T. D. Chicalla, C. E. MacNeily, and R. E. Skaidahl, "The Plutonium-Oxygen System" *J. Nucl. Mat.*, Vol. 12 (1964), pp. 131-141.

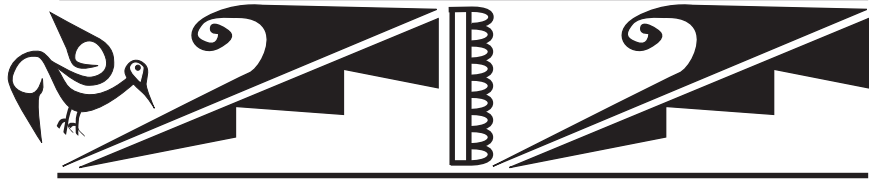
## A Combinatorial Chemistry Approach to the Investigation of Cerium Oxide and Plutonium Oxide Reactions with Small Molecules

We are currently investigating the potential chemistry of the 3013 Standard waste storage containers. These containers are filled with waste that is a mixture of inorganic salts and plutonium oxide that has been calcined to remove water and other volatiles. There has been concern about possible pressure buildup due to the formation of hydrogen or other gases. We are utilizing a combinatorial chemistry approach to investigate a range of possible reactions that may occur in the containers with various concentrations of metal oxides and inorganic salts. We are examining the reaction of  $\text{PuO}_2$  and inorganic salts such as  $\text{CaCl}_2$ ,  $\text{MgCl}_2$ ,  $\text{Ca}(\text{NO}_3)_2$  and  $\text{Mg}(\text{NO}_3)_2$  with small molecules such as  $\text{H}_2\text{O}$ ,  $\text{H}_2$  and  $\text{O}_2$ . Initial studies have involved the use of cerium as a surrogate for plutonium to establish combinatorial techniques for analysis of the reactions. Cerium alkoxides are used as precursors for cerium oxide, which is formed upon calcining above  $800^\circ\text{C}$  in air. Mixtures of cerium and various inorganic salts are measured into wells on stainless steel plates and calcined in a furnace. These reaction plates are then placed in a sealed temperature controlled reactor and allowed to react with  $\text{H}_2\text{O}$ . Examination of the plates by reflectance infrared and Raman spectroscopy allows us to look at water absorption as well reactions of the substrates with the water. The reactor has also been used to examine recombination reactions of hydrogen in compressed air to form water. We have also investigated the reactions of the salt/metal oxide mixtures with the stainless steel plates at elevated temperatures utilizing x-ray fluorescence spectroscopy to examine the composition of the plates.

To investigate the presence and potential chemical evolution of other small molecules on the  $\text{PuO}_2$  surfaces, we have developed and implemented a Raman spectral method for both identification and quantitation of small molecules including nitrates, sulfates, and their probable calcination products (e.g.,  $\text{NO}_x$ s and  $\text{SO}_x$ s). These studies have utilized high surface area  $\text{CeO}_2$  and  $\text{TiO}_2$  as a surrogate for the plutonium oxides. We have adapted a geochemical sieving method to the preparation and homogenization of mixtures of solid phases using wet sieving techniques. This technique is critical because homogeneous mixing of solids to give true solid solutions is the absolute most important step in generating surrogates for this project. With homogeneous mixtures these surrogates more accurately depict scenarios anticipated for Pu oxides in the 3013 cans and provide a better means to test the dynamic range and sensitivity of this method for small molecules. Thus far we have demonstrated this analytical method for both nitrate and sulfate (from the corresponding anhydrous sodium salts). The best results have been obtained using 1064 nm excitation with an FT-Raman spectrometer although excitation wavelengths from the ultraviolet (364 nm) through the visible (488 and 514 nm) and into the near infrared (752 nm) were tested. Calibration curves (spectral response vs. concentration of nitrate or sulfate) have been obtained demonstrating good linear dynamic response and sensitivity. Detection levels corresponding to  $\sim 1\%$ – $2\%$  surface coverage were readily achieved. We are presently examining similar nitrate and sulfate bearing samples following calcination to investigate conversion to the reduced species.

**John T. Brady,  
Benjamin P. Warner,  
Jon S. Bridgewater,  
George J. Havrilla,  
David E. Morris,  
C. Thomas Buscher**  
*Los Alamos National  
Laboratory, Los  
Alamos, NM 87545,  
USA*





## **TRU Waste Forms**



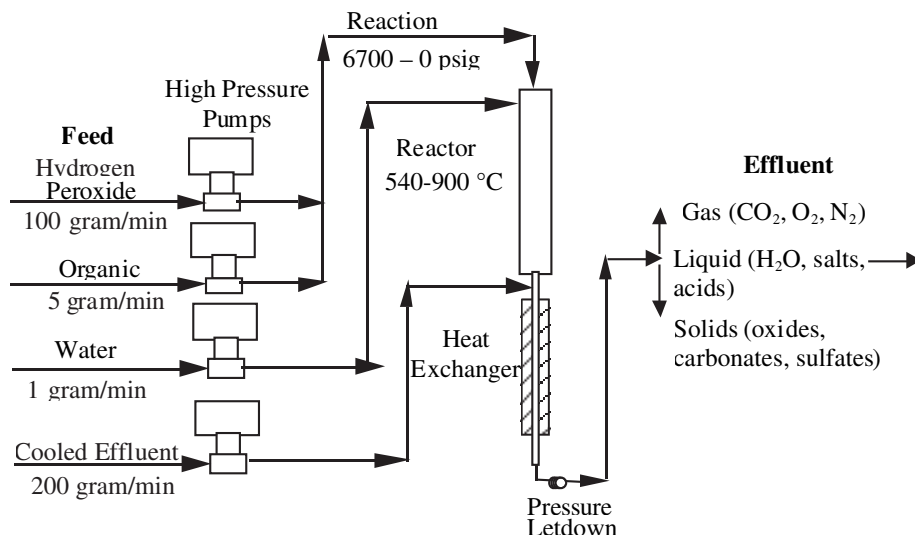
# Destruction of Halogenated Organics with Hydrothermal Processing

## Introduction

Chemical reactions in high temperature water (hydrothermal processing) allow new avenues for effective waste treatment and radionuclide separation. Successful implementation of hydrothermal technologies offers the potential to effectively treat many types of radioactive waste and reduce the storage hazards and the disposal costs, while minimizing the generation of hazardous secondary waste streams.<sup>1-5</sup> Halogenated hazardous organic liquids containing actinides are a difficult to treat category of TRU radioactive wastes. These liquids are typically used for degreasing operations or density measurements and can include trichloroethylene and bromobenzene. Experiments have demonstrated that hydrothermal processes can eliminate hazardous halogenated organics generated by the nuclear industry by the complete oxidation of the organic components to CO<sub>2</sub> and H<sub>2</sub>O.

## Description of the Actual Work

An extensive series of tests on a laboratory scale hydrothermal processing unit demonstrated the complete destruction of radioactive organics.<sup>6</sup> System improvements to the design of this hydrothermal system were developed for the specific treatment of TRU halogenated organic wastes. The modified hydrothermal processing unit, shown in Figure 1. Waste is heated, pressurized if specified, and held at reaction temperature for a time sufficient to complete the desired chemical processes (oxidation, reduction, dissolution). At temperatures above 500°C, reactions are rapid, and oxidation occurs on the time scale of seconds to minutes, and produces simple products (ideally CO<sub>2</sub>, H<sub>2</sub>O, and N<sub>2</sub>). In the reactor, the organic components of the wastes are oxidized to carbon dioxide by reaction with water and 30 wt. % hydrogen peroxide. Nitrate contaminants also react with the organic material and are converted to nitrogen gas. Heteroatoms such as chlorine and bromine are converted to acids or salts depending on the pH of the solution. The speciation of the actinides in the hydrothermal reactor is not yet certain; thus far they have been converted to small insoluble oxide particles that can be separated by filtration.<sup>6</sup>



Laura A. Worl,  
Steven J. Buelow,  
David M. Harradine,  
Dallas Hill,  
Rhonda McInroy,  
Dennis Padilla  
Los Alamos National  
Laboratory, Los  
Alamos, NM 87545,  
USA

Figure 1. Modified configuration of the hydrothermal unit.

## Results

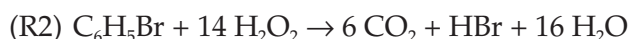
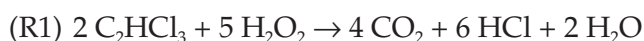
Previous experiments demonstrated the feasibility of using hydrothermal processing for treating halogenated organics, yet the unit only had a capacity for ~1 ml per minute of waste. These results are summarized in Table 1.<sup>6</sup> The modified hydrothermal processing unit, shown in Figure 1, had an increased flow capacity of 5 ml per min of organic waste. The inside diameter of the fluid flow region in the heat exchanger was increased a factor of five from 0.6 mm to 3 mm. To improve flow through the heat exchanger, water (or recycled effluent) is added to the entrance of the heat exchanger. This additional flow improves the transport of solids, and rapidly cools the reactor effluent thus increasing salt solubility. It also decreases the corrosion and creep rates of the heat exchanger.

**Table 1.**  
Hydrothermal  
Processing of  
Halogenated TRU  
Waste.<sup>a</sup>

Organic Composition	Actinide	Effluent pH	TOC Results, (mg/L)		Organic Destruction
			Influent	Effluent	
Carbon tetrachloride	na <sup>b</sup>	nd <sup>c</sup>	11,500	< 0.5	>99.995%
Trichloroacetic acid CCl <sub>3</sub> COOH	na	nd	1000	< 1	99.90%
Trichloroethylene C <sub>2</sub> Cl <sub>3</sub> H	na	nd	1000	< 1	99.90%
1,1,1 Trichloroethane CCl <sub>3</sub> CH <sub>3</sub>	na	nd	1000	1	99.90%
Bromobenzene	AmCl <sub>3</sub>	2.0	18000	7	99.96%
1.5 M trichloroacetic acid	Pu	1.0	1800	<1	99.94%

a) Reaction conditions of 46.2 MPa, 60 seconds, 550<sup>0</sup>C. b) Experiments were conducted in non-radioactive laboratory, c) not determined.

In order to address near-term waste disposal problems at the LANL Plutonium Facility, the heat exchanger was tested under the “worst case” operating conditions - trichloroethylene (TCE) and bromobenzene were processed which produce very acidic effluents. The oxidation reactions for TCE and bromobenzene are given in equations R1 and R2.



Processing TCE with a 10% excess of 30 wt. % hydrogen peroxide produces 9.6 molar hydrochloric acid. Processing bromobenzene under similar conditions produces 0.6 molar hydrobromic acid. In addition to producing highly acidic effluents both compounds are slow to oxidize due to the radical halogen scavengers that slow the oxidation process. Diluting halogen rich compounds via blending with other hydrocarbon rich organic wastes speeds the oxidation reactions.

Modifications to the operating conditions of the reactor were also tested. The reactor operating pressure was lowered from 46.2 MPa to ambient pressure while the operating temperature was increased from 540°C to 900°C. The lower pressure lowers creep rates and allows higher operating temperatures and more flexibility in the design and fabrication of the reactor. The higher temperature increases the rate of reaction and allows use of shorter residence times. To improve mixing in

the reactor at low pressures, the reactor was packed in quartz beads. Under these conditions, the removal of TCE was >99%. Results with bromobenzene were promising at higher temperatures (1000°C). It may be possible to improve bromobenzene destruction under similar conditions by blending the bromobenzene with TCE or another hydrocarbon. Experiments examining this strategy are being conducted.

### References

1. R. Oldenborg, J. M. Robinson, S. J. Buelow, R. B. Dyer, G. Anderson, P. C. Dell'Orco, K. Funk, E. Wilmanns, and K. Knutsen, "Hydrothermal Processing of Inorganic Components of Hanford Tank Wastes," LA-UR-94:3233, LANL (1994).
2. P. C. Dell'Orco, B. R. Foy, E. G. Wilmanns, L. Le, J. Ely, K. Patterson, S. J. Buelow, "Hydrothermal Oxidation of Organic Compounds by Nitrate and Nitrite," ACS Symposium Series Vol. 179, 608 (1995).
3. R. Oldenborg, S. J. Buelow, G. Anderson, G. Baca, R. Brewer, P. C. Dell'Orco, B. R. Foy, K. Knutsen, L. A. Le, R. McInroy, R. McFarland, S. Moore, J.M. Robinson, P. Rodgers, R. Shaw, and E. Wilmanns, "Evaluation of IPM Selection Criteria for Hydrothermal Processing," LA-UR-94-1945, LANL (1994).
4. B. R. Foy, P. C. Dell'Orco, E. Wilmanns, R. McInroy, J. Ely, J. M. Robinson, and S. J. Buelow, "Reduction of Nitrate and Nitrite Under Hydrothermal Conditions," *Physical Chemistry of Aqueous Systems*, ed. H. J. White Jr., J. V. Sengers, D. B. Neumann, and J. C. Bellows, pp. 602-609, Begell House, New York (1995).
5. L. Le, S. J. Buelow, J. H. Roberts, L. A. Worl, D. D. Padilla, G. Baca, V. Contreras, M. Devolder, D. Harradine, D. Hill, R. Martinez, J. McFarlan, R. McFarlan, E. Martinez, M. Mitchell, C. Prenger, J. Roberts, M. Sedillo, K. Veirs, "Hydrothermal Processing Unit for Actinide Contaminated Combustible Wastes - FY96 94-1 R&D Final Report," LA-UR-96:4730, LANL (1996).
6. L. A. Worl, S. J. Buelow, D. M. Harradine, R. Lanning, M. P. Neu, D. D. Padilla, S. D. Reilly, J. H. Roberts, "Demonstration of Hydrothermal Combustible Waste Treatment Process," Los Alamos National Laboratory Report, LAUR-99-2967 (1999).

## Preparation of Plutonium-Bearing Ceramics via Mechanically Activated Precursor

S. V. Chizhevskaya,  
S. V. Stefanovsky  
SIA Radon, Moscow  
119121 Russia

The problem of excess weapons plutonium disposition is suggested to be solved by means of its incorporation in stable ceramics with high chemical durability and radiation resistivity. The most promising host phases for plutonium as well as uranium and neutron poisons (gadolinium, hafnium) are zirconolite, pyrochlore, zircon, zirconia [1,2], and murataite [3]. Their production requires high temperatures and a fine-grained homogeneous precursor to reach final waste form with high quality and low leachability. Currently various routes to homogeneous products preparation such as sol-gel technology, wet-milling, and grinding in a ball or planetary mill are used. The best result demonstrates sol-gel technology but this route is very complicated. An alternative technology for preparation of ceramic precursors is the treatment of the oxide batch with high mechanical energy [4]. Such a treatment produces combination of mechanical (fine milling with formation of various defects, homogenization) and chemical (split bonds with formation of active centers – free radicals, ion-radicals, etc.) effects resulting in higher reactivity of the activated batch.

In our previous work [4] we have demonstrated lowering of the temperature range of formation of titanate phases (zirconolite and pyrochlore) in the mechanically activated batches and improvement of mechanical integrity of the ceramic samples. The best result was achieved using an apparatus with a rotating magnetic field that reduced this range by 100°C–200°C. In the present work we describe a process of preparation of zirconolite ceramics using the mechanically activated precursor.

Composition of the zirconolite ceramic carried over from reference data [2] was as follows (in wt. %): CaO – 13.4, Gd<sub>2</sub>O<sub>3</sub> – 5.9, ZrO<sub>2</sub> – 29.4, PuO<sub>2</sub> – 8.8, TiO<sub>2</sub> – 40.8, Al<sub>2</sub>O<sub>3</sub> – 1.7. Uranium was used as plutonium surrogate in cold tests. The sample production process included preparation of a non-radioactive precursor from CaO, Gd<sub>2</sub>O<sub>3</sub> (neutron poison), ZrO<sub>2</sub>, TiO<sub>2</sub>, and Al<sub>2</sub>O<sub>3</sub> followed by admixing of UO<sub>2</sub> or PuO<sub>2</sub> (dried and calcined uranium or plutonium nitrate solution). To obtain the precursor, oxides mixed and ground in agate mortars were treated either in a planetary mill (PM) Pulverisette-7 (Fritsch, GmbH) or in an apparatus with a rotating magnetic field (ARMF). Particle size distribution was analyzed using an Analysette-22 unit (Fritsch, GmbH).

The duration of mechanical treatment was varied. The longest duration was 30 minutes. Pu-containing batches were compacted (pressure ranged between 50 and 300 MPa) in pellets (80 mm in diameter and 30 mm in thickness) at room temperature followed by sintering in a resistive furnace at 1350°C for 2 hours. Phase composition of the ceramic samples was studied with X-ray diffraction using a DRON-3 diffractometer (Cu K<sub>α</sub> radiation). Linear shrinkage, bending strength, open porosity, apparent density, and water uptake of the ceramic samples were measured using standard techniques.

As follows from Figure 1 (left) particle size distribution after treatment of batches in the ARMF for 15 min and in the PM for 30 min is very similar and strongly different from that produced in the mortar. In particular, in the batches treated in the ARMF and in the PM no particles with size larger than  $\sim 20 \mu\text{m}$  have been found. To obtain the same particle size distribution as the batch after the ARMF, the powder remaining after the PM is strongly agglomerated. After the ARMF the powder requires an additional ultrasonic treatment. Unlike powder after the PM, powder activated in the ARMF for 15 min is not agglomerated and has higher reactivity facilitating its sintering.

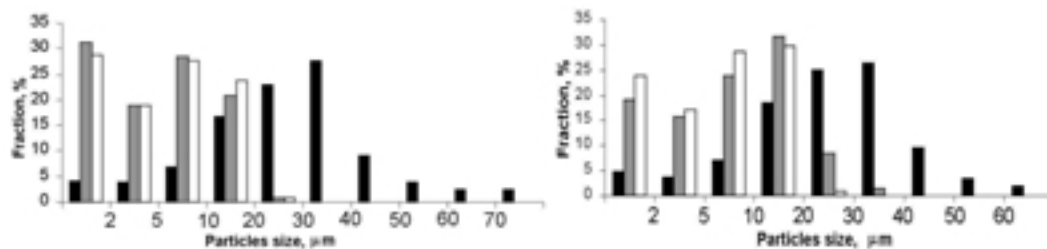


Figure 1 (right) shows that treatment of mixture of ceramic additives in the ARMF following by admixing of  $\text{UO}_2$  gives almost the same particles size distribution as treatment of pre-intermixed  $\text{UO}_2$  and ceramic additives (>95% of particles have size lower 30 mm).

As it has been established from preliminary tests, the duration of mechanical activation in the ARMF longer than 15 min is inexpedient due to secondary agglomeration of fine particles reducing batch reactivity. Pressure to produce mechanically strong pellets was found to be as many as 150 MPa. This produces dense pellets with strong mechanical integrity and low water uptake after heat-treatment and sintering at  $1350^\circ\text{C}$  (Table I). Mechanical activation doesn't affect phase composition of the batch (newly formed phases were not found).

As seen from Table I, the maximum amount of the target phase (zirconolite) in the sample produced by cold pressing of oxide mixture ground in the mortar and sintering at  $1350^\circ\text{C}$  doesn't exceed about 25%. Mechanical treatment/activation in the ARMF or PM increases zirconolite yield to >90%; however, ceramic produced using the ARMF has higher mechanical properties. The highest yield of the target phases (zirconolite and pyrochlore) also occurred in the ceramic sample prepared from ceramic precursor activated in the ARMF and doped with calcined  $\text{UO}_2$ , as compared to ceramic from precursor milled in the PM and also doped with calcined  $\text{UO}_2$ , and ceramic from oxide mixture ground in the mortar at the same temperature ( $1350^\circ\text{C}$ ).

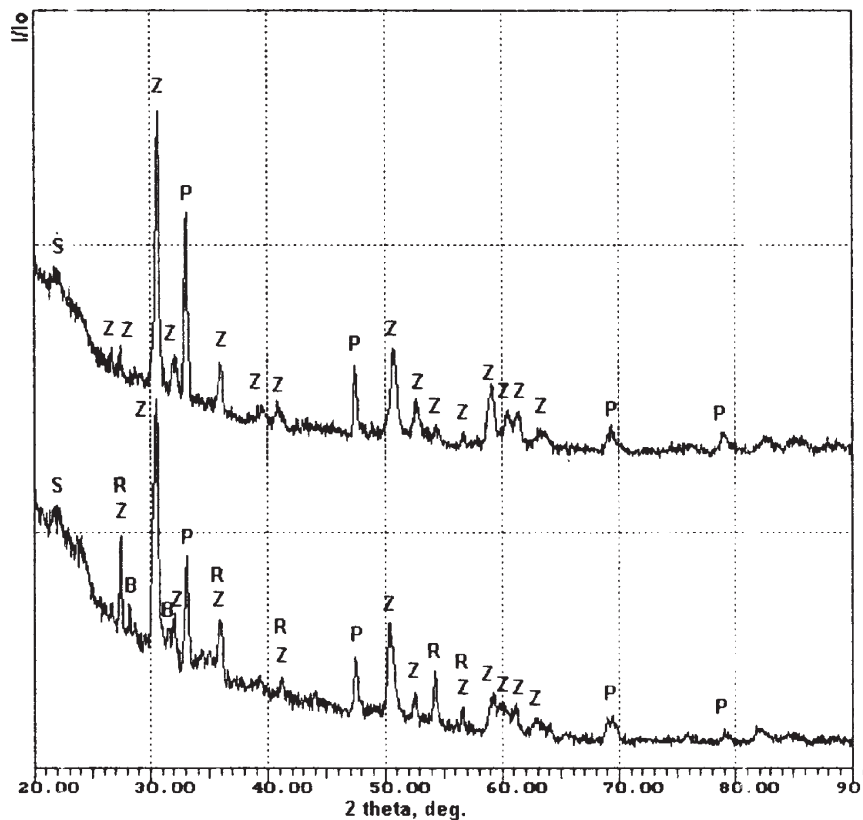
Property	Mortar	ARMF	PM
Target phases content, %	$\sim 25$	$>90$	$>90$
Linear shrinkage, %	0	16.6	16.0
Bending strength, MPa	0	$100.0 \pm 10.7$	$65.6 \pm 4.7$
Open porosity, %	$48.8 \pm 1.3$	$0.3 \pm 0.1$	$1.4 \pm 0.4$
Apparent density, $\text{kg}/\text{dm}^3$	$2.10 \pm 0.05$	$4.07 \pm 0.04$	$3.99 \pm 0.03$
Water uptake, %	$23.2 \pm 3.2$	$0.1 \pm 0.1$	$0.4 \pm 0.1$

Figure 1. Particle size distribution in the batches mechanically treated by different ways. Left – effect of type of treatment (black – mortar, gray – ARMF for 15 min, white – PM for 30 min.). Right – effect of batch preparation method (black – batch from  $\text{UO}_2$  and ceramic additives ground in the mortar, gray - mixture of ceramic additives treated in the ARMF and untreated  $\text{UO}_2$ , white – treated in the ARMF).

Table I. Properties of the Sintered Ceramic Samples Produced Using Different Mechanical Treatment.

Incorporation of Pu rather than U in the ceramics resulted in formation of perovskite with general formula  $(Ca,Gd,Pu)(Ti^{4+}Ti^{3+}Al)O_3$  as an extra phase (Figure 2) due to reduction of some fraction of Pu(IV) to Pu(III). The sample produced via precursor mechanically activated in the ARMF is composed of just zirconolite and perovskite (upper pattern), whereas the sample produced using the PM contains minor unreacted phases (baddeleyite and rutile).

Figure 2. XRD patterns of Pu-doped samples. S – starch, P – perovskite, R – rutile, Z- zirconolite.



## References

1. R. C. Ewing, W.J. Weber, W. Lutze, in *Disposal of Weapon Plutonium*. E. R. Merz, C. E. Walter (eds.). Kluwer Academic Publishers, Hingham, MA 1996. P. 65-83.
2. E. C. Buck, B. Ebbinghaus, A. J. Bakel, J. K. Bates, *Mat. Res. Soc. Symp. Proc.* 465 (1997) 1259.
3. S. V. Stefanovsky, S. V. Yudintsev, B. S. Nikonov, B. I. Omelianenko, A. G. Ptashkin, *Mat. Res. Soc. Symp. Proc.* 556 (1999) 121.
4. S. V. Stefanovsky, S. V. Chezhevskaya, *Phys. Chem. Mat. Treat. (Russ.)* [6] (1999) 81.

## A Single Material Approach to Nuclear Waste Disposal

We are developing a novel concept for microencapsulating and chemically fixing actinide and other heavy element ions in phosphate-rich phases in vitreous silica. Our work is based on a chemically functionalized, porous silica that is termed Diphosil. Diphosil was developed by R. Chiarizia and coworkers in a collaboration between Argonne National Laboratory and the University of Tennessee to selectively sorb most actinide ions from nitric acid solutions [1]. Subsequently, EiChroM Industries received support from the U.S. Department of Energy to demonstrate production of Diphosil on an industrial scale. Diphosphonic acid groups provide the chelating power of Diphosil which, unlike Diphonex® resin [2], contains no sulfonic acid groups.

Although Diphosil is ~90 % silica on a dry weight basis, its organic content raises concern about its suitability as a nuclear waste form for high levels of alpha-emitting isotopes due to the possibility of loss of chelating power by radiolytic destruction of its diphosphonic acid groups and hydrogen generation. Our work is addressing such concerns by destroying the organic content of metal ion-loaded Diphosil and then thermally densifying it to encapsulate the sorbed metal ions in vitreous silica, which is one of the most radiation resistant glasses known. It is of technical importance and fundamental interest that we have shown that thermal densification of Diphosil occurs at 1273 K which is ~300 K lower than the temperatures used to make borosilicate-based nuclear waste glass.

Our present work has shown that thermal processing of Diphosil converts sorbed ions into phosphates and converts its organic content into water and carbon dioxide. Further heating results in densification due to pore collapse and creates a nonporous waste form that is primarily vitreous silica. Progress in optimizing our thermal densification process and studies on characterizing the produced waste form will be reported. Much of our work to date on characterizing Diphosil prior to and following thermally densification has exploited the f-state spectroscopic and photophysical properties of heavy metal ions that were sorbed into Diphosil from 0.8 mole/liter nitric acid. For example, the maximum uptake of trivalent f-element ions by Diphosil was determined by monitoring the optical absorbance of a near-infrared 4f-4f absorption band of trivalent neodymium and found to correspond to one neodymium ion per four phosphorous atoms, which is the same ratio of trivalent metal ions to phosphorous atoms as the most stable methanedisphonic acid complex with trivalent europium ions in solution as determined by molecular mechanics modeling [3]. The photodynamics of sorbed trivalent europium ions prior to and following thermal densification have provided evidence as to the number of its inner sphere coordinated water molecules and the proximity of such sorbed metal ions to each other. Recently, we have extended these studies to actinide ions, beginning with uranyl.

Although Diphosil was developed for selective sorption of actinide ions from nitric acid solution, our work has shown that it is capable of sorbing trivalent metal ions from concentrated phosphoric acid that contains a low concentration of nitric acid. This solution composition corresponds approximately to that expected to be the spent working medium from a combined nitric acid - phosphoric acid oxidation process. This process has been shown to destroy such oxidation-resistant

**James V. Beitz,**  
**Clayton W. Williams**  
*Argonne National  
Laboratory, Argonne,  
IL 60439-4831, USA*

materials as polyethylene and was developed to pilot scale by the Westinghouse Savannah River Company for volume reduction of approximately 1 millions pounds of organic material that is contaminated with Pu-238 [4].

Our current work on Diphosil is being carried out as part of the Nuclear Energy Research Initiative of the Office of Nuclear Energy, Science and Technology of the U. S. Department of Energy under contract W-31-109-ENG-38. The concept of thermally densifying metal ion-loaded Diphosil to create a candidate nuclear waste form emerged from work performed for the Division of Chemical Sciences, Office of Basic Energy Sciences, U. S. Department of Energy.

### References

1. R. Chiarizia, E. P. Horwitz, K. A. D'Arcy, S. D. Alexandratos, and A. W. Trochimczuk, *Solvent Extr. Ion Exchange*, **14**, 1077-1100 (1996).
2. Diphonix is a registered trademark of EiChroM Industries (Darien, IL).
3. K. Nash, *J. Alloys Comp.* **249**, 33-40 (1997).
4. *Nitric - Phosphoric Acid Oxidation of Organic Waste Materials*, R. A. Pierce and J. R. Smith, Westinghouse Savannah River Company Report WSRC-95-0471, dated 1995.

## Immobilization of Pu-Containing Solution using a Porous Crystalline (Gubka) Matrix

Problematic actinide solutions requiring stabilization under Defense Nuclear Facilities Safety Board (DNFSB) Recommendations 94-1 and 2000-1 exist in various compositions at the Savannah River Site (SRS) and the Hanford site. These solutions include isotopes of americium and curium (Am/Cm) at the Savannah River Site and plutonium nitrate solutions at Hanford. A solution stabilization technology using a new silicate matrix, "Gubka," or "sponge" in Russian, has recently been identified. The materials used for this technology will adsorb components such as plutonium, americium, curium and high-level waste from the waste solution at ambient to moderate temperatures, below boiling. Other porous inorganic materials, which were previously tested, included porous glasses, silica gel, foam corundum, porous fireclay (chamotte) and diatomite saturated with the waste components only at solution boiling temperatures; heating at the boiling point is necessary to dry the solid. This paper describes the results of a joint research program of the Russian institutes at St. Petersburg, Krasnoyarsk and the Idaho National Engineering and Environmental Laboratory, which tested the stabilization/immobilization of surrogate actinide solutions containing tracer americium and plutonium using the Gubka matrix.

Gubka material, consisting of glass-ceramic silicate microspheres, was developed by the Institute of Chemistry and Chemical Technology at the Krasnoyarsk Scientific Center from coal power plant fly ash. The Gubka matrix is formed from 10-140 micron cenospheres and has been tested in a number of applications, including high-temperature catalysis,<sup>1</sup> high temperature filtration, and adsorption of problematic solution components. Preliminary studies demonstrated the feasibility of using the Gubka material to stabilize rare earth elements as well as long-lived radionuclides such as technetium-99, zirconium-95 and neptunium. The Gubka material has a high porosity of ~50% and low bulk density of ~0.6 g/cm<sup>3</sup> and has good chemical stability in concentrated nitric acid at temperature 60°C, with mass losses under 1% in three hours. The time of liquid sorption on Gubka is about 30 seconds, and the drying process is finished in about 1 hour at 100°C. Repeated sorption-drying-calcining cycles were performed to achieve the final loading. The surrogate solution of a concentrated filtrate from an oxalate precipitation process, which contained tracer plutonium in a 3.4 M nitric acid, was sorbed by the Gubka matrix. The surrogate solution consisted of added potassium permanganate to the filtrate and was concentrated by evaporation to contain high concentrations of potassium, sodium, aluminum and iron. Chromium, calcium, nickel and magnesium were present in minor amounts. Uranium was used as a surrogate for plutonium. In some cases these solutions were spiked with Pu-239 at 4000 to 10000 Bq/L. The total solution concentration of elements expressed as oxides was about 125.5 g/L. The Gubka sample was dried at 130°C after each cycle, and was calcined at 800°C and 1000°C after the loading cycles were completed. These tests resulted in maximum oxide loading in the Gubka sample of up to about 23 wt. %. The phase compositions of the product are shown in Table 1.

**A.S. Aloy,**  
**N.V. Sapozhnikova,**  
**A.V. Strel'nikov,**  
**D.A. Knecht,**  
*V. G. Khlopin Radium  
Institute, St.  
Petersburg, 194021,  
Russia*

**A.G. Anshits,**  
*Krasnoyarsk Scientific  
Center of Siberian  
Branch of Russian  
Academy of Sciences  
(KSC RAS), 660049,  
Russia*

**A. Tretyakov,**  
*Federal State Unitary  
Enterprise "Mining and  
Chemical Combine"  
(FSUE MCh C),  
Zheleznogorsk,  
Krasnoyarsk Region,  
660033, Russia*

**T. J. Tranter,**  
**J. Macheret**  
*Idaho National  
Engineering and  
Environmental  
Laboratory,  
Idaho Falls, ID 83415,  
USA*

**L. J. Jardine**  
*Lawrence Livermore  
National Laboratory  
(LLNL), Livermore,  
California, 94550,  
USA*

Some of the Gubka samples loaded with oxides were hot pressed. Maximum densification was achieved at 950°C, and linear sample shrinkage of about 35% was reached. The final waste form is a stable ceramic material, suitable for safe, transportation and long-term storage. The detailed results about chemical durability and mechanical properties of the final products will be discussed in the paper.

**Table 1. Phase Composition of Gubka Loaded with Concentrated Simulated Filtrate.**

<b>T, C°</b>	<b>Phase composition</b>	<b>Comments</b>
800	Na <sub>2</sub> U <sub>2</sub> O <sub>7</sub> , (Na <sub>2</sub> UO <sub>4</sub> , UO <sub>2</sub> Cl, KAlSi <sub>2</sub> O <sub>6</sub> , α-Fe <sub>2</sub> O <sub>3</sub> ), amorphous phase	Phase compositions and quantity correlation are the same at both temperatures.
1000		The main crystalline phase is Na <sub>2</sub> U <sub>2</sub> O <sub>7</sub> . The quantities of the other phases are small (traces).

### Reference

1. A. G. Anshits et al., "The Study of Composition of Novel High Temperature Catalysts for Oxidative Conversion of Methane," *Catalysis Today*, **42**, 197 (1998).

# Immobilization of Pu-Containing Wastes into Glass and Ceramics: Results of US-Russia Collaboration

## Introduction

This continuing collaboration between the V.G. Khlopin Radium Institute (KRI) in St. Petersburg, Russia, and Lawrence Livermore National Laboratory (LLNL) in the United States was initiated in 1997. The collaboration is focused on plutonium immobilization to support the disposition of excess weapons plutonium in the US and Russia.

Our work consists primarily of laboratory-scale experiments and studies of borosilicate and phosphate Pu-doped glasses and zircon/zirconia, mono-zirconia, and pyrochlore ceramics. The results were used to compare and evaluate the use of these various materials in Pu immobilization.

## Description

Vitrification of Pu together with high level radioactive wastes (HLW) is a well-known alternative for the immobilization of Pu. During this collaboration, KRI developed and studied an original composition of borosilicate glass (doped with 2.7 wt. % Pu) and of phosphate glass (doped with 4.5 wt. % Pu).

The three ceramic materials studied were zircon/zirconia,  $(Zr,Pu)SiO_4 / (Zr,Pu)O_2$ ; mono-zirconia,  $(Zr,Gd,Pu,\dots)O_2$ , and pyrochlore,  $Ca(Gd,Pu,Hf,U)Ti_2O_7$ . These ceramic materials were chosen because zircon/zirconia and mono-zirconia ceramics doped with 10 wt. % Pu were under consideration in Russia at KRI as attractive Pu waste forms that could be used for the immobilization of actinides; these could then be disposed of in deep geological formations in Russia. The pyrochlore ceramic doped with 10 wt. % Pu and approximately 22 wt. % U was being developed by the US as the matrix for the immobilization of excess US weapons grade Pu.

Our primary goals were to

- Compare each glass.
- Introduce the US experience in the synthesis of the pyrochlore ceramic to Russian specialists, who then would verify the technical results of US teams with independent experiments in Russia.
- Compare the main features of zircon-zirconia and mono-zirconia ceramics with the pyrochlore ceramic in order to provide data to both US and Russian specialists.

All Pu-doped glass and ceramic samples mentioned above were obtained at KRI in the forms of small pellets or beads (1-2 gram of weight each). The Pu-doped samples were studied using x-ray powder diffraction, electron scanning microscopy, microprobe analysis, and leach tests at 25°C and 90°C using the widely accepted MCC-1 test methods developed in the US.

**E. B. Anderson,**  
**A. S. Aloy,**  
**B. E. Burakov**  
*V.G. Khlopin radium  
Institute,  
St. Petersburg, Russia*

**L. J. Jardine**  
*Lawrence Livermore  
National Laboratory,  
Livermore, CA 94550,  
USA*

## Results

Leach tests provided some interesting comparisons. Results obtained indicated that the leach rate of phosphate glass is greater than that of borosilicate glass. The temperature influence on the total leach or dissolution rate is also greater for phosphate glass than borosilicate glass. At 90°C, using the MCC-1 test conditions, the release of Pu and Gd from the phosphate glass was 10 times greater than that from borosilicate glass, and the bulk component releases (Si, B, P, Na) from phosphate glass was two times greater than that from borosilicate glass.

An important aspect of the long-term safety for geologic disposal conditions is the specific behavior of Pu and neutron absorbers such as Gd. At temperatures of 90°C, boron is released very rapidly from borosilicate glass, while the Pu and Gd are released at much lower rates. All ceramic samples-zircon/zirconia, mono-zirconia and US-developed pyrochlore-show higher resistance to Pu leaching by deionized water than either the phosphate or borosilicate glass compositions, despite the fact that some contain separated Pu phases in their ceramic matrices. Zirconia and US-pyrochlore ceramics have almost the same leach rate at 25°C and are also similar at 90°C. The ceramics have different features concerning Am releases under the leach test: pyrochlore ceramic was characterized with a lower level of Am release and the zircon/zirconia ceramic with a higher level of Am release.

This work was performed under the auspices of the U.S. Department of Energy by the Lawrence Livermore National Laboratory under Contract W-7405-Eng-48.

## Performance Evaluation of Pyrochlore Ceramic Waste Forms by Single Pass Flow Through Testing

Titanate-based ceramic waste forms for the disposal of nuclear wastes have been the subjects of numerous studies over the past decades. These studies have generally shown that the chemical durability of titanate ceramic phases such as pyrochlore and zirconolite is better than most other proposed waste forms. Recently, the U.S. Department of Energy selected a titanate as the form of choice for immobilizing surplus weapons-grade plutonium.

In order to assess the performance of this ceramic in a potential Yucca Mountain high-level waste (HLW) repository, it is necessary to understand the kinetics and mechanisms of corrosion of the ceramic under repository conditions. To this end, we are conducting single pass flow-through (SPFT) dissolution tests on ceramics relevant to Pu disposition. The test specimens include both Pu-bearing ceramics and ceramics that incorporate Ce as an analog for Pu. Our tests have been ongoing for over 2.5 years, and are conducted at room temperature and at pH values between 2 and 12. The SPFT test provides the most effective means for assessing the dissolution behavior of materials under conditions far from equilibrium, and can thus be interpreted in terms of a "forward rate," which is reduced under conditions in which the dissolved species are allowed to accumulate in the solution. Therefore, the dissolution rates measured under such far-from-equilibrium conditions are expected to be much higher than the rates under repository conditions, where the groundwaters in contact with degrading waste forms are expected to be relatively stagnant. Rather than measuring the long-term dissolution rates expected in a repository, SPFT experiments provide upper limits, or conservative model parameters for a kinetic model of ceramic dissolution for use in performance assessment.

In SPFT tests, the primary measurements are the concentrations ( $C_i$ ) of ceramic constituents (metal elements) dissolved from a powdered ceramic sample into the effluent buffer solutions as a function of time. A normalized release rate ( $NR_i$ ), or apparent dissolution rate based on element  $i$  is calculated by the following equation:

$$NR_i = \frac{10^{-9} C_i * Q}{S * m * X_i}$$

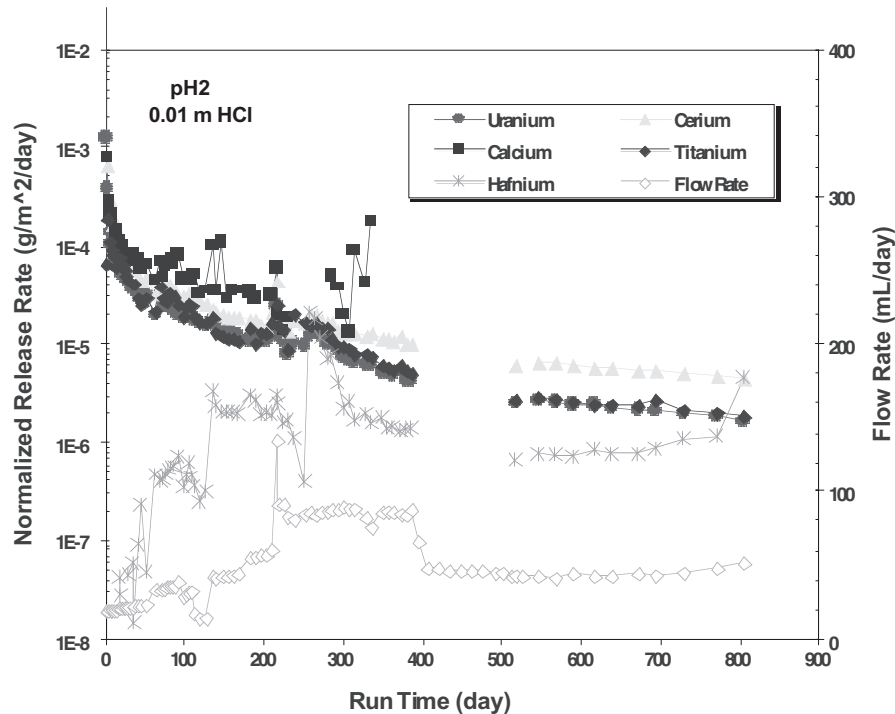
where  $C_i$  is the concentration (ng/mL, corrected with relevant background value) of element  $i$  in a leachate,  $Q$  is the flow rate (mL/day) of effluent buffer solution,  $S$  is the surface area (m<sup>2</sup>/g) of tested sample,  $m$  is mass (g) of the sample, and  $X_i$  is the weight fraction of element  $i$  in the sample.

If the sample dissolves congruently, then all the normalized rates will be the same (*i.e.*, all elements will yield the same rate). Although the flow rate is included in the equation above, the  $NR_i$  will be independent of flow rate ( $Q$ ) if the dissolution of  $i^{\text{th}}$  element is not influenced by the concentration of that element in solution. As an example, Figure 1 shows the release rates of all the major elements in a pyrochlore-based ceramic [(Ca)(Hf,U,Ce)Ti<sub>2</sub>O<sub>7</sub>] at pH 2 as functions of time. The flow rate of the pH 2 buffer solution is plotted along with the release rates.

**P. Zhao**  
G. T. Seaborg Institute  
for Transactinium  
Science  
**W. L. Bourcier,**  
**B. K. Esser,**  
**H. F. Shaw**  
Lawrence Livermore  
National Laboratory,  
Livermore, CA 94551,  
USA

From Figure 1 we can see that the releases of all elements except Hf are nearly congruent. The normalized release rates (except Hf) are also nearly independent of flow rate, indicating that their release rates are not solubility controlled at this pH. The plot also shows a decrease in the rate with time throughout the duration of the tests. This trend may indicate a formation of an alteration layer (enriched in Hf) that is slowing further dissolution.

Figure 1. Normalized release rates of elements and flow rate of pH 2 buffer solution as a function of time.



Our test results have shown that elemental releases become progressively more incongruent as pH increases from 2 to 8. Dissolution rates reach a minimum in the pH range of 8 to 10. For the Ce analog ceramics, the order of release is  $\text{Ca,Ce} > \text{U} > \text{Ti,Hf}$  in weak acidic buffer solutions, and it becomes  $\text{Ca} > \text{U} > \text{Ce, Ti, Hf}$  in solutions with  $\text{pH} > 8$ . Comparable release rates are also observed in SPFT for Pu-containing ceramic, the order of element release tends to be  $\text{Ca} > \text{U} > \text{Gd, Pu} > \text{Ti, Hf}$  in the pH range 2-6. Dissolution rates at all pHs continuously decrease over time, suggesting that long-term rate control of the ceramic dissolution process may be due to transport of water or dissolved species through a leached layer that acts to passivate the surface of the ceramic phase. More complete results, including a discussion of possible dissolution mechanisms, and characterization of the altered solids will be presented at the conference.

### Acknowledgment

This work was performed under the auspices of the U.S. Department of Energy by University of California Lawrence Livermore National Laboratory under contract No. W-7405-Eng-48.

## Experience of V. G. Khlopin Radium Institute on Synthesis and Investigation of Pu-Doped Ceramics

Actinide (An)-doped (An = U, Pu, Np, Am, Cm) ceramics are currently being developed at the V. G. Khlopin Radium Institute for immobilization of weapons-grade Pu and other actinides. These include zircon,  $(Zr,An)SiO_4$ ; zirconia,  $(Zr,An)O_2$ ; mono-phase cubic zirconia,  $(Zr,Gd,An)O_2$ ; garnet,  $(Y,Gd,An)_3(Al,Ga,An)_5O_{12}$ , and perovskite,  $(Y,Gd,An)(Al,Ga)O_3$  [1–3]. We advocate using cold pressing followed by sintering in air at 1450°C–1500°C as the optimal synthesis method for zircon/ zirconia, and mono-phase cubic zirconia ceramics. Garnet/perovskite ceramics, which are attractive for immobilization of actinide-containing waste materials of complex chemical compositions, can be synthesized by melting the oxides at temperatures from 1300°C–1900°C using a “cold crucible” synthesis method.

Polycrystalline samples of these materials were obtained in our laboratory and investigated using SEM, XRD and other methods. These include two samples of Pu-doped zircon  $(Zr,Pu)SiO_4$  (which contains an insignificant amount of secondary zirconia) that were synthesized from sol-gel starting materials sintered in air at 1450°C for 4 hours followed by 1500°C for 3 hours. The zircon samples have the following average compositions: (in samples one and two, respectively) (from electron microprobe analysis, in wt. % element): Zr-45.4 and 46.5; Pu-6.9 and 6.1; Si-15.2 and 14.1. Mono-phase cubic zirconia  $(Zr,Gd,Pu)O_2$ , were synthesized from co-precipitated Zr-Gd-Pu oxalates sintered in air at 1450°C for 2 hours followed by 1500°C for 3 hours. The zirconia material has the following average composition (from electron microprobe analysis, in wt. % element): Zr-48.6; Gd-20.9; Pu-10.3. The garnet/perovskite,  $(Gd,Ce,Ca)_3(Al,Ga,Pu,Sn)_5O_{12}/(Gd,Ce,Ca)(Al,Ga,Pu,Sn)O_3$ , ceramic was obtained from mixed oxide powders melted in air using a hydrogen torch at 1600-1700°C for 10 minutes. The average composition (from electron microprobe analysis, in wt. % element) for the garnet phase is: Gd-36.0; Ce-5.5; Al-12.0; Ga-10.0; Ca-6.0; Pu-5.3; Sn-0.1, and for perovskite phase: Gd-58.0; Ce-4.0; Al-10.0; Ga-0.4; Ca-1.0; Pu-6.5; Sn-0.2.

Our research has shown that mono-phase cubic zirconia has the highest loading capacity for Pu (not less than 10 wt. %) in the form of Zr-Pu solid solution. Zircon host-phase provides complete incorporation of 6.9 wt. % Pu into zircon crystalline structure; however, higher Pu loading into initial precursor phases causes formation of separated  $PuO_2$  in the final polycrystalline zircon. Incorporation of actinides into the garnet and perovskite crystal structures depends on waste chemical composition, and in our experiments we were able to incorporate approximately 5–6 wt. % Pu. We will also discuss the industrial scale applications of these suggested ceramic waste forms.

**B. E. Burakov,  
E. B. Anderson,  
V. G. Khlopin**  
*Radium Institute,  
St. Petersburg,  
194021, Russia*

## References

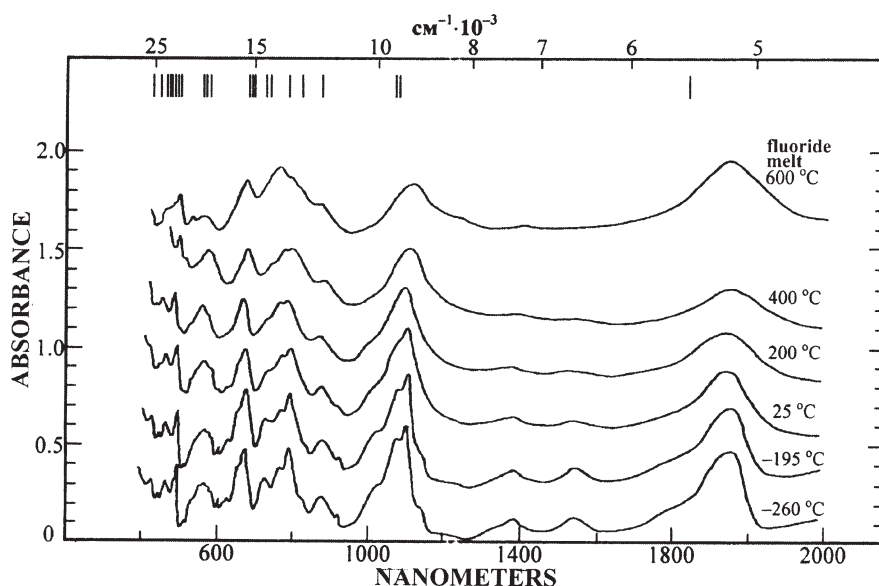
1. Burakov, B. E, Strykanova, E. E. (1998), Garnet Solid Solution of  $Y_3Al_5O_{12}$ - $Gd_3Ga_5O_{12}$ - $Y_3Ga_5O_{12}$  (YAG-GGG-YGG) as a Prospective Crystalline Host-Phase for Pu Immobilization in the Presence of Ga, *Proceedings of the International Conference Waste Management'98, Tucson, Arizona, USA, 1-5/03/1998, CD version, <http://localhost:6017/html/sess34/34-05/34-05.htm>*.
2. Burakov, B. E, Anderson, E. B. (1998), Development of Crystalline Ceramic for Immobilization of TRU Wastes in V. G. Khlopin Radium Institute, *Proceedings of the 2<sup>nd</sup> NUCEF International Symposium NUCEF'98, 16-17/11/98, Hitachinaka, Ibaraki, Japan, JAERI-Conf.99-004 (Part I), 295-306*.
3. Burakov, B. E, Anderson, E. B, Knecht, D. A (1999), Ceramic Forms for Immobilizing Pu Using Zr, Y, Al Metal Additives, *Environmental Issues and Waste Management Technologies IV*, American Ceramic Society, Westerville, Ohio 349-356.

## Absorption Spectra of Plutonium in Phosphate and Borosilicate Glasses

The aim of this work is to characterize the oxidation states and coordination behavior of Pu in glasses used for excess weapons plutonium-containing materials and waste immobilization. To this end, we studied absorption spectra of Pu in the borosilicate glass of the composition developed at Khlopin Radium Institute, as well as absorption spectra of Pu in an aluminophosphate glass (for the first time, as far as we know).

Temperature dependencies of the Pu spectra (0.4-2.5  $\mu$ ) were studied in the range from -260°C (12 K) to the temperatures slightly exceeding those corresponding to the maximum crystallization rates of the glasses (450 $\pm$ 10°C for the phosphate glass and 570 $\pm$ 10°C for the borosilicate glass).

As an example, absorption spectra of Pu (up to 400°C) are shown in Fig. 1, and the wavelengths of the principal maxima of both phosphate and borosilicate glasses are given in Table 1.



Yu .A. Barbanel',  
A. S. Aloy,  
V. V. Kolin,  
V. P. Kotlin,  
A. V. Trofimenko  
V. G. Khlopin Radium  
Institute, St.  
Petersburg, Russia

Figure 1. Absorption spectra of Pu in phosphate glass. For comparison, the absorption spectrum of Pu (IV) in the LiF-NaF-KF (46.5-11.5-42 mol %) eutectic melt at 600oC [3] is also presented (upper line). In the top, the Pu4+ free ion energy levels are plotted basing on the data in Ref. [4].

System	T, °C	$\lambda$ , nm								
Borosilicate glass	-260	-	631	656	754	799	854	1046	1106	1760
	25	-	634	660	760	801	854	1060	1103	1785
	(25)**	-	(635)	(659)	(760)	(793)	-	(1069)	(1108)	(1786)
Phosphate glass	500	-	635	662	662	806	876	-	1100	-
	-260	-	-	665	758	783	870	-	1096	1956
	25	-	-	665	761	782	867	-	1095	1944
Fluoride melt	400	485	-	666	763	786	873	-	1098	1945
	600	482	-	660	745	-	-	-	1102	1936

\*For comparison, the data for fluoride melt are also presented.

\*\*The data from Ref. 1 are given in parentheses.

Table 1. Observed Band Positions for Pu (IV) in Borosilicate and Phosphate Glasses.\*

Although the borosilicate glass used in this work differs in the composition from that in Ref. 1 (in particular, it is lower in Si and higher in B), the room-temperature spectrum (to be given in our presentation along with both low- and high-temperature spectra) is quite similar to the corresponding spectrum in Ref. 1. Also, as seen from Table 1, the observed band positions do not markedly differ from those in Ref. 1 (values in parentheses). In accordance with the findings by Karraker<sup>2</sup> and Eller *et al.*,<sup>1</sup> we can conclude that at room temperature plutonium exists in our borosilicate glass as Pu(IV). Since no principal changes in the spectra (except for the appearance of a fine structure at low temperatures) are observed with varying the temperature, we can suggest that the same valence state is predominant throughout the temperature range studied.

As for the phosphate glass (Fig. 1.), the absorption features characteristic of Pu(III) (the maxima at 1530 and 1380 nm and enhanced absorption near 555 nm) are clearly seen from the spectra, along with the strong Pu(IV) bands whose wavelengths are listed in Table 1. As seen from Fig. 1, the features assigned by us to Pu(III), especially the maxima at 1530 and 1380 nm, strengthen with lowering the temperature. Notably, the latter maxima are observed in the spectral region 1300-1600 nm, where no optical transitions belonging to Pu(IV) can appear in accordance with the Carnall and Crosswhite's energy level data [4] plotted in the top of the figure. The intense absorption in the region 1300-1600 nm was observed by us earlier for Pu(III) spectra in chloride and fluoride melts; it was assigned to hypersensitive transitions, predominantly to  ${}^6F_{1/2} \leftarrow {}^6H_{5/2}$  [3].

It should also be emphasized that the spectra of Pu(IV) in phosphate glass (Fig. 1 and Table 1) strikingly resemble its spectrum in fluoride melt obtained by us earlier;<sup>3</sup> the coordination number 8 may be inferred for Pu in the both media. This offers promise of further detailed comparison of the Pu spectra in glass and molten salts. Moreover, both a wide range of optical transparency of molten salts in the near infra-red and lesser overlapping of principal bands in this region will probably make molten salts more suited, compared to aqueous solutions, as reference media for inferring the valence states and coordination properties of the f- and d-elements in glasses used for waste immobilization.

### Acknowledgments

Authors thank Dr. Leslie Jardine (LLNL) for the attention to this work and support.

Work performed under the auspices of the U.S. Department of Energy by Lawrence Livermore National Laboratory under Contract W-7405-Eng-48 and under specific LLNL Agreement - B 501118.

## References

1. Eller P. G., Jarvinnen G. D., Purson J. G., Penneman R. A., Ryan R. R., Lytle F. W. and Greeger R. B. // *Radiochim. Acta*. 1985. Vol. 37, P. 17.
2. Karraker D. G. // *J. Am. Ceram. Soc.* 1982. Vol. 65, N 1, P. 53.
3. Yu. A. Barbanel', *Coordination chemistry of f-elements in melts (in Russian)*, Energoatomizdat, Moscow (1985), and refs. therein.
4. W. T. Carnall, H. M. Crosswhite, *Optical spectra of actinide ions in compounds and in solution*. Argonne National Laboratory report, ANL-84-90. Argonne, Illinois (1985).

## Microstructure and Thermodynamics of of Zirconolite- and Pyrochlore-Dominated Synroc Samples: HRTEM and AEM Investigation

**Huifang Xu**  
University of  
New Mexico,  
Albuquerque, New  
Mexico 87131, USA

**Yifeng Wang**  
Sandia National  
Laboratories,  
Carlsbad, New  
Mexico 88220, USA

Development of highly durable waste forms is the key to permanent disposal of high-level waste (HLW), including surplus weapons-usable plutonium in geologic repositories. *Synroc* is a durable titanate ceramic waste form with zirconolite ( $\text{CaZrTi}_2\text{O}_7$ ), pyrochlore ( $\text{Ca}(\text{U,Pu})\text{Ti}_2\text{O}_7$ ), perovskite ( $\text{CaTiO}_3$ ), hollandite as major crystalline phases and has been shown to be particularly promising for immobilizing various high level wastes. The concept of *Synroc* was originally proposed by Ringwood et al. in Australia, and the first *Synroc* fabrication technology was developed by Dosch et al. at Sandia National Laboratories. During the last two decades, *Synroc* has been subjected to extensive studies. *Synroc* immobilizes radionuclides by incorporating them into appropriate mineral structures and forming solid solutions. With large polyhedra (with coordination numbers ranging from 7 to 12) in mineral structures, *Synroc* is able to accommodate a wide range of radionuclides (e.g., actinides, Pu, U, Ba, Sr, Cs, Rb, Tc, etc.) as well as neutron poisons (e.g., Gd). U- and Pu-loaded *Synroc* is generally dominated by phases of pyrochlore and zirconolite, a derivative structure of pyrochlore. The pyrochlore phase can incorporate more Pu than the zirconolite phase. Various *Synroc* formulations (e.g., *Synroc-C*, *Synroc-D*, *Synroc-E*, *Synroc-F* etc.) have been developed for specific HLWs. *Synroc* has been shown to be much more chemically durable and radiation-resistant than borosilicate glass waste forms.

*Synroc* waste forms can be prepared by either a sol-gel method or a melting. The *Synroc* prepared by the sol-gel method is usually fine-grained and relatively uniform. Textural heterogeneity in the *Synroc* can directly impact the incorporation of radionuclides into crystalline phases and the resistance of *Synroc* to leaching processes. In this paper, we study the mineralogy and microstructure evolution of a *Synroc* crystallized from a melt with zirconolite ( $\text{CaZrTi}_2\text{O}_7$ ) composition. A  $\text{CaCeTi}_2\text{O}_7$  composition was also described.

Scanning electron microscopy (SEM), high-resolution transmission electron microscopy (HRTEM), and analytical electron microscopy (AEM) studies have been conducted on samples crystallized from melts with a composition of zirconolite  $\{(\text{Ca}_{0.9}\text{Gd}_{0.1})\text{Zr}(\text{Ti}_{1.9}\text{Al}_{0.1})_2\text{O}_7\}$  and  $\text{CaCeTi}_2\text{O}_7$ . The formation of a whole suite of *Synroc* phases (zirconia,  $\text{ZrTiO}_4$ , zirconolite, perovskite, and rutile) has been observed. In the  $\text{CaZrTi}_2\text{O}_7$  system, the formation of these minerals follows the crystallization sequence of Ti-bearing zirconia  $\rightarrow$   $\text{ZrTiO}_4$  phase  $\rightarrow$  Zr-rich zirconolite  $\rightarrow$  Zr-poor zirconolite  $\rightarrow$  rutile/perovskite. This sequence is induced by a fractional crystallization process, in which Zr-rich mineral phases tend to crystallize first, resulting in continuous depletion of Zr in melt. Consistent with this melt compositional evolution, the Zr content in the zirconolite decreases from the area next to the  $\text{ZrTiO}_4$  phase to areas next to rutile or perovskite. High-resolution TEM images show that there are no glassy phases at the grain boundary between zirconolite and perovskite. The fractional crystallization-induced textural heterogeneity may have a significant impact on the incorporation of radionuclides into crystalline phases and the resistance of radionuclides to leaching processes. Exsolution lamellae and multiple twinning resulting from the phase transition from tetragonal zirconia to monoclinic zirconia may decrease

durability of the Synroc. Fast cooling of the melt may produce more zirconolite phase and relatively uniform texture. In the system of Ce-pyrochlore ( $\text{CaCeTi}_2\text{O}_7$ ), there are no glass-like materials at the grain boundaries. Non-stoichiometry of the Ce-pyrochlore results from small amount (up to 20%) of trivalent Ce in the Ce-pyrochlore. In general, however, a Synroc prepared by melting is less uniform in texture than that prepared by a sol-gel method. Phase diagrams for zirconolite and pyrochlore systems are also proposed.

# Electron Microscopy Study of a Radioactive Glass-Bonded Sodalite Ceramic Waste Form

Wharton Sinkler,  
Thomas P. O'Holleran,  
Tanya L. Moschetti  
Argonne National  
Laboratory - West,  
PO Box 2528 Idaho  
Falls, ID 83403

## 1. Introduction

Argonne National Laboratory has developed a process to immobilize a high-level waste (HLW) stream consisting of spent electrolyte halide salts by incorporating these into a ceramic waste form (CWF)<sup>1-3</sup>. The salt electrolyte, a (Li,K)Cl eutectic, is used for electrometallurgical treatment of metallic spent nuclear fuel (SNF). In the course of processing, the salt retains active fission products and plutonium as well as sodium from the fuel bonding. The first step in treating the spent electrolyte is to absorb (occlude) the salt into a Linde Type A (LTA) zeolite. Occlusion reduces the quantity of free chloride to less than 0.5% of that present in the initial salt. The salt occluded zeolite is then mixed with a borosilicate glass and hot isostatically pressed (HIPed) to produce the CWF. The HIP conditions convert the LTA zeolite to sodalite. This paper presents the first results of scanning and transmission electron microscopy (SEM and TEM) characterizations of a CWF made from salt used to electrorefine Experimental Breeder Reactor II (EBR II) driver fuel elements. The goals of the study are to gain a detailed understanding of microstructure and phase formation. This serves as a guide for process development, and also towards interpreting leach test results and developing models to predict long-term repository performance.

## 2. Experimental

The CWF was produced by blending salt waste from electrorefinement of 100 EBR II driver elements with LTA zeolite at 500°C in a mixture containing 10.5 wt% salt. The salt-occluded zeolite was mixed with 25 wt% glass frit and HIP'ed at 850°C and 100 MPa for 1 h at temperature. The HIP cans were cut open and core drilled to obtain specimens. SEM samples were mounted in epoxy and polished to a 1200 grit finish using silicon carbide paper. They were then coated with conductive film prior to examination in a Zeiss DSM 960A SEM. TEM samples were first mechanically thinned and core drilled to obtain a 3 mm disk of approximately 120 mm thickness. Following dimpling, final thinning was performed by ion milling. The samples were given a thin carbon coating and were examined using a JEOL 2010 TEM.

## 3. Results and Discussion

The overall microstructure of these materials is illustrated in a SEM micrograph shown in Figure 1a. Two types of regions are predominant in the SEM image. The first is polycrystalline sodalite, which has a rough or uneven contrast. Also, a number of extended glass regions are visible. Actinide bearing phases in Fig. 1a are seen as bright features preferentially located at sodalite/glass interfaces, or along boundaries between sodalite regions.

The actinide rich phase detected in SEM was further investigated using TEM. Fig. 1b is a bright field TEM image of a glass region between two polycrystalline sodalite granules. In the image, the fine-grained dark phase within the glass was identified using energy dispersive spectroscopy and electron diffraction as a (U,Pu)O<sub>2</sub> solid solution. As shown, it tends to occur within the glass near the

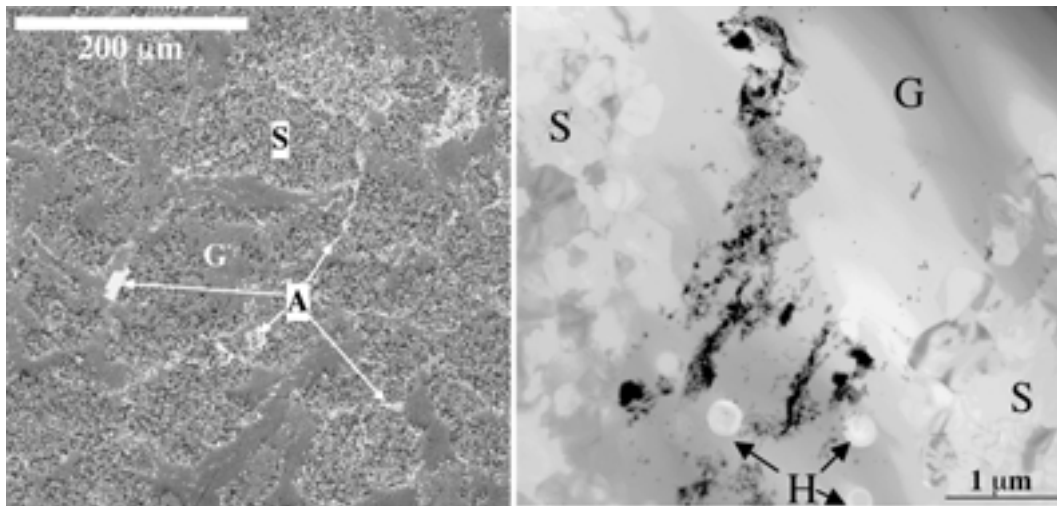


Figure 1. a) Back scattered scanning electron micrograph showing sodalite (S), glass (G), and actinide bearing phases (A). The apparent porosity in the sodalite is a sample preparation artifact. b) Bright field TEM image. Dark phase in glass is (U,Pu)O<sub>2</sub>, with grain sizes as small as 20 nm. H: indicates examples of halite crystals.

glass/sodalite boundary. In addition to the (U,Pu)O<sub>2</sub> phase, crystals of halite can be seen. Analysis of the salt occluded zeolite feed material has shown that uranium and plutonium chloride species react during occlusion with residual water in the zeolite to form oxides that deposit on the surface of the zeolite granules. During HIPing, the glass dissolves some of the zeolite/sodalite, leaving the (U,Pu)O<sub>2</sub> crystals within the glass, and also precipitating sodium chloride. This hypothesis is supported by x-ray diffraction results, which indicate halite forms during the HIP process, and analytical microscopy, which has revealed concentration gradients in the glass near the surfaces of sodalite regions. Because of the fine-grained (U,Pu)O<sub>2</sub> microstructure, most of the plutonium released during leach tests is likely released as colloids. The mechanism of plutonium release is of great interest from a repository performance standpoint, and is under study using a comprehensive test matrix of immersion tests.

### Acknowledgments

This work was supported by the Department of Energy, Nuclear Energy Research and Development Program, under contract No. W-31-109-ENG-38.

### References

1. R. W. Benedict and H. F. McFarlane, "EBR II Spent Fuel Treatment Demonstration Project Status," *Radwaste* 5 (1998).
2. T. L. Moschetti, T. P. O'Holleran, S. M. Frank, S. G. Johnson, D. W. Esh and K. M. Goff, *Ceramic Transactions* 94, to be published (2000).
3. W. Sinkler, D. W. Esh, T. P. O'Holleran, S. M. Frank, T. L. Moschetti, K. M. Goff, and S. G. Johnson, *Ceramic Transactions* 94, to be published (2000).

## Site Preferences of Actinide Cations in [NZP] Compounds

**H. T. Hawkins,  
D. R. Spearing,  
D. M. Smith,  
F. G. Hampel,  
D. K. Veirs**

*Los Alamos National  
Laboratory, Los  
Alamos, NM 87545  
USA*

**B. E. Scheetz,**  
*Materials Research  
Laboratory, The  
Pennsylvania State  
University, University  
Park, PA 16802.*

Compounds adopting the sodium dizirconium tris(phosphate) ( $\text{NaZr}_2(\text{PO}_4)_3$ ) structure type belong to the [NZP] structural family of compounds. [NZP] compounds possess desirable properties that would permit their application as hosts for the actinides.<sup>1-3</sup> These properties include compositional flexibility (i.e., three structural sites that can accommodate a variety of different cations),<sup>4-6</sup> high thermal stability,<sup>7</sup> negligible thermal expansion,<sup>8-10</sup> and resistance to radiation damage.<sup>11</sup> Experimental data indicate that [NZP] compounds resist dissolution and release of constituents over a wide range of experimental conditions.<sup>12,13</sup> Moreover, [NZP] compounds may be synthesized by both conventional and novel methods and may be heat treated or sintered at modest temperatures (800°C–1350°C) in open or restricted systems.<sup>2</sup>

The ease and flexibility of synthesizing these compounds, coupled with their attractive combination of thermal and chemical stability, make [NZP] compounds ideal hosts for the actinides. The desirable properties of this structural family are attributed to the [NZP] structure, a three-dimensional anionic framework of strongly bonded polyhedra that provides the stability and flexibility necessary to form continuous ranges of solid solution with approximately two-thirds of all known elements.<sup>4</sup> The [NZP] structure, which may be represented by the general formula  $M'M''_{1-3}A_2(\text{PO}_4)_3$ , offers two types of sites for chemical substitutions: an octahedral framework site (A) and interstitial sites ( $M'$  and  $M''$ ). Tetravalent and trivalent transition metal cations, such as  $\text{Ti}^{4+}$ ,  $\text{Hf}^{4+}$ ,  $\text{Zr}^{4+}$ ,  $\text{Fe}^{3+}$ , and  $\text{Sc}^{3+}$  have been shown to occupy A with corresponding changes in framework dimensions and/or symmetry; these changes are coupled with changes in the size and oxidation state of the A site occupant. Trivalent lanthanide cations ( $\text{Ln}^{3+}$ ) have been shown to occupy  $M'$  and to form [NZP] compounds of  $\text{Ln}_{1/3}A_2(\text{PO}_4)_3$  stoichiometry.<sup>5</sup>

As the chemistries of the actinides show similarities to those of the transition metals and the lanthanides,<sup>14</sup> our work is aimed at examining the site preference of actinide cations in [NZP] and establishing the ranges of solid solubility between [NZP] compounds and alkali actinide phosphates of similar stoichiometry, such as  $\text{KU}_2(\text{PO}_4)_3$ . Actinide-bearing [NZP] compounds and alkali actinide phosphates were prepared under carefully controlled conditions using special equipment to ensure their safe handling. A battery of structural and spectroscopic techniques including powder X-ray diffraction (coupled with the Rietveld method<sup>15</sup>) and diffuse reflectance spectroscopy were used to probe the structure of the actinide-bearing [NZP] compounds and to determine the chemical states and local coordination environments of the actinide dopants therein.

Our recent work established the preference of  $\text{U}^{4+}$  for the octahedrally-coordinated A site in [NZP].<sup>16</sup> Compounds in the series  $\text{KZr}_{2-x}\text{U}_x(\text{PO}_4)_3$  ( $0 \leq x \leq 0.20$ ;  $x = 2$ ) were prepared from sol-gel derived precursors in an argon environment. Rietveld refined X-ray powder diffraction data of  $\text{KZr}_{2-x}\text{U}_x(\text{PO}_4)_3$  ( $0 \leq x \leq 0.20$ ) confirmed an [NZP] structure and suggested random occupation of A by  $\text{U}^{4+}/\text{Zr}^{4+}$  and  $\text{K}^+$  occupation of  $M'$  only. The presence of U(IV) was established by comparison of the diffuse reflectance spectra of  $\text{KZr}_{2-x}\text{U}_x(\text{PO}_4)_3$  ( $0 \leq x \leq 0.20$ ) with those of other U(IV) phosphates. Using the Rietveld method and an ab-initio approach, we solved the structure of  $\text{KU}_2(\text{PO}_4)_3$ , the end member of the  $\text{KZr}_{2-x}\text{U}_x(\text{PO}_4)_3$  series.

$\text{KU}_2(\text{PO}_4)_3$  adopts a monoclinic structure that is not isostructural with [NZP], which suggests incomplete solid solubility of  $\text{KU}_2(\text{PO}_4)_3$  in [NZP].

Compounds in the series  $\text{KZr}_{2-x}\text{Pu}_x(\text{PO}_4)_3$  ( $0 \leq x \leq 0.35$ ;  $x = 2$ ) were prepared with a solution-based method followed by heat treatments in air at  $1000^\circ\text{C}$ , thus avoiding the reduction of Pu(IV) to Pu(III). The Rietveld method was applied to the powder X-ray structure refinement of compounds in the series  $\text{KZr}_{2-x}\text{Pu}_x(\text{PO}_4)_3$  ( $0 \leq x \leq 0.35$ ) to obtain precise structural parameters, and to the quantitative analysis of those samples that were prepared as mixtures of two or more phases. Powder X-ray diffraction data of  $\text{KZr}_{2-x}\text{Pu}_x(\text{PO}_4)_3$  ( $0 \leq x \leq 0.05$ ) confirmed an [NZP] structure and showed an increase in the volume of the unit cell with increasing values of  $x$ ; samples of nominal composition  $\text{KZr}_{2-x}\text{Pu}_x(\text{PO}_4)_3$  ( $0.05 \leq x \leq 0.35$ ) were prepared as mixtures of two or more phases, one of which is isostructural with [NZP].

Alternative synthesis routes to Pu(III/IV)-bearing [NZP] compounds are being explored so that phase-pure compounds may be prepared, and the site preference of  $\text{Pu}^{3+}$  and  $\text{Pu}^{4+}$  may be examined. Characterization of long-term aging effects in actinide-doped [NZP] compounds and determination of the stability of the [NZP] structure in the presence of a radiation field are left to future investigations.

### References

1. Roy, R.; Vance, E. R.; Alamo, J. *Mater. Res. Bull.* **1982**, *17*, 585–589.
2. Scheetz, B. E.; Agrawal, D. K.; Breval, E.; Roy, R. *Waste Manage.* **1994**, *14*, 489–505.
3. Hawkins, H. T.; Scheetz, B. E.; Guthrie, G. D. in *Scientific Basis for Nuclear Waste Management XX*; Gray, W. J., Triay, I. R., Eds.; Materials Research Society: Boston, MA, 1996; Vol. 465, pp 387–394.
4. Alamo, J. *Solid State Ionics* **1993**, *63–65*, 547–561.
5. Alami Talbi, M.; Brochu, R.; Parent, C.; Rabardel, L.; Le Flem, G. *J. Solid State Chem.* **1994**, *110*, 350–355.
6. Kasthuri Rangan, K.; Gopalakrishnan, J. *Inorg. Chem.* **1995**, *34*, 1969–1972.
7. Agrawal, D. K. *J. Mater. Ed.* **1994**, *16*, 139–165.
8. Lenain, G. E.; McKinstry, H. A.; Limaye, S. Y.; Woodward, A. *Mater. Res. Bull.* **1984**, *19*, 1451–1456.
9. Agrawal, D. K.; Roy, R. *J. Mater. Sci.* **1985**, *20*, 4617–4623.
10. Oota, T.; Yamai, I. *J. Am. Ceram. Soc.* **1986**, *69*, 1–6.
11. Kryukova, A. I.; Kulikov, I. A.; Artem'eva, G. Y.; Pechenevskaya, O. V.; Alferov, V. A. *Radiokhimiya* **1992**, *34*, 82–89.
12. Orlova, A. I.; Zyranov, V. N.; Kotel'nikov, A. R.; Demarin, V. T.; Rakitina, E. V. *Radiokhimiya* **1993**, *35*, 120–126.

13. Orlova, A. I.; Zyryanov, V. N.; Egor'kova, O. V.; Demarin, V. T. *Radiokhimiya* **1996**, *38*, 20–23.
14. Kaltsoyannis, N.; Scott, P. *The elements*; Oxford University Press, Inc.: New York, 1999.
15. Rietveld, H. M. J. *Appl. Crystallogr.* **1969**, *2*, 65–71.
16. Hawkins, H. T.; Spearing, D. R.; Veirs, D. K.; Danis, J. A.; Smith, D. M.; Tait, C. D.; Runde, W. H.; Scheetz, B. E. *Chem. Mater.* **1999**, *11*, 2851–2857.

## Actinide -Zirconia Based Materials for Nuclear Applications: Cubic Stabilized Zirconia Versus Pyrochlore Oxide

Concepts about nuclear energy and nuclear materials have changed considerably over the past six decades. Regardless of one's position on the nuclear generation of electric power, there are serious needs for pursuing fundamental and technological science of existing actinide materials. These needs are best addressed by obtaining an atomic and molecular understanding of these actinides and actinide containing materials. Although electro-nuclear energy is considered less polluting in terms of uncontrolled releases (e.g.,  $\text{SO}_2$ , heavy metals,  $\text{CO}_2$ , etc.) into the environment, its use produces solid wastes, which offer a challenge for scientists. Fortunately, concepts are being developed to appropriately handle<sup>1</sup> these materials after irradiation, reprocessing, etc.

One envisioned strategy for addressing several radionuclides of concern, once they are partitioned, is to transmute ("burn"/"incinerate") them in a dedicated reactor or some specific neutron source system, (e.g., accelerator driven system, "ADS") to provide a more suitable material for disposal. The topic of this paper addresses important materials science issues of americium and/or curium materials that are attractive for different nuclear applications, including disposal/storage options.

One disposal approach is to "recycle" americium and/or curium in a uranium- or plutonium-free host, which would avoid production of additional actinides by neutron capture processes. For this application, it would be necessary to provide a structurally and thermochemically stable material for americium and/or curium. This material would need to meet several criteria concerning neutron cross section, chemical inertness with cladding and/or coolant, melting point, phase stability, thermal conductivity, etc. Potential candidates as  $\text{MgO}$ ,  $\text{Y}_2\text{O}_3$ ,  $\text{MgAl}_2\text{O}_4$ ,  $\text{CeO}_2$ ,  $\text{CeN}$ , and others have already been envisioned for this application.<sup>2,3</sup>

We have pursued studies of zirconia-based compounds that can provide either an inert matrix or a diluent in multiphase systems, for incineration/transmutation of actinides (Pu, Am, Cm, etc.) We have incorporated and studied structural aspects of actinides incorporated in cubic, zirconia-based materials (both with and without yttria stabilization), as well as in zirconia-based pyrochlore oxides. From this work, we concluded that cubic yttria-stabilized zirconia (Y-CSZ) materials, which are well known refractory ceramics, would be suitable for transmutation schemes for americium and/or curium. Several experiments have already demonstrated that cubic stabilized zirconia materials are very resistant to neutron irradiation and damages related to fission processes.<sup>4</sup>

One particularly attractive material is a 25 mol % yttria-stabilized matrix, which offers a stable, single phase (fluorite-type structure) material that can incorporate significant quantities of americium and/or curium oxides. In a study with americium, we examined the structural and phase behavior of the  $\text{AmO}_2\text{-ZrO}_2\text{-YO}_{1.5}$  ternary system (see Fig. 1), and also determined that the cubic lattice parameters of the products were linear with the americium composition.

**P. E. Raison**

*Commissariat à  
l'Energie Atomique  
CEA-CADARACHE  
DRN/DEC/SPUA/  
LACA*

*13108 St Paul lez  
Durance, France*

**R. G. Haire**

*Oak Ridge National  
Laboratory, Oak  
Ridge, TN 37831-  
6375, USA*

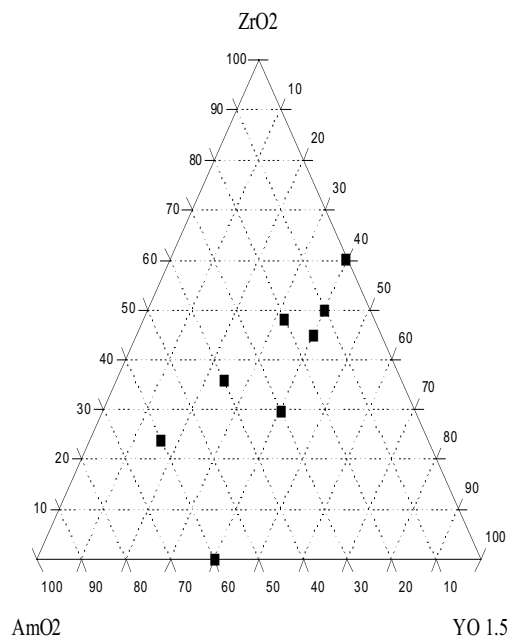
Zirconia-based pyrochlore oxides, which also form refractory ceramics, offer another potential matrix for the transmutation of americium and curium or the incineration of plutonium. The particular pyrochlore oxides discussed here have several common aspects with the components of Synroc,<sup>5</sup> although they exhibit structural differences. They consist of the actinide plus zirconium, and have the general formula,  $A_2B_2O_7$  (where A = actinide and B = zirconium). The “pyrochlore” terminology comes from the structural similarity of the material to the mineral, “pyrochlore.” An interesting aspect of these oxides is that they can exhibit a large domain of homogeneity, which is reflected by the linear variation of cell parameter for the americium containing materials up to 60 mole %  $AmO_2$ .

The presentation will compare and discuss the structural properties of these fluorite-type and pyrochlore-type zirconia systems. In addition, the fundamental physicochemical aspects of these materials with regard to their application in transmutation/incineration schemes will be compared to other materials that have been considered for such applications.

### References

1. B. Barre “The future of nuclear energy in the world,” J. of Alloys and Comp., 271/273 (1998) 1.
2. H. Kleykamp, “Selection of materials as diluents for burning of plutonium fuels in nuclear reactors,” J. Nuc. Mat 275 (1999) 1.
3. A. Languille, P. Millet, J. Rouault, S. Pillon, “Nuclear fuels for actinides burning, CAPRA and SPIN program status,” J. Alloys and Comp., 271/273(1998) 517.
4. K.E. Sickafus, Hj. Matzke, Th. Hartmann, K. Yasuda, J. A. Valdez, P. Chodak III, M. Nastasi, R.A. Verrall, “Radiation damage effects in zirconia,” J. Nucl. Mat., 274 (1999) 66.
5. A. E. Ringwood, S. E. Kesson, K. D. Reeve, D. M. Levins and E. J. Ramm, in “Radioactive waste forms for the future,” eds., W. Lutz and R. C. Ewing, (Elsevier, Amsterdam, 1988), pp.233-334.

Figure 1. The pseudo ternary system  $AmO_2$ - $ZrO_2$ - $YO_{1.5}$ .



## Fundamental Aspects of Actinide-Zirconium Pyrochlore Oxides: Systematic Comparison of the Pu, Am, Cm, Bk and Cf Systems

Zirconium- and hafnium-based oxide materials have gained attraction for various nuclear applications. These materials have features in common with one of the early, well-publicized inorganic ceramics for immobilizing nuclear waste. Synrock, which is a multi-phased titanate system. There have been extensive efforts to establish the materials science and technological application of these materials with the goal of resolving important issues of the nuclear community. As a result, many of these efforts have concentrated on specific f-elements.

Several fundamental science issues are encountered when pursuing the application of these materials, and there have been a number of sophisticated studies performed on them. Our efforts on these materials concentrated on exploring systematically the fundamental solid state chemistry of selected types of these f-element, zirconium- or hafnium-based oxides. We have synthesized and studied polycrystalline pyrochlore oxides of the general formula,  $An_2M_2O_7$  and solid solutions of  $(An,M)O_2$ , where An is considered trivalent Pu, Am, Cm, Bk and Cf, and M is tetravalent Zr or Hf).

Our interests have addressed the fundamental structural and chemical properties of these oxide systems. We pursued both the crystal chemical constraints of the oxide matrices, as well as the importance of the chemistry of the f-elements. By incorporating five actinide elements in our studies, we were able to compare systematically the materials science of these materials with the fundamental chemistry and electronic configurations of these actinides employed. It is expected that this basic information will be useful technologically in the realm of tailor-made materials for different applications.

The polycrystalline pyrochlore oxides discussed here have the general formula of  $A_2M_2O_7$ ; more precisely,  $A_2B_2O_6O^*X$ , where the one oxygen is in a special site (general position) and the X is an oxygen vacancy. The structure can be visualized as a fluorite-type cell with a double unit cell and an ordered deficiency of oxygen atoms. If the oxygen vacancy is filled fully (e.g., the trivalent actinide ion is oxidized fully), a solid solution of the dioxides may be generated. Formation of this pyrochlore structure is possible only if  $A^{3+}$  is larger than  $B^{4+}$ , and the ratio  $r_{A^{3+}}/r_{B^{4+}}$  is between 1.46 and 1.80. Using accepted values for  $An^{3+}$  radii, this suggests such pyrochlore oxides would form for the actinides through Es in the series.

From a structural standpoint, the special oxygen site (located in 48f, space group Fd3m, no. 227) has one unknown structural parameter, x. Generally, such parameters are obtained from diffraction experiments, but given the difficulty with radioactive materials and the limited quantities of these higher actinides, we explored a calculation approach based on valence-bond relationships, where priori assumptions about the nature of the chemical bonds or knowledge of the radii are not required. From the experimental cell parameter, it is then possible to deduce the structural parameter, x. We have used this approach to estimate this parameter for these actinide pyrochlores and several lanthanide pyrochlores.

**R. G. Haire**  
Oak Ridge National  
Laboratory, Oak  
Ridge, TN 37831-  
6375, USA

**P. E. Raison**  
Commissariat à l'  
Energie Atomique,  
CEA-Cadarache DRN/  
DEC/SPUA/LACA  
108 St. Paul lez  
Durance, France

One observes an excellent correlation between the ionic radii of the trivalent metal ions of actinides and lanthanides and the lattice parameters of the pyrochlores. This relationship is useful in conceiving and/or forming custom pyrochlore ceramics for various technological applications. This relationship also provides predictability of crystal lattice parameters and/or the degree of reduction of the f element for pure or mixed f-element pyrochlore oxides.

For f-elements that can exhibit both a trivalent and a tetravalent oxidation state, a solid solution of the f-element and the transition metal dioxides may be generated via oxidation of the pyrochlore oxides; the stoichiometry required for the pyrochlore fixes the mole ratio of the metal ions at ~50 mol %. Thus, for some of the f-elements, an oxidation/reduction cycle can be established, that appears as a form of a Born-Haber cycle. This cycle for these pyrochlore oxides involves (1) the reduced pyrochlore oxide; (2) an oxygen-rich pyrochlore oxide; (3) an oxygen deficient dioxide solid solution; and (4) a solid solution of the dioxides. The five transneptunium elements discussed here are all known to form dioxides, but the extent to which this cycle is observed for each element depends on the pseudo-oxidation potential of the f-element and the stabilization afforded by the two crystal forms.

The presentation will present the structural data obtained for the different actinide materials and compare them with known data for the lanthanide elements. Important structural aspects of the pyrochlore oxides, the actinide oxide phase behavior and the pseudo-oxidation potentials of the actinide elements will be discussed in the context of formation and stability of these pyrochlore materials. In addition, comments concerning the physicochemical nature of these materials with regard to their technological applications will be mentioned.

## Identification of Source Term of Plutonium in the Environment Around WIPP Site

The WIPP Site is the first transuranic disposal facility. It lies 2,150 feet underground in stable salt formations. The major radionuclides in the inventory for disposal are plutonium and americium in the contact handled (CH) TRU waste; and cesium, strontium, and plutonium in the remote handled (RH) TRU waste.

The two potential airborne emission sources are from the underground repository and/or from the waste handling building. The air emissions from the waste handling building are filtered through HEPA filtration systems before they are discharged to the environment. However, the airborne effluents from the underground during the normal operation mode are discharged through the ventilation exhaust to the environment without filtration.

Chronic releases are not expected at the WIPP Site because the TRU waste is contained; however, in the most unlikely event of unplanned release, the HEPA filtration system is triggered when a disposal room continuous air monitor (CAM) exceeds the preset alarm level for alpha and beta/gamma. These airborne effluent emissions to the environment are regulated by 40 CFR 191, Subpart A, and 40 CFR 61, Subpart H. The effluent chronic release monitoring of the exhaust shaft is accomplished with fixed air samplers (FAS) with a flow rate of 2.0 cubic feet per minute at station A for compliance purposes.

The source identification and discrimination from radon and thoron progeny imposes certain problems in the underground ventilation to calculate the set point for CAMS. Also, the limitations of collecting representative samples, salt dust loading corrections, and selecting alarm set-point of the CAM to reduce false alarms in relation to DAC- hours are evaluated. The airborne effluent monitoring compliance is achieved with sensitive real-time air monitors, and analysis of air filters from the fixed air samplers.

**Balwan Hooda,**  
**Carl Ortiz**  
*Westinghouse, WIPP,*  
*Carlsbad, NM 88221,*  
*USA*

## Elimination or Reduction of Magnesium Oxide as the Engineered Barrier at the Waste Isolation Pilot Plant

Matthew K. Silva  
Environmental  
Evaluation Group  
Albuquerque, NM  
87109, USA

The Waste Isolation Pilot Plant was built by the U.S. Department of Energy for the deep geologic disposal of transuranic (TRU) waste contaminated with 13 metric tons of  $^{239}\text{Pu}$ . Emplacement began in March 1999 after the U.S. Environmental Protection Agency (EPA) certified<sup>1</sup> that the U.S. Department of Energy (DOE) met the EPA Standards for disposal. Re-certification is required every five years with the first re-certification due in March 2004.

The EPA certification requires the DOE to emplace  $\text{MgO}$  adjacent to each contact handled (CH) TRU waste container for a total of 85,600 tons of magnesium oxide. Shortly after certification and prior to receiving any waste, the DOE Carlsbad Area Office (DOE/CAO) expressed a desire to reduce or eliminate the use of magnesium oxide.<sup>2</sup> Elimination or reduction in the amount of  $\text{MgO}$  reopens a litany of concerns raised during the certification process. The EPA is relying on the  $\text{MgO}$  to

- decrease actinide solubility,
- minimize uncertainty in calculated actinide solubility,
- decrease gas production due to corrosion,
- eliminate carbon dioxide impact on retardation,
- reduce complexation of actinides with chelating agents,
- reduce microbial degradation of organic waste materials,
- reduce availability of mobilizing water,
- reduce water contact with drums by forming dense layers of cementitious material.

The calculated actinide releases over the next 10,000 years must not exceed the amounts specified by the EPA Standards. The performance assessment (PA) calculations credit  $\text{MgO}$  with a reduction in plutonium solubility. The PA also takes credit for the postulated benefits of  $\text{MgO}$  by eliminating certain transport factors from consideration in the calculation. For example, the impact of chelating agents on transport (increased actinide solubility and reduced retardation) is not included in the calculations on the basis that the presence of  $\text{MgO}$  will eliminate such effects.

Given the inherent uncertainty in 10,000 year predictions, the EPA Standards also contain the assurance requirements including the use of natural and engineered barriers. While many alternatives for engineered barriers were examined, one engineered barrier is used—magnesium oxide—as a backfill.

There may be valid reasons for selecting another engineered barrier and eliminating the use of  $\text{MgO}$ . For example, hanging sacks of  $\text{MgO}$  on each container and placing  $\text{MgO}$  on top of each stack of containers is costly and requires workers to be in close proximity to the waste. The results from the Los Alamos Source Term Test Program (STTP) with actual transuranic waste raise serious questions about the behavior of  $\text{MgO}$ . In the one container to which  $\text{MgO}$  was added, the actinide concentrations initially dropped from 90 ppm, then doubled to 200 ppm.<sup>3</sup>

The DOE and EPA provide disparate explanations of the anticipated behavior of MgO in the repository. The EPA maintains that magnesium oxide will hydrate to form brucite, brucite will react with CO<sub>2</sub> to form nesquehonite (observed in SNL experiments), and nesquehonite will rapidly alter to hydromagnesite or hydromagnesite-like solids (not observed in Sandia National Laboratories—SNL experiments).<sup>4</sup> The DOE, on the other hand, maintains that nesquehonite will never be produced in the WIPP.<sup>5</sup>

It is difficult to determine which explanation is correct. Neither argument has the support of directly applicable experimental results. Rather, the arguments rely on inference and extrapolation from experiments designed to address far different questions under far different conditions. For example, the EPA argument relies on the results of scoping experiments conducted by SNL. As noted by the DOE:

It is imperative to note that those experiments were conducted to investigate long-term reactivity of MgO with CO<sub>2</sub>, to address concerns of the Conceptual Model Peer Review Panel (Papenguth et al., 1997). Those experiments were not designed to define the mineral assemblage used in actinide-solubility calculations.<sup>5</sup>

Nonetheless, the observation of nesquehonite with no conversion to hydromagnesite is important. The DOE model for thorium solubility, which was used to represent plutonium solubility, calculated that the presence of nesquehonite would increase actinide solubility. Increasing actinide solubility would promote mobility. By definition, such a finding would disqualify MgO as an engineered barrier.

At WIPP, the MgO must first react with brine to form brucite [Mg(OH)<sub>2</sub>]. SNL<sup>6</sup> observed the formation of Mg(OH)<sub>2</sub> occurs in de-ionized water. But for experiments conducted at 25°C with Salado and Castile brines, there was no formation of brucite after more than a year. It appears that the high salinity found in WIPP brines favors the formation of sorel cement instead. The experiments conducted by SNL also indicate that the formation of brucite is electrolyte dependent. The magnesium ions in WIPP brines appear to inhibit MgO hydration and the reaction to brucite. Brines without magnesium are less inhibiting to hydration of MgO and brucite production. Finally, the anticipated time to form magnesite (MgCO<sub>3</sub>), the mineral phase assumed in the PA calculations, relies on non-linear extrapolation of reaction times determined at much higher temperatures.

## References

1. U.S. Environmental Protection Agency (199), Criteria for the Certification and Recertification of the Waste Isolation Pilot Plant's Compliance with the 40 CFR Part 191 Disposal Regulations: Certification Decision; Final, Federal Register (May 18) vol. 63, no. 95, pp. 27354-27406.
2. Sandia National Laboratories (199), Sandia National Laboratories Compliance and Recertification Program Strategy, Revision 0, January 15.
3. Villareal, R., 1999, The Actinide Source-Term Waste Test Program Experimental Results and Status, November 23, 1999, presentation to the DOE Carlsbad Area Office and the Environmental Evaluation Group, Albuquerque.

4. U.S. Environmental Protection Agency (199), Response to Comments, Criteria for the Certification and Recertification of the Waste Isolation Pilot Plant's Compliance with the 40 CFR Part 191 Disposal Regulations: Certification Decision, EPA Docket A-93-02, V-C-1.
5. Dials, G.E. (199), DOE's February 24, 1998 Response to the December 31, 1997 Comments submitted by EEG to Docket A-93-02.
6. Krumhansl, J. L., Molecke, M. A., Papenguth, H. W., Brush, L. H., A Historical Review of Waste Isolation Pilot Plant Backfill Development, in the 7<sup>th</sup> International Conference Proceedings on Radioactive Waste Management and Environmental Remediation, Nagoya, Japan, September 26–30, 1999.

## Immobilization of Plutonium-Containing Waste into Borobasalt, Piroxen and Andradite Mineral-Like Compositions

Immobilization of plutonium-containing waste with obtaining stable and solid compositions is one of the problems that require a solution while managing radioactive waste. At VNIINM work is under way to select and synthesize matrix compositions for the immobilization of various-origin plutonium waste with the use of a cold crucible induction melting technology (CCIM). This paper presents information on the synthesis in a muffle furnace and in the CCIM zirconium-, uranium- and plutonium-containing borobasalt, piroxen and andradite materials.

In laboratory-scale installations in glove boxes the compositions containing up to 15 wt. %  $\text{CeO}_2$ , up to 10 wt. %  $\text{U}_3\text{O}_8$  and up to 5 wt. %  $\text{PuO}_2$  were obtained. Comparative research of the materials synthesized in the muffle furnace and in the CCIM has shown advantages of the CCIM method.

Research in physico-chemical properties, including the homogeneity and distribution of components in synthesized compositions, with the use of various characterization methods was done.

**Yu. I. Matyunin,  
S. V. Yudin**  
SSC RF VNIINM A.A.  
Bochvar, Russia,  
123060, Moscow,  
Rogov st. 5  
IGEM RAS, Russia,  
109017, Moscow,  
Staromonetny 35

**L. J. Jardine**  
LLNL, P.O. Box 808,  
Livermore, California,  
94550, USA

## Technology and Equipment Based on Induction Melters with “Cold” Crucible for Reprocessing Active Metal Waste

**V. G. Pastushkov,**  
**A. V. Molchanov,**  
**V. P. Serebryakov,**  
**T. V. Smelova,**  
**I. N. Shestoporov**  
SSC RF VNIINM,  
Rogov st. 5, 123060,  
Moscow, Russia, (095)  
190-2371

The operation and, particularly, the decommissioning of nuclear power plants and radiochemical production plants result in substantial quantities of radioactive metal waste (RAMW) having different activity levels ( $5 \times 10^{-4}$  – 40 Ci/kg). The long-term storage of unprocessed RAMW in specially designed storage facilities is economically ineffective and dangerous for the environment. To provide the environmentally safe storage and a drastic reduction in RAMW amounts is achievable by waste decontamination and melting.

The paper discusses specific features of technology, equipment and control of a single stage RAMW decontamination and melting process in an induction furnace equipped with a “cold” crucible. The calculated and experimental data are given on melting high activity level stainless steel and Zr simulating high activity level metal waste. The work is under way in SSC RF VNIINM.

The results are given of investigations in progress to choose and synthesize decontaminating fluxes and to study the properties of resultant ingots and slags and the distribution of the main radionuclides in products of RAMW melting. Other results describe the development of equipment and methods and instruments of remote control and management of RAMW melting and slag vitrification processes.

# Development of Technology for Ammonium Nitrate Dissociation Process

## Introduction

Ammonia and ammonium carbonate are frequently used as reagents in fuel production and processing of liquid radioactive wastes. In particular, liquid radioactive wastes that contain ammonium nitrate are generated during operations of metal precipitation [1]. In closed vessels at elevated temperature, for example in evaporators or deposits in tubing, ammonium nitrate may explode due to generation of gaseous nitrogen oxides [2]. Explosive dissociation of ammonium nitrate occurs mainly in accordance with the equation [3]



The heat of explosive conversion of ammonium nitrate is 157 kJ/kg. The sensitivity of ammonium nitrate to explosion increases in the presence of mineral acids, organic substances and some metals [4, 5, 6]. When ammonium nitrate is slightly heated, it dissociates, forming nitrous oxide in accordance with the equation [7]

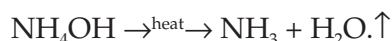
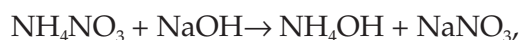


The presence of moisture in amounts of less than 1% has no effect on its susceptibility to an initial impulse, but an increase in moisture content to 2.5% by mass sharply reduces susceptibility to explosion. At moisture content of >2.5% by mass, ammonium nitrate generally does not detonate, and at moisture content of  $\geq 3.0\%$  ammonium nitrate does not explode [8]. Thus, ammonium nitrate solutions are not an explosion hazard. However, in the production of nuclear fuel, there is a possibility of formation of anhydrous ammonium nitrate salts in equipment used for evaporative condensation of solutions containing ammonium nitrate, in wind boxes, and in the lines through which the solutions are transferred.

In this connection, steps have to be taken to rule out conditions that result in explosion. To do that, ammonium nitrate should be removed even prior to the initial stage of its formation. This report gives results of development of a method of dissociating ammonium nitrate.

## Principles of Oxidative Method of Dissociating Ammonium Nitrate

Various methods of dissociating or removing ammonium salts are described in several papers [9, 10, 11]. Some of these methods of dissociating  $\text{NH}_4\text{NO}_3$  are employed in industry with the use of ammonia displacement by alkali, oxidation by nitrogen oxides or gaseous chlorine and the oxidative action of chlorides in a melt of ammonium nitrate. The method of ammonia displacement by alkali entails adding alkali to the solution and heating it. Ammonium is removed as a result of the reactions:



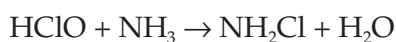
B. S. Zakharkin,  
V. P. Varykhanov,  
V. S. Kucherenko,  
L. N. Solov'yeva,  
V. V. Revyakin  
State Science Center  
of the Russian  
Federation, A. A.  
Bochvar All-Russian  
Research Institute of  
Inorganic Materials,  
123060, Moscow,  
Russia

The process of ammonium removal by the displacement method is fairly simple in use. However, this method does have two significant disadvantages: the additional introduction of salts of sodium or other metals, and the necessity of catching gaseous ammonia, as the concentration limit of flammability (CLF) for ammonia is 15%-28% (by volume) [12].

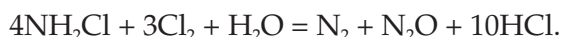
There are also problems with oxidation by gaseous chlorine or nitrogen oxides. First, there is the need for warehousing gas cylinders, and secondly, because of the low efficiency of interaction of gaseous chlorine, for example, as an oxidizer, a large excess of chlorine is needed as compared with the stoichiometric amount. The following reactions occur when ammonia is oxidized by chlorine [13, 14]:



At pH = 5–9 and at ratio  $\text{Cl}_2:\text{NH}_3 < 4.1:1$ , monochlorides only are formed:



At ratio  $\text{Cl}:\text{NH}_3 \geq 7.31:1$ , it dissociates completely:



The described oxidative process of ammonium nitrate dissociation in the presence of chloride ions [14] takes place in melts of ammonium nitrate and cannot be directly used since liquid radioactive wastes ordinarily contain as much as ~2 moles/liter of ammonium nitrate. It is of interest to look at the possibility of dissociating the latter in liquid nitrate wastes by using chlorine ions. Ammonium nitrate may be dissociated on the basis of oxidizing ammonium nitrogen.

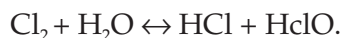
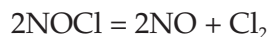
An initial assessment of the possibility of redox reactions can be made on the basis of comparing the redox potential ( $E_0$ ) with respect to a normal hydrogen electrode (Table 1) [15].

**Table 1. Standard redox potentials**

Electrode process	$E_0, \text{V}$
$\text{HClO} + \text{H}^+ + e^- = 1/2\text{Cl}_2 + \text{H}_2\text{O}$	+1.63
$\text{HClO} + \text{H}^+ + 2e^- = \text{Cl}^- + \text{H}_2\text{O}$	+ 1.494
$\text{Cl}_2 + 2e^- = 2\text{Cl}^-$	+1.359
$2\text{HNO}_2 + 4\text{H}^+ + 4e^- = \text{N}_2\text{O} + 3\text{H}_2\text{O}$	+1.297
$2\text{NO}_3^- + 10\text{H}^+ + 8e^- = \text{N}_2\text{O} + 5\text{H}_2\text{O}$	+1.116
$\text{HNO}_2 + 7\text{H}^+ + 6e^- = \text{NH}_4^+ + 2\text{H}_2\text{O}$	+ 0.864
$\text{NO}_3^- + 10\text{H}^+ + 8e^- = \text{NH}_4^+ + 3\text{H}_2\text{O}$	+0.87
$\text{N}_2 + 6\text{H}^+ + 6e^- = 2\text{NH}_3$	+0.057

These data provide a basis for finding conditions of oxidation of ammonium nitrogen in the presence of chlorine-containing ions. Table 1 shows that all electrode processes with chlorine compounds have redox potentials that are more electropositive than for those with compounds that contain nitrogen, including those in which the reduced form is an ammonium ion.

The basis for the redox process is to bring about conditions for the formation of hypochlorous acid that is a strong oxidizer, e.g. by equation [7]



Equilibrium of the last reaction is established instantaneously [16].

The process of oxidation of ammonium nitrogen may take place by reactions (Table 1)

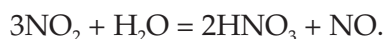
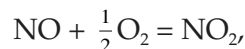
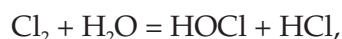
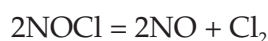


Oxidation by reaction  $2\text{NH}_3 - 6e^-$  ( $E_0 = -0.057 \text{ V}$ ) is unlikely, as this electrode process has a much higher redox potential.

The products of oxidation of ammonium nitrogen may participate in the reduction process until nitrous oxide  $\text{N}_2\text{O}$  is formed (see Table 1).

A solution containing chlorine ions,  $\text{NH}_4\text{NO}_3$  and  $\text{HNO}_3$  must be heated to create an abundance of vapor-gas phase that is sent to a reflux condenser in which the vapor-gas phase will be condensed and returned to the solution as condensate. In the vapor of nitrate solutions, the content of  $\text{HNO}_3$  may attain considerably lower values than in the solution [16], bringing about conditions for oxidation of ammonium nitrogen in the vapor-gas phase. The cyclic process of oxidation–reduction–oxidation of chlorine will continue for as long as ammonium ions remain in the solution. As a result, the ammonium nitrate is entirely dissociated, while the quantity of chlorine ions remains unchanged.

The redox process in the liquid and vapor-gas phase can be described by the following equations:



An examination of processes that occur in two phases (liquid-vapor) shows that the rate of dissociation of ammonium nitrates will depend on various factors: concentration of  $\text{HNO}_3$  in the solution, concentration of chlorine ions, temperature of the solution and so on. The main component of the gas phase that is not absorbed by condensate and does not interact with other components is nitrous oxide ( $\text{N}_2\text{O}$ ). The amount of  $\text{HNO}_3$  and  $\text{HCl}$  remains unchanged during oxidation of ammonium nitrogen.

## Development of Flowchart of Dissolution of Ammonium Nitrate in Liquid Radioactive Wastes

For practical application of this method, an investigation is made of the influence that various factors have on the rate of dissolution of ammonium nitrate for the purpose of determining the optimum parameters of the process. For dissociating nitrous oxide into nitrogen and oxygen, a thermal method is proposed, that is carried out at 900°C:

Fig. 1 shows a flowchart of the way that solutions containing ammonium nitrate are handled.

Process equipment	
Unit No.	Purpose of unit
1	Dissociation of ammonium nitrate and evaporative condensation of solution
2	Condensing components of vapor-gas phase
3	Heat-treating uncondensed components of vapor-gas phase
4	Collecting condensate
5	Mixing solutions: mother liquors, reagents, condensate
6	Evaporative condensation of solutions
7	Condensing vapor phase
8	Collecting condensate
9	Distributive valve for sending condensate to unit No. 1 or No. 4

### Description of Operation of Hardware/Flowchart

1. Reception of solution of 6 m/l of  $\text{HNO}_3$  + 0.2 m/l of HCl in volume of V liters into unit 5 and sequential transfer to unit 6 and unit 1.
2. Heating solution to boiling.
3. Reception into unit 5 of solution containing ammonium nitrate (mother liquor) in volume of V liters.
4. Reception into unit 5 of solution of 1 m/l of  $\text{HNO}_3$  in volume of V liters.
5. Air agitation of solution.
6. Feeding solution to unit 6.
7. Evaporative condensation of solution to volume V liters. Condensation of vapor phase in condenser 7 and collection of condensate in unit 8.
8. Feeding still residue in volume V liters from unit 6 to unit 1 continuously at a rate of V liters/h while unit 1 operates with reflux condenser in direct refrigeration mode and condensate is collected in unit 4. The gas phase is sent from the reflux condenser to the tubular furnace and the ventilation system.
9. Reception into unit 5 of solution in volume of V liters that contains ammonium nitrate.
10. Reception into unit 5 of solution in volume of V liters from unit 4.
11. Air agitation of solution.
12. Feeding solution to unit 6.

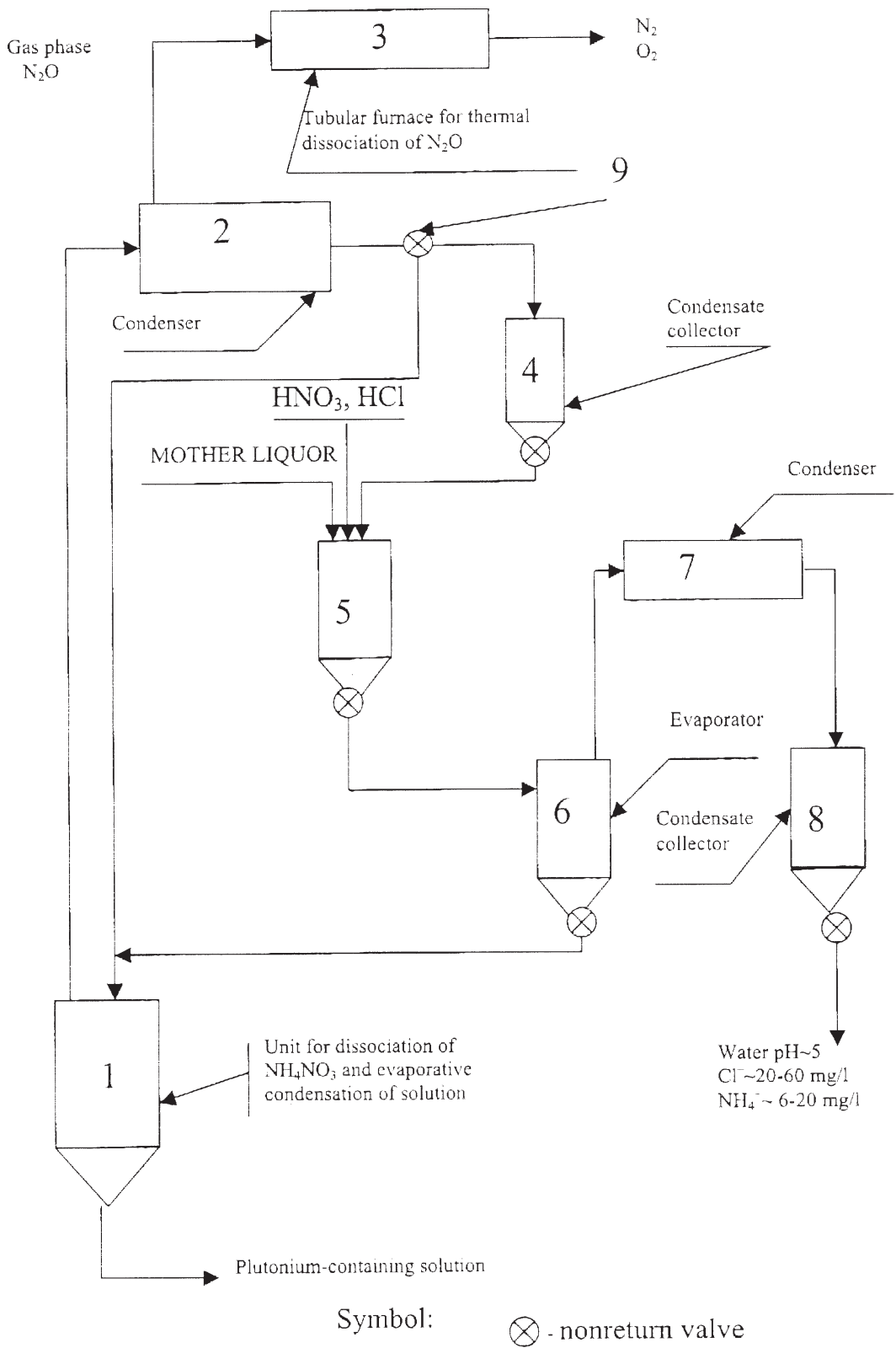


Figure 1. Flowchart of handling solutions that contain  $NH_4NO_3$ .

13. Evaporative condensation of solution to volume V liters. Condensation of vapor phase in condenser 7 and collection of condensate in unit 8.
14. Feeding still residue in volume V liters from unit 6 to unit 1 continuously at a rate of V liters/h while unit 1 operates with reflux condenser in direct refrigeration mode and condensate is collected in unit 4. The gas phase is sent from the reflux condenser to the tubular furnace and the ventilation system.
15. Multiple repetition of operations 9-14 (until accumulation of necessary amount of plutonium in solution).
16. Distilling off HCl from still residue in unit 1 in operation 8 with supply of 12 m/l of HNO from unit 6.

### References

1. Polyakov, A. S., Zakharkin, B. S., Borisov, L. M., Kuchernko, V. S., "Materials of the International Conference on the Nuclear Fuel Cycle," Versailles, France, 11-14 September 1995, pp 640-651.
2. Zakharkin, B. S., Revyakin, V. V. et al., "Materials of the International Conference on the Nuclear Fuel Cycle," Japan, 5-10 October 1997, pp 1157-1162.
3. Bostanjoglo, K. F., Ross, B. D., "Ammonium Nitrate Substances," Moscow, 1940.
4. Nekrasov, B. V., "Course in General Chemistry," Moscow, 1961, p 348.
5. Rozman, B. Yu., "Thermal Stability of Ammonium Nitrate," Leningrad, 1957.
6. Klevke, V. A., Polyakov, N. N., Arsen'yeva, L. Z., "Technology of Nitrogen Fertilizers," Moscow, 1963.
7. Pozin, P. Ye., "Technology of Mineral Fertilizers and Salts," 1957.
8. Smirnov, I. V., "Fire Safety in the Storage of Ammonium Nitrate," Moscow, 1974.
9. Vasil'yev, V. V., Rodicheva, N. A., Uchenyye zapiski Leningradskogo gosudarstvennogo universiteta, seriya khimicheskikh nauk, No 272, p 149, 1959.
10. Agte, A. N., "Trudy Leningradskogo tekhnologicheskogo universiteta im. Lensovetu," Vol 48, Goskhimizdat, 1958, p 182.
11. Kreshkov, A. P., "Principles of Analytical Chemistry," Book 1, Moscow, 1965, pp 184-187.
12. Chemical Encyclopedia, Vol 1, Moscow, 1998, p 278.
13. Slipchenko, V. A., "Upgrading Technology of Purifying Drinking Water. A Textbook," Kiev, 1987, pp 41-43.
14. Dolivo-Dobrovol'skiy et al., "Chemistry and Microbiology of Water," Kiev, 1971, p 158.
15. Rabinovich, V. A., Khavin, Z. Ya., "Concise Chemical Handbook," Leningrad, 1997.
16. Solodushenkov, S. I., Shilov, Ye. A., Zhurnal fizicheskoy khimii, Vol 19, 1945, pp. 409-415.

## The Myth of the “Proliferation-Resistant” Closed Nuclear Fuel Cycle

National nuclear energy programs that engage in reprocessing of spent nuclear fuel (SNF) and the development of “closed” nuclear fuel cycles based on the utilization of plutonium process and store large quantities of weapons-usable nuclear materials in forms vulnerable to diversion or theft by national or subnational groups. In an attempt to blunt criticism of this practice, which is associated with significant nuclear proliferation risk, advocates of closed fuel cycles have recently seized on the notion of “proliferation resistance” to rehabilitate the image of certain reprocessing projects. Proliferation resistance, an idea dating back at least as far as the International Fuel Cycle Evaluation (INFCE) of the late 1970s, is a loosely defined term referring to processes for chemical separation of SNF that do not extract weapons-usable materials in a purified form, so that diversion or theft of these materials during processing or storage is more difficult than for conventional PUREX reprocessing.

Proliferation resistance has been employed as a selling point for a variety of reprocessing proposals which raise significant proliferation concerns, such as the now-defunct Integral Fast Reactor (IFR) program, its direct descendant, the Accelerator Transmutation of Waste (ATW) program, and the proposed U.S.-Russian collaborative fuel cycle research program, which may well include the “BREST” fast reactor being advocated by the Russian Minister of Atomic Energy, Evgeny Adamov. Promoters of these programs argue that they are needed to mitigate proliferation risks posed by the geologic disposal of weapons-usable materials far into the future. However, these advocates have failed to demonstrate how the systems they propose can effectively mitigate the even more severe proliferation risks that would be posed in the near term by large-scale processing of SNF.

In particular, the “ATW Roadmap” released late last year by DOE (“A Roadmap for Developing Accelerator Transmutation of Waste Technology,” DOE/RW-0519, October 1999) describes the development of a large processing capability in the U.S. for commercial SNF, which would appear to violate current U.S. policy. However, ATW promoters argue that this is not the case because the processing technologies it utilizes do not “separate weapons-usable fissile materials at any time during the process.” In this paper, one of the chemical separation technologies which underlies the claim that the ATW proposal is “proliferation-resistant” — the electrometallurgical treatment (EMT) process developed by Argonne National Laboratory - West — will be examined in detail with respect to the following essential criteria:

Does the actinide-bearing product retain a radiation barrier comparable to that of the spent fuel from which it was extracted at every stage of the process?

(2) Is the isotopic mix of the actinide-bearing product significantly less attractive for national or subnational groups than the manufacture of nuclear weapons or than pure plutonium or highly enriched uranium (HEU)?

(3) Is it likely that resources for safeguards and physical protection can be significantly reduced for the “proliferation-resistant” fuel cycle compared to those required for conventional reprocessing and mixed-oxide (MOX) fuel fabrication?

**Edwin S. Lyman, PhD**  
*Nuclear Control  
Institute, Washington,  
DC 20036, USA*

(4) Are the environment, safety and health risks associated with the “proliferation-resistant” fuel cycle an acceptable price to pay for a closed fuel cycle and the speculative (and minimal) reduction in future environmental risk that its promoters claim it can provide?

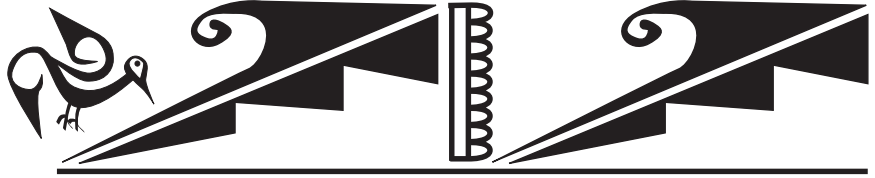
A preliminary analysis indicates that the EMT process fails with respect to all four of these criteria and hence offers insignificant additional proliferation resistance relative to diversion-prone processes like PUREX (plutonium-uranium (reduction) extraction).

For example, with respect to criterion (1), it is noted that a primary emitter of penetrating gamma radiation from the actinide product of EMT is cerium-144 ( $^{144}\text{Ce}$ ), which has a half-life of only 284 days. For the EMT actinide product of typical U.S. commercial spent nuclear fuel that has aged more than ten years, the  $^{144}\text{Ce}$  content and penetrating gamma ray emission of the EMT actinide product is likely to be minimal. In this paper, a shielding analysis of the EMT recycle fuel elements will be conducted to confirm this.

With respect to criterion (2), the proliferation resistance once ascribed to the mix of isotopes in the EMT actinide product is also seen to be minimal, in view of the increasing public awareness that the weapon-usability of some neptunium and americium isotopes is comparable to that of conventional special nuclear materials.

With respect to criterion (3), one notes that the increased difficulty of accurate material accountancy of the actinides in the EMT process stream, coupled with the insignificant reduction in attractiveness of the material, is not likely to lead to a reduction in the safeguards burden relative to conventional fuel cycle activities and may well require compensatory enhancements in containment and surveillance, as well as more frequent inspection and inventory verification.

Finally, criterion (4) is important for placing proliferation resistance into a larger perspective. Even if a process can be designed so that the product stream is always as self-protecting as spent fuel, it is far from clear whether this is a reasonable path forward compared to less complex and hazardous energy technologies.



## **Nuclear Fuels/Isotopes**



## Advanced MOX Fabrication Methods for LWRs

Mixed oxide (MOX) has now become a standard fuel in commercial LWRs. More than 90% of the world's production is made according to the so-called MIMAS process.<sup>1</sup> Moreover, a new fabrication plant using this process is being designed in the US for the disposition of weapon-grade Pu.

MOX fuel burnups of up to 50 GWd/tHM are routinely achieved in commercial reactors in Europe, and the overall behavior is close to UO<sub>2</sub> fuel. However, more ambitious goals up to 70 GWd/tHM have been set, with the aim of reducing further the fuel cycle cost. Most data at high burnup show that fission gas release becomes larger in MOX than in UO<sub>2</sub>. Several explanations have been given: the different physical properties of MOX and the heterogeneous structure of industrial MOX.<sup>2</sup>

The research carried out on advanced MOX fuels at the Transuranium Institute in Karlsruhe contributes to the aim of achieving high burnup. In particular, our efforts are concentrated on following aspects, both related to the fuel microstructure:

- (i) increasing the homogeneity of the Pu distribution in MIMAS fuel. The master blend containing 30% to 40% of PuO<sub>2</sub> is micronized by ball-milling and then blended down to the required Pu content (4% to 10%). After pellet pressing and sintering, the typical microstructure shows Pu-rich agglomerates of about 50 to 150 microns. The aim is to reduce the Pu content in these agglomerates and to enlarge the volume of the U-Pu phase in the pellet.
- (ii) obtaining large grain sizes in MOX, to lower the diffusion of fission gases to grain boundaries. This can be achieved quite easily in sol-gel fuel, which is a homogeneous solid solution (U-Pu)O<sub>2</sub>. Large grains are obtained by modifying the sintering conditions. For MIMAS fuel, practical experience shows that increasing the UO<sub>2</sub> grains cannot be achieved. A grain size increase is, however, observed in the (U,Pu)O<sub>2</sub> phase.

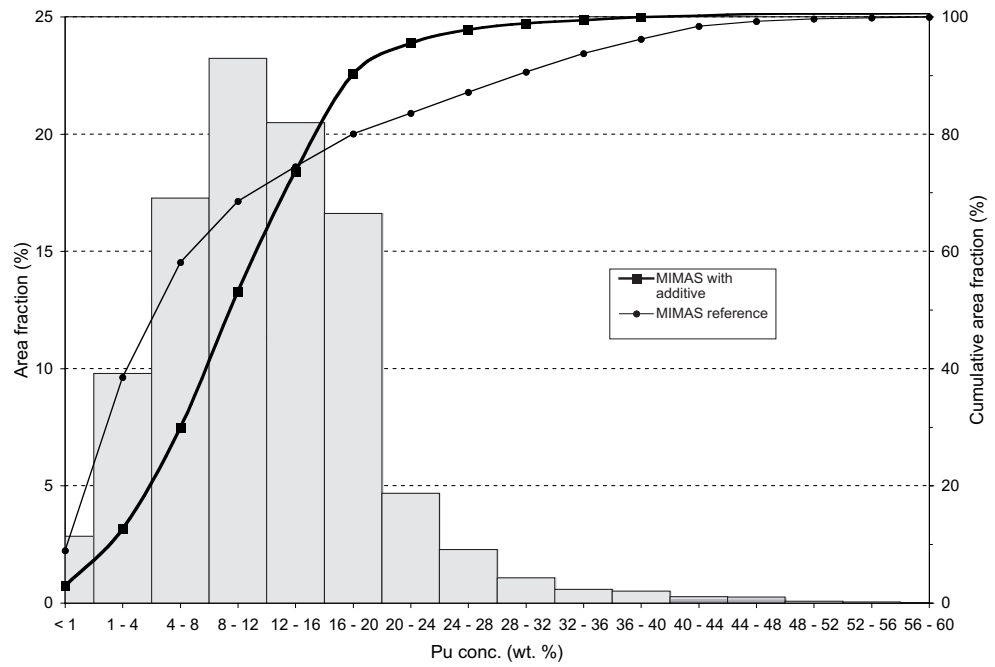
The work described in this paper includes fabrication and characterization results on three fuel types:

- (i) MIMAS with an additive (Al<sub>2</sub>O<sub>3</sub>-SiO<sub>2</sub>) in the secondary blend.
- (ii) MIMAS using a sol-gel UO<sub>2</sub> powder for dilution to increase the interdiffusion process during sintering.
- (iii) Sol-gel MOX with modified sintering conditions (humidity, time).

For each fuel type, the process has been optimized to obtain pellets of good quality in terms of geometry, density, and visual aspect. The pellets have been characterized by etched ceramographies and EPMA. The results show that the main targets have been achieved although improvements are still possible. Grains of up to 50 microns were obtained in the sol-gel MOX, after sintering for 24 h in humidified atmosphere. For the MIMAS, a good homogenization factor is obtained when an additive is used (see Fig. 1). This paper presents further the results of the fuel structure and fabrication parameters on the three fuel types.

**D. Haas,  
J. Somers,  
C. Walker,  
S. Brémier**  
*European  
Commission, JRC,  
Institute for  
Transuranium  
Elements  
D-76125 Karlsruhe,  
Germany*

Figure 1. EPMA results showing the Pu-rich particle distribution in MIMAS fuels.



### References

1. H. Bairiot et al., Overview on MOX fuel fabrication achievements, International Symposium on MOX Fuel Cycle technologies for Medium and Long Term Deployment, Vienna, 17-21 May 1999.
2. P. Blanpain et al., High Burnup MOX Fuel Assembly, TOPFUEL'99, Avignon, 13-15 Sept. 1999.

## Synthesis of the U.S. Specified Ceramics Using MOX Fuel Production Expertise\*

At present, under the auspices of the USA/Russia agreements, joint work is under way to dispose of excess plutonium being withdrawn from nuclear defense programs. A major approach is to produce mixed plutonium-uranium fuel (MOX fuel) for its further burnup in different nuclear reactors. Plutonium-containing materials, which upon their composition or from an economic standpoint cannot be used for MOX fuel production, are to be immobilized into solid ceramic and glass-type matrices with their safe storage and eventual geologic disposal. For an immobilization form in the U.S., it is proposed to use ceramics based on pyrochlore developed at LLNL that is capable of incorporating up to 10 wt. % PuO<sub>2</sub> and 23 wt. % UO<sub>2</sub>. At VNIINM, work was done to assess the possibility of using equipment and expertise of MOX-fuel production to fabricate the ceramics. A few of the ceramic samples were synthesized, and basic physicochemical properties, including the homogeneity of the plutonium and uranium distributions in the matrix, density, and pellet porosity, were also measured.

**V. A. Astafiev,  
A. E. Glushenkov,  
M. Sidelnikov,  
G. B. Borisov,  
O. A. Mansourov**  
*A. A. Bochvar All-  
Purpose Research  
Institute of Inorganic  
Materials (VNIINM)  
123060, Moscow,  
Russia*

**L. J. Jardine**  
*Lawrence Livermore  
National Laboratory  
(LLNL), Livermore,  
California, 94550,  
USA*

\*Work performed under the auspices of the U.S. Department of Energy by Lawrence Livermore National Laboratory under Contract W-7405-Eng-48.

# Research Program for the 660 MeV Proton Accelerator Driven MOX-Plutonium Subcritical Assembly

V. S. Barashenkov,  
V. S. Buttsev,  
G. L. Buttseva,  
S. Ju. Dudarev,  
A. Polanski,  
I. V. Puzynin,  
A. N. Sissakian  
*Joint Institute for  
Nuclear Research,  
Dubna, Russia*

## Introduction

This paper presents the research program of the Experimental Accelerator Driven System (ADS), which employs a subcritical assembly and a 660 MeV proton accelerator operating in the Laboratory of Nuclear Problems at the Joint Institute for Nuclear Research in Dubna. Mixed-oxide (MOX) fuel (25% PuO<sub>2</sub> + 75% UO<sub>2</sub>) designed for the BN-600 reactor use will be adopted for the core of the assembly. The present conceptual design of the experimental subcritical assembly is based on a core nominal unit capacity of 15 kW (thermal). This corresponds to the multiplication coefficient  $k_{\text{eff}} = 0.945$ , energetic gain  $G = 30$ , and accelerator beam power of 0.5 kW.

## Description of the Experimental Setup

As a first step in the study of characteristics of the ADS, a metallic weapon-grade plutonium fuel was proposed ("Pluton" project [1-3]). However, the results of the calculations have shown [4] that MOX fuel would be a better option.

The proposed ADS facility consists of

- a 660 MeV proton accelerator,
- beam bending magnets,
- a spallation target with different material (Pb, W, Pb-Be, Hg),
- the blanket based on MOX fuel of a BN-600 type Russian fast reactor,
- beryllium reflector and concrete shielding,
- control systems, and
- measuring systems.

The following measurements on the test assembly are planned: energetic gain and its variation for different target material compositions, neutron multiplication  $k_{\text{eff}}$  and its variation, neutron generation, neutron spectra, and reaction rates. The kinetics of the processes in the subcritical assembly, produced by the proton-neutron flash in the target inside the MOX fuel zone from the interaction with 660 MeV protons, will be investigated. One of the interesting questions is the stability of the neutron multiplication coefficient value for the subcritical assembly at various energies and intensities of the proton beam.

The proton beam is transported horizontally to the target by bending magnets and through a vacuum track provided by concrete shielding. The proton beam interacts with the target, which is placed in a steel tube. The target is surrounded by a blanket consisting of the MOX fuel. The fuel is placed in a stainless steel vessel with a beryllium reflector and a concrete shield surround the blanket. The target and fuel elements are cooled by a flow of air.

The schematic layout of the subcritical assembly is presented in Fig. 1. Parameters of the ADS facility are presented in Table 1.

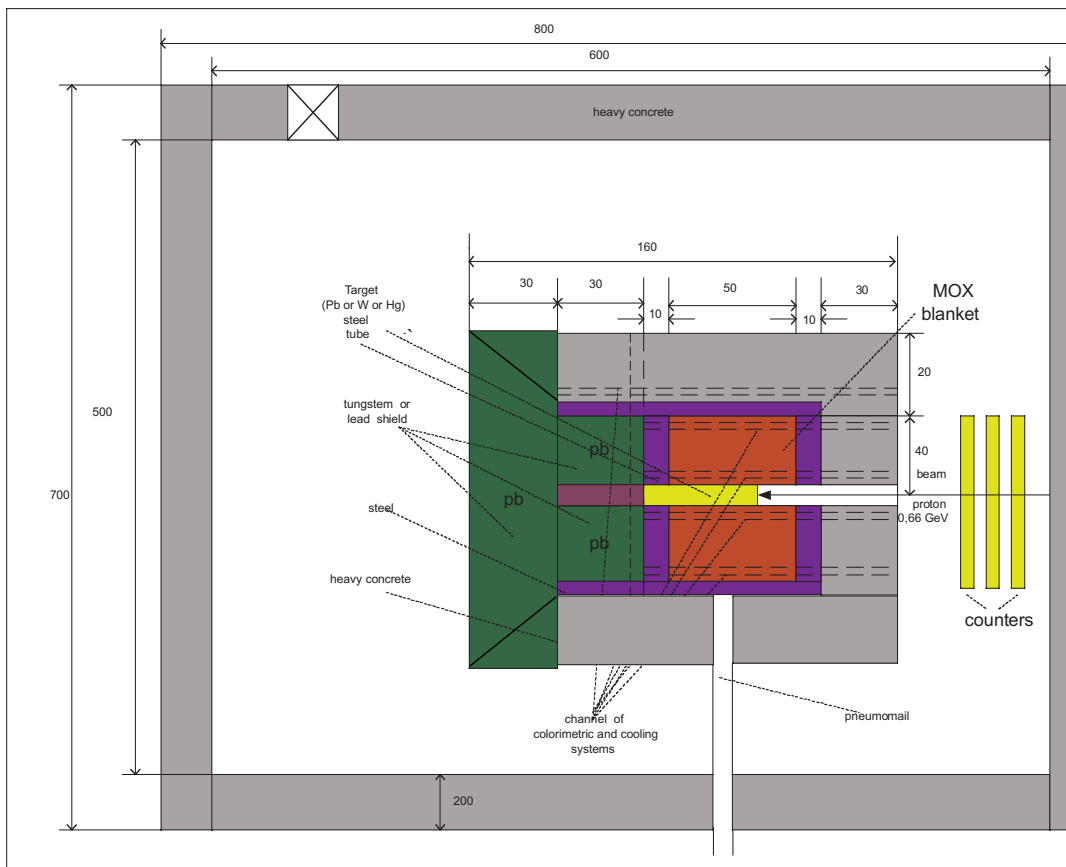


Figure 1. Subcritical assembly scheme (sizes are given in cm).

Fission power	15 kW
Average intensity of produced neutrons	$1.51 \cdot 10^{15}$ n/s
Energetic gain	30
Factor $k_{\text{eff}}$	0.945
Fissile material	$\text{PuO}_2$ (25%), $\text{UO}_2$ (75%)
Density of fissile material	$8.64 \text{ g/cm}^3$
The full length of a fuel element	70 cm
Core length of a fuel element	50 cm
Core diameter (with beryllium)	80 cm
Fuel load	250 kg

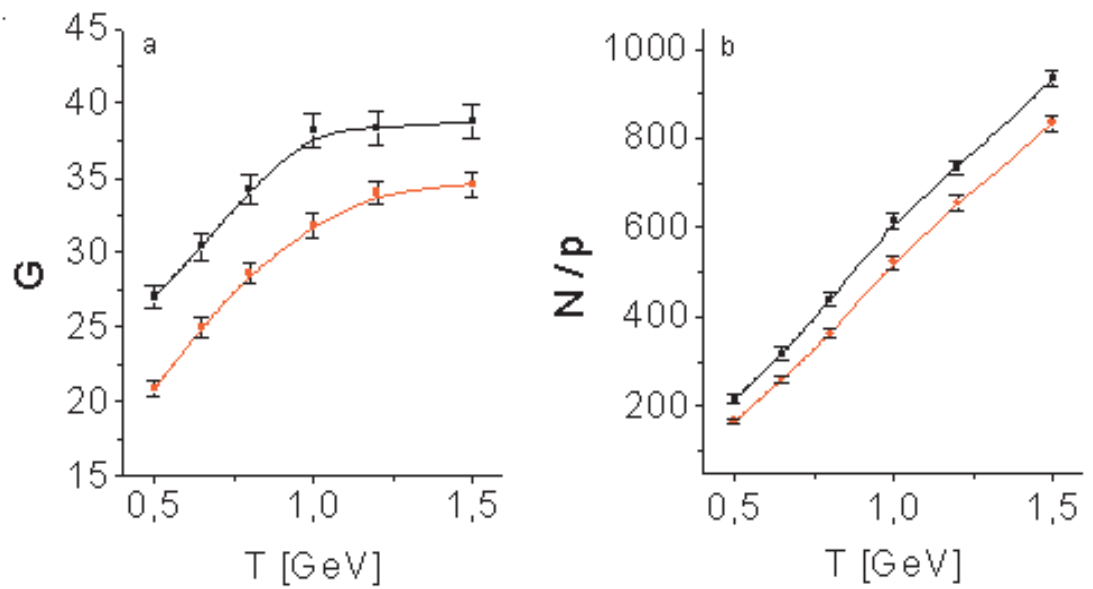
Table 1. Main Parameters of the ADS Facility.

### Results of Monte Carlo Calculations

We have performed a Monte Carlo study of the main parameters of the proposed system. The Dubna Cascade model has been used.

The calculated quantities were the neutron multiplication coefficient, neutron production, and the heat generation in the system. The dependence of the energetic gain and neutron production at various proton beam energies  $T$  for  $k_{\text{eff}} = 0.945$  is presented in Fig. 2. Energetic gain  $G$  is the ratio of the energy produced in the device to the energy delivered by beam.

Figure 2. Energetic gain  $G$  and the number of neutrons per proton ( $N/p$ ) produced in the system vs. incident proton energy  $T$  for  $k_{\text{eff}} = 0.945 / 0.003/$  (The upper curve is for the lead target; the lower curve is for the tungsten target.)



The maximum energetic gain  $G$  is observed for incident proton energy of 1.5 GeV [5]. A decrease in energy gain observed at low energies results from ionization losses of primary protons. For the suggested 660 MeV energy of protons, the energetic gain is only 20% less than for 1.5 GeV. Energetic gain for a lead target is 20% greater than for a tungsten target.

### Research Program

The program of experimental research consists of the following two parts:

- (1) Research on the characteristics and parameters of the electronuclear installation: generation and spectrum of neutrons, heat production per unit of beam power, yield of radioactive isotopes.
- (2) Obtaining nuclear data required for designing a full-scale industrial electronuclear system for energy production and nuclear power radioactive waste transmutation; optimization of unit power; sizes and design of the future energy systems and transmuter; research in material properties connected to the creation of a new type of nuclear energy systems.

In order to perform this program, the following measuring systems have been adopted:

- (1) a neutron spectrometer, in which the neutrons are slowed in a lead column;
- (2) a gamma spectrometry complex with a pneumomail for the express analysis of the radioactive isotopes formed in the field of electronuclear neutrons;
- (3) a calorimetric system on the basis of metal thermometers of resistance, sensitive micro thermocouples, and infrared sensors for measuring the heat production rate in the assembly; and
- (4) an operation mode automatic control system of the experimental installations.

In order to measure the spectra of the neutrons leaving the plutonium assembly and the shielding, it is offered to use a method of spectrometry on the time of slowing down the neutrons in a leaden column. This method is used for the measurement of neutrons spectra at the meson factory of the INR AS Russian Federation. The fast neutrons, generated in a primary target made of lead and tungsten (see Fig. 1) by a 660 MeV proton beam at the Joint Institute for Nuclear Research phasotron, result in fission and consequent breeding of plutonium. These neutrons pass through a steel cladding and get in the leaden column placed in lead shielding (see Fig. 1). On slowing down time in lead, the spectrum of neutrons taking off the limits of the steel shielding of the assembly is measured. The time of slowing down neutrons that is inversely proportional to  $E_n$  is measured by detectors with boron, lithium, and isotopes of uranium and plutonium. The 660 MeV extracted proton beam from the phasotron will be controlled with the help of an external start-up. The phasotron operation's external start-up mode is provided by a package of impulse emitted by the switching system from the pulse generator of the accelerator start-up and allows one to select the needed time interval. The time interval is determined by the slowing down time of the neutrons having the least energy in the spectrum.

To investigate the neutron spectrum in the electronuclear installation, to irradiate and measure the samples in the course of neutron reactions, a pneumomail channel of the POLON brand and a stationary gamma spectrometer of CANBERRA-PACKARD type with an Accu Spec/B card and an integrated signal processor will be installed. In order to deliver the samples of various materials in the active zone (core) of the installation, the tungsten shielding will be provided with a special channel (see Fig.1). The gamma-spectrometer with high efficiency precision resolution is expected to be used for studying the effective cross-section of transmutation of long-living radioactive isotopes in the field of electronuclear neutrons. The results of these studies are of special interest for creation in the future of an industrial scale ecological transmutor.

The automated infrared information-measuring detection system is intended for measurement of heat production in the subcritical assembly. Infrared sensors will be used as detectors. They possess high sensitivity and the possibility of performing a study of space and temporary distribution of heat production in the assembly. In addition to the infrared sensors for calorimetry, other thermometric gauges and detectors such as microthermocouples, thermoresisters, etc., can also be used. However, the infrared methods are selected only from the viewpoint of convenience when working in high radiation conditions. The jamming-protected precision device for measuring the thermal radiation intensity is intended for registration of spectra and measurement of the radiation intensity in the infrared spectrum under the conditions of strong electromagnetic and radiation jamming. It can be used for measurement of one-dimensional structures and the sizes of objects under study, such as emitters and beams of radiation.

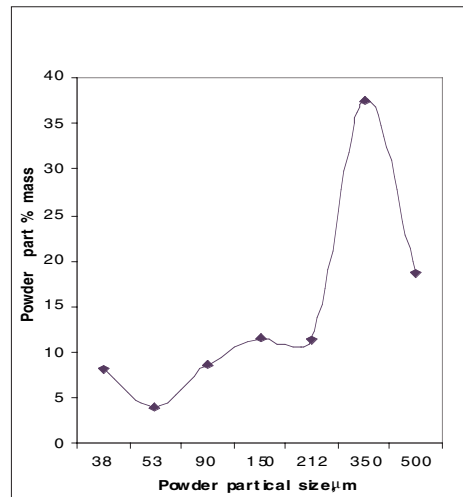
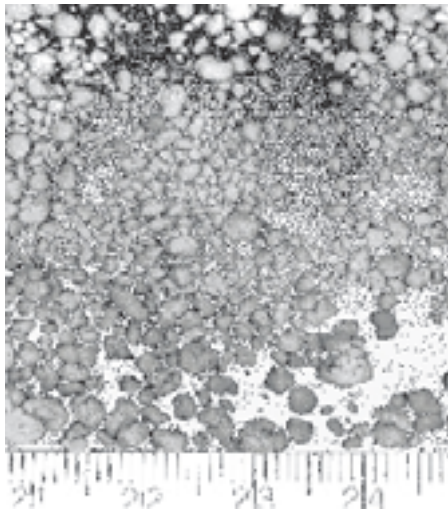
## References

1. V. S. Barashenkov, A. Polanski, I. V. Puzynin, A. N. Sissakian, "An Experimental Accelerator Driven System Based on Plutonium Subcritical Assembly and 660 MeV Proton Accelerator," Proc. 3<sup>rd</sup> Int. Conf. on Accelerator Driven Transmutation Technologies and Applications, June 7-11, 1999, Prague, Czech Republic (CD-ROM edition). Preprint JINR E2-99-207.
2. A. Arkhipov, V. S. Barashenkov, V. S. Buttsev et al., "Research Programme for the 660 MeV proton Accelerator Driven Plutonium Subcritical Assembly," Experimental Nuclear Physics in Europe, ENPE 99 Seville (Spain), 21-26 June 1999, pp. 478-481, Editor AIP.
3. A. Polanski et al., "Based Energy Amplifier Testing Concept," Conf. on Nuclear Energy in Central Europe '98. Terme Catez, Slovenia, 7-10 September 1998, p. 67.
4. A. Polanski, "Monte Carlo Modeling of Electronuclear Processes in Experimental Accelerator Driven Systems," XXVI Mazurian Lakes School of Physics, 1-11 September 1999, Krzyze, Poland. A NATO Advanced Research Workshop, 2-4 Sept. 1999. Acta Phys. Polonica (in press).
5. C. Rubbia et al., "Experimental determination of the energy generated in nuclear cascades by high energy beam," Physics Letters B 348 (1995) 697-709.

## Continuous Process of Powder Production for MOX Fuel Fabrication According to “GRANAT” Technology

During recent years the solution of the problem of commercial mixed-oxide (MOX) fuel production for nuclear reactors in Russia was realized in a number of directions. Earlier the particular emphasis was put in our country on the development of microspherical fuel fabrication technology by internal gelation method (sol-gel process), as the most promising one for commercial fabrication of mixed fuel. Simultaneously in different Institutes of Minatom RF alternative methods were developed, such as mechanical mixing of uranium and plutonium oxides, carbonate coprecipitation (similar to AUPuC method), plasma-chemical, pyrochemical and others. However, today we can say by a number of objective and subjective reasons that in contrast to leading, nuclear power engineering western countries, there is no full-scale fabrication of mixed fuel in Russia.

The paper deals with the solution to the problem of a continuous pilot plant development for mixed oxide fuel powder production on the basis of the home “GRANAT” technology, which had been tested before on a small-scale pilot-commercial batch-operated plant of the same name and confirmed good results.



V. E. Morkovnikov,  
L. S. Raginskiy,  
A. P. Pavlinov,  
V. A. Chernov,  
V. V. Revyakin,  
V. Varikhanov,  
V. N. Revnov  
SSC RF VNNINM  
123060, Russia,  
Moscow

Figure 1.  
Appearance of  
granules after liquid  
granulation process.

Figure 2. Particle  
size distribution of  
powder produced by  
“GRANAT” method  
in continuous mode.

## Fabrication Technology and Characteristics of AmO<sub>2</sub>-MgO Cercecer Materials for Transmutation

**Y. Croixmarie,  
A. Mocellin,  
D. Warin**  
*Commissariat à  
l'Energie  
AtomiqueCEA-  
CADARACHE DRN/  
DEC/SPUA, France*

A large R and D program devoted to transmutation of long-lived radioactive elements is being carried out in France at the CEA, in the frame of a national law voted in 1991. One of the field's concerns is the transmutation of actinides (americium), and several experimental irradiations are planned in order to test the optimized conditions of americium transmutation, namely in a fast reactor.

This paper deals with the fabrication technology and the physico-chemical properties of target materials prepared for the ECRIX experiment in the French PHENIX reactor. The ECRIX target materials consist of pellets made of a ceramic-ceramic type composite in which particles of americium oxide are microdispersed in an inert matrix of magnesium oxide.

The R and D studies and the manufacturing of the Am targets have been conducted in a new laboratory inside the CEA Atalante facility in Marcoule, in which the equipment for the fabrication process and for the characterization techniques have been largely upgraded to provide the necessary quality-controlled materials for the irradiation experiment (transmutation test properties and safety of the experiment).

The essential characteristics of the pellets are the following:

- Americium compound    AmO<sub>x</sub> (1.5<x<1.7)
- Americium content        17±2 wt %
- Inert matrix                Magnesia
- Porosity                    ≤ 5 vol %
- Diameter                    5.18 mm

The R and D results allow us to compare the evolution of the O/Am ratio and of the crystalline phases of the different americium oxides when treated thermally (during the same sintering conditions) as pure AmO<sub>x</sub> material and as dispersed in the inert matrix. These results show, for instance, slower oxygen diffusion phenomena in the cercecer (ceramic-ceramic) materials than in the pure americium oxide ceramics. In the case of a crystalline phase modification during heat treatment, diametrical, volume variations, density and porosity of the cercecer have also been studied.

Distribution of the americium oxide inside the material, which is an essential characteristic of the composite, has been controlled with adjusted ceramographic and gamma scanning methods.

Thermophysical properties of the cercecer materials such as melting temperature, calorific capacity, thermal diffusivity, swelling and sodium chemical compatibility have been measured: most of them are close to those of pure magnesia. Oxygen potentials of the ECRIX cercecer and stoichiometric UO<sub>2</sub> are in the same range.

Thermal stability after high temperature sintering, then room-temperature aging in storing conditions have also been measured according to a possible evolution of the size and phases of the cercer material.

Finally, ECRIX materials, manufactured according to the process clearly defined during the R and D study, exhibit characteristics in accordance with the experiment specifications which should lead, beginning year 2001, to the transmutation experiment of these targets in the fast reactor PHENIX.

With the aim to optimize the transmutation materials, new compounds of americium and new concepts of dispersion in matrix are foreseen: crystalline phases of americium, substituted yttria, and stabilized zirconia are under investigation first with inactive simulating compounds then with americium. These compounds are tested for the microdispersed and macrodispersed concepts.

# Analysis Capabilities for Plutonium-238 Programs

A.S. Wong,  
G. H. Rinehart,  
M. H. Reimus,  
M. E. Pansoy-Hjelvik,  
P. F. Moniz,  
J. C. Brock,  
S. E. Ferrara,  
S. S. Ramsey  
*Los Alamos National  
Laboratory, Los  
Alamos, NM 87545  
USA*

## Introduction

In the past two decades, Los Alamos National Laboratory (LANL) has produced general-purpose heat sources (GPHS) from plutonium-238 oxide for space and other power source applications. One of the most recent GPHS applications was in the Cassini Spacecraft for Saturn exploration.<sup>1</sup> The Power Source Technologies Group (NMT-9) has full capabilities to recover and purify  $^{238}\text{PuO}_2$  from scrap and aged fuels,<sup>2</sup> and to fabricate oxides into fuel pellets for heat sources.<sup>3</sup>

In this presentation, an overview of analysis capabilities that support  $^{238}\text{Pu}$  programs will be discussed. These capabilities include neutron emission rate and calorimetric measurements, metallography/ceramography, ultrasonic examination, particle size determination, and chemical analyses. The data obtained from these measurements provide baseline parameters for fuel clad impact testing, fuel processing, product certifications, and waste disposal. Also several in-line analyses capabilities will be utilized for process control in the full-scale  $^{238}\text{Pu}$  Aqueous Scrap Recovery line in FY01.

## Physical Measurement Capabilities

Neutron Emission Rate Measurements. Spontaneous fission of  $^{238}\text{Pu}$  produces approximately 2220 neutrons per second per gram (n/s/g) of  $\text{PuO}_2$  (at 81% of  $^{238}\text{Pu}$ ).<sup>4</sup> Energetic alpha particles react with light isotopes such as  $^{17}\text{O}$ ,  $^{18}\text{O}$ , and  $^{19}\text{F}$  in  $\text{PuO}_2$  producing additions of 5000 to 20,000 n/s/g via (alpha, n) reactions. In order to reduce the neutron emission rate, a minimum amount of hydrofluoric acid is used in the aqueous process, and the fuel oxide is treated in an  $^{16}\text{O}$  exchange process to reduce  $^{17}\text{O}$  and  $^{18}\text{O}$ . The neutron emission rate of oxide is then measured on a thermal neutron counter.<sup>5</sup> The emission rate in the final products (purified oxides and fuel powder) must be less than 7000 n/s/g of  $^{238}\text{Pu}$ .

Calorimetric Measurements. Calorimetry is used for determining the power output of heat producing materials.  $^{238}\text{Pu}$  has a half-life of 87.74 years and a power output of 0.567 watt per gram. Several types of calorimeters are utilized in the  $^{238}\text{Pu}$  lab to measure low (0 to 5 W with an accuracy of  $\pm 0.003$  W) and high wattage (0 to 200 W with an accuracy of  $\pm 0.5$  W) fuel.<sup>6</sup> Calorimetry is used to verify the amount of special nuclear materials in incoming fuel materials, outgoing scrap, and finished heat source assemblies.

Metallography/ceramography. Metallographic/ceramographic examinations are performed on test components recovered from impact tests to determine possible failure mechanisms. The microstructure of the GPHS clad material, girth welds, and samples of fuel pellets are also examined. A LECO 300 metallograph with magnification range of 8 to 500 X is interfaced to the glovebox line through a unique hood extension that covers but does not enclose the metallographic stage. Metallographic/ceramographic specimens are prepared with standard metallographic equipment. This includes a wafering saw, automated grinding, rough polishing and fine polishing equipment, and a power supply for electrolytic etching.

Ultrasonic Examination. Ultrasonic testing is performed to examine the weld integrity of the  $^{238}\text{PuO}_2$ -fueled clad and simulant-fueled capsules. The instrument we use to perform ultrasonic testing is a 3.5-MHz transducer inspecting system with a 0.5-inch diameter and a 1.5-inch spherical focus in water. The operator must have a minimum of an ASNT Level I ultrasonic testing certification.

Particle size analysis. NMT-9 has in-line capabilities for determining the particle size distribution of fines that are less than 100 micron recovered from impact tests. Impact tests are conducted to determine the response of GPHS to probable launch accident scenarios. Particle size analysis is also used to verify the particle size of milled oxide prior to dissolution. The instrument we use to perform particle size analysis is the Galai CIS-100. Its measurement range is 0.5 to 600 micron.

### **Chemical Analysis Capabilities**

Chemical data of  $^{238}\text{Pu}$  samples (feed oxides, purified oxides, granular  $^{238}\text{Pu}$ , and process solutions) provide necessary baseline parameters and measures for process control, material control and accountability, waste disposal, and product certification. Our chemical analyses are available through collaborative effort with NMT-1 Analytical Chemistry Group.

The purity of plutonium oxide is determined by Pu(III) visible spectrometry. If expected Pu content is low ( $\mu\text{g}$  or less), gross alpha counting is used to calculate the  $^{238}\text{Pu}$  content. Actinide impurity analyses including  $^{234}\text{U}$ ,  $^{241}\text{Am}$ ,  $^{237}\text{Np}$ , and  $^{236}\text{Pu}$  are determined by radiochemical methods (gross alpha and gamma counting, gamma and alpha spectroscopy, and radionuclide separations.) The plutonium isotopic composition is determined by thermo-ionization mass spectrometry (TIMS). Direct-current arc (DC Arc) and inductively coupled plasma mass spectrometry (ICP-MS) techniques are used to determine non-actinide cationic and anionic impurities.

Detailed descriptions of each chemical measurement capability will be given in the presentation.

### **In-Line/On-Line Process Monitoring**

In FY01, the full-scale  $^{238}\text{Pu}$  Aqueous Recovery and Purification Line will be operational at LANL. We are currently installing an on-line gamma system that will monitor Am, U, and Pu gamma rays during the ion-exchange process.<sup>7</sup> The on-line gamma monitoring system will provide real-time elution profiles of actinide impurities that are important for plutonium loss, waste minimization, and process control.

In addition, a solution in-line alpha counter (SILAC) will be used for in-line monitoring of alpha activity in hydroxide filtrate during the full-scale production. By knowing the approximate alpha concentration, we can adjust the operating parameters of the ultra-filtration process to maximize removal of plutonium and uranium from the waste solutions. Farnham and Fowler at LANL<sup>8</sup> developed this SILAC system for real-time monitoring of plutonium and americium concentration in process solutions in the glovebox lines.

## Summary

The Plutonium Facility at LANL is the only place left in the United States with full capabilities of producing  $^{238}\text{Pu}$  heat sources. It is very important for us to maintain and improve our valuable resources in order to support future space applications.

## Acknowledgment

We thank Liz Foltyn, Tim George, and Kevin Ramsey for leading the efforts discussed here. We also thank NMT-1 Analytical Chemistry Group for providing analytical chemistry results for oxides and process solutions, NMT-4 Material Accountability Group for providing calorimetric measurements, and all the personnel who support  $^{238}\text{Pu}$  programs.

## References

1. T. G. George, and E. M. Foltyn, "Production of  $^{238}\text{PuO}_2$  heat sources for the Cassini mission," AIP Conference Proceedings (CONF-980103), Jan 1998.
2. L. D. Schulte, G. H. Rinehart, J. Espinoza, G. L. Silver, K. B. Ramsey, K. G. D. Jarvinen, G. M. Purdy, "Recycle of scrap plutonium-238 oxide fuel to support future radioisotope applications," AIP Conference Proceedings (CONF-980103), Jan 1998.
3. G. H. Rinehart, "Light weight radioisotope heater unit (LWRHU) production for the Cassini mission," AIP Conference Proceedings (CONF-970115), Jan 1997.
4. G. M. Matlack, and C. F. Metz, "Radiation Characteristics of Plutonium-238," LA-3696, Los Alamos National Laboratory, 1967.
5. N-1 Application Note, "Passive neutron coincidence counters," LALP-92-52, Los Alamos National Laboratory, 1992.
6. NIS-5 Application Note, "Heat-Flow Calorimeters," LALP-99-25, Los Alamos National Laboratory, 1999.
7. A. S. Wong, K. B. Ramsey, and M. E. Pansoy-Hjelvik, "On-line Gamma Monitoring System for the  $^{238}\text{Pu}$  Aqueous Recovery Process," ANS Transactions, 15 (81) 1999.
8. J. Farnham and M. M. Fowler, "SILAC Assembly Manual," Los Alamos National Laboratory, August 1998.

## Modeling of Fission Gas Release in MOX Fuel Considering the Distribution of Pu-Rich Particles

The mixed-oxide (MOX) fuel for light-water reactors (LWRs) is fabricated either by direct mechanical blending of  $\text{UO}_2$  and  $\text{PuO}_2$  powders in proportions of the desired Pu content or by two-stage mixing, where the master blend of intermediate Pu content prepared in the first step is mixed with the proper amount of pure  $\text{UO}_2$  in the second stage to get the final Pu content. Therefore, it would be inevitable that incomplete mixing of Pu exists in MOX fuel, resulting in some number of Pu-rich particles with higher Pu content than average for a fuel pellet. In addition, examination of the fabricated MOX pellet indicates that Pu-rich particles have the size distribution that is characteristic of its fabrication method. There is some experimental evidence that fission gas release rates are enhanced in LWR MOX fuel compared with conventional  $\text{UO}_2$  fuel under similar operation conditions. The enhancement in MOX fuel may be attributed to incomplete Pu mixing along with slightly lower thermal conductivity and higher reactivity later in life. Since the last two factors can be considered in terms of fuel temperature, it is required to take into account the heterogeneity effect of MOX fuel on fission gas release.

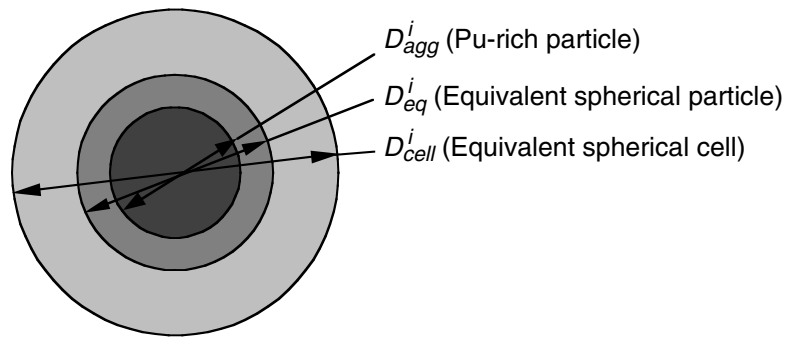
In this paper, a fission gas release model for MOX fuel has been developed for the analysis of the effect of Pu heterogeneity on gas release by considering the distribution of Pu-rich particles. This model is an extension of the previous one [1], which used the assumption that all Pu-rich particles are of the same size. The model uses the concept of the equivalent spherical cell that is composed of an equivalent spherical particle with the diameter of  $D_{eq}^i = D_{agg}^i + 2 * L_{rec}$  and the  $\text{UO}_2$  matrix that surrounds it as shown in Fig.1. Here  $D_{eq}^i$  and  $D_{agg}^i$  represent the diameters of an equivalent spherical particle and a Pu-rich particle for i-th group, respectively, when the Pu-rich particles are divided into n groups according to their size, and  $L_{rec}$  is the recoil length of fission products of about 6 mm. The diameter of an equivalent spherical cell  $D_{cell}^i$  for i-th group is defined in such a way that Pu mass in each equivalent cell is equal to the sum of Pu mass in a Pu-rich particle and that in the  $\text{UO}_2$  matrix. Then the diameter of an equivalent cell is derived as follows using the assumption that Pu content in the Pu-rich particles is the same, irrespective of the group to which they belong, and those in the matrix regions are also the same for all groups:

$$D_{cell}^i = D_{agg}^i \frac{-e_a - e_m}{e_p - e_m},$$

where  $e_a$  is the Pu content in the Pu-rich particle,  $e_p$  the average Pu content in the fuel pellet, and  $e_m$  the Pu content in the  $\text{UO}_2$  matrix. Fission rates both in the equivalent particle and in the  $\text{UO}_2$  matrix are calculated by multiplying the average fission rate in the fuel pellet by their respective ratios of Pu content to the average for a fuel pellet. If the fuel parameters are such that  $D_{eq}^i * D_{cell}^i$ , the i-th group can be treated as homogeneous because in this case the distribution of produced fission gas would be distributed uniformly in the equivalent spherical cell.

Yang-Hyun Koo,  
Byung-Ho Lee,  
Dong-Seong Sohn  
Korea Atomic Energy  
Research Institute,  
Daejeon, Korea

Figure 1. An equivalent spherical cell for a Pu-rich particle of i-th group.

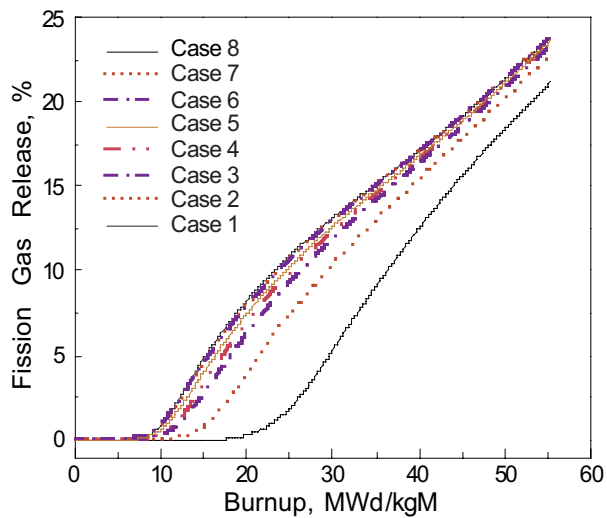


Then the average gas release fraction  $f$  for a fuel pellet with  $n$  groups of Pu-rich particles is expressed as

$$f = \sum_{i=1}^n F_{agg}^i * (REL_{eq}^i + REL_m^i) / \sum_{i=1}^n F_{agg}^i * (PRO_{eq}^i + PRO_m^i),$$

where  $F_{agg}^i$  is the fraction of Pu-rich particles corresponding to the  $i$ -th group of the total number of Pu-rich particles,  $REL_{eq}^i$  and  $PRO_{eq}^i$  are the released and produced amount of fission gas for an equivalent spherical particle of the  $i$ -th group, respectively, and  $REL_m^i$  and  $PRO_m^i$  are the corresponding values for the matrix region in an equivalent spherical cell of the  $i$ -th group.

The model has been incorporated into a computer code, COSMOS [2], and a parametric study has been made to investigate the heterogeneity effect of MOX fuel on gas release for a constant fuel temperature of 900°C and linear power of 250 W/cm. Grain sizes both in the Pu-rich particle and in the UO<sub>2</sub> matrix are all assumed to be 15 μm. In addition, average Pu content of the fuel pellet is taken to be 0.06, while those for Pu-rich particle and UO<sub>2</sub> matrix are given as 0.23 and 0.04, respectively. Fig. 2 shows the calculated results in ascending order of magnitude for 8 cases given in the table below, where the combination of three sizes of Pu-rich particles (20, 30 and 40 μm) are considered. From these calculations, it is confirmed that the more Pu is accumulated in larger Pu-rich particles, the more fission gas is released for the same operating conditions. This is because more fission gas atoms would migrate to the grain boundaries in the larger Pu-rich particles than in the smaller ones due to more production of gas atoms, thereby leading to earlier formation of release paths in the grain boundaries and larger gas release. This phenomenon is dominant at low burnup, where the formation of release path plays a major role in determining the amount of gas released. However, the effect decreases with burnup because at high burnup many gas atoms would be available for release at the grain boundaries with release paths already being established. It can be concluded from this parametric study that the present model explains why there exists some experimental evidence that fission gas release rates are enhanced in LWR MOX fuel compared with conventional UO<sub>2</sub> fuel under similar operation conditions.



	$F_{agg}^1$ (20 $\mu\text{m}$ )	$F_{agg}^2$ (30 $\mu\text{m}$ )	$F_{agg}^3$ (40 $\mu\text{m}$ )
Case 8	0.00	0.00	1.00
Case 7	0.00	0.50	0.50
Case 6	0.50	0.00	0.50
Case 5	0.33	0.33	0.33
Case 4	0.00	1.00	0.00
Case 3	0.50	0.50	0.00
Case 2	1.00	0.00	0.00
Case 1	UO <sub>2</sub>		

Figure 2. Effect of the size distribution of Pu-rich particles on fission gas release.

### References

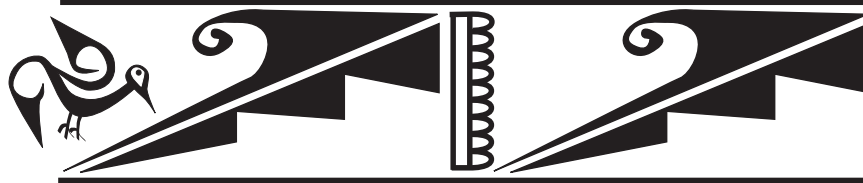
1. Yang-Hyun Koo, Dong-Seong Sohn and P. Strijov, "A Fission Gas Release Model for MOX Fuel and Its Verification," International Symposium on MOX Fuel Cycle Technologies for Medium and Long-Term Deployment, Vienna, Austria, May 17-21, 1999.
2. Yang-Hyun KOO, Byung-Ho LEE and Dong-Seong SOHN, Journal of the Korean Nuclear Society, **30** (1998) 541-554.

## Comparative Analysis of Basic Process Arrangements for Converting Surplus Weapons Grade Plutonium to MOX Fuel

**V. P. Varykhanov,  
E. M. Glagovskiy,  
B. S. Zakharkin,  
V. V. Revyakin and  
O. V. Khauystov**

*State Scientific Center  
of Russian Federation  
A. A. Bochvar All-  
Russia Scientific  
Research Institute of  
Inorganic Materials  
123060 Moscow,  
Russia*

The report looks at basic ways of converting surplus weapons grade plutonium to MOX fuel for fast and light-water reactors. The authors give results of research under standard conditions on the physicochemical and technological characteristics of plutonium and uranium-plutonium dioxides produced by different process arrangements. A comparative analysis is made of the most advanced options for converting plutonium to MOX fuel. The paper gives a process scheme developed by the authors for conversion of weapons grade plutonium to MOX fuel for fast and light-water reactors.



## **Separations & Process Chemistry**



# Technical Challenges in Support of the Plutonium Materials Conversion Program in Russia

## Introduction

The Department of Energy's Plutonium Materials Conversion Program for Russia is designed to assist Russia in defining a path for the destruction of weapons grade plutonium. A similar program is currently defining a program for destruction of US weapons grade plutonium. These two sister programs arose from the September 1998 meeting between President Yeltsin and President Clinton, after which they issued a "Joint statement of principles for management and disposition of plutonium designated as no longer required for defense purposes." The US and Russia have each committed to convert 50 metric tons of plutonium from nuclear weapons programs to forms which are unusable for weapons.

The Russian disposition program includes conversion of plutonium metal to oxide, fabrication of MOX fuel using this oxide, and modification and licensing of reactors to burn MOX fuel. This paper describes the current Russian conversion work in support of the disposition goal and areas that have been identified as suitable for research collaborations.

## Description

There are two overall paths for converting weapons grade Pu into less viable forms: conversion to fuels for nuclear reactors and immobilization into forms from which it is hard to recover plutonium. Russia considers Pu a valuable commodity that can be converted to energy in the form of nuclear fuel with only small amounts being wasted, i.e., immobilized. The US considers Pu a danger that needs to be disposed of safely with smaller amounts being developed as nuclear fuel.

## Results and Significance

The Russian conversion program has focussed on defining the best process for converting Pu to its oxide. Four methods are under consideration:

1. dissolution of metal and reprecipitation using oxalate
2. dissolution of metal and reprecipitation using ammonia
3. a dry method using conversion to hydride and nitride followed by an aqueous purification step (such as is used in the US ARIES process), and
4. a pyroelectrochemical method.

Throughout the last year research has been conducted in Russia in order to define the most effective method. We expect the Russian decision on their choice in the early spring of 2000.

C. F. V. Mason,  
S. J. Zygmunt,  
W. K. Hahn,  
C. A. James,  
D. A. Costa,  
W. H. Smith,  
S. L. Yarbrow

*Los Alamos National  
Laboratory, Los  
Alamos, NM 87545*

There are several areas with continuing technical challenges. Three have been identified, two for aqueous processing and one for pyroelectrochemical processing:

1. A recurring challenge in Pu chemistry is the multiple oxidation states (+3, +4, +6) found in aqueous solution. Many separation processes are based on dissimilar chemical behavior of plutonium in different oxidation states. In the anion exchange purification of Pu solutions, Pu (IV) is retained on the resin while impurities are removed.<sup>1</sup> Plutonium ions are subsequently eluted off the column by reduction to Pu(III). Various reducing agents have been investigated for this purpose.<sup>2</sup> The reducing agent currently used in the US is hydroxylamine while Russia uses hydrazine. The hydroxylamine reduction produces small amounts of nitrogen and nitrous oxide and is inhibited by Pu(III). The hydrazine forms potentially explosive byproducts.
2. The characteristics that affect the dissolution of PuO<sub>2</sub> in nitric acid are incompletely understood.<sup>3</sup> Some of the parameters that exert an influence on the dissolution include the prior processing of PuO<sub>2</sub>, temperature, solid-to-liquid ratio, and the presence of complexing agents. The complexing properties of fluoride exert a catalytic influence on the dissolution with the rate being controlled by the diffusion of fluoride species through the surface oxide film. The speed and completeness of dissolution also affect the economics of fuel production. However, fluoride itself is an impurity that can only be tolerated below certain levels (~ 250 ppm). Further, fluoride attacks glass. The kinetics and mechanism of fluoride catalysis need to be better understood.
3. Gallium is added to weapons grade Pu to stabilize the material in the correct crystallographic phase. This gallium must be removed to convert weapons grade Pu into MOX fuels for consumption in nuclear power reactors. One possibility for carrying out the separation of the two metals is by using selective electrodeposition in a high temperature chloride-based molten salt. However, little is known about the chemical behavior of gallium and gallium oxides in this media due mainly to the difficulty of making accurate measurements at elevated temperatures (>600°C). A solution to this problem is to study the chemical behavior of the element under less severe conditions using room temperature ionic liquids (RTIL). RTILs are liquid at room temperature and have a very wide electrochemical window and a very wide spectroscopic window allowing for more accurate measurements of chemical systems.<sup>4</sup> Information obtained at room temperature can then be extrapolated to estimate the behavior of gallium compounds at the elevated temperatures characteristic of the molten salt systems. Alternatively, it may be possible to develop a process to separate gallium and Pu in an RTIL. A room temperature process could potentially decrease operation time, require the use of simpler equipment, and be less hazardous to the operator.

Collaborative research between the Bochvar Institute of Inorganic Materials, Moscow; the Research Institute for Atomic Reactors, Dimitrovgrad; and the Los Alamos National Laboratory has been initiated. We are planning joint Russian/Los Alamos workshops at Los Alamos to review the current state of the subject followed by laboratory work carried out both in Russia and at Los Alamos.

## References

1. "MOX Fuel Aqueous Polishing Flowsheet Support," S. L. Yarbrow, et al., Los Alamos National Laboratory report LA-CP-98-327 (October 1998).
2. "The Kinetics of the Oxidation-Reduction Reactions of Uranium, Neptunium, Plutonium and Americium in Aqueous Solutions," T. W. Newton, ERDA Critical Review Series, Technical Information Center, Office of Public Affairs, US Energy Research and Development Administration, Oak Ridge, Tennessee (1975).
3. "Plutonium dioxide dissolution in nitric/hydrofluoric acid mixtures- kinetics and mechanism," G. S. Barney, AEC AT(45-1)-2130, Atlantic Richfield Hanford Company, Richland, WA (1973).
4. "Electrochemistry and Spectroscopy of  $UO_2^{2+}$  in acidic  $AlCl_3$ -EMIC," C. J. Anderson, G. R. Choppin, D. J. Pruett, D. A. Costa and W. H. Smith, *Radiochimica Acta*, 84(1), 31-36 (1999).

## Acknowledgments

The authors acknowledge the support of John Baker, Program Manager of the Materials Disposition Program, US Department of Energy.

## CHEMOX: An Integrated Facility for the Conversion of Russian Weapon-Grade Plutonium into Oxide for MOX Fuel Fabrication

**E. Glagovski**

(A. A. Bochvar,  
Russia),

**Y. Kolotilov**

(GSPI, Russia)

**B. Sicard**

(CEA, France),

**F. Josso**

(CEA, France),

**G. Fraize**

(COGEMA, France)

**N. Herlet**

(CEA, France),

**A. Villa**

(COGEMA, France),

**P. Brossard**

(CEA, France)

In the frame of the trilateral agreement between Russia, Germany and France, the CHEMOX (chemistry from metal into oxide) facility is proposed for the conversion of the alloyed plutonium coming from the dismantling of nuclear pits into an oxide suitable for MOX fuel fabrication and irradiation in VVER- or BN-type reactors. For the CHEMOX facility an aqueous conversion process has been chosen for its versatility, and compatibility with known technologies and with existing on-site treatment facilities. The process mainly consists in the following steps:

• A batch dissolution in a mixture of nitric acid and hydrofluoric acid,

• The plutonium purification and recovery by liquid-liquid extraction with an organic solvent,

• The oxide preparation through an intermediate oxalate precipitation and calcination method.

Around that process, the work to be done have been split in two parts: laboratory scale research and development experiments and engineering studies.

The research and development studies are aimed at assessing the conversion process in terms of performance, safety and secondary waste management. The CHEMOX plant will have to convert two tons of weapons grade plutonium per year (extendable up to 5 t/year). For performance the kinetics have to be maximized, especially for the dissolution and the recovery yield at each step, as well as for the recycling of dissolution residues. Plutonium recovery from possible scraps produced in the MOX fabrication plant is also considered. Best conditions for the purification of plutonium from high concentration solutions are looked for. Regarding the safety, such issues as the gas phase evolution during the dissolution, the possible formation of plutonium fluoride complexes (which could precipitate) or the pyrophoricity of dried residues are addressed. Waste management work deals with the validation of gas trapping methods and liquid effluents treatment procedures in accordance with other on-site treatment facilities requirements.

An overview of the engineering development work, taking into large account Russian and French industrial experience is also given. The studies follow the general Russian road-map for the conception and building of new nuclear facilities. The objective of the present work is to give the more precise estimate of the investment and operation costs, which takes into account safety and environmental requirements, and to draw a construction and start-up schedule. Engineering teams have to work in close relations with research and development institutes and with nuclear sites' operational teams to reap maximum benefit from industrial experience. The work includes a detailed description of the plant and of its integration in the Russian nuclear site to be chosen. The licensing procedure is also addressed.

The presentation describes the organization of the work done in the frame of the trilateral collaboration and emphasizes the results obtained.

## Radiation-Chemical Behaviour of Plutonium in Solutions DAMP and TOPO in n-dodecane

The extraction ability of di-isoamylmethylphosphonic acid ether (DAMP), and the octylphosphinoxide (TOPO) is superior to one of TBP and TIAP. Radiation stability of DAMP and TOPO exceeds one of the alkyphosphates. Radiation-chemical behaviour is of interest in this connection. Some questions of radiation-chemical behaviour of Plutonium in gamma-irradiated (to  $2,5 \cdot 10^6$  Gy) solutions of DAMP and TOPO (10% and 5%, respectively) have been studied by spectrophotometry. The concentration of plutonium in solutions was  $1,6 \cdot 10^6$  mol/l.

Complexes Pu(IV) with products of radiolysis of DAMP and TOPO (mono-isoamylmethylphosphonic and di-octylphosphinic acids, respectively) have been found to form in the process of gamma-irradiation of the solution. Radiation-chemical formation yields of these complexes have been found to be 0,6 and 0,3 molec/100 eV. Precipitates of plutonium insoluble compounds with the radiolysis products of the solutions are formed at doses  $1,7 \cdot 10^6$  and  $2,4 \cdot 10^6$  Gy for solutions DAMP and TOPO, respectively.

**D. A. Fedoseev**  
SSC A. A. Bochvar  
All-Russia Research  
Institute of Inorganic  
Materials, Moscow,  
Russia.

## Dissolution of Phosphate Matrices Based on the Thorium Phosphate Diphosphate

**N. Dacheux,**  
**A. C. Thomas,**  
**V. Brandel,**  
**M. Genet**  
*Nuclear Physics*  
*Institute, 91406*  
*Orsay, France*  
*P. Le Coustumer*  
*LMGE, UMR-CNRS,*  
*86022, Poitiers,*  
*France*

Several authors have reported the use of phosphate matrices like apatites, monazites or NZP for the immobilization of actinides coming from an advanced reprocessing or for the final disposal of the excess plutonium from dismantled nuclear weapons. The thorium phosphate diphosphate  $\text{Th}_4(\text{PO}_4)_4\text{P}_2\text{O}_7$  (namely TPD) was also proposed for this purpose. Indeed, its structure allows the replacement of large amounts of tetravalent actinides like uranium, neptunium or plutonium leading to the obtention of solid solutions. The maximum weight loading was estimated to be equal to about 48% for uranium, 33% for neptunium and 26% for plutonium.

Sintered samples (14×5×5 mm) were obtained from a dried residue prepared, after the slow evaporation of a mixture of concentrated solutions, through a simple procedure based on two steps: pressing at room temperature at 100 – 800 MPa then heating at 1250°C for 10 hours. The density measured was equal to 95%–99% of the calculated value.

The behavior of the TPD during leaching tests was also examined varying several parameters like the area/volume ratio ( $S/V$ ), the temperature, the acidity of the leachate, the leaching flow and the phosphate concentration in the solution. As the TPD is very insoluble, several experiments were performed in very acidic conditions (5M and  $10^{-1}$ M  $\text{HNO}_3$ ) in order to increase the dissolution rate. The kinetic was conducted for low  $S/V$  ratio values ( $25 \text{ cm}^{-1}$  –  $692 \text{ cm}^{-1}$ ) while the neoformed phases obtained at the saturation of the solution (thermodynamic equilibrium) were studied for higher  $S/V$  ratios.

The dependence of the TPD dissolution rate on the proton concentration was determined by making experiments on samples doped with trivalent actinides. This study led to a partial order related to  $[\text{H}_3\text{O}^+]$  ( $n$ ) equal to 0.30 – 0.35 while the apparent leaching rate constant ( $k_{298\text{K}}$ ' corresponding to a proton concentration equal to 1M) was evaluated to  $1\text{--}3 \cdot 10^{-5} \text{ g}/(\text{m}^2\cdot\text{d})$  at room temperature. These values were also determined for  $\text{Th}_{4-x}\text{U}_x(\text{PO}_4)_4\text{P}_2\text{O}_7$  (TUPD) and  $\text{Th}_{4-x}\text{Pu}_x(\text{PO}_4)_4\text{P}_2\text{O}_7$  (TPPD) solid solutions. For TUPD solid solutions, the  $n$  and  $k_{373\text{K}}$ ' were found to be 0.40 and  $2.8 \cdot 10^{-4} \text{ g}/(\text{m}^2\cdot\text{d})$ . For TPPD solid solutions, the saturation of the solution seems to be reached for very short leaching times, which does not allow us to get the  $n$  and  $k_{298\text{K}}$ ' determination with a good accuracy in static conditions. Leaching tests in dynamic conditions were conducted to avoid this problem. The  $n$  values determined are consistent with those obtained for several minerals.

The temperature dependence of the dissolution rate was determined for the pure TPD between 4°C and 120°C. The activation energy  $E_A$  deduced from the Arrhenius law was found to  $42 \pm 3 \text{ kJ}\cdot\text{mol}^{-1}$  as shown from Figure 1. It seems to be the same for TUPD solid solutions.

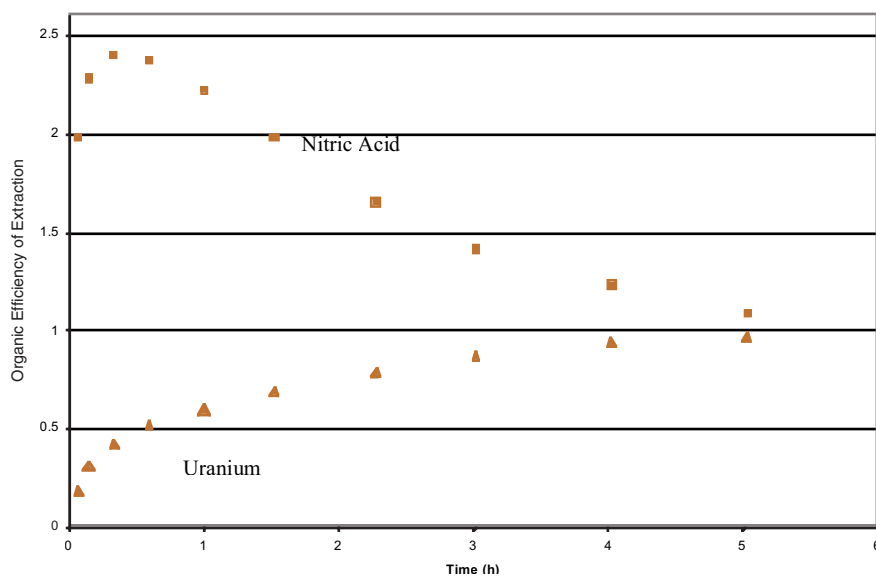
The TPD dissolution rate is also slightly increased by the presence of phosphate ions in the solution. Nevertheless, this increase is significant (more than 10%) for phosphate concentration higher than  $5 \cdot 10^{-2} \text{ M}$ .

## Modelling of Nitric Acid and U(VI) Co-Extraction in Annular Centrifugal Contactors

British Nuclear Fuels Limited (BNFL) is currently developing novel flow sheets for an advanced PUREX process using centrifugal contactors. This technology provides two major advantages. Firstly, centrifugal contactors can process high throughputs of liquid, while being an equipment of small size, compared to pulsed columns for example. Secondly, during the reprocessing of actinides with diluted tributyl phosphate (TBP) solutions, centrifugal contactors also minimise solvent hydrolysis and radiolysis because of the very short contact times involved.

However, the short residence times mean that the rates of mass transfer of the actinides and nitric acid between the aqueous and organic phases assume greater importance than in conventional contactors. As literature about mass transfer in annular centrifugal contactors is scarce, modelling work on the kinetics of extraction of nitric acid was needed to compute precisely the concentration of nitric acid in each phase in the contactor. The concentration-profile of nitric acid in the series of contactors is important, as it determines the distribution coefficient of the actinides in the flow sheet, and therefore the efficiency of the separation. At some experimental conditions, the concentration of nitric acid, in the organic phase, can even be greater than its equilibrium value, posing an additional challenge to process modelling.

In the feed stage of the process, nitric acid is co-extracted with uranium. When the aqueous concentration of uranium (U) is high ( $\approx 200 \text{ g}\cdot\text{l}^{-1}$ ), the organic concentration of nitric acid can exceed its equilibrium value for short contact times. This so-called *overshoot* is an effect of the kinetics of mass transfer, as shown in Figure 1. The organic concentration of nitric acid then decreases, as if the U(VI) were replacing nitric acid that has extracted in excess of that at equilibrium. Overshoot is also reported for the extraction of plutonium (Pu), at similar conditions. Therefore, it is of importance to be able to predict nitric acid overshoot, in order to understand better the behaviour of Pu, and to compute criticality criteria with higher accuracy.



**E. T. Gaubert,  
M. Jobson**  
UMIST, Manchester,  
M60 1QD, UK

**J. E. Birket,  
I. S. Denniss**  
Research and  
Technology, BNFL,  
Sellafield, Seascale,  
Cumbria, CA20 1PG,  
UK

**I. May**  
BNFL Radiochemistry  
Center of Excellence,  
University of  
Manchester, Oxford  
Road, Manchester,  
M13 9PL, UK

**Figure 1. Nitric acid overshoots its equilibrium value while U is extracted (data from Ref. 1).**

A review of the literature shows some disagreements; the majority of researchers state that nitric acid mass transfer is very fast compared to that of actinides. This commonly held view is exemplified by the model of Nitsch and Schoor.<sup>1</sup> They studied extensively the co-extraction of nitric acid and U(VI) in a Lewis cell. Their model embodies a mass transfer coefficient for nitric acid that is twice the mass transfer coefficient of U(VI) ( $120 \text{ g}\cdot\text{l}^{-1}$  of U(VI), 30% TBP). This is in disagreement with observations<sup>2</sup> that the diffusivity of the U(VI)-2TBP complex, in a 30%TBP-dodecane phase, is about 2.5 times greater than the diffusivity of  $\text{HNO}_3\cdot\text{TBP}$ . As the ratio of two mass transfer coefficients is approximately the square root of the ratio of the diffusivity of the two species, the overestimation of the mass transfer coefficient of nitric acid is of a factor 4.

Another mechanism is sometimes advocated to explain fast transfer of nitric acid. It assumes that  $\text{HNO}_3$  would diffuse freely in the organic phase, and faster than U. Free diffusion of nitric acid in the organic phase can be disregarded because dissociation of  $\text{HNO}_3\cdot\text{TBP}$  is less than 0.5%.

In this work an *a priori* mass transfer model is presented that assumes the same overall mass transfer coefficient,  $K$ , for U(VI), nitric acid, and TBP. The approach is semi-empirical. However it relies on the fact that species of similar size should have similar mass transfer coefficients.  $K$  was determined from U(VI) mass transfer experiments, therefore no parameters were fitted to model the behaviour of nitric acid. The model assumes that the equilibrium concentration of nitric acid,  $C^{**}$ , changes with the amount of U(VI) extracted and as the concentration of free TBP decreases.  $C^{**}$  is simply computed by using an existing equilibrium correlation as a function of the free TBP for any time during the extraction process. Hence the driving force for mass transfer,  $(C^{**}-C)$ , where  $C$  is the bulk concentration, also varies with the concentration of U(VI). Mass transfer rates are then given by  $K\cdot(C^{**}-C)$ . At high values of  $C^{**}$ , the flux of nitric acid extracted is limited by the available flux of TBP.

Experimental data were obtained with a single stage miniature centrifugal contactor. The mass balances for nitric acid closed to within 5%. Our simple model can represent the co-extraction of nitric acid and U(VI), with or without overshoot of nitric acid. Furthermore, the validity of the model is proved as it also represents accurately simultaneous back-extraction of nitric acid and extraction of  $200 \text{ g}\cdot\text{l}^{-1}$  of U(VI), in 30% TBP.

However, this model cannot successfully represent co-extraction of nitric acid and U(VI) in to 20% TBP. It would predict an overshoot of nitric acid while no overshoot is observed experimentally. The reason for this is not clear. The model could be extended to represent Pu(IV) and U(VI) and nitric acid co-extraction, provided that a suitable correlation was available to predict the equilibrium concentration of Pu(IV) as a function of the amount of nitric acid and U(VI) extracted. It is possible that chemical reactions kinetics may also be needed, as Pu(IV) and U(VI) would compete for TBP.

## References

1. Nitsch, W., and van Schoor, A., 1983, The Kinetics of Coextraction in the System Uranyl Nitrate, Nitric Acid, Tributylphosphate, *Chemical Engineering Science*, **38**(12): 1947-1957.
2. Marx, G., Gauglitz, R., Friehmelt, V., and Feldner, K. H., 1986, Transport Processes of Actinides in Aqueous and Non-Aqueous Solutions, *Journal of the Less-Common Metals*, **122**: 185-188.

# The Measurement of U(VI) and Np(IV) Mass Transfer in a Single Stage Centrifugal Contactor

## Introduction

BNFL currently operates two reprocessing plants for the conversion of spent nuclear fuel into uranium and plutonium products for fabrication into uranium oxide and mixed uranium and plutonium oxide (MOX) fuels. To safeguard the future commercial viability of this process, BNFL is developing novel single cycle flowsheets that can be operated in conjunction with intensified centrifugal contactors. Recent research has focussed on the effective control of neptunium and two hydroxamic acids, formohydroxamic acid (FHA) and acetohydroxamic acid (AHA), which have been shown to selectively complex and strip Np(IV) into aqueous nitric acid from a U(VI) product stream in 30% TBP/OK (tributyl phosphate in odourless kerosene).<sup>[1]</sup> A countercurrent centrifugal contactor trial has proven the viability of this process<sup>[2]</sup> although there was some discrepancy between the modelled and experimental data obtained from this trial. The most likely cause of this discrepancy is an inadequate understanding of Np(IV) mass transfer in the presence of hydroxamic acids. By undertaking single stage centrifugal contactor trials using flowsheet specific feed concentrations it was hoped that a better understanding of Np(IV) mass transfer could be obtained which could in turn be used to increase the accuracy and reliability of the flowsheet model.

## Results and Discussion

Initially a series of single stage trials were undertaken to monitor the extraction of U(VI) in the absence of either Np(IV) or hydroxamic acids to test the viability of using a 1cm rotor diameter annular single stage centrifugal contactor to monitor mass transfer (the contactor used was based on the Argonne design<sup>3</sup>). The trials were run with an aqueous phase containing variable concentrations of nitric acid and U(VI) and a 30% TBP/OK organic phase containing variable loadings of nitric acid. Two physical parameters were also varied; rotor speed and feedstock flow rates (both aqueous and organic phases). Results clearly indicated that contact time and phase mixing efficiencies had a major influence on U(VI) mass transfer efficiency (i.e., both flow rates and rotor speeds). Of all the chemical parameters tested the only one that appeared to have any significant effect was the amount of free TBP, and then only at high initial aqueous phase U(VI) concentrations (~200g/l). For most conditions it could therefore be assumed that the overall mass transfer coefficient for U(VI) is independent of chemical effects.

The next single stage contactor trials initiated were for Np(IV) extraction and again contact time significantly affected mass transfer efficiency i.e. at higher flow rates Np(IV) mass transfer decreased. However, of more interest was the decrease in extraction rate of Np(IV) compared with U(VI), which is indicative of a comparatively slow chemical reaction between Np(IV) and TBP (Figure 1). The rate of Np(IV) extraction is increased when U(VI) is also loaded into the system suggesting that the presence of U(VI) leads to an increase in the rate of chemical interaction between Np(IV) and TBP.

**I. May**

*BNFL Radiochemical  
Centre of Excellence,  
University of  
Manchester,  
Manchester, M13 9P,  
Great Britain*

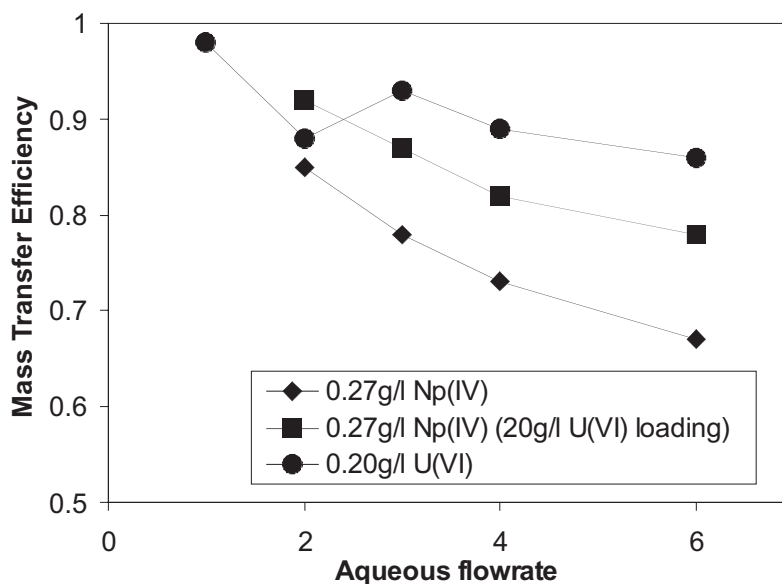
**E. J. Birkett,**

**I. S. Denniss**  
*BNFL Sellafield,  
Seascale, Cumbria,  
CA20 1PG, Great  
Britain*

**E. T. Gaubert,**

**M. Jobson**  
*UMIST, Manchester,  
M60 1Q, Great Britain*

Figure 1. Mass transfer efficiencies for U(VI) and Np(IV) calculated from single stage centrifugal contactor data. The organic:aqueous flow rate ratio = 2:1 and aqueous  $[HNO_3] = 2.0M$ .



Finally, single stage centrifugal contactor Np(IV) strip experiments were undertaken in the presence and absence of hydroxamic acids and U(VI). Preliminary results confirmed that both the presence of hydroxamic acids in the initial aqueous phase and U(VI) in the organic phase lead to an increase in Np(IV) stripping at all the flow rates tested. Also, due to the decreased surface area for the Np(IV) strip experiments (6:1 organic:aqueous ratio) compared with the Np(IV) extract experiments (2:1 organic:aqueous ratio) there is a subsequent decrease in Np(IV) mass transfer efficiency.

### Conclusion

Single stage contactor trials have confirmed that actinide mass transfer efficiency is significantly lowered as phase contact time is lowered. It has also been shown that the rate of mass transfer for Np(IV) is also significantly lower than for U(VI). A further assessment is ongoing to ascertain the effects of U(VI) and hydroxamic acids on the mass transfer efficiency of Np(IV) stripping, which will then be incorporated into flowsheet models.

### References

1. The application of formo- and aceto- hydroxamic acids in nuclear fuel reprocessing, R. J. Taylor, I. May, A. L. Wallwork, I. S. Denniss, N. J. Hill, B. Ya. Galkin, B. Ya. Zilberman and Yu. S. Fedorov, *J. Alloys & Comp.*, **271-273**, 1998, 534-537.
2. The development of chemical flowsheets for an advanced purex process, A. L. Wallwork, P. Bothwell, J. E. Birkett, I. S. Denniss, R. J. Taylor and I. May, accepted for publication *The Proceedings of the International Solvent Extraction Conference*, '99.
3. Annular centrifugal contactors for solvent extraction, R. A. Leonard, G. J. Bernstein, A. A. Ziegler and R. H. Peltó, *Sep. Science and Tech.*, **15(4)**, 1980, 925-943.

## Actinide Chemistry in Room Temperature Ionic Liquids: Actinide Chemistry in RTIL Systems (Why?)

Room temperature ionic liquids (RTILs) have potential throughout the nuclear industry in the recovery and purification of actinide elements, as reactor components, as waste disposal forms, and potentially as media for the storage and/or separation of spent nuclear fuels. Due to their unique dissolution properties, RTILs can be used as substitutes for solvents currently used in the extraction of uranium from native ores, and in the dissolution and reprocessing of spent nuclear fuels. Potential benefits include greater uranium and plutonium recovery efficiencies and the ability to recycle the solvent, leading to a decrease in waste generation and lower overall production costs. Another potential area of interest is in the use of RTILs as solvents for the recovery and purification of actinide elements. Many of the current recovery processes are redox based and are carried out in high temperature molten salt systems. These processes are inefficient, require extreme operating conditions and generate large quantities of contaminated residues. Substituting RTILs for the high temperature melts and performing these reactions at ambient temperature would allow for greater control over the reactions, leading to much higher yields and higher final product purity. The development of room temperature, low-pressure processes would mitigate the safety concerns associated with high temperature operations. Also the ability to recycle these extremely low vapor pressure solvents would lead to significantly less waste generation. Finally, the unique ability to adjust the acid/base properties of some of the RTIL melts, coupled with the lack of interference from hydrolysis reactions, creates an opportunity to obtain much more detailed information on the fundamental chemical behavior of actinide compounds. This knowledge can be instrumental in the development of the next generation of actinide separation and purification processes.

Research efforts in our laboratory focus on determining the chemical properties (i.e., solubility, complexation, redox properties, etc.) of actinide species in RTIL systems. We are currently involved in RTIL projects ranging from the spectroscopic characterization of actinide complexes by  $O^{17}$ NMR, low temperature UV-Vis, and EXAFS, to the enhanced dissolution and separation of actinide oxides in room temperature ionic liquids. We have extensive experience in the electrochemical characterization of actinide complexes in ionic melts and are focusing efforts in support of the Accelerator Transmutation of Waste (ATW) and Advanced Design and Production Technologies (ADAPT) programs. Ultimately we would like to be able to compare the chemistries observed in the RTIL systems with the high temperature molten salt systems currently in use in the actinide recovery and purification processes. The results of our study will allow us to evaluate the potential of ionic liquids as alternative solvents in the nuclear industry.

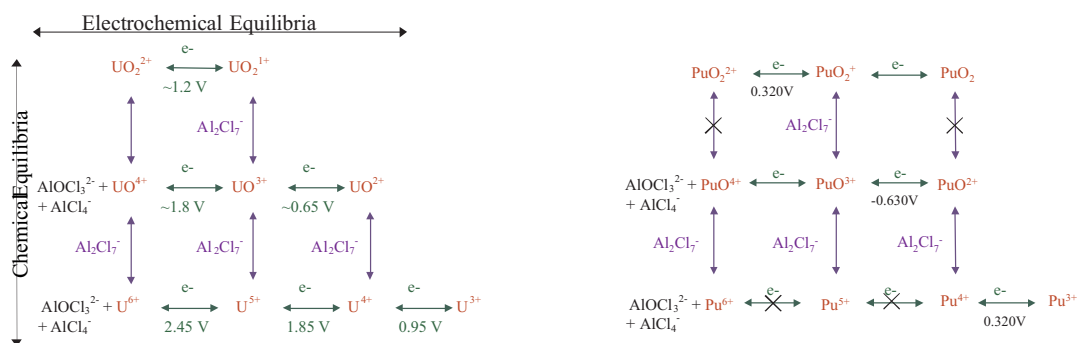
We have previously reported on the redox behavior of uranyl chloride in room temperature acidic 1-ethyl-3-methyl imidazolium chloride by electrochemical and spectroscopic techniques.<sup>1,2</sup> The uranyl moiety is unstable to oxygen loss in this melt with the concomitant in-growth of a uranium (V) chloride species. We proposed that an equilibrium is established between the Lewis acidic  $Al_2Cl_7$  and the uranium oxy-chloride species (Figure 1). Similar behavior may be expected for plutonium oxide species. Spectroscopic and electrochemical results on uranium and plutonium in the +3, +4, +5 and +6 oxidation states will be presented at this

David A. Costa,  
Wayne H. Smith,  
Kent D. Abney,  
Warren J. Oldham  
*Los Alamos National  
Laboratory, Los  
Alamos, NM 87544  
USA*

conference. We have demonstrated that a basic EMIC/ $\text{AlCl}_3$  solution of  $\text{PuCl}_3$  displays one reversible oxidation and an irreversible reduction. The reversible wave has been confirmed to be associated with the Pu (III)/Pu (IV) redox couple by comparison with the CV of an authentic sample of  $\text{Cs}_2\text{PuCl}_6$ . The irreversible reduction wave is believed to come from the reduction of a plutonium oxide contaminant. We propose an equilibrium diagram similar to that presented for uranium to explain these results (Figure 2). New calculations on the critical mass of RTIL Pu systems will also be presented.

**Figure 1.**  
Mechanism for the reaction of  $\text{UO}_2^{2+}$  with an acidic  $\text{AlCl}_3$ /EMIC RTIL.

**Figure 2.** Possible reaction pathways for  $\text{PuO}_2^{2+}$  in  $\text{AlCl}_3$ /EMIC RTIL.



## References

1. Anderson, C. J.; Choppin, G. R.; Pruett, D. J.; Costa, D. A.; Smith, W. H., *Rad. Chem. Acta.* 84, 31-36 (1999).
2. David A. Costa, Wayne H. Smith; Proceedings of the Eleventh International Symposium on Molten Salts, P. C. Trulove, H. C. De Long, G. R. Stafford, S. Deki, PV 98-11, p. 266, The Electrochemical Proceedings Series, Pennington, NJ 1998.
3. David A. Costa, Wayne H. Smith; Proceedings of the Eleventh International Symposium on Molten Salts, P.C. Trulove, H.C. De Long, G.R. Stafford, S. Deki, **PV 98-11**, p. 266, The Electrochemical Proceedings Series, Pennington, NJ 1998.

## Oxidation of Pu(IV) and Pu(V) with Sodium Hypochlorite

The hypochlorite ion ( $\text{OCl}^-$ ), a major product of the radiolysis of water in solutions containing high concentrations of chloride, can be expected to influence the oxidation state distribution of plutonium in these solutions. Since plutonium has significantly different chemistry in each of its oxidation states, knowledge of the oxidation state distribution of plutonium and of the kinetics of transfer between these oxidation states is essential for modeling the behavior of plutonium in aqueous systems and for design of efficient remediation procedures for plutonium containing wastes.

The oxidation of Pu(IV) with sodium hypochlorite has been investigated in alkaline media (0.4 - 16 M NaOH) with millimolar concentrations of plutonium by Garnov et al.<sup>1</sup> The authors report the oxidation of Pu(IV) to Pu(VI) at a rate that increases with the concentration of hypochlorite, with temperature, and with alkalinity. However, no quantitative measures of the reaction rate were reported. The oxidation of Pu(IV) under the influence of its own alpha radiation has been investigated by Bueppelmann et al.<sup>2</sup> in solutions of sodium chloride. These authors reported oxidation of Pu(IV) to Pu(V) in solutions of < 3 M NaCl, whereas oxidation was to Pu(VI) at higher chloride concentrations. The oxidation reaction, shown to be due to hypochlorite, had a rate which increased with pH, salinity and specific activity of the solution. However, again no quantitative measures of the rate constants were reported nor a rate equation.

In this study, the kinetics of the oxidation of tracer concentrations of Pu(IV) and Pu(V) with sodium hypochlorite have been investigated. By varying the pH and the concentration of sodium hypochlorite, the dependence of the reaction with respect to the concentration of  $\text{H}^+$  and of hypochlorite were studied.

The oxidation state distribution of plutonium in solution was monitored by a ultrafiltration procedure combined with solvent extraction using thenoyltrifluoroacetone, TTA, and di-(2-ethylhexyl)-phosphoric acid, HDEHP, as extractants. After removing any polymeric, hydrolytic species of Pu(IV) from solution by ultrafiltration, two parallel extraction steps were performed. Use of 0.5 M TTA in cyclohexane extracted Pu(IV) from an aqueous phase containing 0.6 M  $\text{HNO}_3$  while Pu(V) and Pu(VI) remained in the aqueous phase. A parallel extraction step using 0.05 M HDEHP in heptane extracted Pu(IV) and Pu(VI) into an organic phase at pH 0, leaving Pu(V) in the aqueous phase. The results of the two extractions allowed evaluation of the individual fractions of Pu(IV), (V) and (VI).

The rate of the oxidation of Pu(IV) to Pu(V) and Pu(VI) was found to be dependent on the pH and the concentration of sodium hypochlorite. Increasing the concentration of sodium hypochlorite leads to a faster oxidation of Pu(IV) and yields higher concentrations of the oxidized species of Pu(V) and Pu(VI). The oxidation of Pu(V) to Pu(VI) could not be observed within the time frame of the

**G. R. Choppin,  
A. Morgenstern**  
Florida State  
University,  
Tallahassee, FL-  
32306-4390, USA

experiments of up to three weeks. In the pH range from 6 to 9 in the presence of 0.2 M NaOCl no significant oxidation of Pu(V) to Pu(VI) was found. Further experiments are being conducted to define the mechanisms of the redox reactions of Pu(IV), (V) and (VI) in the presence of hypochlorite.

This research was supported under Grant No. 54893 of the Environmental Management Science Program, Office of Science and Technology, Office of Environmental Management, United States Department of Energy (DOE). However, any opinions, findings, conclusions, or recommendations expressed herein are those of the authors' and do not necessarily reflect the views of the DOE.

### References

1. Garnov, A. Yu., Yusov, A. B., Shilov, V. P., Krot, N. N., Radiochemistry 40(1) (1998) 17-21.
2. Bueppelmann, K., Magirus, S., Lierse, Ch., Kim, J. I., J. Less Comm. Met. 122 (1986) 329-336.

# Contribution of the “Simple Solutions” Concept to Estimate Density of Concentrated Solutions

## Introduction

In order to calculate criticality parameters of nuclear fuel solution systems, number density of nuclides are needed and generally estimated from density equations.<sup>1</sup> Most of the relations allowing the calculation of the density of aqueous solutions containing the electrolytes  $\text{HNO}_3\text{-UO}_2(\text{NO}_3)_2\text{-Pu}(\text{NO}_3)_4$ , usually called “nitrate dilution laws” are strictly empirical. They are obtained from a fit of assumed polynomial expressions on experimental data of density. Out of their interpolation range, such mathematical expressions show discrepancies between calculated and experimental data. The biggest discrepancies appear in the high concentrations range and can be higher than three percent.

## Description of the Actual Work

In this study, a physico-chemical approach based on the isopiestic mixtures rule is suggested. The behaviour followed by these mixtures was first observed in 1936 by ZDANOVSKII<sup>2</sup> and expressed as: “Binary solutions (*i.e.*, one electrolyte in water) having a same water activity are mixed without variation of this water activity value.” The isopiestic behaviour is followed by many multi-component solutions in particular nitrate solutions.<sup>3,4</sup> With regards to this behaviour, a set of basic thermodynamic expressions has been pointed out by Ryazanov and Vdovenko<sup>5</sup> in 1965 concerning enthalpy, entropy, volume of mixtures, activity and osmotic coefficient of the components. In particular, a very simple relation for the density is obtained from the volume mixture expression depending on only two physico-chemical variables:

- concentration of each component in the mixture and in their respective binary solutions having the same water activity as the mixture,
- density of each component respectively in the binary solution having the same water activity as the mixture.

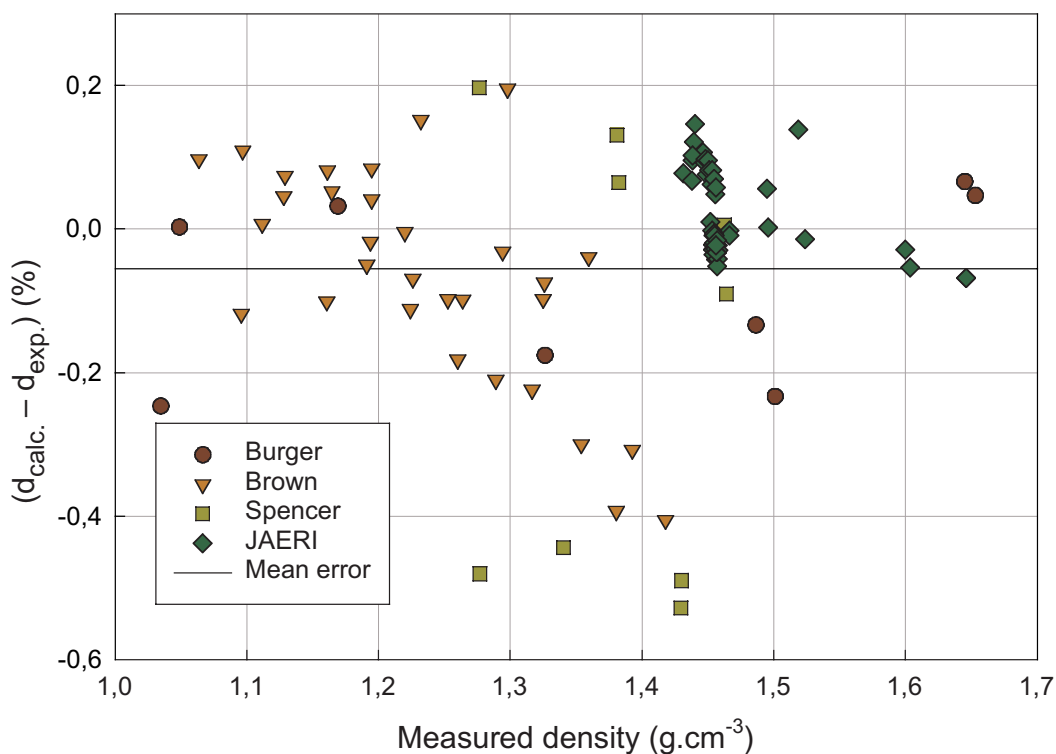
Therefore, the calculation needs the knowledge of binary data of each component (water activity, density and concentration) at the same temperature as the mixture. Such experimental data are largely published in the literature and are available for nitric acid and uranyl nitrate.<sup>6</sup> Nevertheless, nitric acid binary data show large discrepancies between the authors and need to be revised. This extensive work has been done by Charrin<sup>7</sup> during his PhD. In the field of this work, density data of uranyl nitrate binary solutions have been tabulated by incorporating recent experimental data<sup>8</sup> to older published tables.<sup>9-11</sup>

## Results

The performance of this relation has been checked on experimental density data of ternary solutions  $\text{HNO}_3\text{-UO}_2(\text{NO}_3)_2\text{-H}_2\text{O}$  available in the literature<sup>8,11-13</sup> as shown on Figure 1. The Ryazanov-Vdovenko relation has been also validated on new density data of quaternary mixtures  $\text{HNO}_3\text{-UO}_2(\text{NO}_3)_2\text{-Pu}(\text{NO}_3)_4\text{-H}_2\text{O}$ .<sup>14</sup> The mean deviation between experimental and estimated values is always lower than 0.3 percent.

Christian Sorel,  
Philippe Moisy,  
Binh Dinh,  
Pierre Blanc  
French Atomic Energy  
Commission DCC/  
DRRV/SEMP – CEA  
Valrhô BP171 30207  
Bagnols sur Cèze,  
France

Figure 1.  
Comparison  
between  
experimental and  
calculated densities  
of  $\text{HNO}_3/\text{UO}_2(\text{NO}_3)_2/$   
 $\text{H}_2\text{O}$  solutions at  
 $25^\circ\text{C}$ .



### References

1. Tachimori, S.; Ami, N.; Miyoshi, Y., "Calculation of Criticality Parameters for Uranium and/or Plutonium Nitrate Solutions, I (Evaluation of Density and Atomic Number Density of the Solutions)," Japan Atomic Energy Research Inst., 1983.
2. Zdanovskii, A. B., *Trudy Solyanoi Lab. Akad. Nauk. SSSR* **1936**, 6.
3. Kirgintsev, A. N.; Luk'yanov, A. V., *Russ. J. Phys. Chem.* **1966**, 40, 953-956.
4. Chen, H.; Sangster, J.; Teng, T. T.; Lenzi, F., *Can. J. Chem. Eng.* **1973**, 51, 234-241.
5. Vdovenko, V. M.; Ryazanov, M. A., *Sov. Radiochem.* **1965**, 7, 368-474.
6. Goldberg, R. N., *J. Phys. Chem. Ref. Data* **1979**, 8, 1005-1050.
7. Charrin, N.; Moisy, P.; Garcia-Argotte, S.; Blanc, P. *Radiochimica Acta* **2000**.
8. Brown, N. L.; Coubrough, A.; Allan, C. G., "The Use of a Digital Density Meter for Reprocessing Plant Analysis of Aqueous Uranyl Nitrate in Nitric Acid," United Kingdom Atomic Energy Authority, 1980.
9. Kaputinskii, A. F.; Lipilina, I. I., *Bull. Acad. Sc. USSR, Div. Chem. Sc.* **1956**, 661-668.
10. Grant, W. E.; Darch, W. J.; Bowden, S. T.; Jones, W. J., *J. Phys. Chem.* **1948**, 52, 1227-1236.
11. Burger, L. L.; Rahn, I. M.; Schmidt, H. R.; Slansky, C. H., "Properties of the System: Uranyl Nitrate - Aluminium Nitrate - Nitric Acid (or Sodium Hydroxyde) - Sodium Nitrate - Water - Hexone," General Electric Compagny, 1949.

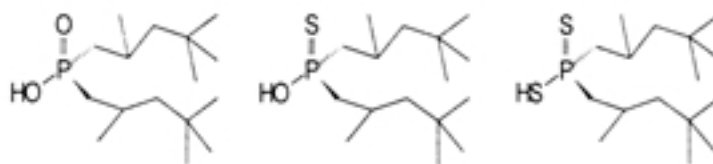
12. Spencer, B. B., Fourth International Conference on Facility Operations - Safeguards Interface, Albuquerque, New Mexico, 1991.
13. Anno, J., Réunion d'échanges techniques en sûreté criticité JAERI/IPSN-SEC.
14. Charrin, N., Université Pierre et Marie Curie, 1999.

## Structural Studies of f-Element Complexes with Soft Donor Extractants

Mark P. Jensen,  
Andrew H. Bond,  
Kenneth L. Nash  
Argonne National  
Laboratory, Argonne,  
Illinois 60439-4831

Given the chemical similarity of the trivalent lanthanide (Ln) and actinide (An) cations, traditional hydrometallurgical separations of these two groups are difficult. Bonding in f-element complexes is dominated by electrostatic (hard-hard) interactions. A given hard donor ligand will differentiate between hard cations based on their size and charge, but since the trivalent f-ions have the same charge, hard donor ligands can only separate these cations by size. Unfortunately, the lanthanide and actinide contractions give the most abundant Ln fission products and trivalent An species similar ionic radii, making the strong bonds of the f-element cations with oxygen donor ligands useless for direct Ln/An separations. Consequently, successful hydrometallurgical Ln/An separations must exploit the slightly stronger interactions of  $An^{3+}$  with ligands containing softer (more covalent) donors like nitrogen or sulfur. For example, extraction of  $Am^{3+}$  by bis(2,4,4-trimethylpentyl)dithiophosphinic acid has previously been shown to be 6000 times greater than  $Eu^{3+}$ , while related phosphinic acid extractants containing hard oxygen donors discriminate between  $Ln^{3+}$  and  $An^{3+}$  only on the basis of cation size. Despite this, most of our understanding of f-element complexation is based on studies with hard oxygen donor ligands because they form stronger complexes with f-element cations. To better understand the unique features and structural implications of An-soft donor interactions, we used solvent extraction, extended x-ray absorption fine structure (EXAFS), and optical spectroscopy to study both the lanthanide and actinide complexes of a series of dialkylphosphinic acid extractants, bis(2,4,4-trimethylpentyl)phosphinic acid, bis(2,4,4-trimethylpentyl)monothiophosphinic acid, and bis(2,4,4-trimethylpentyl)dithiophosphinic acid, which are the primary components of the commercial extractants Cyanex 272, Cyanex 302, and Cyanex 301.

Figure 1. Bis(2,4,4-trimethylpentyl)-phosphinic acid based extractants used in this study.



Using the Actinide Synchrotron Facility and a BESSRC beamline at the Argonne National Laboratory Advanced Photon Source, we examined the structures of a series of  $Sm^{3+}$  (Shannon radius 1.098 Å for coordination number 6) and  $Cm^{3+}$  (Shannon radius 1.11 Å for coordination number 6) complexes of the phosphinic acid based extractants Cyanex 272, Cyanex 302, and Cyanex 301 by EXAFS. Since the cations are nearly the same size, their electrostatic interactions with ligands should be similar, and any structural differences in metal-ligand coordination should arise from increased covalence in the actinide-ligand bonds. Samples were prepared by solvent extraction of the relevant cations from 1.0 M  $NaNO_3$  buffered between pH 3 and 5, depending on the extractant, into a 1.0 M solution of the extractant in *n*-dodecane. Analysis of the EXAFS and supporting UV-visible spectra shows that the first coordination sphere around the metal ion does not change when a trivalent actinide is substituted for a lanthanide of the same size. This is expected in the case of the phosphinic and monothiophosphinic acids, which contain hard oxygen donors and show little preference for  $Ln^{3+}$  or  $An^{3+}$ . However,

even though extraction of the Cm-Cyanex 301 complex is much stronger than the Sm-Cyanex 301 complex, the metal-sulfur bond distances are indistinguishable for the Sm and Cm complexes with Cyanex 301. Also, only sulfur donors are detected in the inner-sphere of the organic phase Cyanex 301 complexes despite the affinity of  $\text{Ln}^{3+}$  and  $\text{An}^{3+}$  for the water and nitrate present in the system. Within the error limits of the EXAFS experiment and analysis, the presumed greater covalence of the Cm-S bonds does not result in measurably shorter bonds or differences in  $\text{Ln}^{3+}$  and  $\text{An}^{3+}$  coordination. Thus the structural manifestations of the stronger An-soft donor ligand bonds are more subtle than those observed in other cases where ionic bonding predominates.

Work performed under the auspices of the US Department of Energy, Office of Basic Energy Sciences, Division of Chemical Science, under contract W-31-109-ENG-38.

## Lewis Base Binding Affinities and Redox Properties of Plutonium Complexes

Susan M. Oldham,  
Ann R. Schake,  
Carol J. Burns,  
Arthur N. Morgan III,  
Richard C. Schnabel,  
Benjamin P. Warner,  
David A. Costa,  
Wayne H. Smith  
Los Alamos National  
Laboratory, Los  
Alamos, NM 87545  
Eckerd College, St.  
Petersburg, FL 33711

Fundamental chemistry of the actinide elements provides key support for the mission at Los Alamos, especially for future efforts in science-based stockpile stewardship, plutonium processing, and waste stabilization. In contrast to other aspects of Pu research, knowledge of molecular chemistry is relatively underdeveloped. This knowledge, however, will provide the basis for the development of process-related chemistry, separations chemistry, stockpile stewardship, and advances in metallurgical properties relevant to the weapons mission of the Laboratory.

As part of the *actinide molecular science* competency development effort, the initial goal of this work is to synthesize and investigate several series of complexes, varying by actinide metal, ligand set, and oxidation state. We are examining the reactivity of plutonium and neptunium organometallic complexes to elucidate fundamental chemical parameters of the metals. These reactions will be compared to those of the known corresponding uranium complexes in order to recognize trends among the actinide elements and to document differences in chemical behavior.

Reactions we are investigating include one- and two-electron oxidations, as well as ligand exchange processes. Oxidation chemistry is significant in the plutonium-uranium (reduction) extraction (PUREX) process for separation of uranium and plutonium. Understanding ligand exchange processes is also important in current separation methods, as well as for development of new extractants for application in environmental decontamination and waste remediation efforts.

Current separations methods in use or under investigation rely on the extraction of actinide species from acidic aqueous solution into a solid or liquid organic phase. Examples of solid organic extractants used in separation chemistry are based on polymer-bound b-phosphorylcarboxamides (CMPOs), which function by oxygen bond chelation. Liquid phase extractants include tributylphosphate, CMPOs, and malonamides. The three major functional groups of these solid and liquid chelating complexes are ketones, phosphoryls, and amides. These functional groups are the basis of the ligands we have chosen for our studies as well-defined solution phase mimics of actinide processing chemicals. We have investigated the binding of these ligand types to a homoleptic Pu(III) complex,  $\text{Pu}(\text{OAr})_3$  ( $\text{Ar}=2,6\text{-di-}t\text{-butylphenyl}$ ), as shown in Figure 1. Using these simple, well-defined complexes, we have determined binding affinities and exchange rates for metal-ligand interactions for a series of these Lewis bases. The exchange process is associative, even with the large aryloxy ancillary ligands. Importantly, the binding affinities of the ligands mirror those of comparable ligands in acidic-aqueous Pu(III) chemistry.

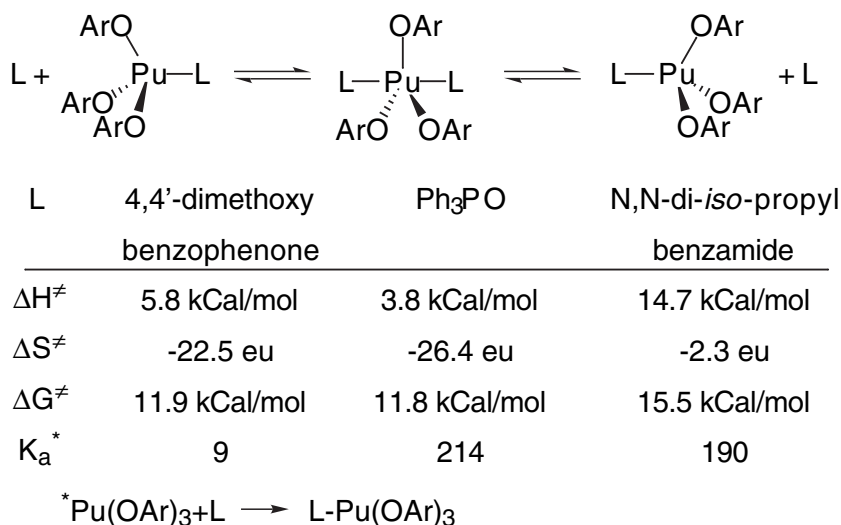


Figure 1. Self-exchange reactions between Pu(OAr)<sub>3</sub> and ligands.

Redox chemistry is important in the PUREX process. We have previously reported on the oxidation chemistry of the uranium(III) tris aryloxy complex. We have extended this chemistry to plutonium, and the synthesis, characterization, and oxidation chemistry of these plutonium analogs will be discussed. The differences in the chemical behavior of uranium and plutonium will be discussed based on the differences in redox behavior of the complexes. Results from these investigations as well as methods for designing experiments with these difficult to manipulate elements will be discussed.

## QSAR of Distribution Coefficients for $\text{Pu}(\text{NO}_3)_6^{2-}$ Complexes Using Molecular Mechanics

**Eddie Moody**  
Los Alamos National  
Laboratory, Los  
Alamos, NM 87545,  
USA

Anion exchange in nitric acid is a frequently used process for the recovery of plutonium from a wide range of impure materials. The large coordination sphere (up to 12 coordinate) of plutonium enables it to form anionic complexes in high nitrate media where few other metals form competing anionic species. This unique chemical behavior is exploited by the anion-exchange process used in the Plutonium Facility at Los Alamos National Lab. Plutonium recovery operations in nitric acid currently use Reillex HPQ®, a macroporous polymer of N-methylated 4-vinylpyridine crosslinked with divinylbenzene.

Under typical anion-exchange conditions, sorption of a dianionic species requires complexation to two separate cationic resin sites. The orientation and availability of these sites for cooperative interactions with a dianion is not well controlled. We have synthesized and evaluated several series of bifunctional resins where the structure of the anion-receptor site is well defined. These resins are synthesized via N-derivatization of pyridinium units from a base poly(4-vinylpyridine) resin with a second cationic site such that the two anion-exchange sites are linked by 'spacer' arms of varying length and flexibility. Plutonium sorption data from nitric acid media has been reported for these materials,<sup>1</sup> and these results indicate that the controlled geometry of the anion-exchange sites has a positive impact upon the sorption of the actinide dianion.

Modeling the interactions of actinide hexanitrate complexes with the dicationic resin sites is a complex, multi-stage process. We report herein the modeling of the electrostatic interactions of the plutonium hexanitrate dianion with 'free' analogues of the resin dicationic sites for three series of resins.

Although any individual  $\text{Pu}(\text{NO}_3)_6^{2-}$  moiety docks and undocks with the cationic sites of the anion-exchange resin repeatedly, we can consider this process to be a single docking operation in that one complex has moved from the solution phase onto a solid phase in the macroscopic sense. In this docking procedure, there are many forces at work (i.e. electrostatics, sterics, London forces, entropy forces, cavitation, phase change enthalpies, dispersion forces, etc.). Here, we consider only sterics and electrostatic forces between the  $\text{Pu}(\text{NO}_3)_6^{2-}$  complex and the resin. The impact of the weaker components upon the total attractive force can be included, but agreement with experimental data is very good using only steric and electrostatic forces.

Steric interactions are considered to be the primary repulsive forces. While the 5f orbitals are extremely important within the  $\text{Pu}(\text{NO}_3)_6^{2-}$  complex, the radial distribution of these orbitals beyond 6 Å is negligible.<sup>2</sup> HyperChem<sup>3</sup> predicts the distance between the plutonium atom to the closest hydrogen on any of dications to be ca. 5 Å and from the plutonium atom to the closest heavy atom to be over 6 Å. Therefore, the following discussion does not consider f-orbital contributions to the interactions of the actinide complex with the dication.

$K_{\text{eq}}$  can be derived from classical thermodynamics, eq 1. In all of the following discussions, we assume a closed system at constant T. Gibbs free energy can be greatly simplified, however, because our quantitative structure-activity relation-

ship (QSAR) scheme is based upon *differences* in  $\Delta G$  (under conditions in which  $\Delta G \approx \Delta U + \text{constants}$ ). Our assumptions, discussed below, allow all terms except for  $\Delta U$ , which can be computed very efficiently, to be dropped from consideration.

$$K_{eq} = e^{\frac{-\Delta G}{RT}} \quad (1)$$

The usually intractable entropic terms become minor contributors when looking at  $\Delta(\Delta G)$ . Certainly, the SdT is zero at constant T. The entropy term TdS is difficult to calculate accurately, and a fundamental premise of this work is the assumption that  $\Delta(\text{TdS})$  for the docking of a  $\text{Pu}(\text{NO}_3)_6^{2-}$  to the dicationic sites is essentially zero within a series of very similar resins where the dicationic sites differ only in the number of methylene groups separating the two cationic moieties. The TdS term itself is undoubtedly quite large, but the  $\Delta(\text{TdS}) \sim 0$  approximation is supported by the quality of our empirical correlations. A stickiness factor (SF), defined as the sum of the intermolecular electrostatic moments, is calculated with partial and formal charges at the MM+<sup>3</sup> optimized structure of each ion pair. Empirical correlation between the calculated SF, using either partial charges or formal charges, and the experimentally-determined distribution coefficients for plutonium uptake is very good and strongly suggests that this methodology can be further developed in the future to allow *a priori* predictive capabilities.

### References

1. Marsh, S. F.; Jarvinen, G. D.; Bartsch, R. A.; *Reactive Polymers* **1997**, *35*, 75-80.
2. Freeman, A. J.; Lander, G. H.; *Handbook on the Physics and Chemistry of the Actinides*; Freeman, A. J.; Lander, G. H., Ed.; North-Holland: Amsterdam, 1984; Vol. 1..
3. HyperChem *HyperChem*; 5.1 ed.; HyperChem, Ed.; Hypercube, Inc.: 1115 NW 4th Street, Gainesville, Florida 32601, USA.

# Materials Compatibility for $^{238}\text{Pu}$ - $\text{HNO}_3$ /HF Solution Containment: $^{238}\text{Pu}$ Aqueous Processing

M. A. Reimus,  
M. E. Pansoy-Hjelvik,  
G. Silver,  
J. Brock, J. Nixon,  
K. B. Ramsey,  
P. Moniz  
*Los Alamos National  
Laboratory, Los  
Alamos, NM 87545,  
USA*

## Introduction

The Power Source Technologies Group at Los Alamos National Laboratory is building a  $^{238}\text{Pu}$  Aqueous Scrap Recovery Line at the Plutonium Facility. The process line incorporates several unit operations including dissolution, filtration, ion exchange, and precipitation. During 1997-1999, studies were carried out to determine the chemistry used in the full-scale process. Other studies focussed on the engineering design of the operation. Part of the engineering design was to determine, in compatibility studies, the materials for reaction and storage vessels which will contain corrosive  $^{238}\text{Pu}$ - $\text{HNO}_3$ /HF solutions. The full-scale line is to be operational by the end of year 2000.

Hydrofluoric acid is known to be very corrosive. In aqueous solutions, HF forms soluble complexes with Pu thereby enhancing the dissolution of solid  $^{238}\text{PuO}_2$ . In other chemical applications, HF etches the surfaces of most materials. As a consequence, it is predicted that the use of HF in the aqueous line could introduce impurities into the Pu solution from the etching of storage and reaction vessels. Corrosion due to the high alpha radiation of  $^{238}\text{Pu}$  is also anticipated.

One compatibility study examined the feasibility of using Inconel alloys, stainless steel or tantalum as the material of construction for the storage of  $^{238}\text{Pu}$  mixtures of concentrated nitric acid and hydrofluoric acid.<sup>1</sup> Tantalum was shown to be superior to the other materials, so it was selected as the material for the dissolution vessel and storage tanks. Another study determined the suitability of Pyrex columns for ion exchange. The studies showed that hydrofluoric acid does not significantly etch Pyrex, and that minimal Si is leached into the  $^{238}\text{Pu}$ - $\text{HNO}_3$ /HF solutions.

## Experimental

In separate metal compatibility studies, a coupon of each metal was immersed in a test solvent at room temperature for 340 hours or kept at reflux for 100 hours. The solvent contained Ce(IV) or  $^{238}\text{Pu}$ , concentrated nitric acid, and hydrofluoric acid. Ce(IV) was chosen as an oxidizing cation similar to Pu(IV), though it lacks the alpha-radiations of  $^{238}\text{Pu}$ . Weighed, duplicate control coupons of the metals were immersed in the test solvent. After the end of the exposure periods, the coupons were removed from the test solutions, and the corrosion products were carefully removed from the base metals. The coupons were then weighed and examined under a microscope.<sup>2,3</sup>

In the Pyrex compatibility studies, two cylindrical Pyrex ion exchange columns were used. One column contained 100 mL of a mixture containing  $^{238}\text{Pu}$  in 7.0 M nitric acid and 0.1 molar hydrofluoric acid. The second column contained 100 mL of 7.0 M nitric acid. Samples of both columns were taken at regular time intervals. The samples were analyzed for Si content by ICP-AES (inductively coupled plasma-atomic emission spectrometry) to determine Si concentration versus time. The plutonium concentration in each sample was determined by proportional counting.

## Results

In the metal compatibility studies, coupon weight loss measurements and analysis of the spent solvents indicated that tantalum and its 2.5% tungsten alloy have superior resistance to the corrosive Ce or  $^{238}\text{Pu}$  in acid solutions. Thus, dissolution and storage vessels are being constructed of these materials.

The Pyrex compatibility studies indicated that silicon is not significantly leached into the plutonium nitric acid solution over a period of 1008 hours. This time corresponds to approximately 300 ion exchange runs during full-scale operations. These results confirmed that Pyrex can be used for the ion exchange columns in the aqueous processing of  $^{238}\text{Pu}$ .

## Summary

A  $^{238}\text{Pu}$  Aqueous Scrap Recovery Line is being built at the Los Alamos National Laboratory Plutonium Facility. Several studies have investigated the materials of construction for dissolution and storage, and the ion exchange columns. The materials must not leach its constituents into the corrosive  $^{238}\text{Pu}\text{-HNO}_3/\text{HF}$  solutions. Our studies have determined that tantalum or its tungsten alloy is suitable for the dissolution and storage vessels, and Pyrex is suitable for the ion exchange columns.

## References

1. Reimus, M. A. and Silver, G. L., "Metals for the Containment of Nitric Acid Solutions of Plutonium-238," *J. of Radioanalytical and Nuclear Chemistry*, V. 242, N. 2 (1999).
2. ASTM G1-90, Standard Practice for Preparing, Cleaning, and Evaluating Corrosion Test Specimens (Reapproved 1994). Annual Book of ASTM Standards, 1998.
3. ASTM G31-72, Standard Practice for Laboratory Immersion Corrosion Testing of Metals (Reapproved 1995), Annual Book of ASTM Standards, 1998.

# Process Parameters Optimization in Ion Exchange $^{238}\text{Pu}$ Aqueous Processing

M. E. Pansoy-Hjelvik,  
J. Nixon,  
J. Laurinat,  
J. Brock,  
G. Silver,  
M. Reimus,  
K. B. Ramsey  
*Los Alamos National  
Laboratory, Los  
Alamos, NM 87545,  
USA*

## Introduction

An aqueous recovery line is being built at the Los Alamos National Laboratory Plutonium Facility to purify scrap plutonium-238 dioxide. The oxide is used in the fabrication of general-purpose heat sources (GPHS) or light-weight radioisotope heater units (LWRHUs). The heat sources supply energy to thermoelectric generators that power spacecraft for deep space missions and heat critical components in the cold environment of space.

The purification of  $^{238}\text{PuO}_2$  is necessary because the scrap contains unacceptable amounts of daughter product  $^{234}\text{U}$  and other impurities. The impurities make the heat source heavier but contribute no heat and may react adversely with other components. Aqueous purification requires a nitric acid/hydrofluoric acid mixture at reflux to dissolve the powdered oxide, followed by oxalate precipitation, filtration, and calcination to produce the pure oxide. Nitrate anion exchange processing prior to oxalate precipitation is necessary when the  $^{238}\text{PuO}_2$  material contains gross amounts of impurities.

This paper describes bench-scale efforts (5-7 grams of  $^{238}\text{Pu}$ ) to optimize the ion exchange process for  $^{234}\text{U}$  separation with minimal  $^{238}\text{Pu}$  losses to the effluent and wash liquids. The bench-scale experiments also determine the methodology to be used for the full-scale process: 5 kg  $^{238}\text{Pu}$  annual throughput. Heat transfer calculations used to determine the thermal gradients expected during ion exchange processing are also described. The calculations were performed in collaboration with Westinghouse Savannah River Technology Center (WSRTC) and provide information for the design of the full-scale ion exchange equipment.

## Chemical Pretreatment

The Pu(IV)-hexanitrate complex formed in 7 molar (M) nitric acid sorbs onto the Reillex-HPQ resin during ion exchange. Maintaining all of the Pu in the tetravalent state is difficult because of the highly oxidizing environment that develops in 7 M nitric acid containing  $^{238}\text{Pu}$ . Most of the plutonium in the 7 M acid is expected to exist in the Pu(IV) tetravalent state. However, the high alpha activity of 17 Ci/gm  $^{238}\text{Pu}$  generates Pu(VI). The hexavalent state of Pu sorbs weakly on the resin leading to loss of Pu from the column. Bench-scale studies have shown that chemical pretreatment is necessary for maintaining  $^{238}\text{Pu}$  in the tetravalent oxidation state. Chemical pretreatment consists of adding urea, ferrous ammonium sulfate, and sodium nitrite to a 3 M nitric acid solution of the Pu. Without pretreatment, a large percentage of  $^{238}\text{Pu}$  is lost to the effluent and wash streams. Pretreatment reduces the losses to less than 1%.

## Thermal Gradient Calculations

Heat transfer analysis was made to demonstrate that heat from the  $^{238}\text{Pu}$  will not cause the resin temperature to rise to the point where the resin degrades significantly. The calculations are based on previous work at the WSRTC Waste Recov-

ery facility, performed in support of the  $^{238}\text{Pu}$  production campaign to provide material to Los Alamos National Laboratory for heat source fabrication. The calculations determine the amount of  $^{238}\text{Pu}$  that can be safely processed in one column operation within our glovebox environment.

Calculations were executed by using finite difference equations, incorporating models for absorption and elution of  $^{238}\text{Pu}$  and for forced and natural convection within the resin bed. The calculations determine the maximum resin temperature during loading, washing, and elution of the plutonium. They also predict equilibrium temperature of the resin should fluid flow to the column be interrupted.

### Summary

The implementation of full-scale nitrate anion exchange processing of  $^{238}\text{Pu}$  feedstock is underway, and is part of the  $^{238}\text{Pu}$  Aqueous Recovery Line for the purification of scrap  $^{238}\text{PuO}_2$ . Concurrent efforts include bench-scale experiments to determine optimal pretreatment and elution parameters and the conditions that will minimize the effects of decay heat during loading, washing, and elution of the column. The calculations will permit us to determine the maximum amount of plutonium that can be safely processed in one operation within our glovebox environment. The optimal pretreatment scheme will be applied during full-scale processing, with efficient  $^{234}\text{U}$  separation and minimal  $^{238}\text{Pu}$  losses.

## Plutonium Pyrochemical Salts Oxidation and Distillation Processing: Residue Stabilization and Fundamental Studies

Donna M. Smith,  
Mary P. Neu,  
Eduardo Garcia,  
Vonda R. Dole  
*Los Alamos National  
Laboratory, Los  
Alamos, NM 87545*

Vanadium pentoxide,  $V_2O_5$ , has been proposed as an oxidant for the stabilization of pyrochemical salt residues from plutonium pyrochemical processes at the Rocky Flats Environmental Test Site because of its large reduction potential and its ability to react via normal solid-state reactions (i.e. no solvents are required). The pyrochemical salt residues contain plutonium in reactive forms and lower oxidation states (the most common forms being  $Pu^0$ ,  $PuOCl$ , and  $PuCl_{13}$ ) along with several alkali or alkaline earth chlorides. These residues present an environmental hazard because compounds with plutonium in oxidation states less than IV are unstable with respect to air-oxidation, and deleterious reactions with water and other small molecules can occur. The ideal stabilization process would result in the concentration of a Pu-rich heel containing primarily  $PuO_2$ , an ideal form for long-term storage or disposition, and a Pu-poor salt phase, that may be disposed of as low-level waste.

When  $V_2O_5$  was used to oxidize actual process residues, results were highly variable. There are no published reports of the chemical oxidation of plutonium with vanadium pentoxide in molten salts; in addition, the solid-state reaction chemistry of plutonium with vanadium oxides has not been well studied. This work is the first systematic study of the chemical oxidation of plutonium with vanadium pentoxide.

The reaction chemistry of  $PuCl_{13}$ ,  $Pu^0$  and  $PuOCl$  with  $V_2O_5$  in the presence and absence of a NaCl/KCl salt matrix and under a variety of conditions will be presented. Our studies are intended to address three distinct questions: (1) Is  $V_2O_5$  a suitable oxidant to convert  $Pu^0$  and  $Pu(III)$  to  $Pu(IV)$ ? (2) What is the identity of the reaction products, and are they volatile? And (3) what are the optimal process conditions for these reactions?

Results of the  $PuCl_{13}$  reactions indicate an equal to or greater than 1:1  $PuCl_{13}:V_2O_5$  ratio is needed for complete oxidation of  $PuCl_{13}$ . Products from 3:2  $PuCl_{13}:V_2O_5$  reactions clearly contain unreacted  $PuCl_{13}$ . Increasing the amount of  $V_2O_5$  from one to two equivalents increases the contribution of side reactions, including reactions of  $V_2O_5$  with the process equipment and/or salt matrix, and produces undesirable non-volatile ternary and quaternary vanadium compounds.

The  $Pu^0$  oxidations are more complex than the  $PuCl_{13}$  oxidations. More unreacted  $Pu^0$  remains in a reaction using more equivalents of  $V_2O_5$  than a reaction using a smaller amount of  $V_2O_5$ . The lack of predictability of these reactions may be due to several factors and will be discussed. Complete oxidation of  $Pu^0$  to  $Pu(IV)$  in the presence of the salt matrix does not occur with up to six equivalents of  $V_2O_5$ . Chlorine is detected in the off-gas of the  $Pu^0$  oxidations, indicating the salt matrix participates in the reaction(s) that hinder oxidation. The interference of the salt matrix is further confirmed by the fact that conversion of  $Pu^0$  to  $Pu(IV)$  occurs almost instantaneously in the absence of the salt matrix.

Reactions involving  $PuOCl$  are similar to the  $PuCl_{13}$  oxidations. Greater than a 1:1  $PuOCl:V_2O_5$  ratio is required to achieve adequate conversion of the plutonium phase to  $PuO_2$ .

## Americium Extraction from Plutonium Metal

The concentration of americium in plutonium metal increases with time through the decay of the plutonium-241 isotope. Development of the electrorefining process at Los Alamos showed about 75% of the americium could be removed. This led to the development of a process using  $\text{MgCl}_2$  to extract the americium into a  $\text{NaCl-KCl}$  salt, a process which required 2 cycles to remove >90% of the americium. An increased extraction could be obtained using  $\text{MgCl}_2$  in  $\text{CaCl}_2\text{-NaCl}$ . Further development using  $\text{PuCl}_3$  in  $\text{CaCl}_2$  showed >90% of the americium could be removed in a single pass. A survey of potential single and binary solvent salt systems showed the amount of americium extracted was dependent on the solvent salt used with the greatest extraction occurring in  $\text{CaCl}_2$ .

Initial attempts at the Atomic Weapon Establishment (Great Britain) to remove the americium used  $\text{PuCl}_3$  in  $\text{CaCl}_2$  and resulted in extractions of >90% being achieved in a single pass. This required an additional processing step to make the  $\text{PuCl}_3$ . Impurities in the  $\text{PuCl}_3$  were transferred into the product metal.

To limit the transfer of impurities the use of  $\text{MgCl}_2$  was investigated. Two sets of experiments were carried out using either 13.5 or 9 moles of  $\text{MgCl}_2$  in  $\text{CaCl}_2$  per mole of americium in the metal. The materials were contained within a magnesia crucible and stirred at 200 rpm for 105 minutes at about  $850^\circ\text{C}$  in a furnace with a continual flow of argon. At the end of the process a metallic deposit, presumed to be magnesium, had formed in the cooler parts of the furnace. The metal and salt phases were readily separated. The results, which are summarised in Table 1, show about 90% of the americium was extracted with  $\text{MgCl}_2$ , which is only slightly lower than the 93% extracted with an equivalent amount of  $\text{PuCl}_3$ . Surprisingly there appeared to be no advantage in using the higher level of  $\text{MgCl}_2$ . Chemical analysis showed magnesium was present on the surface of the metal product; there was no detectable transfer of other impurities into the product metal. The magnesium was readily removed in a vacuum casting operation.

Extractant	Extractant : Am Molar Ratio	Am Extracted %	Metal Yield %
$\text{PuCl}_3$	6.0	93.7	99.4
$\text{MgCl}_2$	13.3	89.6	98.2
$\text{MgCl}_2$	9.0	90.6	98.8

There is a slightly lower metal yield when using  $\text{MgCl}_2$  because plutonium as well as americium is oxidised by the  $\text{MgCl}_2$ . When compared with the use of  $\text{PuCl}_3$  as the extractant, the plutonium content of the residue salt is less.

A single stage process using  $\text{MgCl}_2$  in  $\text{CaCl}_2$  has been demonstrated to remove 90% of the americium from plutonium with no transfer of impurities to the product metal except magnesium, which is readily removed in a vacuum casting operation.

© British Crown Copyright 2000/MOD

Published with the permission of Her Britannic Majesty's Stationary Office

R. F. Watson  
AWE, Aldermaston,  
Great Britain

# Dry Process for Recovering Gallium from Weapons Plutonium using a Rotary Furnace Equipped with a Copper Collector

**C. V. Philip,**  
**Rayford G. Anthony,**  
**Chokkaram Shivraj,**  
**Elizabeth Philip,**  
**W. Wilson Pitt**  
*Texas A&M*  
*University, College*  
*Station, TX*

**Max Roundhill**  
*Texas Tech*  
*University, Lubbock,*  
*TX*

**Carl Beard**  
*The University of*  
*Texas, Austin, TX*

## Introduction

Currently the separation of gallium from weapons plutonium is achieved using complex aqueous processing involving solvent extraction and ion exchange; this process generates large quantities of wastewater containing radioactive materials. At Los Alamos National Laboratory, researchers have been developing a simpler alternative process referred to as the thermally induced gallium removal (TIGR) process; vaporized gallium suboxide is swept away by passing hydrogen/argon over gallium trioxide/plutonium oxide heated at 1100°C or higher. During the TIGR process some of the gallium suboxide prematurely decomposes to gallium metal and gallium trioxide, which deposit on furnace and vent surfaces.

The efforts at Texas A&M University are directed towards learning more about the behavior of gallium suboxide and determining how the reduction of vaporized gallium suboxide on a copper surface can be used to develop an effective "gallium collector," which can be incorporated into the TIGR process.

## Description of the actual work

A Horizontal rotary furnace with a quartz reactor vessel (Carbolite) was refitted and used for the experiments. Each experiment was conducted at 1000°C for approximately six hours with H<sub>2</sub>/Ar used as the reducing gas.

## Results

Gallium was deposited on a copper collector as a Ga/Cu alloy in most cases. If the conditions were not optimal for Ga/Cu alloy formation, white deposits condensed on the copper collector, and a black/gray dust deposited downstream on the exit lines and vents. We concluded from our experimental results that the gallium removal and the Ga/Cu alloy formation are dependent on the shape and the temperature of the copper collector and the flow rate of the reducing gas (H<sub>2</sub>/Ar). At 900°C–1000°C, if the geometry and surface area of the copper collector are appropriate, the gallium suboxide (volatile) is reduced and deposited as Ga/Cu alloy on the copper collector; neither the white deposit formed nor the black/gray dust collected on parts downstream. Generally three separate activities were observed: Ga/Cu alloy formation, condensation of white deposits, and black/gray dust evolution. The black/gray dust evolves during very fast flow rates with insufficient copper collector surface area at high temperature zones (800°C–1000°C). White deposits are formed when the surface area of copper collector is adequate at 800 – 900°C zones but inadequate at 900°C–1000°C zones. Only Ga/Cu alloy is formed when the surface area of copper is adequate at 900°C–1000°C zones. The Ga/Cu alloy formation is extremely fast, and the necessary surface area of copper is very low (10 – 15 cm<sup>2</sup>). Since copper is an excellent conductor of heat, the copper collector must be shaped correctly for adequate surface area with minimum heat loss via conduction. A good copper collector should also have several tubular channels large enough for gas flow so that the condensed Ga/Cu alloy does not plug the flow of gases. We have two successful designs. The first successful design is composed of an outer hexagonal packing of

six copper tubes (1/4" OD, 1/8" ID, 1" long) encompassing another copper tube in the center. The second successful design is a 3/4" copper rod with sixteen tubular holes (5/32"). The copper collectors with smaller tubular holes were plugged up with Ga/Cu alloy. When the collector with larger holes was used, a black/gray dust formed. When the two successful designs for the copper collector were used, both the condensation of white products and the formation of

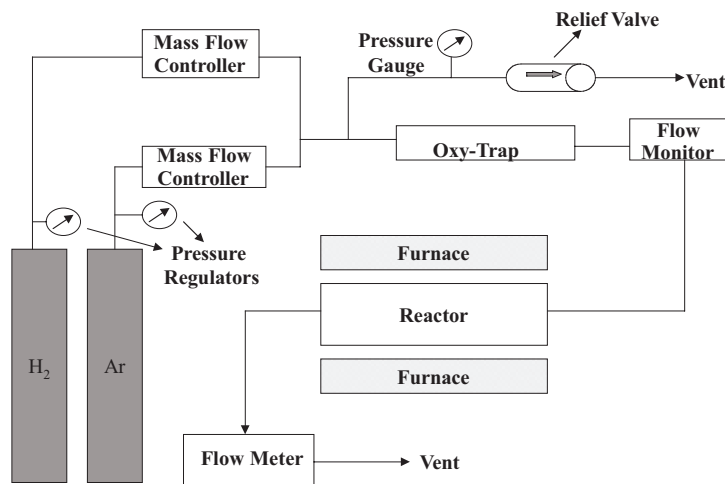
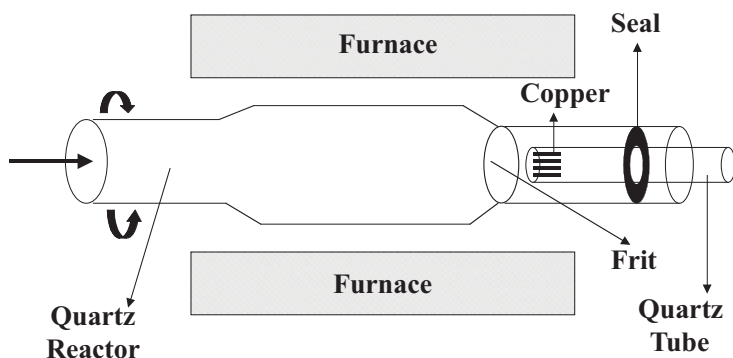


Figure 1. Schematics of gallium separation process.



Reactor Setup

Figure 2. Schematics of furnace and quartz reactor vessel.

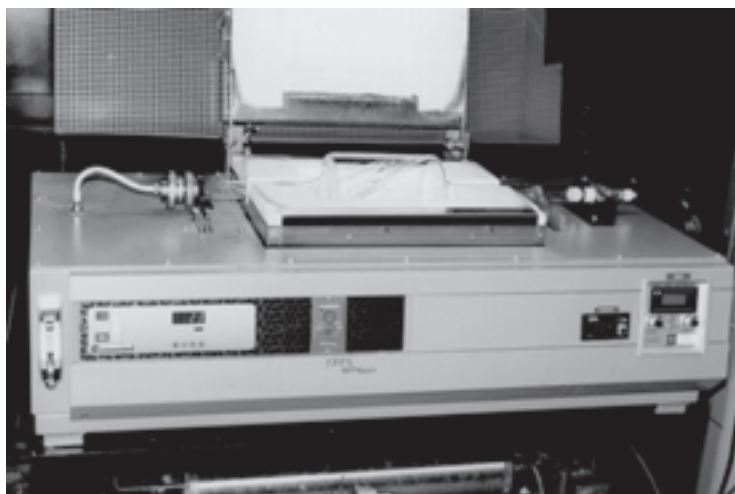


Figure 3. Rotary furnace used for conducting gallium removal experiments.

black/gray dust were completely eliminated. Additionally, droplets of Ga/Cu alloy did not drip from the copper collector as we had observed in our earlier experiments with the quartz "U" tube reactors. The rate of Ga removal is directly proportional to flow rate of H<sub>2</sub>/Ar. At 1000 ml/minute, about 1.75 g of Ga is deposited on copper collector in six hours. At 500 ml/minute, only half the amount is collected. The diameter of the tested copper collector is only 0.75 in. Most of the deposition is on the first quarter inch of the front end. The quartz reactor, which survived several cycles of heating and cooling without any cracking due to thermal stress, is thermally very stable and inert. The results of our recent experiments clearly indicate that using a copper collector with the TIGR process make it feasible for commercial use.

### Bibliography

1. C. V. Philip, W. W. Pitt and C. A. Beard. "Investigation in Gallium Removal," Amarillo National Resource Center for Plutonium, ANRCP-1997-3, Nov 1997.
2. "Gallium removal process developed by Amarillo center looks promising," Nuclear Materials Monitor, Exchange/Monitor Publications, Inc., page 5, Mar 1998.
3. "Plutonium may become peacetime fuel," Ingenuity, Texas Engineering Experiment Station, page 3, May/June 1998.
4. Elizabeth Philip, C. V. Philip, Rayford G. Anthony, Chokkaram Sivaraj, W. Wilson Pitt, Max Roundhill, and Carl Beard, "Dry Process Using Copper-Collector for Recovering Gallium from Weapons Plutonium," The International Youth Forum: Youth and the Plutonium Challenge July 5-10, 1998, Obninsk, Russia.
5. C. V. Philip, Chokkaram Sivaraj, Rayford G. Anthony, Elizabeth Philip, Venkat Tulasi, Igor Carron, W. Wilson Pitt, Max Roundhill, and Carl Beard, "Collector for Recovering Gallium from Weapons Plutonium," The Researchers Conference, Amarillo, TX, July 21 - 22, 1998.
6. C. V. Philip, R. G. Anthony, C. Sivaraj, and C. Beard. "Copper Collector in a Rotary Reactor Furnace for the Removal and Recovery of Gallium from Ga<sub>2</sub>O<sub>3</sub>/PuO<sub>2</sub>," Twenty-third Annual Actinide Separations Conference, June 7-10, 1999, page 36.
7. C. V. Philip, R. G. Anthony, C. Sivaraj, and C. Beard, "Rotary Reactor Furnace for the Reduction of Gallium trioxide and Deposition of Gallium on a Copper Collector," 1999 Researchers' Conference Proceedings, Amarillo National Resource Center for Plutonium, July 19-21, 1999, page 53.
8. H. F. Koch, D. M. M. Roundhill, C. V. Philip, and R. G. Anthony, "Analysis of Gallium in Mixtures with Cerium and Copper by the Inductively Coupled Plasma-Atomic Emission."

This paper was prepared with the support of the U.S. Department of Energy (DOE), Cooperative Agreement No. DE-FC04-95AL85832. However, any opinions, findings, conclusions, or recommendations expressed herein are those of the author(s) and do not necessarily reflect the views of DOE. This work was conducted through the Amarillo National Resource Center for Plutonium.

# Purification of Plutonium via Electromagnetic Levitation

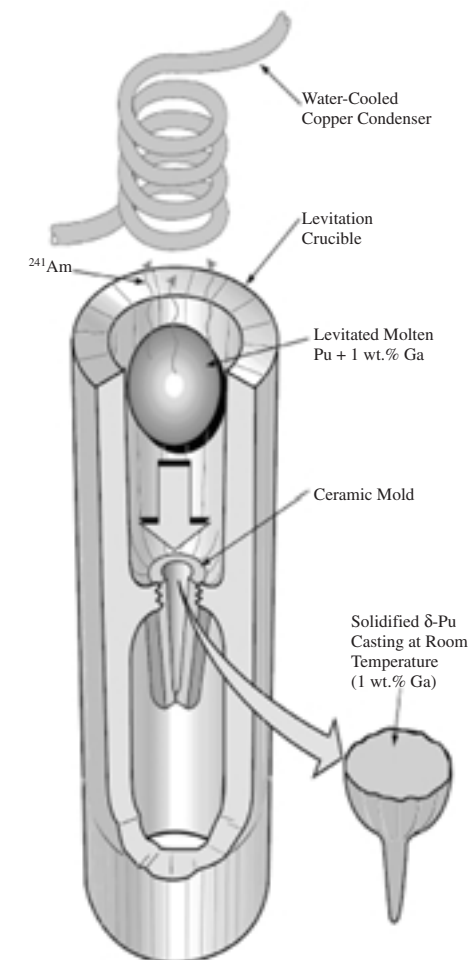
## Abstract

Plutonium metal that has been double electrorefined (ER) was further purified via zone refining, using a levitated molten zone to minimize the introduction of impurities. The temperature of the molten zone was 750°C, and the atmosphere was 10<sup>-5</sup> Pa. A total of ten zone refining passes were made at a travel rate of 1.5 cm/hr. In order to study the efficiency of the zone refining process, core samples were taken after every two zone refining passes in five locations along the length plutonium specimen. Several impurities were reduced to levels below that of instrument detection limits, and it appears that six sequential zone refining passes are required to obtain the highest purity metal. The total impurity concentration (sum of 75 elements) in the cleanest portion of the plutonium specimen was 130 ppm (excluding N, O, F, Cl, and Br), and uranium contributes 110 ppm to the 130 ppm. The zone-refined metal was then used in an in situ distillation, alloying, and casting step to prepare tapered specimens for single-crystal growth experiments. Specifically, <sup>241</sup>Am was distilled from Pu metal by levitating Pu metal with 1 wt. % Ga in the melt in a Crystallox vertical electromagnetic levitation crucible at 10<sup>-5</sup> Pa (Figure 1). The Pu is alloyed with Ga to stabilize the δ phase (fcc symmetry) upon solidification. The Pu was chill-cast directly from the electromagnetic levitation field into 1-cm tapered specimens. A water-cooled ceramic mold was used, and the Pu metal was cooled at a rate of 100°C/min. A microstructure examination of the specimen showed 10 x 25 mm acicular grains with an as-cast density of 15.938 g/cm<sup>3</sup> (± 0.002 g/cm<sup>3</sup>). Experimental results from zone refining will be presented together with some examples of measurements using the pure plutonium metal.

## Introduction

An understanding of atomic-scale properties of the metal plutonium can only follow from high purity samples that have been well characterized. The purification of plutonium, beyond levels obtained in the ER process, are required to meet the stringent demands of the elegant measurements of solid state and thermodynamic properties. Furthermore, newly prepared plutonium samples serve as a standard frame of reference for aged-plutonium.

Plutonium metal processing at Los Alamos includes a molten salt extraction (MSE) step, followed by one or two ER runs.



J. C. Lashley,  
M. S. Blau,  
J. R. Quagliano  
*Los Alamos National  
Laboratory, Los  
Alamos, NM 87545,  
USA*

**Figure 1.** In situ americium distillation, alloying, and chill-casting step. A mixture of α-Pu and Ga are added in a levitation crucible. The mixture is heated to the melt while suspended in a magnetic levitation field. As the Ga mixes with the Pu in the melt, it will stabilize the δ phase upon solidification. While in the melt, <sup>241</sup>Am distilled from the Pu is collected onto a water-cooled condenser. Next, the furnace power is reduced, and Pu is cast directly from the electromagnetic field into a ceramic mold.

In these two processes, molten Pu exhibits a strong affinity for the crucible materials, the atmosphere, and the anode/cathode materials [1-4]. The daughter products that grow into Pu over time are always present as impurities, and they add a new degree of complexity to purification. The principal daughter products of Pu are isotopes of uranium and americium. The  $^{235}\text{U}$  nuclei grows into Pu from the  $\alpha$ -decay of the  $^{239}\text{Pu}$  nuclei, and  $^{241}\text{Am}$  is present from the  $\beta$ -decay of the  $^{241}\text{Pu}$  nuclei [5]. Typically, the  $^{235}\text{U}$  nuclei grows into Pu at 30 ppm per year, and  $^{241}\text{Am}$  grows in at 120 ppm per year depending on the initial  $^{241}\text{Pu}$  composition.

We report the purification of Pu using zone refining along with a complete solute profile for a total of 75 trace impurity elements commonly found in Pu. Inductively coupled plasma mass spectrometry (ICP-MS) and atomic emission spectroscopy (ICP-AES) measure the trace impurities reported. These methods detect a suite of 75 trace impurities, and the total impurity levels are quantified to the 100-ppm level, which corresponds to 99.99 wt. % metal.

### Experimental Procedure and Results

All work is carried out in a glove box under an argon or vacuum atmosphere. Starting material for the initial series of runs was double-ER Pu that is cast into rods having a total impurity level of 447 ppm. The ER process used a feed of recycled Pu alloys, and all specimens had a density greater than  $19\text{ g/cm}^3$ . The double-ER rods were further purified by passing a 10 mm-wide molten floating zone ten times through a cast rod at a travel rate of 1.5 cm/h at  $10^{-5}$  Pa. Zone refining was done at reduced pressures with a levitated molten zone to take advantage of volatile impurities.

The floating molten zone was induction melted using a radio-frequency-power-induced electric current. The crucible acts as a transformer inducing a current in the Pu sample in a direction opposite to the current in the crucible. Magnetic fields in the crucible and the plutonium are opposed, causing repulsion and levitation of the plutonium a small distance from the crucible walls (Figure 1). The induction parameters used for the zone refiner was a 50-kHz frequency at 20 kW of power. Core samples were removed for analysis after every two passes using a cobalt drill bit powered with a variable speed drill motor under an atmosphere of argon.

The final trace element analysis with error bars of the zone-refined rods will be discussed. It appears that there is no added benefit to making more than six zone refining passes because the total uranium concentration (110 ppm) is being approached in the clean section of the rod. The uranium concentration is uniform over the entire length of the rod after eight passes. Presumably this is due to a small slope of the fusion line in the limit of infinite dilution on the plutonium-uranium phase diagram.

The zone-refined rod, weighing approximately 240 g, was placed in a water-chilled copper crucible along with sufficient gallium to make a 1 wt. % alloy. The Crystallox levitation crucible was in a vertical position. The bottom of the crucible was fitted with a 1-cm tapered Mycor ceramic mold (Figure 1). The vertical crucible operates in the same manner as the zone refining crucible described above with the exception of the induction parameters. A water-cooled copper condenser was located above the crucible to trap the volatile  $^{241}\text{Am}$ . Next, the

alloy is chill-cast directly from the magnetic field into a ceramic mold at the bottom of the crucible by reducing the furnace power. The cooling rates of the Pu castings are measured using an infrared thermometer.

There are two operative purification processes occurring simultaneously: zone refining and vacuum distillation of volatile elements. This fact makes comparing the data to thermodynamic models problematic. Furthermore, it is very difficult to experimentally determine a Henry's Law constant in the limit of infinite dilution for all of the impurity elements present. The purified metal has been utilized in many experiments including nuclear cross section studies, elasticity measurements using resonant ultrasound (RUS), and photoemission spectroscopy studies using a laser plasma light source (LPLS).

### References

1. J. C. Lashley, M. S. Blau, K. P. Staudhammer, and R. A. Pereyra, *J. Nucl. Mater.*, 274 (1999), 315.
2. J. A. Leary and L. J. Mullins, LA-3356-MS, Los Alamos Scientific Laboratory (1965).
3. L. J. Mullins and J. A. Leary, *I & EC Process Des. and Dev.*, 4(4) (1965), 394.
4. B. Blumenthal and M. B. Brodsky, "The Preparation of High Purity Plutonium" in *PLUTONIUM 1960* (Cleaver-Hume Press Ltd., London).
5. G. T. Seaborg and W. D. Loveland, *The Elements Beyond Uranium* (John Wiley & Sons, INC., New York, 1990).

# **$^{238}\text{Pu}$ Recovery and Salt Disposition from the Molten Salt Oxidation Process**

**M. L. Remerowski,  
Jay J. Stimmel,  
Amy S. Wong,  
Kevin B. Ramsey**  
*Los Alamos National  
Laboratory, Los  
Alamos, NM 87545,  
USA*

## **Introduction**

Rockwell International developed the Molten Salt Oxidation (MSO) process in the 70s and 80s for treating hazardous and radioactive waste.<sup>1</sup> It is an innovative way of treating waste to remove the organic component by complete oxidation to water and carbon dioxide in the salt matrix, leaving only the inorganics, including actinides and heavy metals, in the salt. There are a number of advantages to using MSO,<sup>2</sup> including substantial reduction in waste volume and the possibility of recovering the radioactive component from transuranic waste. Our full-scale  $^{238}\text{Pu}$  aqueous scrap recovery operation will be integrated with the MSO process to recover  $^{238}\text{Pu}$  from the spent salt. The feed for the MSO process will consist of process residues and legacy waste. The organic process residues to be treated are generated by all  $^{238}\text{Pu}$  process operations, including scrap recovery, fuel processing, and pellet encapsulation. The legacy waste and process residues will consist of PVC bags, plastic bottles and labware, Tygon tubing, cheesecloth, unleaded rubber gloves, anti-C clothing, and tape.

Organic material oxidizes almost completely in the molten sodium carbonate medium in the presence of oxygen, leaving the  $^{238}\text{Pu}$  and any other inorganic material in the salt matrix. The salt will no longer promote suitable oxidation when the content becomes either too high in inorganic material, e.g., metal oxides, or the carbonate has been replaced by chlorine (or other acidic species) from sources like highly chlorinated PVC bag-out bags. At that point, the salt is “spent” and must be replaced to ensure process efficiency. We intend to reclaim the  $^{238}\text{Pu}$  using techniques implemented in our aqueous scrap recovery of  $^{238}\text{Pu}$  operation and recycling usable salt and water produced by the MSO process. This will be the first application of this technology to the treatment of  $^{238}\text{Pu}$  contaminated process residues and transuranic waste, which will require the operations to be engineered to glovebox work.

## **Work in Progress**

We have begun designing and optimizing our recovery and recycling processes by experimenting with samples of “spent salt” produced by MSO treatment of surrogate waste in the reaction vessel at the Naval Surface Warfare Center-Indian Head. One salt was produced by treating surrogate waste containing pyrolysis ash spiked with cerium. The other salt contains residues from MSO treatment of materials similar to those used in  $^{238}\text{Pu}$  processing, e.g., Tygon tubing, PVC bag-out bags, HDPE bottles.

Using these two salt samples, we will present results from our investigations of (1) potential vessel corrosion products and inorganic material introduced by “fillers” in the organic feed material, (2) the separation of the surrogate, corrosion products, and other inorganic material into water soluble and insoluble portions, (3) methods to separate the surrogate from the other constituents in the spent salt, and (4) the best method for salt recycling in a glovebox environment.

We plan to install and operate a bench-scale MSO processing unit in the Los Alamos National Laboratory (LANL) Plutonium Facility and will optimize the recovery of  $^{238}\text{Pu}$  from the spent salt, and the salt recycling method, using the results of our pilot studies as a starting point. This bench-scale processing unit will be used to treat pyrolysis ash containing several grams of  $^{238}\text{Pu}$ .

### Summary

We will use the bench-scale  $^{238}\text{Pu}$  aqueous recovery process to extract  $^{238}\text{Pu}$  from the spent salt of MSO processing. We will optimize the process for  $^{238}\text{Pu}$  recovery and salt recycling by conducting surrogate testing followed by processing salts from MSO treatment of  $^{238}\text{Pu}$  contaminated process residues. The results of our surrogate studies will be presented. By integrating the full-scale  $^{238}\text{Pu}$  aqueous recovery process with a full-scale MSO process, we will further minimize waste volume and maximize recovery of  $^{238}\text{Pu}$  from processing.

### References

1. L. F. Grantham, D. E. McKenzie, R. D. Oldenkamp and W. L. Richards; "Disposal of Transuranic Solid Waste using Atomics International's Molten Salt Combustion Process, II," AI-ERDA-13169 UC-70, Rockwell International, Canoga Park, CA (March 15, 1976).
2. J. J. Stimmel and K. B. Ramsey; "Stabilization of  $^{238}\text{Pu}$ -Contaminated Combustible Waste by Molten Salt Oxidation," Pu-Futures 2000 Conference, Santa Fe, NM (July 10-13, 2000)

# Stabilization of $^{238}\text{Pu}$ -Contaminated Combustible Waste by Molten Salt Oxidation

Jay J. Stimmel,  
Mary Lynn Remerowski,  
Kevin B. Ramsey  
*Los Alamos National  
Laboratory,  
Los Alamos, NM  
87545, USA*

J. Mark Heslop  
*Naval Surface Warfare  
Center-Indian Head  
Division, Indian Head,  
MD 20640, USA*

## Introduction

The legacy inventory of  $^{238}\text{Pu}$ -contaminated waste at LANL includes more than 7000 kilograms of combustible process residues containing more than 2 kg of  $^{238}\text{Pu}$ . The same quality that makes  $^{238}\text{Pu}$  attractive for heat source applications, a specific activity of 17 curies per gram, makes disposal of  $^{238}\text{Pu}$ -contaminated waste difficult. The Waste Isolation Pilot Plant (WIPP) thermal load limit of 0.26 gram  $^{238}\text{Pu}$  per drum for  $^{238}\text{Pu}$ -contaminated combustible waste would result in the generation of approximately 8000 drums of TRU waste for WIPP disposal.

Molten salt oxidation, a thermal process, will be used to remove the organic matrix from combustible  $^{238}\text{Pu}$ -contaminated materials. The combustible materials, which are contaminated with residual quantities of  $^{238}\text{Pu}$ , consist of common materials, such as polypropylene bottles, high-density polyethylene bottles, PVC bag-out bags, Tygon™ tubing, and cheesecloth wipes. The residues will be size reduced and injected into molten sodium carbonate salt with excess air. The salt functions as a catalyst to convert the organic material into water and carbon dioxide. Reactive species, such as chlorine and fluorine, react with the molten salt to form neutralized salts, which minimizes off-gas treatment requirements. Plutonium and other metals form metal oxides or salts. The  $^{238}\text{Pu}$  will be recovered from the saturated salt by aqueous chemical separation.

## Current Activities

Surrogate studies were conducted using the molten salt oxidation system at the Naval Surface Warfare Center-Indian Head Division. This system uses a rotary feed system and an alumina molten salt oxidation vessel. The combustible materials were tested individually and together in a homogenized mixture. A slurry containing pyrolyzed cheesecloth ash spiked with cerium oxide, which is used as a surrogate for plutonium, and ethylene glycol were also treated in the molten salt oxidation vessel.

Process optimization studies for the size reduction equipment are currently being conducted. A commercial granulator is being used to size reduce the combustible materials. The granulator, which uses a staggered wave rotor configuration, required minor modifications for use in a glovebox.

Fabrication of the bench scale molten salt oxidation system will soon be completed. Optimization studies and testing with this system will be conducted in a "cold" lab and in the Los Alamos National Laboratory Plutonium Facility.

The final design for the full-scale molten salt oxidation system is nearly complete. This system will be operated inside of a glovebox in the Plutonium Facility. The system incorporates a unique design with internal heating and external cooling. A protective "skull" layer of salt protects the reactor from corrosion. This extends the life of the vessel and reduces maintenance. The unit will have a throughput of 2 kilograms per hour.

## Results

An average destruction efficiency of 99.99% was achieved for the surrogate testing conducted at Indian Head. There were difficulties feeding the cheesecloth and pyrolyzed cheesecloth ash individually into the system. The cheesecloth was mixed with the other materials in a homogenized mixture to facilitate the feeding of the material. The destruction efficiency for the mixture was 99.97%. The pyrolysis ash was mixed with ethylene glycol, and the slurry was pumped into the MSO reactor. The results from the surrogate study will be presented. Results from the size reduction process optimization study and bench scale molten salt oxidation studies will also be presented.

# Low Temperature Reaction of Reillex $\phi$ HPQ and Nitric Acid

William J. Crooks III,  
Edward A. Kyser III,  
Steven R. Walter  
Westinghouse  
Savannah River  
Company, Aiken, SC,  
29808, USA

## Introduction

Despite reports<sup>1,2,3,4</sup> of the relative inertness of Reillex $\phi$  HPQ anion exchange resin to chemical and radiological degradation, a low temperature exothermic reaction was identified for this resin in nitric acid using the Reactive System Screening Tool<sup>5</sup> (RSST). The purpose of this work is to characterize the low temperature exothermic reaction, investigate its origin, and evaluate the risks it introduces to plutonium processing at the Savannah River Site.

## Description of the actual work

The RSST calorimeter allows for efficient screening of runaway reactions as a function of temperature. The reaction of Reillex $\phi$  HPQ, Ionac $\phi$  A-641 and irradiated Reillex $\phi$  HPQ $\phi$  anion exchange resins (all in nitrate form) with nitric acid were compared in the RSST. The thermal effects were evaluated as a function of nitric acid concentration, cerium (IV) loading (as a simulant for plutonium (IV)), and damage caused by previous irradiation of the resin. Much of this work focused on the low temperature exothermic reaction observed for Reillex $\phi$  HPQ-nitric acid mixtures. Off-gases associated with this low temperature exotherm were identified by gas chromatography-mass spectrometry (GC-MS), the final nitric acid concentration was determined by titration, and the solid resin residue was characterized by FTIR.

## Results

Incidents involving undesirable self-accelerated exothermic reactions between organic resins and nitric acid solutions have been well documented. As expected, all resins studied displayed runaway reaction behavior at temperatures in excess of 100°C.

Generally, for all resin-nitric acid mixtures studied, higher nitric acid concentrations decreased the time to the maximum rate of reaction but did not increase the intensity of the exotherm, and cerium (IV) had little to no effect on the reactivity of the resin-nitric acid systems.

Surprisingly, Reillex $\phi$  HPQ displayed an additional low temperature exotherm that initiated at about 69°C and reached a maximum rate about 80°C (see table).

Table.  
Characteristics of  
the Low and High  
Temperature  
Exotherms for  
Reillex $\phi$  HPQ-8  
Molar Nitric Acid  
Mixtures.

Exotherm	Reaction Onset T (°C)	Max. T (°C)	Max. $\Delta T/\Delta t$ (°C/min)	Max. $\Delta P/\Delta t$ (psi/min)
Low	69°C (4)	80 (4)	2 (1)	0.3 (0.1)
High	> 100°C	248 (1)	105 (40)	274 (21)

While this low temperature exotherm is small in magnitude (2°C/min  $\pm$  1), gaseous products were identified in the off-gas, leading to concerns of pressurization in the ion exchange column. FTIR analysis of the solid resin residue identified a

carbonyl stretching frequency at  $1700\text{ cm}^{-1}$  that was not present in the unreacted resin. A study of the reaction of various model compounds with nitric acid in the RSST suggests the reactive sites are the ethylbenzene pendant groups, which were introduced during resin production as an impurity in the divinylstyrene reactant.

Interestingly, the Reillex $\phi$  HPQ that had been irradiated prior to the test showed no low temperature exotherm, evidence that irradiation caused the exothermic reaction to occur. These results indicate that the low temperature exothermic reaction may be initiated by radiological or chemical attack. Therefore, a chemical pretreatment was developed that eliminates the exotherm.

### References

1. C. T. Busher, R. J. Donohoe, S. L. Mecklenburg, J. M. Berg, C. D. Tait, K. M. Huchton, and D. E. Morris, *Applied Spectroscopy*, 1999, 53 (8), 943-953.
2. S. F. Marsh, "The Effects of In Situ Alpha-Particle Irradiation on Six Strong-Base Ion Exchange Resin," Los Alamos National Laboratory report LA-12055 (April 1991).
3. S. F. Marsh, "The Effects of Ionizing Radiation on Reillex $\phi$  HPQ, a New Macroporous Polyvinylpyridine Resin, and on Four Conventional Polystyrene Anion Exchange Resins, Los Alamos National Laboratory report LA-11912 (November 1990).
4. S. F. Marsh, "Reillex $\phi$  HPQ: A New, Macroporous Polyvinylpyridine Resin for Separating Plutonium Using Nitrate Anion Exchange," *Solvent Extraction and Ion Exchange*, 1989, 7(5), 889-908.
5. Manufactured by Fauske and Associates, Inc., 16W070 West 83<sup>rd</sup> Street, Burr Ridge, IL, 60521.

# Molten Salt Fuels for Treatment of Plutonium and Radwastes in ADS Critical Systems

Victor V. Ignatiev  
RRC–Kurchatov  
Institute,  
Moscow, 123182,  
Russian Federation

## Abstract

Introduction of the innovative reactor concept of the incinerator type in the future nuclear power system should provide the following:

- Low Plutonium and Minor Actinides Total Inventory in the Nuclear Fuel Cycle ( $M$ )
- Reduced Actinides Total Losses to Waste ( $W$ )
- Minimal Uranium-235 Support
- Minimal Neutron Captures Outside Actinides (Coolant & Structural Material Activation Products).

Estimations have shown strong dependence of the first two parameters ( $M$  and  $W$ ), which are responsible for incinerator efficiency, from the burnup ( $c$ ) reached in the core of an incinerator and the actinides mass flow rate in the fuel cycle ( $A(t) = G(t) / Q(t)$ , where  $G(t)$  = amount of TRU fed to the process during  $t$ , and  $Q(t)$  = electricity produced during ( $t$ ).

For example, in a multirecycling mode and a co-processing case with the assumption that single cycle losses in fuel reprocessing ( $a$ ) and fabrication ( $b$ ). When  $a, b \ll c$ , we could obtain the following approximate equations:

$$M \approx A(\tau) \cdot \tau \cdot [1 + (a + b + c) - 1] \approx A(\tau) \cdot \tau \cdot (1 + c) / c, \text{ kg TRU / GWe, (at equilibrium)} \quad (1)$$

$$W = W_{rec} + W'_{rem} \approx A(t) \cdot [(a + b) / c + (1 - c)^{t/\tau}], \text{ kg TRU / TWhe, (at the end of scenario)} \quad (2)$$

where  $W_{rec}$  = recycling losses,  $W'_{rem}$  = residual inventory,  $\tau$  = turnaround time of one recycle.

The interest in the MSR type of incinerator stems mainly from an increased burnup time in the system, reduced actinides mass flow rate and relatively low waste stream when purifying and reconstituting the fuel. It is natural to expect that in the future the molten salt reactor (MSR) technology could find a role in symbiosis with standard reactors in the management of plutonium, minor actinides and possibly fission products.

The advantages of the MSR as a burner reactor follow not only from a possibility for its effective combination with the dry technique of fuel processing, which has a prospect to have low cost and produce a small volumes of wastes, but also from its capability to use fuel of different nuclide compositions. The MSRs have the flexibility to utilize different fissile fuel in continuous operation with no special modification of the core as it was demonstrated during MSRE operation for  $^{233,235}\text{U}$  and Pu. The MSRs further can tolerate denaturing and dilution of the fuel, as well as contamination by lanthanides.

The results of recent studies have demonstrated that a broad range of the molten salt reactors of the TRU burner type (MSB) operating in critical or accelerator driven modes with  $\text{PuF}_3$  and minor actinides as the fuel is conceptually feasible. At one end of this range is the well thermalized graphite moderator reactor in which fluid fuel consists of a molten mixture of  $^7\text{Li, Be/F}$  or  $\text{Na, Be/F}$ , containing appropriate quantities of plutonium and minor

actinides as trifluorides. At the other end is a MSB operating with a fast spectrum without a graphite moderator, in which there is a solvent system prepared from NaF-  ${}^7\text{LiF}$  (and/or other possible constituents, like  $\text{ZrF}_4$ ,  $\text{PbF}_2$ ,  $\text{CaF}_2$ ). This MSB concept can have a concentration of  $\text{PuF}_3$  much higher than that of previous ones. Phase behavior of some such mixtures appears suitable to permit use of a high concentration of  $\text{PuF}_3$  in melts whose freezing point will be acceptable for single fluid MSBs. The basic reactor flowsheet for the MSB is essentially the same as that for the reference ORNL designs, in which a single molten salt containing both fissile and fertile materials serves as both the fuel and coolant. The only differences are in the core/blanket configuration, details of the fuel salt composition and the fission product cleanup system. A U-free fuel matrix, as well as addition of  $\text{ThF}_4$  and  $\text{UF}_4$  in homogeneous solution, are conceptually feasible for MSB.

The simpler MSB concept would completely eliminate on-line chemical processing of the fuel salt for removal of fission products. In order to achieve high burnup results the stripping of gaseous fission products would be retained, and some batch-wise treatment to control oxide contamination probably would be required. This reactor needs routine additions of TRU fuel, probably with some  ${}^{235}\text{U}$  support, but would not require replacement or removal of the in plant inventory except at the end of the plant lifetime- $t_p$ . If we denote actinides concentration in the fuel by  $\rho_c$ , heat generated in actinides by  $B$ , plant efficiency by  $\eta$ , capacity factor by  $\phi$  and core / auxiliaries volumes by  $V_{in}/V_{out}$ , we can calculate actinide mass flow rate  $A(t_p)$  for one reactor lifetime from the following equation:

$$A(t_p) \approx [\rho_c \cdot (1 + V_{out}/V_{in}) / (q_c \cdot t_p) + c / B] / (\eta \cdot \phi), \text{ kg TRU / TWh.} \quad (3)$$

The primary feature in the MSB concept is a high-power density -  $q_c$ . Indeed, the principal shortcoming of the single fluid concept of course is the substantial investments of the fissile material in the heat transfer circuit and elsewhere outside the reactor core ( $V_{out}$ ). Obviously, these investments will increase with the increase of the core specific power  $q_c$ , because the removal power density in the external power circuit is limited primarily by heat transfer and pressure drop considerations. An optimum salt discard rate exists, for which the fuel burnup time is balanced against the increasing of the core inventory and fuel makeup, which increase due to neutron balance worsening. In addition, there is a minimum discard rate required to limit the concentration of An/Ln trifluorides in the circulating fuel to an acceptable level. Adding a batch or on-line chemical facility to the single-pass reactor provides the second conceptual line, based on uranium and TRU recycling, as often as necessary. Fluoride volatility method, converting  $\text{UF}_4$  to gaseous  $\text{UF}_6$  and uranium oxide precipitation are proven methods for recovery of uranium from molten fluoride salt.

This contribution summarizes the available R&D which led to selection of the fuel compositions for MSB. Special characteristics of behavior of TRUs and fission products during power operation of MSB concepts are presented.

The present paper briefly reviews the processing developments underlying the prior MSR programs and relates them to the fuel treatment requirements for the MSB concept, including permissible range of fission product cleanup cycle times and removal times. Status and development needs in the thermodynamic properties of fluorides, fission product cleanup methods and container materials compatibility with the working fluids for the fission product cleanup unit are discussed.

To solve some of the essential issues mentioned in previous sections, Russian Institutes: RFNC–All–Russian Institute of Technical Physics, (Chelyabinsk–70), RRC–Kurchatov Institute (Moscow), Institute of Chemical Technology (Moscow) and Institute of High Temperature Electrochemistry (Ekaterinburg) have submitted to the ISTC the Project#1606: *Experimental study of molten salt technology for safe, low waste and proliferation resistant treatment of radwaste and plutonium in accelerator driven and critical systems.*

## High Level Waste Partitioning Studies at the Research Centre Jülich

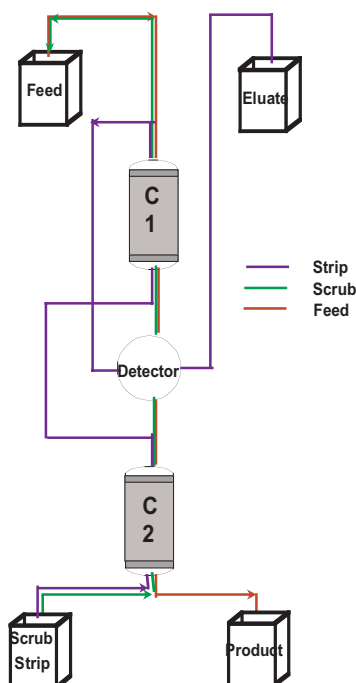
Partitioning of high level radioactive waste (HLW) into long-lived and short-lived radionuclides is now under discussion as an alternative to conventional nuclear waste management concepts. This strategy aims at reducing the long term hazard potential of waste repositories. Basic experimental data of the partitioning systems, but also technical scale operations of the separation units are needed for a meaningful cost-risk-benefit assessment of such a strategy. In the "Forschungszentrum Juelich," we focus on the decontamination of HLW solutions from the actinides including the non-recovered fuel components uranium and plutonium.

In future industrial scale applications, such processes will follow spent fuel reprocessing, and countercurrent solvent extraction will be the chosen technique. In research, however, this technique constitutes almost insurmountable difficulties, such as the continuous mode of operation requiring shift work and extra health physics and medical standby service, an extended effort for feed supply and removal of the process waste and non-routine safety measures even for artificial fission product solutions, due to the high  $\alpha$ -activity of the investigated contaminants. In addition, appropriate extractants are either extremely expensive or even not commercially available.

To this end, we determined solid phase extraction carried out in columns and operated in the front chromatographic mode as a suitable alternative. This technique is on the one hand closely related to liquid-liquid extraction regarding the chemical system; on the other hand, it can be operated batchwise, it can be scaled down easily to minimal throughputs ( $\sim 50$  ml feed/d  $\leq$  throughput  $\leq 20$  l feed/d), and it shows a very small extractant consumption (we processed in 100 working days  $2$  m<sup>3</sup> feed solution with 200 g extractant and did not observe any deterioration of the extractant).

In contrast to liquid-liquid extraction, solid phase extraction is operated in non-equilibrated states, thus requiring on-line monitoring of the contaminants with detectors, that respond to very low solute concentrations at the column outlet. For  $\alpha$ -emitters, such detectors are not yet available. We overcame this impediment by introducing the "Twin Column Concept" (Figure 1).

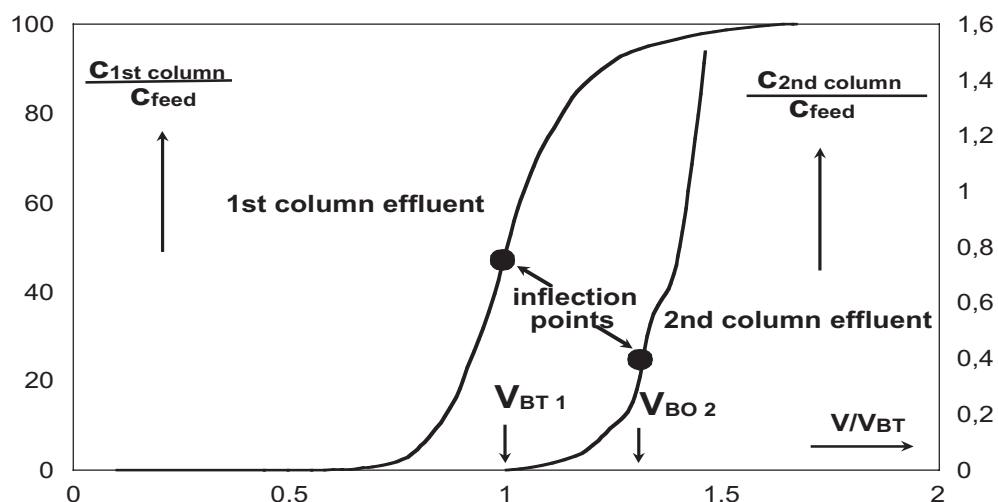
The column is divided into two identical parts and a detector is placed between the columns measuring the solute concentration in the first column effluent during the loading stage. The detector is a handmade solid scintillation flow detector which is selective for  $\alpha$  particles. At well defined volumes, the effluent concentrations of the two columns are correlated to each other (Figure 2) due to the different extraction mechanism at the column wall and the column interior.



**Ulrich Wenzel**  
Forschungszentrum  
Juelich - Institute for  
Safety Research and  
Reactor Technology  
D-52425 Jülich,  
Germany

Figure 1. Twin column concept.

Figure 2.  
Chromatograms of  
1st and 2nd  
column.



We can thus terminate the decontamination at a 2<sup>nd</sup> effluent concentration below the detection limit, while still obtaining a detector signal from the effluent of column 1, that can be evaluated with acceptable accuracy.

For the subsequent scrub stage, we apply a countercurrent flow, which prevents the tubing system behind column 2 from solute contamination. Again, we place the detector between the two columns, as scrubbing serves only to displace the non-extracted feed in the column carrier. Consequently, the scrub ends up in the feed tank. During the strip stage, we apply countercurrent flow and place the detector behind column 1 terminating the strip when the detector shows the background signal.

We have tested the twin column unit by decontaminating artificial waste solutions from the actinides Np, U, Pu, Am and Cm. We adjusted the feed to 2 M HNO<sub>3</sub> and stabilized Pu in the trivalent, Np in the tetravalent state using ascorbic acid and urea. The chromatographic support was composed of Amberchrom 71 C (a polymethacrylate) coated with a 59 wt % TBP (tri-butyl phosphate) solution containing 15 wt % CMPO (n-octyl phenyl N,N diisobutyl methyl phosphine oxide). This chromatographic support retained the actinides in the range of Cm(III) < Am(III) < Pu(III) < U(VI) < Np(IV). We achieved decontamination factors of (300 regarding Cm(III), the compound being least retained). The lanthanides were coextracted together with the actinides.

At present, we use the twin column unit for separating the actinides from the lanthanides using aromatic derivatives of dithiophosphoric acid as extractant. However, a large variety of extraction systems can be investigated that way in a technical scale by economizing the costs to those limits, which are nowadays imposed on research facilities.

# Modeling Hollow Fiber Membrane Separations Using Voronoi Tessellations

## Introduction

Hollow fiber membrane modules have their filaments randomly packed in the shell. The maldistribution of flow on the shell side leads to different mass transfer driving forces on the individual fibers. This makes the correct sizing of HFM contactors for process applications uncertain. By use of the method of Voronoi tessellations each fiber can be treated individually and the results summed. This puts us one step closer to an a priori design algorithm. The goal of this work is to develop a self-contained design procedure that will allow chemical process engineers to correctly predict the performance of the unit without the use of totally ad hoc methods. This implies that both the driving force on the shell side and the interface mass transfer in the pore must be handled correctly. In this work we consider systems with interface reaction. Further, we are employing pseudo first order kinetics for actinide separation. And we develop a software module compatible with a commercial simulator.

## Description of the Actual Work

In this work we combine film theory and facilitation factors in a simple way to model the extraction of uranyl nitrate from nitric acid into tributyl phosphate/diisopropylbenzene organic solution. We use independently obtained kinetic rate constants from data that minimizes diffusional mass transfer to obtain as close to a pure kinetic rate constant parameter as possible. The physical mass transfer constants are calculated using correlations. The model of maldistribution of flow on the shell side of the module is random sequential adsorption packing theory and the computational geometry concepts of Voronoi tessellations. A good representation of randomness, boundary effects, and area open to flow and mass transfer for each individual random filament placement can be obtained using the techniques. The model correlates well with experimental data.

## Results

Results shown in Rogers and Long (1997) show that the Voronoi tessellation method is superior to competing methods for computing mass transfer, and it eliminates mass adjustable parameters in the calculations. In the present work, the small error introduced by employing boundary polygons is corrected. The results are improved over the earlier case.

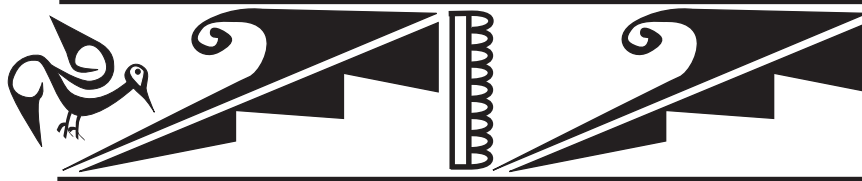
## Reference

1. Rogers, J. and Long, R. "Modelling hollow fiber membrane contactors using film theory, Voronoi tessellations, and facilitation factors for systems with interface reactions" *J. Membrane Science*, 134 (1997) 1-17.

**Richard Long,**  
**Tsun-Teng Liang,**  
**John Rogers**  
*New Mexico State*  
*University, Las*  
*Cruces, NM 88003,*  
*USA*

**Steve Yarbrow**  
*Los Alamos National*  
*Laboratory, Los*  
*Alamos, NM 87545*



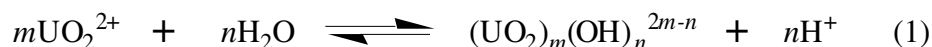


## **Actinides in the Environment**



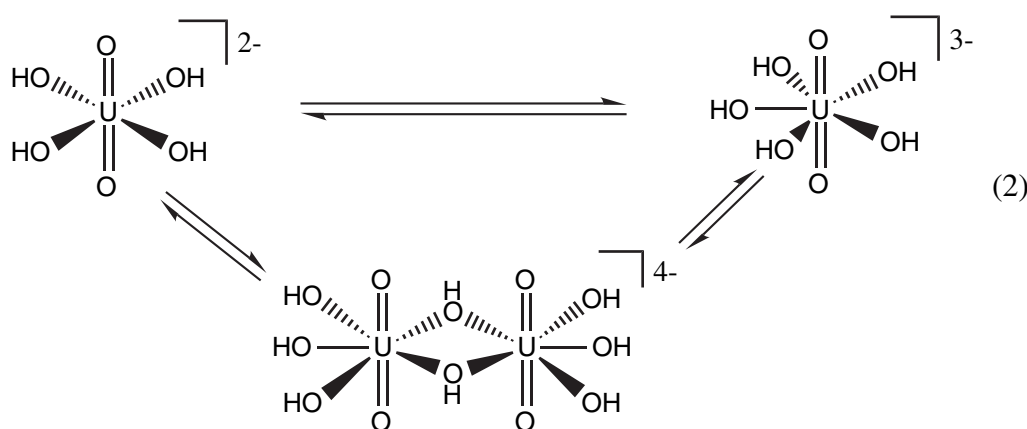
## Identification of Oligomeric Uranyl Complexes under Highly Alkaline Conditions

The aqueous chemistry of the uranyl(VI) ion ( $\text{UO}_2^{2+}$ ) under acidic and near-neutral conditions has been very well studied. The chemistry under these conditions centers around hydrolysis reactions, which result in the formation of a series of oligomeric U(VI) species as in eq. 1.<sup>1</sup> The formation of these products begins at



pH = 3 and is highly dependent upon the concentrations of both  $\text{UO}_2^{2+}$  and  $\text{OH}^-$ , with the predominant species consisting of monomers, dimers and trimers. However, the aqueous solution chemistry of the uranyl ion under strongly alkaline conditions is only poorly understood. We are interested in studying the species involved in the uranyl hydrolysis equilibria in order to gain an initial understanding of this chemistry, which may then translate to the chemistry of the  $\text{NpO}_2^{2+}$  and  $\text{PuO}_2^{2+}$  ions that are present in relatively high concentrations in aging waste tanks within the DOE complex.

By utilizing X-ray absorption methods, e.g., extended x-ray absorption fine structure (EXAFS) and single crystal x-ray diffraction (XRD), as well as Raman, UV-Vis and fluorescence spectroscopy, we have shown that an equilibrium exists between the monomeric uranyl hydroxide species  $\text{UO}_2(\text{OH})_4^{2-}$  and  $\text{UO}_2(\text{OH})_5^{3-}$ , which is dependent upon hydroxide concentration. Upon further study of this system, we have now determined that a new hydrolysis product is present in equilibrium with the monomeric uranyl hydroxide species, which is favored at higher  $\text{UO}_2^{2+}$  concentrations. Based upon several different methods of characterization, we are favoring the formulation for this new species as the dimeric uranyl hydroxide species  $[(\text{UO}_2)(\text{OH})_3(\text{m-OH})]_2^{4-}$  (eq. 2). This formulation is



consistent with electronic absorption and emission studies, which show a marked dependence on uranyl concentrations. The UV-Vis spectrum of this species exhibits a structured band with  $\lambda_{\text{max}} = 412 \text{ nm}$  and  $\epsilon = 45 \text{ M}^{-1}\text{cm}^{-1}$ , with a large tail into the UV region that begins at 375 nm. Both of these bands are red-shifted with respect to the corresponding peaks in the spectrum of the monomeric uranyl

Wayde V. Konze,  
David L. Clark,  
Steven D. Conradson,  
J. Donohoe,  
John C. Gordon,  
Pamela L. Gordon,  
D. Webster Keogh,  
David E. Morris,  
C. Drew Tait  
G. T. Seaborg Institute  
for Transactinium  
Science and Los  
Alamos National  
Laboratory, Los  
Alamos, NM 87545,  
USA

hydroxide equilibrium solution, and the molar absorptivity for the peak with  $\lambda_{\text{max}} = 412 \text{ nm}$  is increased. Similar features have been observed previously in the UV-Vis spectra of systems where oligomeric species are present.<sup>2</sup> The Raman spectrum for this new species exhibits a O=U=O  $\nu_1$  frequency at  $816 \text{ cm}^{-1}$ , which is higher in energy compared to the monomeric solution species at  $786 \text{ cm}^{-1}$ .

We have isolated this new species as a gel from solutions containing relatively high  $\text{UO}_2^{2+}$  concentrations (50 mM) and relatively low TMAOH concentrations (0.5M). This gel was found to exhibit the same Raman peak at  $816 \text{ cm}^{-1}$  and the same emission spectrum as that from solution. When the gel was washed with THF, a yellow solid was obtained, which exhibited the same Raman peak at  $816 \text{ cm}^{-1}$  and the same emission spectrum as that of the gel and from solution. This solid was also probed by diffuse reflectance UV-Vis and showed a very similar spectrum to that of the solution spectrum, suggesting that the same species is present in solution, in the gel and in the solid.

By probing solutions with high  $\text{UO}_2^{2+}$  concentrations (50 mM) and even lower TMAOH concentrations (100 mM), we were able to isolate and characterize a new phase of schoepite. A single crystal x-ray diffraction analysis revealed a schoepite structure  $[(\text{UO}_2)_4\text{O}(\text{OH})_6] \cdot 6\text{H}_2\text{O}$ , which crystallized in a different space group ( $P_{\text{bcn}}$ ) with a significantly higher density than that of the previous crystallographically characterized material.<sup>3</sup> The main difference in structural features of this new phase is that all of the  $\text{UO}_2^{2+}$  units contain five-coordinate equatorial planes, while the previously characterized phase contains alternating four- and five-coordinate equatorial planes.

### References

1. Palmer, D. A.; Nguyen-Trung, C., *J. Solution Chem.* **1995**, *24*, 1281.
2. Meinrath, G., *J. Radioanal. Nucl. Chem.* **1997**, *224*, 119.
3. Finch, R. J.; Cooper, M. A.; Hawthorne, F. C.; Ewing, R. C., *Can. Mineral.* **1996**, *34*, 1071.

# Process Support Conditions for Dissolving Metallic Plutonium in a Mixture of Nitric and Hydrofluoric Acids

## Introduction

The process of dissolving metallic plutonium is based on a method that uses a mixture of nitric and hydrofluoric acids. The choice of this method is cited in comparison primarily with the method of dissolving Pu in hydrochloric acid solutions [1]. Dissolution is done in mixtures of 4-12 moles/liter of nitric acid and 0.2-0.4 mole/liter of hydrofluoric acid with boiling of the solution. The process of dissolving plutonium releases about 90 liters of gas per kg of metal. For practical purposes, the volume and composition of the gas depend only slightly on the concentration of the acids and the solid:liquid ratio. Hydrogen content in the gas phase does not exceed 0.45% (by volume), which is much less than the lower limit of explosivity of a mixture of hydrogen with air. Composition of the gas phase (in percent by volume):  $H_2 = 0.31-0.45$ ,  $N_2 = 23.8-29.0$ ,  $N_2O = 1.31-1.62$ ,  $NO = 22.4-28.1$ . Insoluble residues do not contain pyrophoric compounds. Dissolution is done in a dissolver made of EP-630 steel.

Process support of safe dissolution of metallic plutonium in a mixture of nitric and hydrofluoric acids is described in report [2]. Data obtained previously by experiment and published in [1] have enabled further research for the purpose of obtaining additional information for process engineering of dissolution.

## Factors That Influence the Process of Dissolution

A study has been done on the effect that various factors have on the process of dissolving metallic plutonium in mixtures of nitric and hydrofluoric acids:

- concentration of acids and solid:liquid ratio on the completeness of dissolution of metallic plutonium,
- surface area (aggregate state) of the specimen on rate of dissolution of metallic plutonium,
- temperature of solutions,
- intensity and method of agitating solutions,
- kinetics and gas release in dissolution process,
- conditions of dissolution on composition and volume of gas phase,
- amount of surface of plutonium specimens on volume and composition of gas phase released during dissolution,
- amount of surface of metallic plutonium on rate of gas release.

The range covered by the study was with respect to concentrations of nitric acid 4-13 moles/liter, of hydrofluoric acid — 0.15-0.3 mole/liter, volume-mass (solid:liquid) ratio — 1:5, 1:10, 1:15 and 1:20.

**B. S. Zakharkin,  
V. P. Varykhanov,  
V. S. Kucherenko,  
L. N. Solov'yeva**  
*State Science Center  
of the Russian  
Federation, A. A.  
Bochvar All-Russian  
Research Institute of  
Inorganic Materials,  
123060, g. Moskva,  
Russia*

Based on these studies, the following has been established:

- the rate of dissolution of metallic plutonium and the rate of gas release as it is being dissolved are directly proportional,
- the composition and volume of gas phase released during dissolution do not depend on the area of the specimens and the concentration of reagents,
- the content of hydrogen in the gas phase throughout the dissolution process is less than the lower limit of explosivity in a mixture with air,
- reducing the surface area of specimens of metallic plutonium reduces the maximum values of rates of gas release and dissolution of metallic plutonium,
- the method of agitating the solution — mechanical stirring or bubbling with inert gas or air — has practically no effect on the rate of dissolution at boiling temperatures of the solution,
- the completeness of dissolution decreases with decreasing temperature.

### Discussion of Results

The data of our studies confirm that the basis of the process of dissolving metallic plutonium in mixtures of  $\text{HNO}_3$  and  $\text{HF}$  is comprised of two stages that occur simultaneously: dissolution of the oxide film due to interaction with  $\text{HF}$ , and interaction of metallic plutonium with  $\text{HNO}_3$ . This is confirmed by the kinetic dependence of the rate of dissolution: it is not subject to the kinetic dependence of dissolution of plutonium oxide [3].

Dissolution of the oxide layer on the surface of the metal increases its penetrability for diffusion of nitric acid molecules into the metal. As the nitric acid interacts with  $\text{Pu}$ , an oxide layer is formed once again. Thus, processes of formation and dissolution of the oxide layer on the surface of the metal go on continually. The maximum values of rates of dissolution and gas release correspond to the minimum amount of oxide layer.

As metallic plutonium interacts with  $\text{HNO}_3$ , atomic hydrogen is formed on the surface of the metal [1] that is absorbed by nitric acid as a result of a redox reaction with formation of nitrogen compounds of various degrees of oxidation: nitric oxide, nitrogen dioxide, nitrous oxide and molecular nitrogen.

The abundant gas phase released during dissolution brings about conditions for intensifying convection in the solution. Convective agitation is likewise increased by raising the temperature of the solution [4]. The processes of dissolution of solid phase in solutions with release of gas phase are described in [5], and it is shown that increasing the concentration of reagent with a concomitant increase in the rate of release of gas phase stops agitation from having an effect on the rate of dissolution. Thus, two factors — abundant liberated gas phase and boiling of the solution — bring about conditions that cancel the effect of various methods of agitation on the rate of dissolution of metallic plutonium in a mixture of  $\text{HNO}_3$  and  $\text{HF}$  as the solution boils.

The rates of gas release and dissolution of plutonium while the solution is boiling change throughout the process. Their maximum values are reached midway through the process and drop to the minimum at the end. To make the course of the dissolution process more uniform and reduce the aggressiveness of the me-

dium, consideration could be given to the possibility of using fluorine ions in the form of fluorine-containing compounds other than HF without serious detriment to the parameters of dissolution. This is based on a two-stage mechanism of the course of dissolution of metallic plutonium and plutonium oxide in mixtures of nitric and hydrofluoric acids.

### References

1. Polyakov, A. S., Zakharkin, B. S., Borisov, L. M., Kucherenko, V. S., "Materials of the International Conference on the Nuclear Fuel Cycle," Versailles, France, 11-14 September 1995, pp 640-651.
2. Borisov, L. M., Revyakin, V. V., Varykhanov, V. P., Gitkovich, Ye. S., Kucherenko, V. S., "Process Support of Safety in Converting Plutonium to Nuclear Fuel," report to the fourth US-Russian seminar on handling nuclear-hazardous materials, Amarillo, Texas, 15-23 March 1997.
3. Nikitina, G. P. et al., "Existing Methods of Dissolving Plutonium Dioxide. 1. Dissolving in Mineral Acids and Their Mixtures," *Radiokhimiya*, Vol 39, No 1, St. Petersburg, 1997, pp 14-27.
4. Kireyev, V. A., "A Course in Physical Chemistry," Moscow, 1956, pp 687 ff.
5. Aksel'rud, G. A., Molchanov, A. D., "Dissolution of Solids," Vol 1, Moscow, 1997, pp 34-40.

## Investigation of Radiation-Chemical Behaviour of Plutonium in the Groundwaters and Soils

D. A. Fedoseev,  
M. Yo. Dunaeva,  
M. V. Vladimirova  
SSC A.A. Bochvar  
All-Russia Research  
Institute of Inorganic  
Materials, Moscow,  
Russia

The valent state of plutonium in a model heterogeneous system—groundwater-plutonium dioxide—has been studied by spectrophotometry in the process of exposition in time both with and without gamma-irradiation (to 450 kGy).

Concentrations of plutonium in the groundwater (after separation from suspension) exposed during six months without irradiation have been found to be 42 mg/l. The absorption spectrum of the solution resembles one of that of the hydroxopolimere of Pu(IV), though an extinction coefficient for peak at 400 nm (6500 l/mol·cm) is significantly superior to literature values (150 l/mol·cm). This obstacle permits to us conclude, that hydroxopolimere is solvated by being dissolved in a liquid organic complexing agent, for example, by fulvo-acid.

The concentration of plutonium in the water, exposed with plutonium dioxide during two years (without irradiation) has been found to be 18 mg/l. The absorption spectrum of the solution has no bands that are features of Pu(IV), but are those for Pu(III) and Pu(V).

Apparently, part of the Pu(IV) has been sorbed on the suspension particles (64%), and a second part (36%) has been transformed into Pu(III) and Pu(V).



The concentration of plutonium in water with plutonium dioxide, exposed during six months at gamma-irradiation (absorbed dose is 430 kGy) is 32 mg/l. The bands of Pu(III) and of Pu(V) are observed on the absorption spectra. Apparently, in addition to the disproportionation reaction there are the following radiation-chemical reactions:



Apparently, radiolytic effects increase the formation rate of Pu(III) and Pu(V), which are more mobile forms of plutonium in groundwater than Pu(IV).

# Polymeric Species of Pu in Low Ionic Strength Media

## Introduction

The U.S. Government has declared that approximately 50 tons of plutonium is surplus to U.S. needs and should be set aside for eventual disposition. The U.S. is currently following a dual path for the disposition of this plutonium: immobilization and irradiation of mixed-oxide fuel.<sup>1</sup>

Some fraction of this plutonium material that is undesirable for use in mixed-oxide fuel will be immobilized in a titanate ceramic and disposed of in a geologic repository for high-level waste. The remainder of Pu will be fabricated into mixed-oxide fuel and irradiated in domestic light-water reactors. The resulting spent fuel would also be disposed of in a geologic repository for high-level waste. The proposed U.S. repository would be at the Yucca Mountain site in Nevada.

Plutonium present in the disposal forms, either ceramics or spent fuel, must remain isolated from the biosphere over the geologic repository regulatory performance period, which is currently 10,000 years. Contamination of the biosphere could result from slow dissolution of the disposal forms followed by transport of the dissolution products into the biosphere by flowing ground water. Measurable amounts of apparently soluble plutonium can be released if plutonium dioxide is exposed to water under some conditions.<sup>2</sup> Furthermore, recent studies in Nevada near the Yucca Mountain Site revealed that plutonium, associated with the colloidal fraction of the groundwater, was detected over a kilometer from its source within 30 years after it was placed underground for nuclear weapons testing.<sup>3</sup> It was not clear whether plutonium was transported as an intrinsic plutonium colloid or as plutonium sorbed onto colloidal clay or zeolite particles.

## Description of Work and Results

The formation of plutonium colloids was studied in a surrogate Yucca Mountain groundwater similar in composition to water from well J-13 at the Nevada Test Site. Experiments were conducted at several pH under an air atmosphere at 25°C. Pu(V) is the dominant oxidation state of plutonium in water at atmospheric oxygen fugacity.<sup>2</sup> Solutions containing  $10^{-4}$  M Pu(V) and  $10^{-6}$  M Pu(V) were produced in J-13 surrogate at pH 1, 3, 6, 8, and 11, and the plutonium solutions were monitored for several months. Aliquots were taken periodically and analyzed using ultrafiltration and liquid scintillation spectrometry. Several times during the experiment, the plutonium oxidation state distribution was determined using solvent extraction techniques.

The results show that the Pu(V) oxidation state dominated under conditions relevant to natural systems. For both plutonium concentrations, 10% to 25% of the plutonium in every sample was present as a non-extractable, suspended form of plutonium that passed through a 0.01-micron filter. We infer that this material was a polymeric form of plutonium.

The plutonium species distribution under the conditions of the experiment was calculated using the Geochemist's Workbench package.<sup>4</sup> The calculated and experimentally determined total concentrations of dissolved plutonium were in

V. V. Romanovski,  
C. E. Palmer,  
H. F. Shaw,  
W. L. Bourcier,  
L. J. Jardine  
*Lawrence Livermore  
National Laboratory,  
Livermore, CA 94550,  
USA*

reasonable agreement only if one accounts for the polymeric plutonium. There are no polymeric plutonium species represented in the thermodynamic database used to model the experiments.<sup>5</sup> The fact that polymeric species were present in significant quantities in our experiments raises the question of their long-term stability and their possible role in long-term plutonium transport in the underground environment of a geologic repository. This work is focused on collecting data to address this possible transport role of plutonium as a colloid.

### References

1. DOE (U.S. Department of Energy), Surplus Plutonium Disposition Draft Environmental Impact Statement Summary, DOE/EIS-0283-D, Office of Fissile Materials Disposition, Washington, D.C., July 1998.
2. Heaton, R. C., Jones, W. M., Coffelt, K. P., "Plutonium release from radioisotope heat sources into aqueous systems," Los Alamos National Laboratory, LA-11668-MS, December 1989, Government Reports 91 (19), (152, 431).
3. Kersting, A. B., Efurud, D. W., Finnegan, D. L., Rokop, D. J., Smith, D. K., and Thompson, J. L., "Migration of plutonium in ground water at the Nevada Test Site," *Nature*, 397, 56 (1999).
4. Craig M. Bethke and The Board of Trustees of the University of Illinois, The Geochemist's Workbench™, Release 3.0.2, Urbana, Illinois, 1991-98.
5. Johnson, J. W., and Lundeen, S. R., (1994) GEMBOCHS thermodynamic datafiles for use with the EQ3/6 software package, Lawrence Livermore National Laboratory, Report Number LLNL-YMP milestone report MOL72, 99; 126 p.

## Solubility and Speciation of Plutonium(VI) Carbonates and Hydroxides

Plutonium exists in the environment as a result of the nuclear fuel and weapons cycle and nuclear weapons testing. Carbonate and hydroxide are ubiquitous in the environment while chloride is a principal component in brines such as those native to the Waste Isolation Pilot Plant (WIPP) site. Thus, the characterization of plutonium complexes formed with  $\text{CO}_3^{2-}$ ,  $\text{OH}^-$ , and  $\text{Cl}^-$  is important for predicting the behavior of plutonium in the environment. Plutonium(VI) is known to form under oxidizing conditions, and we are investigating the structure, solubility and speciation of plutonium(VI) carbonates and hydroxides.

Despite the importance of plutonium(VI) carbonates, only a limited amount of thermodynamic data exists.<sup>1-4</sup> We are investigating the solubility and speciation of the plutonium(VI) carbonate system under conditions relevant to the environment. Based upon solution thermodynamic studies (potentiometric and spectrophotometric), we determined that the monocarbonato species,  $\text{PuO}_2\text{CO}_{3(\text{aq})}$ , has the largest relevant stability range. We prepared the corresponding solid phase,  $\text{PuO}_2\text{CO}_{3(\text{s})}$ , and characterized the pink-tan solid using powder XRD, EXAFS, and diffuse reflectance. We have measured the solubility of  $\text{PuO}_2\text{CO}_3$  in NaCl and  $\text{NaClO}_4$  solutions as a function of pH and ionic strength (0.1 to 5.6 m). The concentration of soluble plutonium in solution was calculated from liquid scintillation counting and spectroscopic data. Spectroscopy also reveals the plutonium oxidation state. We have determined the solubility product of  $\text{PuO}_2\text{CO}_3$  to be  $\log K_{\text{sp}} = -13.8$  (0.1 m NaCl),  $\log K_{\text{sp}} = -14.0$  (5.6 m NaCl) and  $\log K_{\text{sp}} = -14.4$  (5.6 m  $\text{NaClO}_4$ ).

The solubility product of  $\text{PuO}_2\text{CO}_3$  as a function of ionic strength is shown in Figure 1 along with available literature reference values for  $\text{PuO}_2\text{CO}_3$  and  $\text{UO}_2\text{CO}_3$ . Based upon our results and the few data available in the literature, we find that plutonyl carbonate is significantly more soluble in NaCl than in  $\text{NaClO}_4$ . This difference is due to the formation of chloro complexes  $\text{PuO}_2\text{Cl}_x^{2-x}$ . In

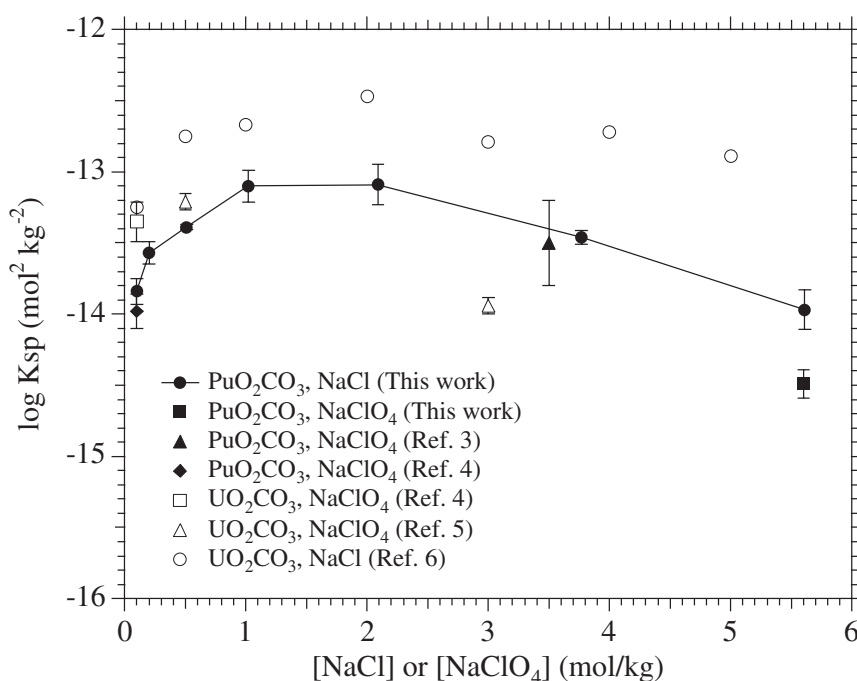
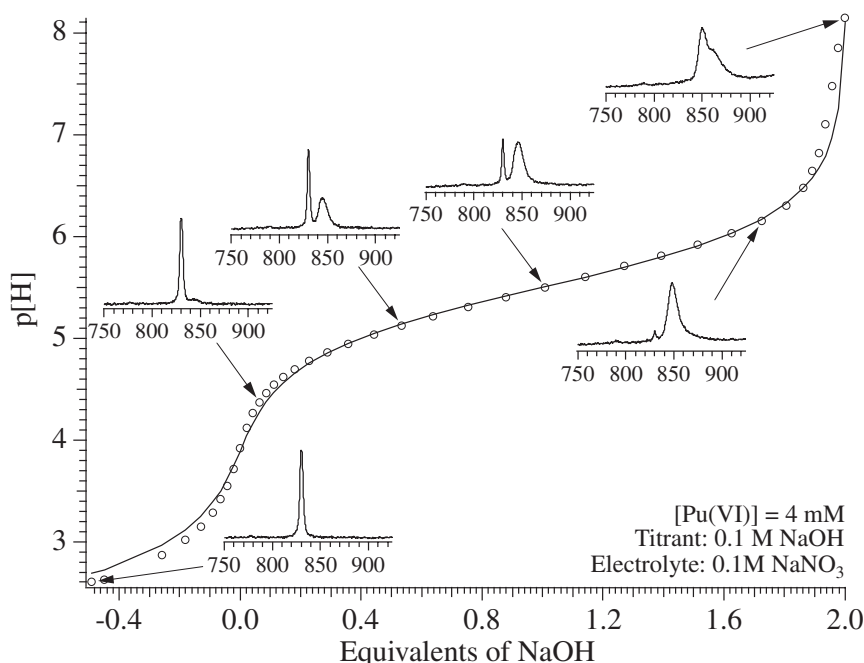


Figure 1. Overall solubility of  $\text{PuO}_2\text{CO}_3$  and  $\text{UO}_2\text{CO}_3$  in NaCl and  $\text{NaClO}_4$ .

separate studies we determined the formation constants of the mono and bis chloro complexes to be  $\log \beta^\circ = 0.23 \pm 0.03$  and  $-1.7 \pm 0.2$ , respectively.<sup>7</sup> From the first day in the 5.6 m  $\text{NaClO}_4$  and the more dilute  $\text{NaCl}$  solubility experiments optical absorbance spectra of the filtered solution showed absorbance bands indicative of both Pu(V) and Pu(VI). The surface of the solid also underwent a gradual color change from pink-tan to bright green. Characterization of the aged solid by diffuse reflectance spectroscopy and powder XRD shows that it is a mixture of the starting  $\text{PuO}_2\text{CO}_3$  solid and insoluble polymeric Pu(IV) hydroxide. We conclude that the Pu(V) present in solution disproportionated to form Pu(VI) and polymeric Pu(IV) hydroxide. We note that Pu(VI) in low ionic strength carbonate solutions is reduced to Pu(V) within hours to days, while concentrated  $\text{NaCl}$  appears to stabilize the higher oxidation state, presumably via chloro complexation and the radiolytic production of hypochlorite. Additional results from solution thermodynamic and structural studies will be presented.

We have begun to investigate and characterize the initial plutonium(VI) hydrolysis species. Uranium(VI) hydrolysis has been studied thoroughly.<sup>8</sup> In contrast, only a handful of publications on plutonium(VI) hydrolysis chemistry exist, and evidence indicates uranium and plutonium exhibit markedly different speciation. We are collecting potentiometric and spectrophotometric data to determine formation constants as a function of plutonium concentration and solution ionic strength (see Figure 2). Higher order oligomeric and polymeric plutonium(VI) hydrolysis products readily form and impede the study of expected initial hydrolysis species such as  $\text{PuO}_2\text{OH}^+$  and  $\text{PuO}_2(\text{OH})_2$ . Preliminary studies focused on solutions with  $10^{-2}$  to  $10^{-3}$  M Pu(VI) but we have extended our investigation to lower plutonium concentrations ( $10^{-4}$  M). At these lower concentrations we see evidence for fewer hydrolysis species and different absorbance maxima suggesting a change in speciation. We are also isolating plutonium(VI) hydroxide solids for characterization and comparison to solution species.

**Figure 2.**  
Plutonium(VI)  
hydrolysis  
potentiometric  
titration. Insets show  
solution optical  
spectra as hydrolysis  
progresses.



## References

1. M. P. Neu, S. D. Reilly, W. Runde In *Materials Research Society Symposium Proceedings Series, II. Scientific Basis for Nuclear Waste Management XX*, Vol 465, p. 759.
2. G. Meinrath, Y. Kato, T. Kimura, Z. Yoshida, *Radiochim. Acta* **84**, 21 (1999).
3. P. Robouch, P. Vitorge, *Inorg. Chim. Acta* **140**, 239 (1987).
4. I. Pashalidis, W. Runde, J. I. Kim, *Radiochim. Acta* **61**, 141 (1993).
5. I. Grenthe, *et al.*, *J. Chem. Soc., Dalton* 2439 (1984).
6. W. Runde, *et al.*, unpublished results.
7. W. Runde, S. D. Reilly, M. P. Neu, *Geochim. Cosmochim. Acta* **63**, 3443 (1999).
8. I. Grenthe, *et al.*, *Chemical Thermodynamics of Uranium*; Elsevier Science Publishing Company, Inc.: North-Holland, 1992; Vol. 1.

## Plutonium in the Environment: Speciation, Solubility, and the Relevance of Pu(VI)

**W. Runde,  
D. Efurd,  
M. P. Neu,  
S. D. Reilly,  
C. VanPelt,  
S. D. Conradson**  
*Los Alamos National  
Laboratory, Los  
Alamos, NM 87545,  
USA*

The critical role of plutonium in long-term and interim storage of nuclear waste attracts great attention to its fate under environmental conditions. The unique feature of plutonium, the ability to occur in multiple oxidation states simultaneously, complicates its geochemistry. For decades  $\text{PuO}_2$  has been considered the most stable form of Pu with the lowest solubility and lowest mobility among the actinide oxides/hydroxides. However, recent reports have raised concern on the stability of  $\text{PuO}_2$ . Colloidal transport of Pu at the Nevada Test Site and absorption of oxygen in the presence of water to form a higher oxide,  $\text{PuO}_{2+x}$ , indicated the potential implications for the long-term storage of plutonium. In specific, the formation of a "superoxide" in which more than 25% of the Pu(IV) is oxidized to soluble Pu(VI) raised concerns regarding the safety of underground storage facilities.

We combined fundamental chemical studies, site-specific investigations, and geochemical modelling to evaluate the understanding of the environmental behavior of plutonium. Solubility studies were conducted in J-13 water from the Yucca Mountain site representing the range of natural waters of low ionic strength. In these waters, amorphous plutonium oxide/hydroxide and/or colloidal Pu(IV) dominated the solubility-controlling solid. X-ray absorption spectroscopy studies revealed the +IV oxidation state to be prevalent. Geochemical modelling showed that at neutral pH, the Pu solubility is controlled by the solubility of the Pu(IV) solid at Eh (the redox potential of the solution) < 300 mV. Increasing Eh results in the stabilization of Pu(V). Maintaining the high Eh and increasing pH results in the stabilization of Pu(VI). While Pu(V) is the most stable oxidation state at neutral pH, the formation of Pu(VI) causes a significant increase in Pu solubility due to the formation of highly soluble anionic Pu(VI) carbonate complexes. The stability of these complexes increase with carbonate concentrations. At the carbonate concentrations common for natural waters, Pu(VI) is calculated to be stable only at pH above 9 (Figure 1).

The stability of Pu(VI) was tested at varying pH and NaCl concentrations. At low pH and chloride concentration Pu(VI) is unstable towards reduction and green Pu(IV) solid precipitates from oversaturation. Increase in chloride and pH stabilizes Pu(VI), most likely due to radiolysis and complexation reactions. Radiolytic formation of oxidizing species, such as  $\text{ClO}^-$ , at  $[\text{NaCl}] > 2 \text{ M}$  may create an oxidizing system and Pu(IV) is oxidized to Pu(VI). In the presence of reductive agents, such as Fe, Pu(VI) rapidly reduces to lower oxidation states, Pu(V) and Pu(IV).

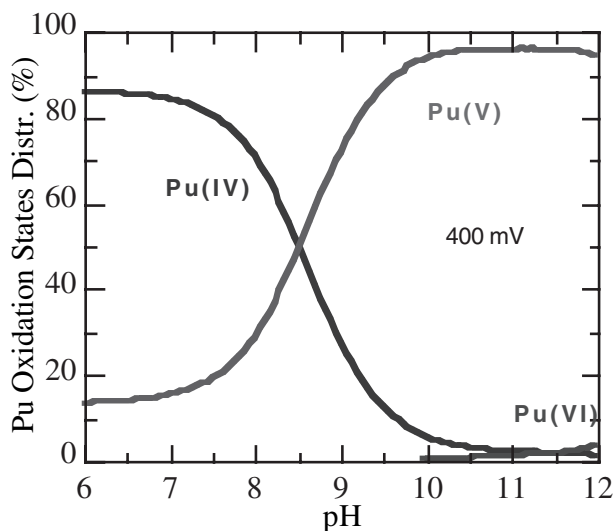


Figure 1. Pu oxidation state distribution at 400 mV and 500 mV. The carbonate concentration was maintained at 1 millimolar.

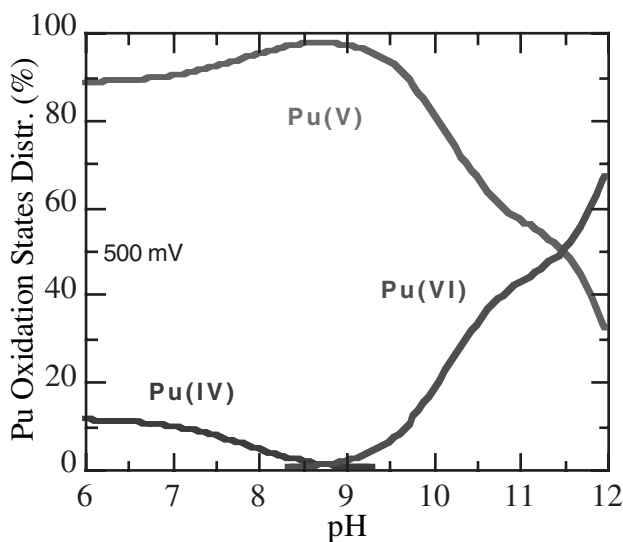


Figure 2. Pu oxidation state distribution at 400 mV and 500 mV. The carbonate concentration was maintained at 1 millimolar.

Geochemical modelling predicts Pu(IV) in its low soluble solid oxide/hydroxide form that predominates over most natural conditions. We studied the speciation of Pu in contaminated soil from the Rocky Flats Environmental Test Site (RFETS). X-ray absorbance data on soil samples from the RFETS indicate the Pu present is tetravalent and structurally similar to the highly stable and immobile  $\text{PuO}_2$ . Dissolution reactions are ongoing to determine the release rate and Pu concentration boundaries. Here we evaluate the present understanding of plutonium environmental chemistry and discuss how solid phase stability, solution speciation, and redox potential interact and influence the solubility of plutonium in natural systems.

## Immobilizing U from Solution by Immobilized Sulfate-Reducing Bacteria of *Desulfovibrio desulfuricans*

Huifang Xu,  
Larry L. Barton  
University of New  
Mexico, Albuquerque,  
NM 87131, USA

The solubility of uranium is dependent on its oxidation state. Under oxidizing environments, uranium will exist in the form of uranyl ( $\text{UO}_2^{2+}$ ) ion that complexes with carbonate ( $\text{CO}_3^{2-}$ ) and organic ligands. When carbonate is present in aerobic solutions, uranyl forms highly soluble metal complexes of  $\text{UO}_2\text{CO}_3^0$ ,  $\text{UO}_2(\text{CO}_3)_2^{2-}$ , and  $\text{UO}_2(\text{CO}_3)_3^{4-}$ . Waste water from the nuclear industries is important because oxidative dissolution of nuclear waste results in the formation of very soluble oxy-cations, such as of  $\text{UO}_2^{2+}$  and  $\text{PuO}_2^{2+}$ . In order to immobilize the uranium in water, uranium may be reduced to insoluble uraninite ( $\text{UO}_2$ ). Recent studies have demonstrated that *Desulfovibrio desulfuricans* and other sulfate-reducing bacteria are capable of reducing uranyl and other metals by enzyme-mediated reactions. This biological process involving reduction of heavy metals can effectively remove these materials from solution. The detoxification process is known as dissimilatory reduction and occurs when electrons from molecular hydrogen ( $\text{H}_2$ ) or lactate are transferred to oxidized metal ions such as selenate or  $\text{UO}_2^{2+}$ . In at least one instance, the dissimilatory reduction of uranyl ion is coupled to the growth of a sulfate-reducing bacterium, *Desulfotomaculum reducens*.

Previous studies of bacteria-induced uranyl reduction focus on solution chemistry where the amount of uranyl ion removed from solution is measured. In one transmission electron microscopy (TEM) report using whole cells of bacteria, aggregates of uraninite and iron sulfide precipitates were apparent, and uraninite crystals were suggested as extracellular products.

As determined by transmission electron microscopy, the reduction of uranyl acetate by immobilized cells of *Desulfovibrio desulfuricans* results in the production of black uraninite nanocrystals precipitated outside the cell. Some nanocrystals are associated with outer membranes of the cell as revealed from cross sections of these metabolically active sulfate-reducing bacteria. The nanocrystals have an average diameter of 5 nm and have anhedral shape. It is proposed that cytochrome in these cells has an important role in the reduction of uranyl through transferring electron from molecular hydrogen or lactic acid to uranyl ions.

## Interaction of Actinides with Aerobic Soil Bacteria

The production and testing of nuclear weapons, nuclear reactor accidents, and accidents during the transport of nuclear weapons have caused significant environmental contamination with radionuclides. Their migration behavior is controlled by a variety of complex chemical and geochemical reactions such as solubility, sorption on the geo-matrix, hydrolysis, redox reactions, and complexation reactions with inorganic, organic, and biological ligands. In addition, microorganisms can strongly influence the actinides' transport behavior by both direct interaction (biosorption, bioaccumulation, oxidation, and reduction reactions) and indirect interaction (change of pH and redox potential), thus immobilizing or mobilizing the radionuclides. Extensive studies were performed on the interaction of uranium with different kinds of bacteria (aerobic and anaerobic).<sup>1</sup> Nevertheless, very little information is available for transuranic elements such as Np, Am, Cm, and especially Pu.<sup>2</sup>

Plutonium can exhibit several oxidation states, e.g., 4+, 5+, and 6+, in aqueous solution under environmental conditions. Most papers on the interaction of Pu with bacteria contain only data on the amount of uptake, but generally lack information on the plutonium oxidation state and the nature of the binding.<sup>3-5</sup> Because Pu is a redox active metal, the interaction with the biomass can cause changes of the oxidation state. For a better understanding of these processes, the speciation of the bacterial plutonium complexes formed is necessary. In recent years, first attempts were made to characterize the reduction products of Pu(IV) after contact with iron-reducing bacteria.<sup>6</sup> Increased solubilization on hydrous PuO<sub>2</sub>(s) under anaerobic conditions was observed in the presence of these bacteria. Unfortunately, the predicted reduction of Pu(IV) to Pu(III) could not be proved by absorption spectroscopy. Our research focuses on the interaction of aerobic bacteria with hexa- and pentavalent plutonium. We used two different strains for our studies, *Bacillus sphaericus* (ATTC 14577) and *Pseudomonas stutzeri* (ATTC 17588), that are representatives of the main aerobic groups of soil bacteria present in the upper soil layers. The investigation included quantitative studies to determine the binding of Pu as a function of biomass. To characterize the formed Pu species, we used optical absorption spectroscopy and x-ray absorption spectroscopic (EXAFS/XANES).

The accumulation studies have shown that these soil bacteria accumulate large amounts of Pu(VI). The sorption efficiency toward Pu(VI) decreased with increasing biomass concentration due to increased agglomeration of the bacteria and a decreased total surface area and number of available complexing groups at higher biomass concentrations. The spores of *Bacillus sphaericus* showed a higher biosorption than the vegetative cells at low biomass concentration. It decreased significantly with increasing biomass concentration. At higher biomass concentrations (>0.77 g/L) the vegetative cells of both strains and the spores of *B. sphaericus* showed comparable sorption efficiencies. Our earlier studies on the interaction of U(VI) with different *Bacillus* strains have shown that the uranium is bound to phosphate groups of the cell surface.<sup>7,8</sup> The uranium bound to the biomass was almost quantitatively released by extracting the biomass with EDTA. These results indicate that uranium forms surface complexes with functional groups of the bacterial cells and is not transported into the cells. To obtain similar information on the binding strength and the reversibility of bacterial Pu complexes, we extracted the plutonium bound to the cells with 0.01 M EDTA solution (pH 5.2). The pluto-

**P. J. Panak**

*The Glenn T. Seaborg  
Center, Lawrence  
Berkeley National  
Laboratory, Berkeley,  
CA 94702, USA*

**H. Nitsche**

*University of  
California, Berkeley,  
Berkeley, CA 94720,  
USA*

nium bound to the biomass was almost quantitatively released for all biomass concentrations. In agreement to the uranium *Bacilli* complexes, these results indicate that the plutonium is bound to the cell walls and is not transported to the inside of the cells. The complex formed with the functional groups of the cell surface is less stable than the EDTA complex. We observed no significant differences of extraction behavior between the different strains or between the vegetative cells and the spores.

Using optical absorption spectroscopy, we found that the initial amount of Pu(VI) and Pu(V) decreased with increasing concentration of the biomass. The spectra also confirmed that not stable Pu(VI) and Pu(V) bacterial complexes were formed. Synchrotron-based x-ray absorption spectra (XANES and EXAFS) revealed that the plutonium, initially present as Pu(VI), was reduced to Pu(IV), which was coordinated to phosphate groups of the bacterial cells. This is the first observation of actinide reduction by aerobic soil bacteria. Possible explanations for this behavior will be discussed.

### References

1. Francis, A. J., Characteristics of Nuclear and Fossil Energy Wastes, *Experientia* **46**, 794–796 (1990).
2. Francis, A. J., Biotransformation of Uranium and Other Actinides in Radioactive Wastes, *J. Alloys Comp.* 271–273, 78–84 (1998).
3. Wildung, R. E., Garland, T. R., The Relationship of Microbial Processes to the Fate and Behavior of Transuranic Elements in Soils, Plants, and Animals, in *Transuranic Elements in the Environment*, pp. 300–335, Ed. W. C. Hanson, DOE/TIC-22800, Technical Information Center, US Department of Energy, Washington, DC (1980).
4. Francis, A. J., et al., Role of Bacteria as Biocolloids in the Transport of Actinides from a Deep Underground Radioactive Waste Repository, *Radiochim. Acta* **82**, 347–354 (1998).
5. Streitmeier, B. A., et al., Plutonium Interaction with a Bacterial strain Isolated from the Waste Isolation Pilot Plant (WIPP) Environment, American Chemical Society, Division of Environmental Chemistry, Preprints of Extended Abstract, Vol. 36(2) (1996).
6. Rusin, et al, Solubilization of Plutonium Hydrous Oxide by Iron-Reducing Bacteria, *Environ. Sci. Technol.* **28**, 1686–1690 (1994).
7. Panak, et al, Complex Formation of U(VI) with *Bacillus*-Isolates from a Uranium Mining Waste Pile, *Radiochim. Acta*, in press.
8. Hening, C., et al., EXAFS Investigation of U(VI)-Complexes with Different Bacteria, Forschungszentrum Rossendorf, Institut für Radiochemie, Report-FZR 272, 88 (1999).

## Plutonium Uptake by Common Soil Aerobes

Radionuclide contamination in soils and groundwater poses a risk to both human and environmental health. The DOE has identified 12 sites with significant U contamination in the soils and ground water, and 10 sites with Pu contamination.<sup>1</sup> It is important to study the interactions of common soil microbes with these radionuclides both to understand the environmental fate of these contaminants and to evaluate the potential of biological techniques to remediate contaminated soils and water.

We have undertaken a study of the potential for common soil aerobes to take up Pu and U by the same mechanisms used in the uptake of Fe(III). All known soil microbes use siderophores, biologically produced low molecular-weight chelating agents, to scavenge Fe(III) from the environment. In the presence of oxygen iron exists only in the insoluble ferric form. Complexation by a siderophore solubilizes the Fe(III) and plays a crucial role in transporting Fe into the cell. The same mechanisms that allow for Fe uptake by microbes have also been shown to be responsible for the uptake of other metal ions. Both Ga and Cr complexes have been demonstrated to form stable complexes with some common siderophores and to be taken up by cells in the same manner as Fe. Single crystal X-ray diffraction and solution spectroscopic studies have shown that both Pu and U form stable complexes with the siderophore desferrioxamine-B (DFO-B) and that the Pu complex is structurally similar to the Fe complex. Based on this evidence, we hypothesized that similar uptake of DFO-B complexed with Fe, Pu, and U ions would occur.

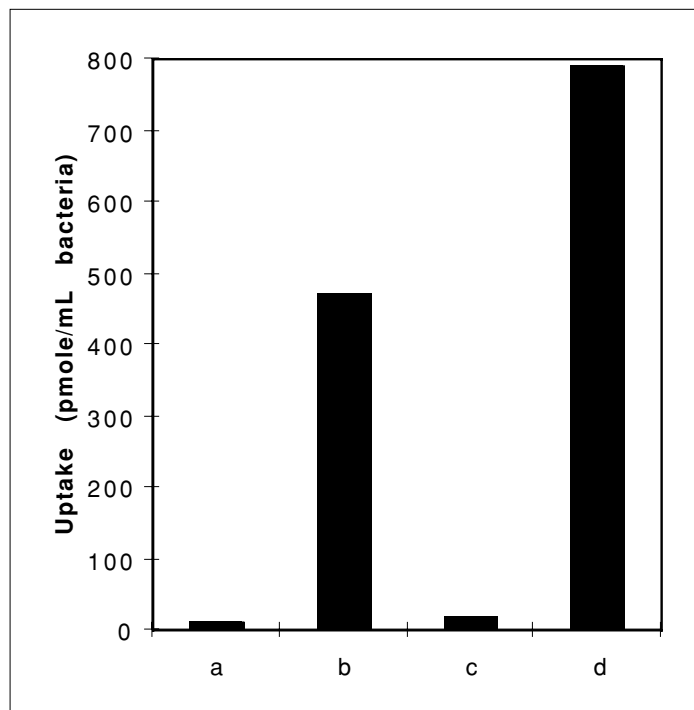
The common soil aerobes *Aureobacterium flavescens* (JG-9) and *Streptomyces pilosus* were chosen for these uptake experiments. Both organisms are known to take up the Fe-DFO complex. In the case of *S. pilosus*, the natural producer of DFO, the mechanism and kinetics of uptake have been extensively studied.<sup>2</sup> JG-9 is appropriate because it is a siderophore auxotroph, producing no siderophore of its own. We can therefore assure that all uptake is associated with a DFO complex. The siderophore DFO-B is a convenient choice for uptake experiments because it is inexpensive, readily available, and is known to exhibit Fe uptake capabilities in many different microorganisms.

Procedures for uptake experiments have been developed for many different organisms, including *S. pilosus*<sup>2</sup> and JG-9.<sup>3</sup> The microorganisms are grown on rich media to achieve high cell density. They are transferred to an iron-deficient minimal media for incubation or growth for a day or two to 'starve' the cells for Fe. Directly before the experiment, the cells are washed and resuspended in minimal media. The addition of metal-DFO complex to a culture of a known cell density determines the start of the experiment. Aliquots of the cell culture are removed at various time points over the course of an hour and filtered by vacuum filtration. The cells are retained on the filter while the soluble metal complex passes through. Scintillation counting of the filter allows for a determination of the amount metal taken up by the bacteria. The use of metal-free media and glassware, coupled with the use of metal radio-isotopes ensures that the scintillation counts represent the total amount of metal taken up by the bacteria.

Seth John,  
Christy Ruggiero,  
Larry Hersman,  
Mary Neu  
Alamos National  
Laboratory, Los  
Alamos, NM 87545,  
USA

Siderophore-mediated uptake of  $^{55}\text{Fe}$  by JG-9 has been clearly demonstrated (Fig. 1). When the cells are inoculated with an iron-DFO complex, in the presence of NTA, significant Fe uptake is observed. The rate of uptake declines significantly with time and uptake is generally complete after an hour. When media are inoculated with Fe-NTA complex in the absence of DFO, iron uptake is negligible. Although uptake has not clearly been established with plutonium, Pu is similarly associated with the cells at a much higher level in the presence of DFO. Preliminary results also indicate uptake of Fe and Pu by *S. pilosus*. Further experiments will quantify the amount and rate of uptake and elucidate the mechanism of metal-siderophore uptake.

**Figure 1. Fe and Pu uptake by the microbacterium JG-9 after 54 minutes incubation (a)  $^{55}\text{Fe}$  in the absence of DFO (b)  $^{55}\text{Fe}$  in the presence of DFO. Results are similar for JG-9 after 40 min. incubation with (c)  $^{239}\text{Pu}$  in the absence of and (d)  $^{239}\text{Pu}$  in the presence of DFO.**



### References

1. R. G. Riley and J. M. Zachara (1992), U.S. Department of Energy, Office of Energy Research, Subsurface Science Program, DOE/ER-0547-T 1.
2. Raymond, K., and Muller, Gertraud (1984), Specificity and Mechanism of Ferrioxamine-Mediated Iron Transport in *Streptomyces Pilosus*. *J. Bacteriol.* **160**:304-312.
3. Estep, M., Armstrong, J. E., and Van Baalen, C. (1975), Evidence for the Occurrence of Specific Iron (III)-Binding Compounds in Near-shore Marine Ecosystems. *Applied Microbiology.* **30**:186-188.

# XAS of Uranium(VI) Sorbed onto Silica, Alumina, and Montmorillonite

## Introduction

The purpose of this work is to determine the speciation (oxidation state and molecular structure) of uranium sorbed onto surfaces of silica, alumina, and montmorillonite, in order to investigate the modes of uranium sorption on these minerals. Characterization of actinide sorption onto silicates, aluminates, and aluminosilicates such as montmorillonite is vital for the prediction of the environmental impact and risk assessment of actinide migration from nuclear waste storage sites, underground test sites, and mining sites.

## Description of Experiment

A <2  $\mu\text{m}$  fraction of SAz-1 calcium-montmorillonite from Cheto, Arizona was washed with 2 M NaCl to convert it to the sodium form, rinsed, and freeze dried prior to loading with uranium. The  $\gamma\text{-Al}_2\text{O}_3$  and amorphous  $\text{SiO}_2$  used in the experiment were obtained from Alfa Aesar and were loaded with uranium without any pretreatment steps. These minerals were loaded with U(VI) using solutions of  $\text{UO}_2(\text{NO}_3)_2 \cdot 6\text{H}_2\text{O}$  (Mallinkrodt) and adjusted to the desired pH using NaOH or  $\text{HNO}_3$ . NaCl was added to three of the montmorillonite mixtures to determine the effect of varying ionic strength. All mixtures were kept open to atmospheric  $\text{CO}_2(\text{g})$  and were agitated at ambient temperature conditions using a gyratory shaker for approximately 5 days. The solid phases were then filtered and the resulting wet paste samples sealed in plastic vials for EXAFS analysis. Prior to EXAFS analysis final solution pH and uranium concentration were measured in order to measure pH and % sorption.

Uranium  $L_{\text{III}}$ -edge X-ray absorption spectra for two of the samples were collected on beamline X23A2 at the National Synchrotron Light Source (NSLS) using a Si(311) double-crystal monochromator. Spectra for the remaining samples were collected at the Stanford Synchrotron Radiation Laboratory (SSRL) on beamline 2-3 using a Si (220) double-crystal monochromator. All spectra were collected in transmission mode at room temperature using argon-filled ionization chambers, and energy calibrated by simultaneous measurement of the transmission spectrum of a solid uranyl nitrate hexahydrate standard that was placed in the x-ray beam downstream from the sample. The data were analyzed using standard procedures contained in the suite of programs EXAFSPAK from G. George of SSRL.

## Results

The preservation of the uranyl structure ( $\text{UO}_2^{2+}$ ) was observed in all of the samples. EXAFS analysis determined axial oxygen bond lengths of ca. 1.8 Å along with the presence of ~5 equatorial oxygen atoms at longer bond lengths (2.3-2.5 Å). The XANES spectra also confirm this result displaying features indicative of the multiple scattering from the linear O-U-O configuration in the  $\text{UO}_2^{2+}$  structure.

E. R. Sylwester,  
P. G. Allen,  
E. A. Hudson  
*Lawrence Livermore  
National Laboratory  
Livermore, CA  
94551, USA*

On montmorillonite within the pH range 3.2 to 4.1, the equatorial oxygens are observed to form a single shell at ca. 2.4 Å similar to the structure of the “free” aquo ion. Additionally, no evidence of longer-range interactions is observed. These results are consistent with previous results for uranyl sorption on montmorillonite at pH 2 and 3.3.<sup>1,2</sup> Based on this evidence the uranyl is believed to exist as a monomeric oxo-cation surrounded by an outer hydration shell, and surface adsorption by the montmorillonite occurs most likely through an outer-sphere mechanism. Uptake trends with ionic strength support a cation-exchange adsorption mechanism at pH ca. 4.1, as expected.

At a pH of 6.41, a split equatorial shell is observed in the uranyl structure. This split shell is interpreted as evidence of inner-sphere complexation with the surface, in agreement with previous work performed at a similar pH and ionic strength on kaolinite.<sup>3</sup> The lack of any U-U interactions in the sample again suggests the formation of monomeric surface complexes rather than precipitated solids. The combination of neutral pH and high ionic strength is expected to suppress cation exchange in favor of complexation by surface hydroxyl groups, explaining the observed difference between the EXAFS of this sample compared to the lower pH montmorillonite samples. Taken together, the montmorillonite results suggest a transition from an outer-sphere cation-exchange adsorption mechanism at lower pH to an inner-sphere surface complexation mechanism at near neutral pH.

In contrast to the results on montmorillonite, the EXAFS data for uranyl sorbed onto silica and  $\gamma$ -alumina at low pH display a split in the equatorial shells, forming two distinct shells at ca. 2.35 Å and 2.50 Å. This bond heterogeneity and the absence of near-neighbor U-U interactions are attributed to the formation of mononuclear, inner-sphere surface complexes on these materials at low pH. These results are in agreement with previous EXAFS studies of uranyl sorption on silica gel.<sup>4</sup>

At near-neutral (> 6) pH on silica and  $\gamma$ -alumina, a shell of U atoms was detected at 4.0 Å. For silica, an additional shell of Si atoms was clearly observed at 3.1 Å. The observation of U-U interactions suggests the formation of polynuclear surface complexes or precipitates, while the U-Si interaction at 3.1 Å is consistent with the uranyl group binding to SiO<sub>2</sub> surface subunits in a bidentate fashion. However, because EXAFS only detects average structure, it is difficult to differentiate between the following two physical models: one in which the U-U and U-Si interactions are contained within the same species or a model where these interactions originate from separate, chemically distinct species (i.e., a mixture of monomeric surface complexes + surface precipitates).

## References

1. Chisholm-Brause C., Conradson S. D., Buscher C. T., Eller P. G., Morris D.E. (1994): Speciation of Uranyl Sorbed at Multiple Binding Sites on Montmorillonite, *Geochim. Cosmochim. Acta.*, **58**, 3625-3631.
2. Dent A. J., Ramsay J. D., Swanton S. W. (1992): An EXAFS Study of Uranyl Ion in Solution and Sorbed onto Silica and Montmorillonite Clay Colloids, *J. Colloid Interface Sci.* **150**, 45-59.
3. Thompson H. S., Parks G. A., Brown G. E. Jr. (1998): Structure and Composition of Uranium<sup>VI</sup> Sorption Complexes at the Kaolinite-Water Interface, in *Adsorption of Metals by Geomedia* (ed. E. A. Jenne). Chap. 16, pp 349-370. Academic Press, San Diego, CA.
4. Reich T., Moll H., Denecke A., Geipel G., Bernhard G., Mitche H, Allen P. G., Bucher J. J., Kaltsoyannis N., Edelstein N. M., Shuh D. K. (1996): Characterization of Hydrated Uranyl Silicate by EXAFS, *Radiochim. Acta* **74**, 219-223.

# Interactions of Mixed Uranium Oxides with Synthetic Groundwater and Humic Acid Using Batch Methods: Solubility Determinations, Experimental and Calculated

David N. Kurk,  
Gregory R. Choppin

Florida State  
University,  
Tallahassee, FL  
32306-4390, USA

James D. Navratil  
Bechtel BWXT Idaho,  
LLC, INEEL, Idaho  
Falls, ID 83415-3915,  
USA (currently located  
at Clemson  
University-Clemson  
Research Park,  
Anderson, SC 29625-  
6510 USA)

## Introduction

The possibility of container compromise within nuclear waste repositories makes it necessary to investigate potential interactions between the repository environment and the materials proposed for storage. Dissolution of the repository contents into the groundwater could result in migration of the radionuclides from the repository. This possible scenario necessitates the investigation of the waste materials solubility in groundwater.

The goal of this research was to determine the solubility of mixed uranium oxides in synthetic groundwater of the Snake River plain, under oxic and anoxic conditions at constant pH, in the presence and absence of humic acid. The values for the uranium solubility obtained experimentally and by calculations were compared.

## Experimental

Anoxic experiments were performed in a glovebox containing a water saturated, dinitrogen atmosphere at ambient temperature ( $20^{\circ}\text{C} \pm 2^{\circ}\text{C}$ ). All anoxic pH and Eh measurements as well as sampling and sample preparation were performed within the glovebox. Oxic experiments were performed on a bench top, exposed to ambient conditions.

Synthetic groundwater resembling the Snake River Aquifer was used for all experiments (see table). Mixed uranium oxides were used as the source of uranium. The humic acid used had a 4.3% ash value and when present in solution, its concentration was 1 ppm.

Fluorinated, high-density polyethylene (HDPE) 2 L bottles stirred with a teflon coated magnetic stir bar, were filled with 1.80 L of the synthetic groundwater, to which approximately 0.330 g of uranium oxide was added. The pH was measured with a semi-micro glass combination electrode and adjusted to a value of 8.00. The Eh measurements were performed using a platinum/silver-silver chloride combination electrode and their accuracy was checked using "Zobell's" solution.

Sampling procedures. Stirring was ceased approximately two hours before sampling. A bottle was sampled by withdrawing approximately 2 mL of solution with a 5 mL disposable syringe. The Eh and pH were measured. Sample aliquots were filtered through a 0.22  $\mu\text{m}$  hydrophilic nylon syringe filter into a silanized glass vial. Using a calibrated pipette, 1.00 mL of a 1.00 M ultra pure nitric acid solution was placed into a 5 mL glass vial, followed by the addition of 1.00 mL of the filtered solution. The vial was stoppered and stored until measured for uranium content. Duplicate samples from each bottle were taken. The pH was adjusted to 8.00.

Uranium concentrations were measured on a high-resolution, magnetic-sector ICP-MS instrument.

## Results

The solubility experiment was performed for a total of 180 days. After a period of 104 days all samples reached equilibrium. A plot of uranium concentration in solution versus time is given in the figure below, with error bars set at 2s (95.5% confidence). In the

absence of humics, the solubility of uranium was  $0.098 \pm 0.002$  g/L in anoxic conditions and  $0.114 \pm 0.002$  g/L in oxic conditions. In the presence of humics, the solubility of uranium was  $0.094 \pm 0.003$  g/L in anoxic conditions and  $0.112 \pm 0.001$  g/L in oxic conditions.

Uranium solubility calculations were performed using published data for

uranium stability constants and solubility products. Results indicated that in the absence of humic acid, the oxic uranium solubility should be 0.117 g/L, which is very close to the experimental value. Calculations indicated that  $\text{CaUO}_4$  controls the overall uranium solubility.

The Eh reached a stable value of  $+138 \pm 4$  mV for anoxic samples and  $+220 \pm 5$  mV for oxic samples. The pH of oxic solutions between samplings increased to approximately 8.2, while for anoxic solutions it remained around 8.0. BET analysis showed that oxides had a surface area of  $3.561 \pm 0.003$  m<sup>2</sup>/g. Sieving resulted in approximately 33% of the oxides being less than 170 mesh. XRD analysis indicated that a mixture of uranium oxides were present in the sample.

The results of these experiments imply the possibility of uranium oxides leaching into groundwater. Uranium entering the groundwater from a mixed oxide form is not a slow process on a geological time scale. The presence of humic acid at 1ppm levels does not influence the uranium concentration as significantly as the presence of oxic conditions. Uranium solubility is less under anoxic conditions than under oxic conditions. The difference between oxic and anoxic solubility though does not imply that anoxic solubility should be ignored. The solubility calculations support the experimental findings of this research.

Sodium	$2.48 \cdot 10^{-2}$ M
Magnesium	$7.00 \cdot 10^{-4}$ M
Calcium	$2.50 \cdot 10^{-4}$ M
Potassium	$2.56 \cdot 10^{-4}$ M
Silicon	$3.57 \cdot 10^{-4}$ M
Carbonate	$1.23 \cdot 10^{-2}$ M
Sulfate	$3.65 \cdot 10^{-3}$ M
Chloride	$6.21 \cdot 10^{-3}$ M
Fluoride	$1.05 \cdot 10^{-3}$ M
Nitrate	$1.26 \cdot 10^{-4}$ M

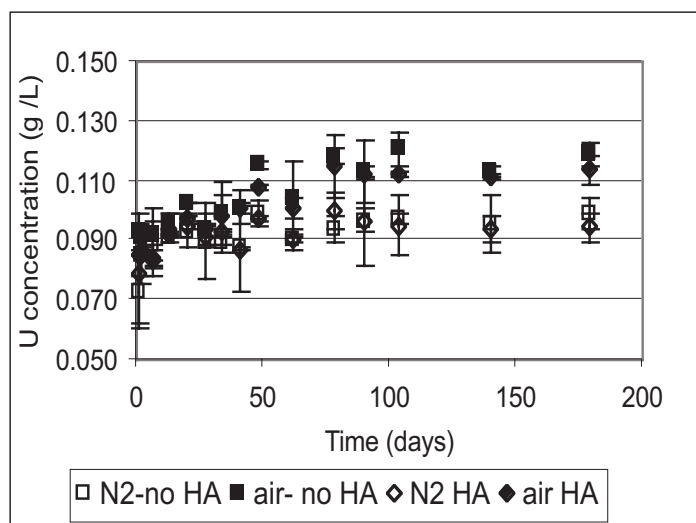


Figure 1. Uranium concentration in solution vs. time.

Table 1. Synthetic Groundwater Formulation.

## Actinide Interactions with Aerobic Soil Microbes and Their Exudates: The Reduction of Plutonium with Desferrioxamine Siderophores

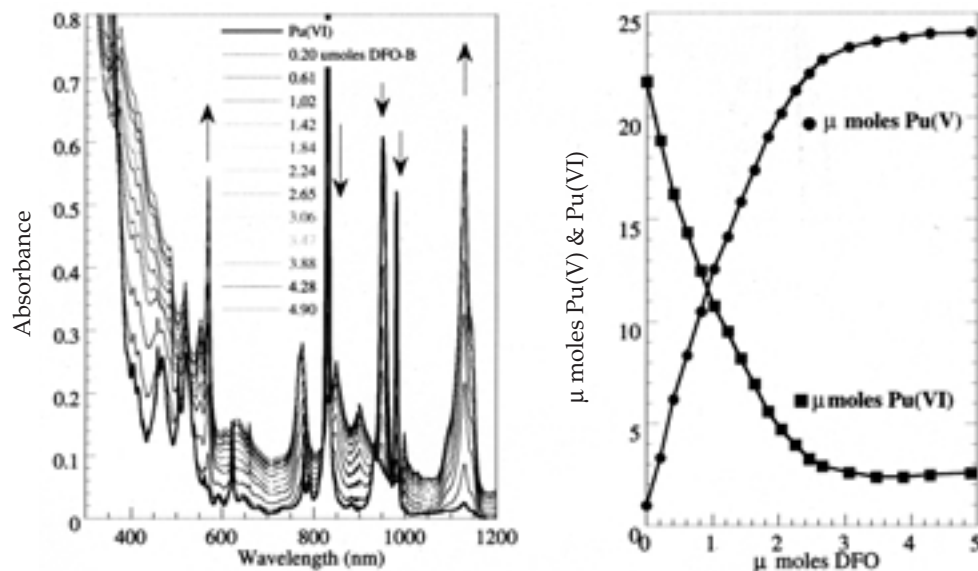
C. E. Ruggiero,  
J. H. Matonic,  
M. P. Neu,  
S. P. Reilly  
Los Alamos National  
Laboratory, Los  
Alamos, NM 87545,  
USA

Plutonium is thought to exist mostly as very low soluble and/or strongly sorbed plutonium(IV) hydroxide and oxide species in the environment, and therefore, has low risk of becoming mobile or bioavailable. However, compounds that solubilize plutonium can significantly increase its bioavailability and mobility. We are examining the fundamental inorganic chemistry of actinides with one type of biogenic chelator, microbial siderophores, in order to understand how they could affect actinide biogeochemistry. Siderophores are low molecular weight, strong metal chelating agents produced by most microbes in order to bind and deliver iron into microbial cells via active transport systems.

We are examining the interactions of plutonium with the tri-hydroxamate siderophores desferrioxamine E and B (DFO-B and DFO-E). Hydroxamate siderophores have been estimated to be present in 0.1-0.01  $\mu\text{M}$  concentrations in soils.<sup>[1]</sup> The stability constant for the Pu(IV)-DFO-B species formed at neutral pH has been estimated to be  $\log b_{110} = 30.8$ .<sup>[2]</sup> We have found that no matter what oxidation state of Pu is present initially (III, IV, V, VI), desferrioxamines rapidly and irreversibly form the Pu(IV)DFO complex at environmentally relevant solution pH: Pu(IV) is a thermodynamic sink. Here we focus on the reduction of Pu(VI) and Pu(V) with desferrioxamine (DFO).

When a solution of DFO is added to a solution of Pu(VI) at  $\sim\text{pH}=2$  in an equal molar ratio, the Pu(VI) is instantly reduced to Pu(V). This occurs as rapidly as could be detected even at concentrations as low as 0.04 mM Pu. Stoichiometric titration of Pu(VI) into a DFO solution showed that up to 12 equivalents of Pu could be reduced per desferrioxamine-B(DFO-B) or desferrioxamine-E (DFO-E) (Figure 1). This corresponds to 4 reducing equivalents per hydroxamate of the DFO molecule. The DFO is oxidized and cleaved during the reduction, as evidenced by changes in the nuclear magnetic resonance (NMR) spectra of DFO with added Pu(VI). There is no apparent binding of DFO to Pu(V), even when the ligand is in 1000x excess.

Figure 1. Titration of DFO-B into an aqueous solution of Pu(VI) ( $I_{\text{max}} = 831, 952, 982 \text{ nm}$ ) showing reduction of 12 molar equivalents of Pu(VI) to aqueous Pu(V) ( $I_{\text{max}} = 569, 775, 1129 \text{ nm}$ ) per molar equivalent DFO-B.



The Pu(V) solution that initially forms slowly reduces and the Pu(IV)DFO complex is observed spectroscopically. At pH 1 to 5.5, the reduction is significantly slower than the initial reduction of Pu(VI) to Pu(V), taking months to fully reduce. Above pH 5.5, Pu(V) is instantly and irreversibly reduced to Pu(IV), with the amount of Pu(IV) instantly formed proportional to the pH.

Both the rate of the initial reduction of Pu(VI) to Pu(V) and the subsequent reduction of Pu(V) to Pu(IV) depend on the ratio of DFO to Pu. At ratios of one molar equivalent DFO to one to four molar equivalents plutonium, the reduction of Pu(VI) to Pu(V) is instant; at ratios of one molar equivalent DFO to six or twelve molar equivalents plutonium, the rate of reduction is slower, but still very rapid (< 1 hour). In the reaction at a ratio of 1 DFO: 12 Pu, up to 20% Pu(VI) still present after 10 minutes, and a second absorbance peak at 350 nm is observed in the ultraviolet-visible (UV-Vis) absorption spectrum. This is likely a Pu(VI)-DFO species; its UV max is similar to U(VI)-DFO, which is inert to reduction. The rate of reduction of the Pu(V) to Pu(IV) is faster with higher DFO ratios. At a ratio of one molar equivalent DFO to 12 molar equivalents plutonium, where the DFO is completely reacted, only Pu(V) is detectable in solution over time, but a precipitate, presumably Pu(IV)colloid, slowly forms. This can be explained by the presence of intact DFO remaining in solution in the reactions with fewer equivalent of plutonium, which would act as a thermodynamic driving force for the formation of Pu(IV)-DFO, whereas in the reactions with 12 equivalents plutonium, there is no Pu(IV) driving force.

When Pu(VI) is added to a solution of the Pu(IV)-DFO-B complex at pH=2, the Pu(VI) is also rapidly reduced, despite the fact the DFO-B is coordinated to the Pu(IV) already. Variable temperature (VT)-NMR indicates that the Pu(IV)-DFO complex is highly fluxional, and may involve equilibrium with free DFO-B at this pH, which would allow for DFO-B interaction with and reduction of the Pu(VI).

The environmental presence of hydroxamate siderophores, the high binding affinity for Pu(IV), and the large reducing capacity for Pu(VI) and Pu(V), suggest that these siderophores could significantly effect plutonium biogeochemistry.

### References

1. P. E. Powell, G. R. Cline, C. P. P. Reid, P. J. Szanislo, *Nature* **1980**, 287, 833-834.
2. N. V. Jarvis, R. D. Hancock *Inorg. Chim. Acta* **1991**, 182(2), 229-232.

## Interactions of Microbial Exopolymers with Actinides

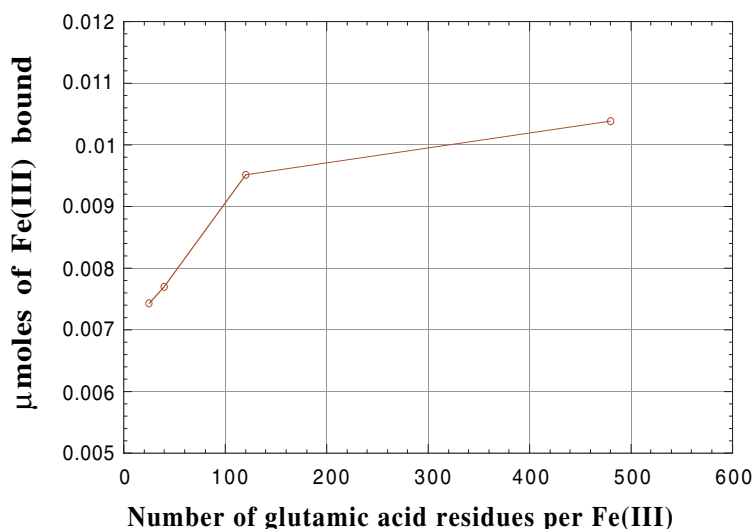
Mitchell T. Johnson,  
Dawn J. Chitwood,  
Lee He,  
Mary P. Neu  
Los Alamos National  
Laboratory, Los  
Alamos, NM 87545,  
USA

The development of viable bioremediation strategies for radionuclide contaminated soils, sediments and ground waters at DOE sites is a formidable challenge. Ubiquitous microorganisms can absorb, oxidize, reduce and/or precipitate actinides and thereby affect the speciation, solubility, bioavailability, and migration of these toxic metals. Actinides can interact directly with microorganisms, i.e., via sorption to the cell wall, and indirectly via reaction with their byproducts, such as extracellular polymers. However, very little is known about the fundamental chemistry of any microbial-actinide interactions or their impact on environmental processes. Our goal is to fully characterize specific microbial-actinide interactions and determine how they may be exploited to effect environmental actinide mobility/immobility and remediation efforts.

Under environmental conditions the chemistry that occurs in the sediments, ground waters and soils is very complex. The elucidation of the fundamental chemical mechanisms that are responsible for the interactions between metal ions and the microbial extracellular materials have begun in our lab with the study of a well characterized extracellular polymer (exopolymer) produced by *Bacillus licheniformis*, which consists of repeating  $\gamma$ -polyglutamic acid residues. The uniformity of the polymer was optimized by growth at 30°C for 14 hours on Medium E plates. The yield of purified polymer is approximately 65 mg per liter of medium. The molecular weight of the polymer is very sensitive to growth time and purification conditions. Under these conditions, a molecular weight of 800 kD with a narrow polydispersity, as determined by GPC (gel permeation chromatography), is consistently obtained. A more detailed description of the growth conditions, polymer stability, and other exopolymer characteristics have been recently reported.<sup>1</sup> R. J. C. McLean and co-workers reported the binding of other transition metals including Fe(III), which we use for the baseline of our experimental methods described herein.

First the absolute binding of the polymer was investigated using a stock solution of Fe(III) nitrate. A stock solution of 1 mg/mL of polymer was dissolved in 0.10 NaNO<sub>3</sub> and kept at 4°C until addition of iron. Four solutions were prepared with metal to glutamic acid residue ratios of 1:1, 1:5, 1:10, and 1:50 with the pH at 5.0 ± 0.2. Each of the ratios was corrected for the addition of the <sup>55</sup>Fe radionuclide (1.5% of total iron). The iron-exopolymer solutions were then vigorously mixed for 2 minutes each and then transferred to a 50,000 molecular weight cut-off membrane and vacuum filtered. Two subsequent 1 mL rinses with NaNO<sub>3</sub> solution were conducted, and the filters were allowed to evacuate to dryness. The amount of bound (on filter) and unbound (in filtrate) metal was then quantified by scintillation counting. Many control experiments were conducted to assure an accurate background subtraction for the amount of metal absorbed by the filter membrane. The amount of Fe(III) absorbed to the filter after two 1 mL washes of 0.10 M NaNO<sub>3</sub> is 5% of iron added to sample. The results are shown in Figure 1, which agree with the absolute metal binding reported by McLean.<sup>2</sup>

The chemistry of plutonium in the environment is essential to understanding what types of remediation efforts are feasible. A stock solution of <sup>239</sup>Pu(IV) nitrate was subjected to similar conditions as shown above. Once again the stock solution of <sup>239</sup>Pu(IV) was added to a solution of the polyglutamic acid exopolymer and



vigorously mixed for 2 minutes and filtered as described above. In these experiments it is essential that the reaction be done quickly so as not to form large Pu colloids, which may not pass through the filter membranes. Prior to the experiments, controls were conducted and the retention of Pu on the membrane did

Figure 1. Absolute Fe(III) binding.

not exceed 3% of total Pu. The results of the Pu bound to the polymer as quantified by scintillation counting of the filter membrane are displayed in Figure 2.

These results show very similar binding characteristics for  $^{239}\text{Pu(IV)}$  and Fe(III). We are currently investigating the uranyl binding of this exopolymer, and these results will also be presented.

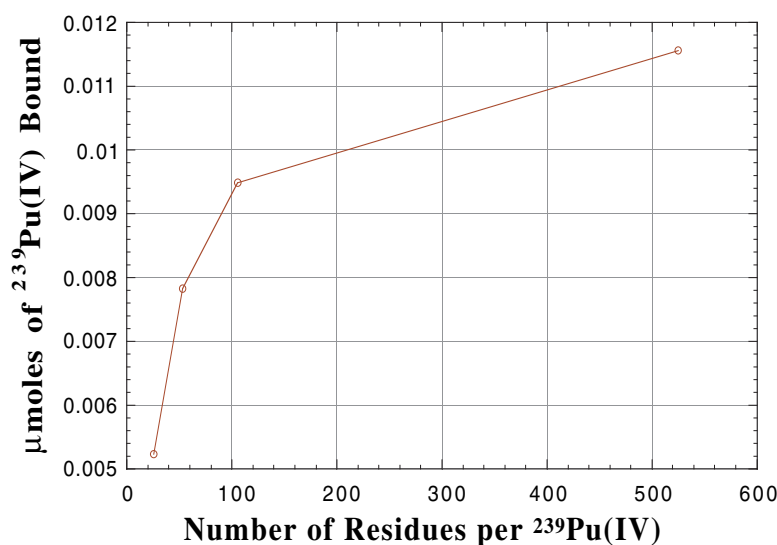


Figure 2. Absolute  $^{239}\text{Pu(IV)}$  binding.

Microbes, such as *Rhodococcus erythropolis*, can also produce high molecular weight exopolymers (1.1 kD) consisting of

saccharide repeat units, rather than amino acids. This polysaccharide contains about 12% of glurouronic acid, which is an important feature in the binding of metals. The Fe(III),  $^{239}\text{Pu(IV)}$  and uranyl binding will also be presented and contrasted to the exopolymer produced by *B. licheniformis*.

### References

1. L. He, M. P. Neu, L. A. Vanderberg, *Env. Sci. & Tech*, in press.
2. (a) R. J. C. McLean, D. Beauchemin, L. Chepman, T. L. Beveridge, *Appl. Envir. Microbiol.* 1990, 56, 3671. (b) R. J. C. Mclean, D. Fortin, D. A. Brown, *Can. J. Microbiol.* 1996, 42, 392.

## The Behaviour of Pu under Repository Conditions

**Jordi Bruno,  
Esther Cera,  
Lara Duro,  
Mireia Grivé**  
QuantiSci S.L., Parc  
Tecnològic del Vallés,  
E-08290 Cerdanyola,  
Spain

**Trygve Erikssen**  
Royal Institute of  
Technology, S-100 44  
Stockholm, Sweden

**Ulla-Britt Eklund**  
Studsвик Nuclear,  
Studsвик, Nyköping,  
Sweden

**Kastriot Spahiu**  
SKB, Swedish Nuclear  
Fuel and Waste  
Management,  
S-10240, Stockholm,  
Sweden

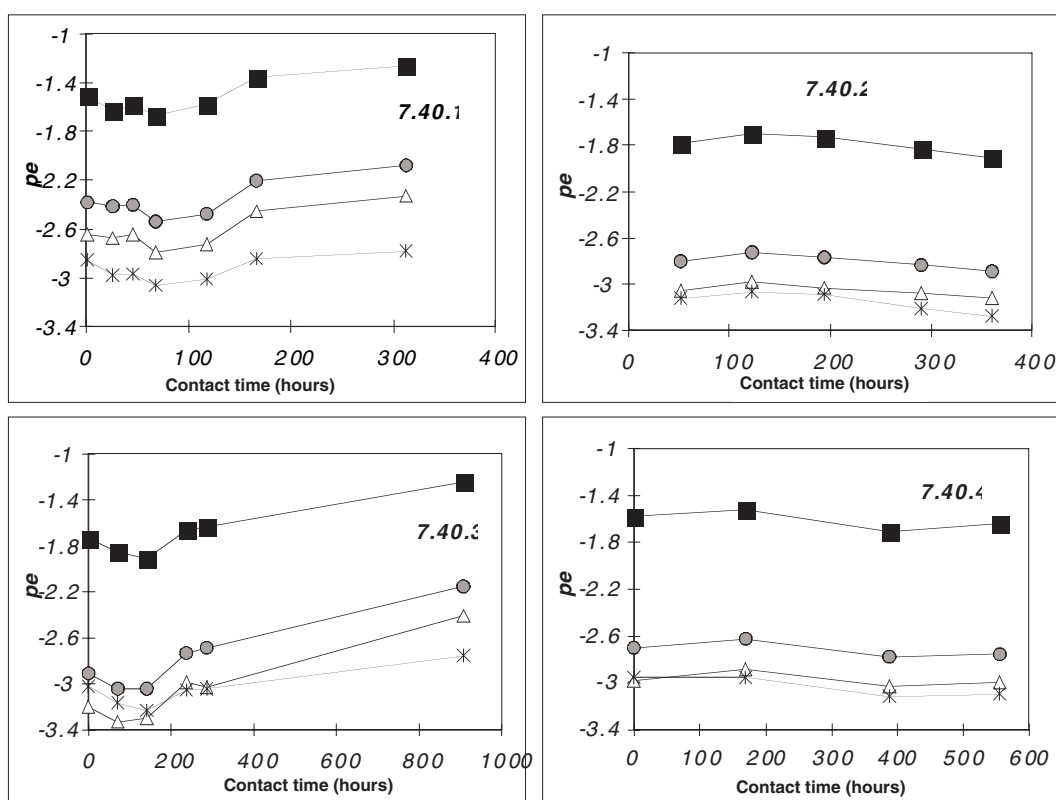
Plutonium is one of the key elements concerning the performance assessment of spent nuclear fuel repositories. Consequently, a large effort has been done in order to understand its dissolution behaviour under repository conditions. In this work we will present the experiences accumulated in a series of spent fuel dissolution tests performed under well-controlled chemical conditions. The experimental behaviour of Pu will be discussed by using different kinetic and thermodynamic modelling approaches.

The careful experimental conditions together with the detailed analysis of the radiolytic products involved in the experiments have allowed us to define the redox state of the experimental system, (see Figure 1). By using this information together with the analytical data we have been able to estimate the saturation state of the most probable solid phases which are able to control Pu solubility under repository conditions.

The kinetic and thermodynamic analysis indicate that the Pu solubility is controlled by the ageing of a poorly structured Pu(OH)<sub>4</sub>(s) (see Figure 2).

The implications for the behaviour of Pu under the reducing conditions prevailing on a SKB type repository and the need for additional experimental data will be discussed.

**Figure 1. Calculated  $p_e$  in experiments 7.40.1 (left upper), 7.40.2 (right upper), 7.40.3 (left lower) and 7.40.4 (right lower). Grey circles stand for electron balance values; white triangles stand for uranium equilibrium values; black squares correspond to TcO<sub>2</sub> equilibrium values and crosses correspond to Tc(m) equilibrium values.**



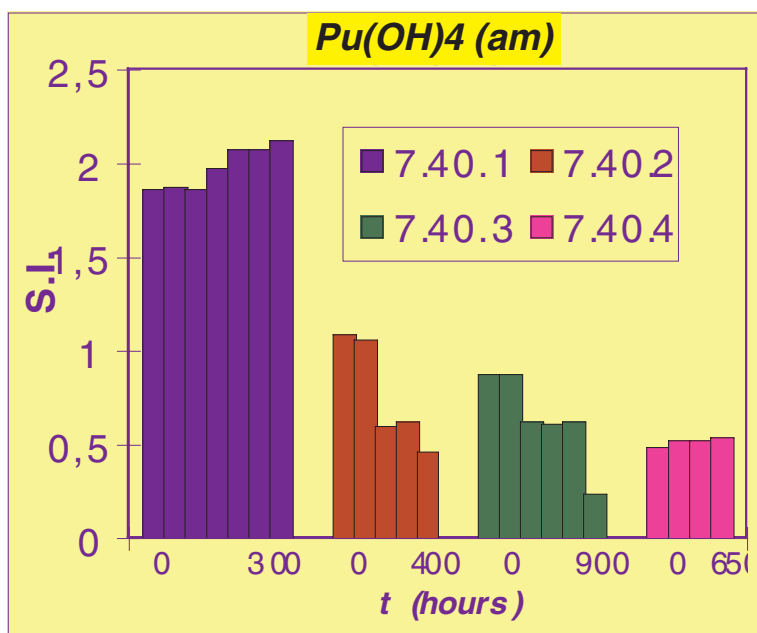


Figure 2. Evolution of calculated saturation index with dissolution time with respect to Pu(OH)4(am).

## Interaction of Plutonium and Uranium with Apatite Mineral Surfaces

Craig E. Van Pelt,  
Mavis Lin,  
Donna M. Smith,  
Wolfgang H. Runde  
*Los Alamos National  
Laboratory, Los  
Alamos, NM 87545,  
USA*

The identification and characterization of the chemical and physical interactions occurring at the solution-water interface is essential to design most effective remediation strategies as well as to predict the mobility of contaminants in the environment.<sup>1,2</sup> Phosphate materials have been used successfully for reprocessing of plutonium and remediation of sites contaminated with heavy metals, including the actinides.<sup>3</sup> The use of phosphate-bearing materials as effective agent for actinides is based upon the low solubility of actinide phosphates and the high stabilities of phosphate complexes in solution. As such, apatites commonly occur in the environment and are the principle mineral components of phosphate rock. The retention of heavy metals and actinides by apatite has been under investigation for some time.<sup>4,6</sup> While apatite has been recognized as reducing soluble actinide concentrations effectively, the fundamental principles of the interfacial chemical processes remain unknown. Both precipitation of low soluble actinide solids (U, Th) as well as surface sorption have been reported as interaction mechanisms. The sorption of metals to apatite (natural, synthetic, and fishbone) is prevalent in the literature with many researchers reporting distribution coefficients ( $K_d$ ) for the apatite uptake.<sup>4,6</sup> However, the reported  $K_d$  values for the apatite-actinide systems do not distinguish between actinide precipitation and actinide sorption on the mineral surface.

This study involves the interaction of plutonium(IV, V, and VI) and uranium(VI) with a natural apatite mineral surface at varying metal concentrations and pHs under atmospheric conditions. The retention factors or  $K_d$  values (in the case of sorption) were calculated by difference knowing the initial actinide concentration and determining the concentration of the actinides in solution. The degree of retention varied with the total actinide concentration. Surface precipitation (see Figure 1 showing uranium(VI) crystals on apatite surface) was identified by using scanning electron microscopy (SEM) at  $[U(VI)] > 10^{-5}$  M. The surface precipitate was characterized using fluorescence, FT-Raman, and attenuated total reflectance (ATR) FTIR spectroscopies. FT-Raman and ATR-FTIR spectroscopies allowed the analysis of the solid in the presence of the aqueous supernatant resulting in the surface denticity of the sorbed cation by comparing the spectra to that of known multidentate phosphate compounds. Uranium samples were also analyzed using fluorescence spectroscopy in a similar manner to the vibrational spectra relating sorbed species to known uranium phosphate complexes (Figure 2). Extended X-ray Absorption Fine Structure spectroscopy was used to investigate the local coordination environment around the absorbing f-element and to determine the coordination number and bond lengths. Studies are ongoing to investigate the kinetics of  $UO_2^{2+}$  sorption to the apatite using batch experiments in which the  $UO_2^{2+}$  solution concentration was monitored as a function of time.

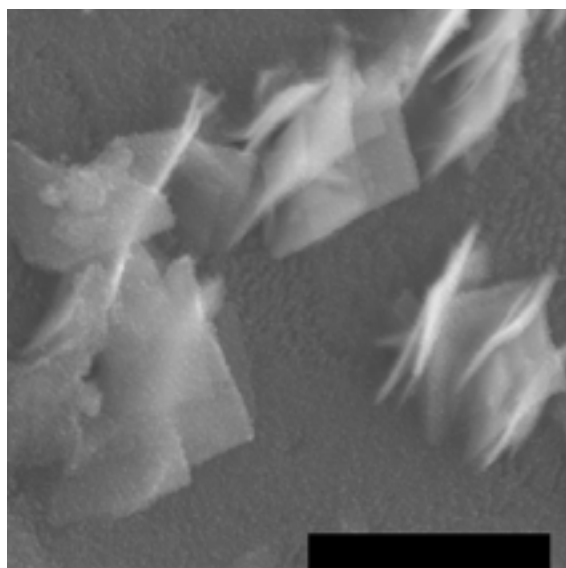


Figure 1. Uranium crystals on apatite.

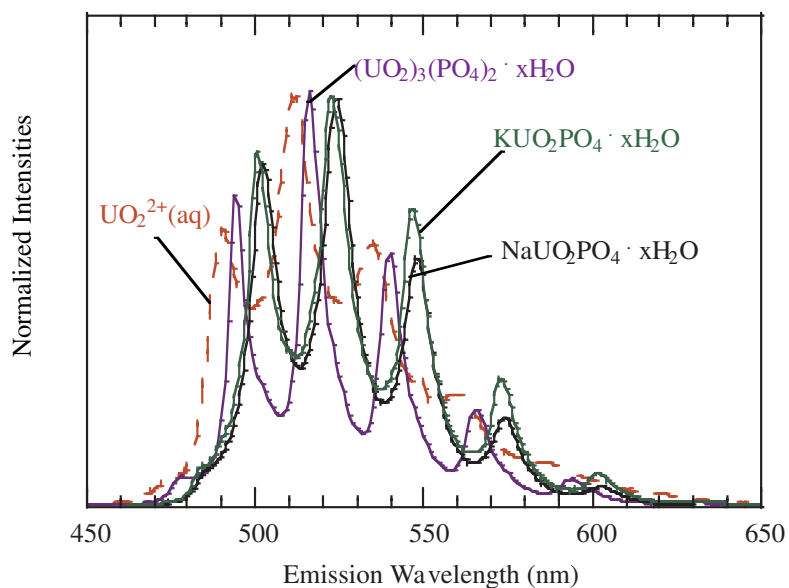


Figure 2. Uranyl phosphate fluorescence.

### References

1. Lenhart, J. J.; Honeyman, B. D., *Geochim. Cosmochim. Acta* **1999**, 63, 2891-2901.
2. Bargar, J. R.; Reitmeyer, R.; Davis, J. A., *Environ. Sci. Technol.* **1999**, 33, 2481-2484.
3. Katz, J. J.; Seaborg, G. T.; Morss, L. R., *The Chemistry of the Actinide Elements*; 2nd ed.; Chapman and Hall: London, 1986.
4. Chen, X. B.; Wright, J. V.; Conca, J. L.; Peurrung, L. M., *Environ. Sci. Technol.* **1997**, 31, 624-631.
5. Admassu, W.; Breese, T. J., *Haz. Mat.* **1999**, 69, 187-196.
6. Bostick, W. D.; Stevenson, R. J.; Jarabek, R. J.; Conca, J. L., *Adv. Env. Res.* **1999**, 3, U9-&.

# Equilibrium, Kinetic and Reactive Transport Models for Pu: Employing Numerical Methods to Uncover the Nature of the Intrinsic Colloid

Jon M. Schwantes,  
Bill Batchelor  
Texas A&M  
University, College  
Station, TX 77843,  
USA

## Introduction

Future missions for the Department of Defense include processing plutonium for vitrification and conversion to mixed oxide fuels for commercial use. Such processing could result in the production of Pu-containing waste and unplanned releases of Pu to the environment. Some releases related to plutonium processing have occurred in the past. However, scientists are currently not able to explain the observed behavior of plutonium in natural systems. For example, classical filtration theory predicts that plutonium transport within groundwater should be limited to a few tens of meters.<sup>1</sup> Experimental observations, however, show that plutonium is present in groundwater at distances orders of magnitude farther away from its source than predicted.<sup>2</sup> Before adequate disposal practices can be designed for plutonium, its behavior in these systems must be better understood. The overall goal of this project is to develop equilibrium, kinetic and reactive transport models that describe the behavior of Pu in aqueous systems and to apply these models to natural and engineered systems.

Scientists have not been able to predict plutonium behavior because of its extremely complex chemistry in aqueous systems. Its chemistry is more complex than all the other elements, with the likely exception of carbon. Due to similarity in redox potentials, Pu exists simultaneously in four different oxidation states under environmental conditions.<sup>3</sup> These oxidation states include  $\text{Pu}^{3+}$ ,  $\text{Pu}^{4+}$ ,  $\text{PuO}_2^+$  and  $\text{PuO}_2^{2+}$  (the V and VI oxidation states exist as linear dioxoions in solution), and each is capable of following a different chemical pathway in the environment. Each particular oxidation state is related to the others via redox mechanisms such as disproportionation and electron transfer that are unique to Pu.

Perhaps the greatest challenge scientists and modelers face in trying to unravel the mystery of Pu chemistry, is Pu sorption to countless different possible surfaces present as substrate or as particles suspended in natural solutions. Natural colloid-facilitated transport, a result of sorption processes, is blamed for extended mobility of Pu at many waste sites.<sup>1,4-8</sup> Sorption processes are usually considered important for the IV and VI oxidation states, with partitioning being greatest for the former.<sup>9,10</sup>

Also problematic when attempting to predict behavior, Pu readily forms mixed valence, inorganic colloids through hydrolysis and polymerization, followed by aggregation.<sup>11-18</sup> This is often the predominant form of Pu at many DOE sites where highly-concentrated liquid waste was disposed of or where the proximity to historic bomb testing sites predisposes the area to aolian transport.<sup>2, 6, 8, 19</sup>

Inorganic Pu colloids may provide another means, besides transport via natural colloids, of explaining observed long-range mobility of plutonium. For this reason, great attention was given in this project to describing the formation and aging of mixed-valence plutonium oxy/hydroxide polymers. Although these polymeric species aggregate into colloids much slower than the rate at which direct sorption of Pu(IV) onto natural colloids would occur, aging of these Pu colloids will form progressively more stable, possibly irreversible, morphs of the

solid<sup>11, 20-24</sup>. As with sorption, natural reductants and oxidants may significantly affect the solubility of these solid Pu particles.<sup>25</sup>

## Methodology

The first task for this project was to develop an equilibrium model describing the environmental behavior of plutonium. This equilibrium model is based on the HATCHES thermodynamic database and supplemented by data derived from an extensive literature search of over 200 scientific publications and government documents. Specific emphasis was placed during the designing of the equilibrium model on the overall goal of linking reaction kinetics and 1-D flow code. For instance, the dissolved species of Pu(IV) may account for an insignificant portion of the total Pu in solution and therefore might not be included in an equilibrium model. However, if the presence of that species affects the reaction rates of other environmentally-important species, that component must be included in this equilibrium model.

Possibly the single greatest limitation that chemical modelers currently face is the lack of well-defined equilibrium constants for various chemical species. This limitation is especially true in the case of Pu chemistry, where potentially behavior-controlling multi-valent, polymeric species are too small and/or too complex to be accurately described by experimental analysis. Controlling species are known (or suspected), but there is a lack of accurate equilibrium constants to describe the reactions that form them.

Hand calculations can be made for simple equilibrium models, but computer-based tools are desirable for a complex system such as one containing unknown plutonium species. Because the model predictions are not usually linearly related to the unknown coefficients, a non-linear regression is required. This means that an iterative solution technique is needed. A computer program module has been developed that integrates a Gauss-Newton nonlinear regression routine with the chemical equilibrium modeling power of PHREEQC to enable inverse calculations of unknown or poorly defined equilibrium constants. This module is called INVRS\_EQ1.

The behavior of plutonium in nature is inherently dependent on the role redox reactions play in all aspects of its chemistry, including sorption/desorption and precipitation/dissolution. Many of these redox reactions may be kinetically controlled and reach steady state far away from equilibrium. Equilibrium models alone are therefore ill equipped to predict such complex behavior.

Other tasks for this project include developing reactive transport models that integrate equilibrium models with reaction kinetics. This integral approach will have the capability to describe behavior controlled by reaction kinetics, given an appropriately extensive database of kinetic constants. To assist in the development of a database of kinetic constants, a module similar to that of INVRS\_EQ1 is currently being developed to enable inverse calculations of unknown or poorly-defined kinetic constants. Results of the literature search and inverse calculations of equilibrium and kinetic constants pertaining to the mixed valence oxy/hydroxide plutonium polymer will be discussed.

## References

1. McDowell-Boyer, L. M., Hunt, J. R. & Sitar, N., *Wat. Resour. Res.* 22, 1901-1921 (1986).
2. Kersting, A. B., D. W. Efurud, D. L. Finnegan, D. J. Rokop, D. K. Smith, and J. L. Thompson, *Nature*, 397, 7, 56-59 (1999).
3. Choppin, G. R., and B. E. Stout, *Chem. Brit.*, 12, 1126-1129 (1991).
4. Buddemeier, R. W., and J. R. Hunt, *Appl. Geochem.*, v. 3, pp. 535-548 (1988).
5. Penrose, W. R., W. L. Polzer, E. H. Essington, D. M. Nelson, and K. A. Orlandini, *ES&T*, 24, 228-234 (1990).
6. Jakubick, A. T., In: *Transuranium nuclides in the environment*, San Francisco, 17-21 November 1975, 74-62 (1976).
7. Hakonson, T. E., J. W. Nyhan, and W. D. Purtymun, In: *Transuranium nuclides in the environment*, San Francisco, 17-21 November 1975, 175-189 (1976).
8. Price, S. M., and L. L. Ames, In: *Transuranium nuclides in the environment*, San Francisco, 17-21 November 1975, 191-211 (1976).
9. Bondietti, E. A., S. A. Reynolds, and M. H. Shanks, In: *Transuranium nuclides in the environment*, San Francisco, 17-21 November 1975, 273-287 (1976).
10. Nelson, D. M., R. P. Larsen, and W. R. Penrose, In: *Symposium on Environmental Research for Actinide Elements*, 27-48 (1987).
11. Lloyd, M. H. and R. G., *Haire. Radiochimica Acta*, 25, 139-145 (1978).
12. Bell, J. T., C. F. Coleman, D. A. Costanzo, and R. E. Biggers, *J. Inorg. Nuc. Chem.*, 35, 629-632 (1973).
13. Bell, J. T., D. A. Costanzo, and R. E. Biggers, *J. Inorg. Nuc. Chem.*, 35, 623-628 (1973).
14. Costanzo, D. A., R. E. Biggers, and J. T. Bell, 1973. *J. Inorg. Nuc. Chem.*, 35, 609-622 (1973).
15. Neu et al., Paper presented at the Pu Futures Conference, Santa Fe, New Mexico (1997).
16. Rai, D., and J. L. Swanson, *Nucl. Tech.*, 54, 107-112 (1981).
17. Aston, S. R., *Mar. Chem.*, 8, 4, 319-325 (1980).
18. Taube, M., In: *Nuclear chemistry in monographs*, Volume 4, 69-86 (1974).
19. Tamura, T., In: *Transuranium nuclides in the environment*, San Francisco, 17-21 November 1975, 213-229 (1976).
20. Ockenden, D. W., and G. A. Welch, *Chem. Ab. number* 653 (1956).

21. Haschke, J. M. and T. E. Rickett, *J. of Alloy. Comp.*, 252, 148-156 (1997).
22. Williams, L. A., G. A. Parks, and D. A. Crerar, *J. Sed. Petro.*, 55, 3, 301-311 (1985).
23. Williams, L. A. and D. A. Crerar, *J. Sed. Petro.*, 55, 3, 312-321 (1985).
24. Haschke, J. M., T. H. Allen, L. A. Morales, *Science*, 287, 285-287 (2000).
25. Madic, C., P. Berger, and X. Machuron-Mandard, In: *Transuranium elements: a half century*, 200<sup>th</sup> ACS National Meeting, Washington DC, August 26-31, 1990, 457-468 (1992).

